I.O.S.

STATUS REPORT ON RESEARCH AT THE INSTITUTE OF OCEANOGRAPHIC SCIENCES RELATED TO THE POSSIBLE DISPOSAL OF RADIOACTIVE WASTE ON OR BENEATH THE SEAFLOOR APRIL 1979 – MARCH 1984

EDITED

BY

B. BOOTY

REPORT NO. 204

1985

OCEAN DISPOSAL OF HIGH LEVEL RADIOACTIVE WASTE
A RESEARCH REPORT PREPARED FOR THE DEPARTMENT
OF THE ENVIRONMENT

NATURAL ENVIRONMENT RESEARCH COUNCIL

INSTITUTE OF OCEANOGRAPHIC SCIENCES

INSTITUTE OF OCEANOGRAPHIC SCIENCES

Wormley, Godalming,
Surrey, GU8 5UB.
(0428 - 79 - 4141)

(Director: Dr. A.S. Laughton FRS)

Bidston Observatory,
Birkenhead,
Merseyside, L43 7RA.
(051 - 653 - 8633)

(Assistant Director: Dr. D.E. Cartwright FRS)

Crossway,
Taunton,
Somerset, TA1 2DW.
(0823 - 86211)

(Assistant Director: M.J. Tucker)

When citing this document in a bibliography the reference should be given as follows:-

BOOTY, B. [Ed.] 1985 Status report on research at the Institute of Oceanographic Sciences related to the possible disposal of radioactive waste on or beneath the seafloor: April 1979 - March 1984. *Institute of Oceanographic Sciences, Report*, No. 204, 333pp.

INSTITUTE OF OCEANOGRAPHIC SCIENCES

WORMLEY

Status report on research at the Institute of Oceanographic Sciences related to the possible disposal of radioactive waste on or beneath the seafloor

April 1979 - March 1984

edited

by

B. Booty

I.O.S. Report No. 204

1985

DEPARTMENT OF THE ENVIRONMENT

RADIOACTIVE WASTE MANAGEMENT

RESEARCH PROGRAMME 1979/1984

DoE Report No. DoE/RW /85/003

Contract Title:

DoE Reference: DGR 481/176, DGR 481/177, DGR 481/178, DGR 481/179,

PECD7/9/023

Report Title: Status report on research at the Institute of Oceanographic Sciences related to the possible disposal of radioactive waste on or beneath the seafloor: April 1979 - March 1984 edited by B. Booty.

Date of Submission to DOE 1984

Abstract

This report summarises all of the research carried out by the Institute of Oceanographic Sciences in connection with the possible disposal of radioactive waste at sea. It covers the period April 1 1979 to March 31 1984.

All the work mentioned here is reported upon, usually in much greater detail, in a series of individual reports.

Keywords
299 - DoE sponsored research
15 - Heat generating
93 - Disposal on deep ocean bed
94 - Disposal under deep ocean bed

CONTENTS

CHAPTER 1

INTRODUCTION

The Institute of Oceanographic Sciences has carried out a five year programme of oceanographic and marine biological investigations aimed at a better understanding of the problems and possibilities associated with the disposal of radioactive waste in the oceans.

The work has been funded by the Department of the Environment through five separate contracts as follows:

DGR 481/176 - Studies of the benthic boundary layer in relation to the disposal of radioactive waste

The objective of this contract is to examine the processes which control the characteristics of the benthic boundary layer and would control the dispersal of radioactive material released into it. The approach to the problems has been through mathematical modelling of the processes involved backed up by observation in the deep ocean.

DGR 481/177 - The properties of ocean sediments in relation to the disposal of radioactive waste

The objective is to establish the physical, chemical and geotechnical properties of marine sediments suitable for the emplacement of radioactive waste. Studies have been made of a wide range of properties of sediments, the pore water within the sediments and particulate matter in the ocean.

DGR 481/178 - Biological transfer of materials between sea bed and surface

This is an investigation of midwater and sea bottom biota aimed at identifying and quantifying biological processes by which radionuclides may be transferred through the deep ocean environment for the development and validation of predictive mathematical models.

DGR 481/179 - Selection and evaluation of sites for the disposal of radioactive waste

The tasks are to identify potential areas for the disposal of radioactive waste in the ocean bed and to establish generic characteristics of representative areas. Studies have been carried out of selected areas in the North Atlantic to determine the history and stability of sediments in those areas.

PECD 7/9/023 - Dispersion in the deep waters of the Eastern North Atlantic

The principle objective of this contract is to acquire systems and make measurements to permit estimates to be made of advection and the ability of the ocean to disperse radioactivity. The Department has funded specific ocean circulation studies carried out by the Institute of Oceanographic Sciences and also the Institute's participation in international longer term measurements.

This report is intended as a summary of all the work, is self contained and is laid out in a manner which it is hoped will present the overall picture while at the same time acting as a worthwhile reference. Considerably more detail than is presented here is available in the many individual reports the work has generated. Research into the problems of the disposal in the ocean of radioactive waste is continuing under revised contracts with revised objectives and work schedules.

CHAPTER 2

SELECTION AND EVALUATION OF AREAS AND SITES

In 1979, following the production of IOS Report 77, a set of site selection guidelines was drawn up and used to carry out a preliminary assessment of areas in the North Atlantic that might prove suitable for HLRW disposal (Searle, 1979). The guidelines were broadly classified as relating to the stability of the disposal site, the suitability of the sub-seabed disposal medium, oceanographic, biological, operational and general factors. They have now been published (Searle, 1984).

IOS work has been confined to the North Atlantic ocean, although the progress of US and Japanese studies of the North Pacific has been followed closely through the OECD Nuclear Energy Agency's Seabed Working Group (SWG). Indeed, throughout the IOS work there has been close cooperation with other nations through the SWG, with IOS providing the UK representatives of the SWG's Site Selection and Sediment and Rock Task Groups. This international cooperation has been particularly important with regard to studies in the Great Meteor East area (GME), where most of the early work including the majority of the high resolution seismic profiling was carried out by the Dutch Geological Survey (RGD). Details of SWG activities are contained in Anderson (1980, 1981, 1982, 1983).

Our site selection studies have concentrated on five specific areas. Kings Trough (KTF) and Great Meteor West (GMW) are typical of the lower flanks of the Mid-Atlantic Ridge, and were expected to have more or less continuous sequences of calcareous pelagic sediment. GME, Cape Verde One (CV1) and Nares Abyssal Plain (NAP) are distal abyssal plains where the uppermost hundred metres or so of sediment are fine-grained turbidites (predominantly clay at NAP and calcareous at CV1 and GME). A reconnaissance of the southern Cape Verde Abyssal Plain was also carried out (McGiveron, 1981; Kidd and Searle, 1984), but it was eventually decided that the area did not warrant further investigation at present because of the evidence of strong bottom transport of sediments (Kidd and Searle, 1984). The upper parts of the Mid-Atlantic Ridge and the more proximal parts of the abyssal plains and continental margins were considered either to have too little sediment or for the sediment to be too unstable for them to be considered as potential disposal areas.

Three compilations of previously existing data have been carried out at IOS. First, available seismic reflection data were compiled to produce a map of average widths of sediment basins throughout the North Atlantic (Searle, 1979). Secondly, a compilation of seismic reflection and core data was made for the distal abyssal plains between 30°N and 45°N (McGiveron, 1980) to complement a similar French compilation to the south. Finally, a copmpilation and analysis of all existing geophysical data in the KTF area was undertaken and included in the report of that area (Kidd et al, 1983).

A 2 kHz hull-mounted profiler was developed for RRS Discovery and was tested on Cruise 106 in December 1979 (Kidd et al, 1980). It was subsequently replaced by a towed 3.5 kHz profiler, also developed at IOS. These profilers provide vertical resolution of 2-5m and penetration of up to 80m. A near-bottom profiler, giving a penetration of over 30m and resolution of 20cm was built and successfully tested on Discovery Cruise 118 February-March, 1981 (Francis et al, 1981). Finally, a survey camera system (WASP) was built. It has the capacity of taking up to 1600 frames each covering 25 to 100m^2, on each lowering.

Seven cruises have contained a large component of site selection work. Discovery 118 (Francis et al, 1981) and 134 (Francis et al, 1983) and 144 (Schultheiss et al, 1984) worked at GME only; Farnella 3/81 (Searle et al, 1982) worked at GME and CV1; Farnella 8 (Revie et al, 1983) worked at NAP; and Farnella 9 (Revie et al, 1983) worked at KTF. All the Farnella cruises carried the long-range sidescan sonar GLORIA; the others carried a variety of geophysical equipment including airgun seismic reflection profilers and 2 kHz or 3.5 kHz profilers. In addition, a small amount of 2 kHz profiling was carried out over NAP during Discovery 108 (Anon, 1980).

Early work at GMW by RGD demonstrated the widespread occurrence of debris flows and other types of sediment instability (Kuijpers, 1982). It was therefore decided not to investigate the area further.

The CV1 area has been studied in detail by French workers (Auffret et al, 1984) and was covered by our GLORIA reconnaissance of the Cape Verde Basin (Kidd and Searle, 1984; Searle et al, 1982). There is considerable evidence of energetic bottom sediment transport and the existence of shallow, massive sand beds. We have therefore not pursued further investigations there.

IOS studies of NAP have been largely restricted to the GLORIA survey. Further investigations are being carried out by our Dutch, American and Canadian colleagues. Preliminary results suggest that the sedimentary environment may be somewhat more heterogenous than GME, but perhaps with less faulting (see below).

Work at KTF to the end of 1982 has been reported by Kidd et al (1983). Additional work has been carried out on Discovery Cruise 134. The area is situated at 41°-43°N 21°-24°W, in depths of 3400-4000m (Figure 2.2). Sediments consist of alternating calcareous oozes and marls in the uppermost 80m or so, underlain by ooze and chalk. Sediment thickness is in the range 300-800m. It is concluded that areas on the order of 10-30km wide and several 10s of kilometres long exist that are free of scarps or basement outcrops. These are mostly sedimented basins. Near the edges of the basins there is evidence of small-scale sediment slumping or non-deposition and possibly erosion. Minor slumping and hiatuses have been observed in some cores remote from the edges of the basins. Drilling by the Deep Sea Drilling Project (Kidd & Ruddiman, 1983; Kidd, 1984) has documented continuous sedimentation over the last 30 My. Pore-water samples taken from the drilled cores show linear gradients of Ca and Mg, which imply pore-water advection of less than 10^{-4}cm y^{-1} (T.R.S. Wilson, personal communication, 1984).

GME and NAP are now the two sites at which NEA/SWG work is being concentrated, and most IOS effort in recent years has been spent on GME. The area lies between 30.5° and 33°N, 23° and 26°W, in a water depth of 5400m. It is a flat, distal abyssal plain, broken by occasional abyssal hills (some with outcrops of igneous crust) a few hundred metres high (Figure 2.3). Evidence of strong turbidity current transport and debris flows exists east of 24°W, (Simm & Kidd, 1984) but west of there the surface of the abyssal plain appears fairly uniform and stable. Turbidites probably make up the bulk of the uppermost 125m, and are likely to be underlain by pelagic clay and carbonate. Sediment thickness is generally around 250-1250m. The largest basin lies between 31.2° and 31.8°N, 24.0° to 25.0°W. However, this area is characterised by small faults (Duin et al, 1984) spaced 10-20km apart which offset the sediments below about 15m depth. A smaller basin around 31.2°N, 25.3°W appears to be fault free at present. A detailed report of the GME area is in preparation (Searle et al, 1984).

In conclusion, there are areas within KTF, GME, and probably NAP where sediments appear to be adequately thick and stable for waste disposal, but these areas are

only on the order of 20km wide. It appears very difficult to find wider areas in the Atlantic that are reasonably homogenous and present a history of sediment stability.

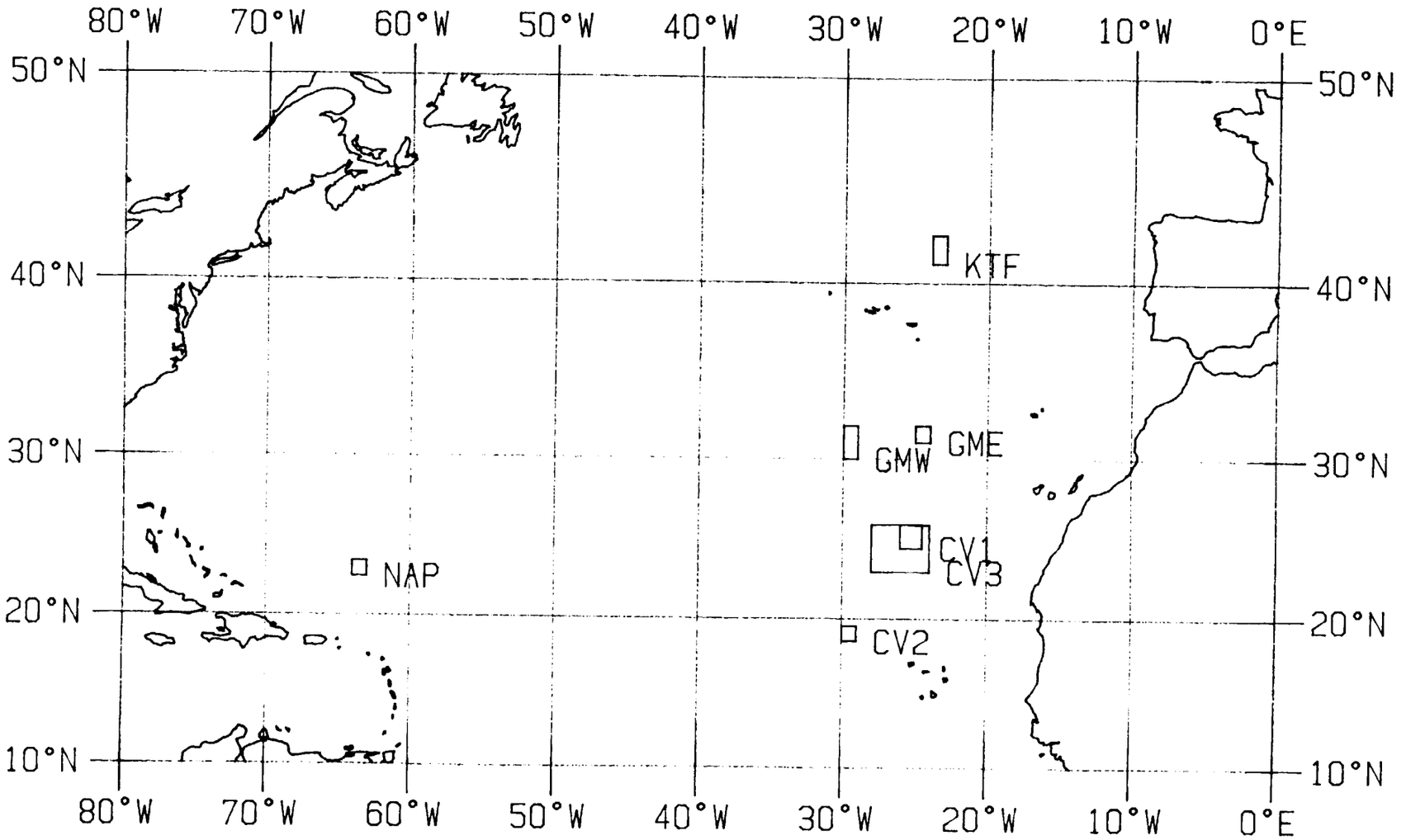

Figure 2.1 High level radioactive waste disposal study areas examined by the Institute of Oceanographic Sciences in the period 1979-1984.

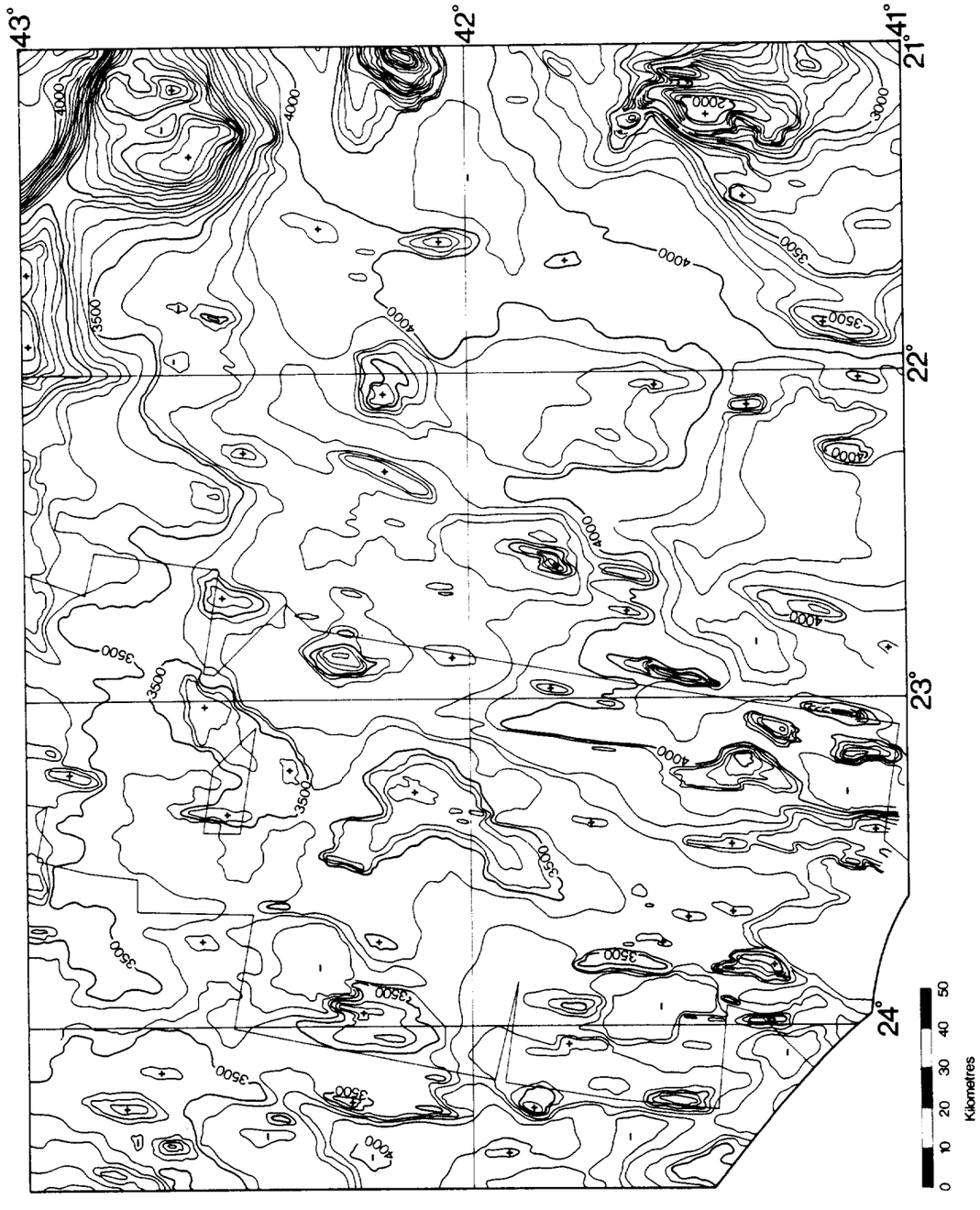

Figure 2.2 Bathymetry of KTF in corrected metres.

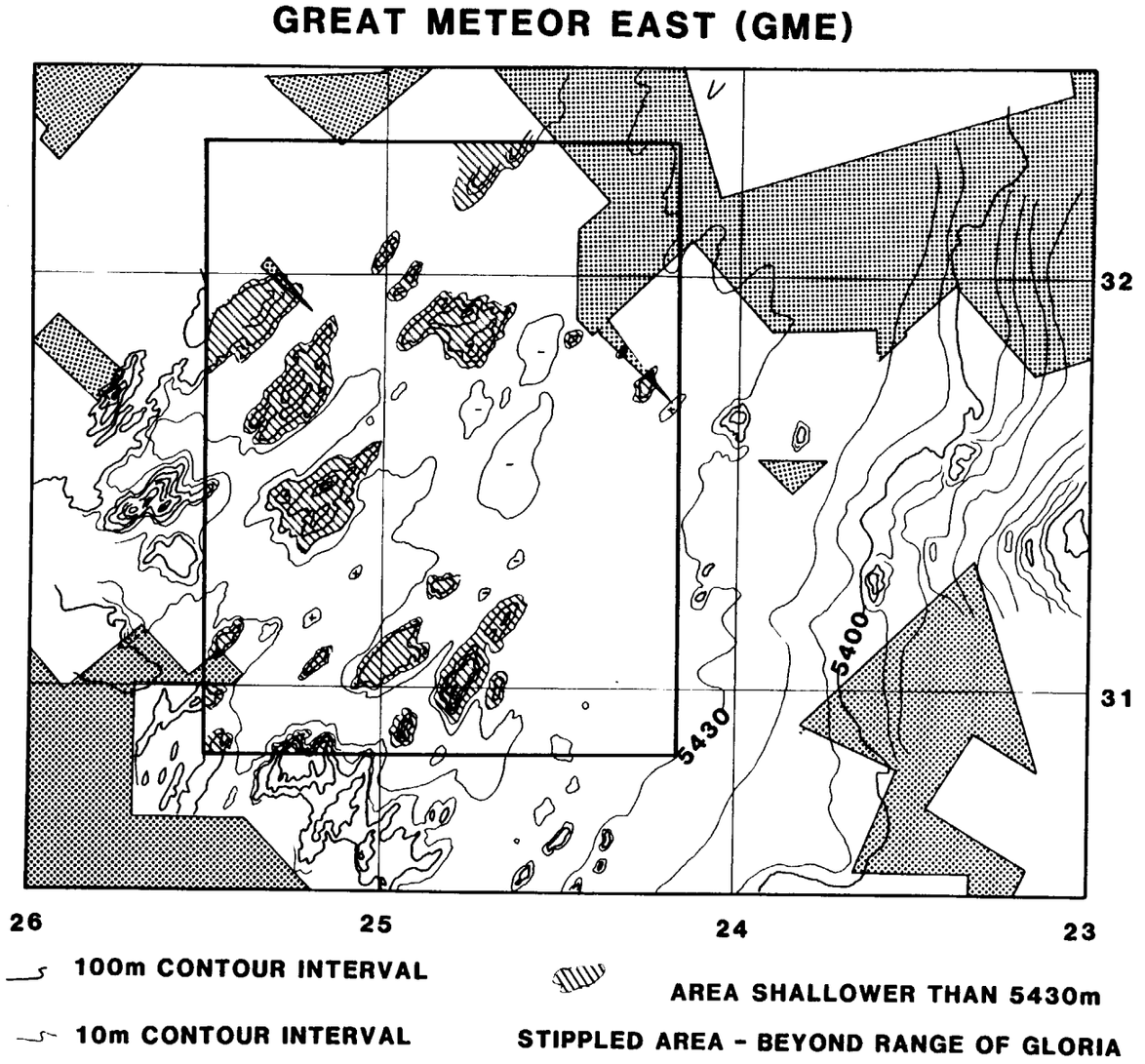

Figure 2.3 Bathymetry of GME in corrected metres.

CHAPTER 3

REGIONAL STUDIES

3.i Estimation of Seismic Risk at Atlantic Ocean Intra-Plate Sites

Earthquakes recorded by the World Seismological Network have been used to assess the seismic hazard for sites within the Atlantic Ocean intra-plate region. For the period for which we have the most complete data (1964-1979) over 100 events can be identified as occurring within the intra-plate regions of the Atlantic (Lilwall, 1982). From these data it is possible to identify a region of greater than average activity to the East and North-East of the Caribbean, which may be the result of slight relative motion of the North and South American plates. Such a zone may not truly represent an oceanic intra-plate region and the data were excluded from seismic risk estimates. Seismicity appears relatively uniform over the remaining regions but overall activity in the South Atlantic is about half that in the north even after correction for network detection thresholds. Relocation and examination of events prior to 1964 gives a similar difference in activity although the zone of high activity near the Caribbean is less evident (Lilwall, 1982).

The largest earthquake for the period 1964-1979 had a magnitude of 6.4 on the surface wave scale (M_s) whilst during the whole period for which we have data (1913-1979) the largest magnitude recorded is 7.2. An extreme value analysis of the magnitude of all the oceanic intra-plate events gives a value of 7.3 for the upper limit and therefore 7.5 would be a conservative upper bound to assume in seismic risk estimation. Below this value the seismicity for North Atlantic intraplate events can be described by the magnitude frequency relation:

$$\text{Log}_{10} N = -5.63 - 0.44\ M_s$$

where N is the number of earthquakes per annum per square km with magnitude greater than M_s.

The larger events are capable of causing considerable damage and liquefaction effects near their epicentre. The seismic risk at any given site, however, depends on the spatial distribution of the above seismicity with respect to the site. If the seismicity is everywhere uniform over long periods then assuming attenuation relations used for land sites the return period for 0.1g peak acceleration (a point at which slope instability and liquefaction may occur) is estimated to be circa 10,000 years. If, as suspected in published work on these earthquakes, the seismicity is concentrated along zones of weakness such as fracture zones, then the return period in such zones may be as short as 2000 years.

In addition to the above analysis of teleseismically recorded earthquakes, a start was made on monitoring the GME area with ocean bottom seismographs for small local events on Discovery Cruise 118 in 1981. Work on the seismicity project was temporarily suspended in April 1982 due to funding constraints, it being considered more sensible at that time to concentrate the available resources behind other projects. However, the concentration of future work in the GME area and the discovery there of faults in the sediment close to the sea bed now makes the monitoring of local seismicity in that area by ocean bottom seismograph an important field of future study. The objectives of this work would be two-fold:

i. Determining whether there are any local concentrations of seismic activity in the area, possibly along the traces of fracture zones.

ii. Establishing whether the faulting observed in the shallow sediments is associated with underlying faulting in the lithified rocks.

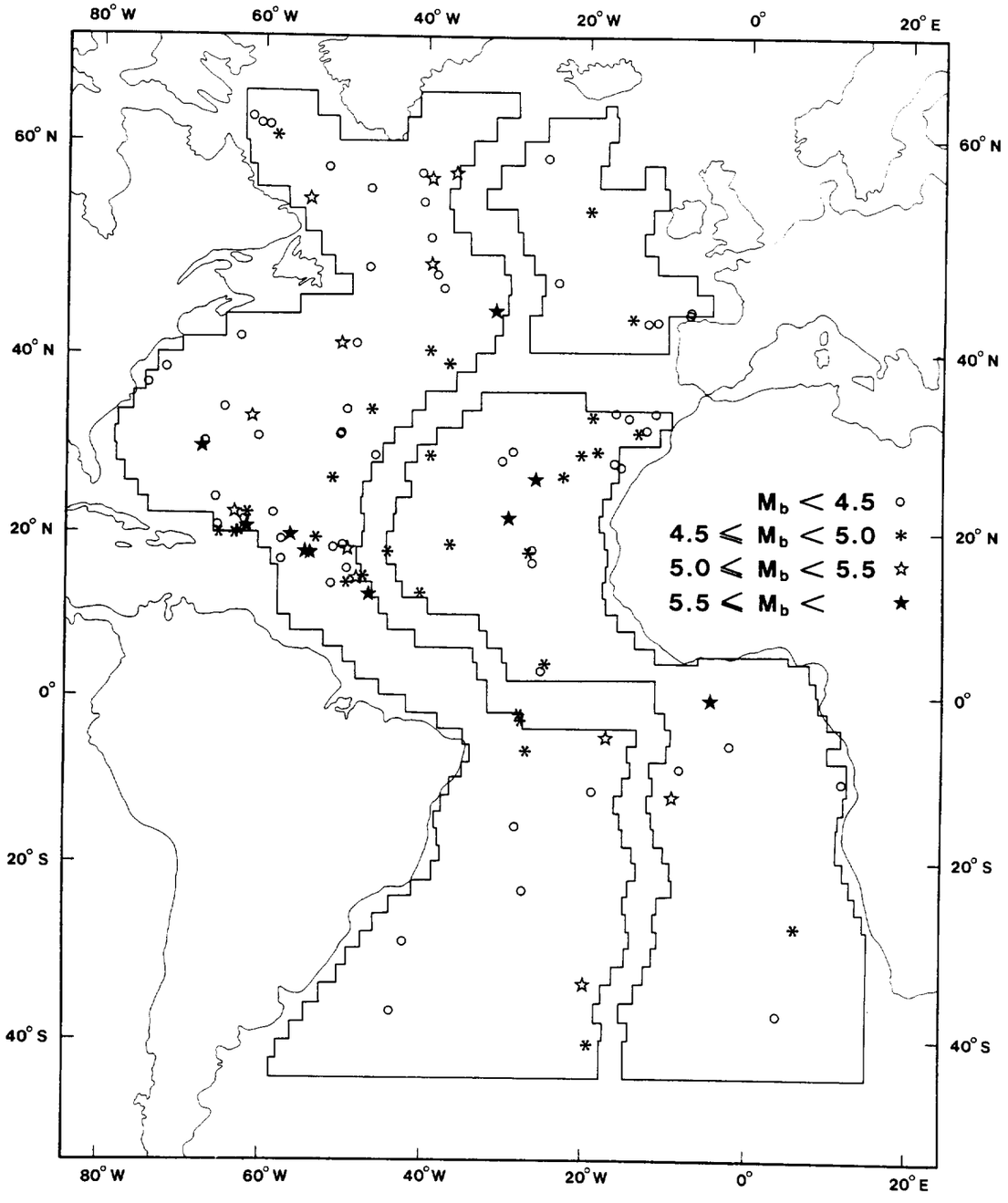

Figure 3.i.1 Teleseismically observed intraplate earthquakes in the Atlantic Ocean during the period 1964-1979 inclusive.

3.ii Physical Properties of Sediments

The objective of this work was to investigate and assess the physical properties of deep-sea sediments in HLRW study areas. In particular it is intended to quantify pore water advection velocities as low as 0.1 mm/year. The innovative nature of some of the research has meant that a significant amount of development work has been necessary.

Two major parameters need to be measured before the vertical pore water speed can be calculated; these are the permeability and the differential pore pressure gradient within the sediment column. Whilst it is desirable that both these should be measured in situ it is argued that values of permeability can be measured accurately in the laboratory from core samples. Consequently an apparatus has been developed at IOS which allows sediment permeability to be measured at decreasing void ratios during a back pressured consolidation test. Data already collected from over 60 samples have established the major differences in permeabilities between various sediment types and how this changes as a function of burial depth and void ratio (Schultheiss & Gunn, 1984) (Figure 3.ii.1). Samples from two study areas in the North Atlantic, Kings Trough Flank (KTF) and Great Meteor East (GME), have been compared with samples of Red Clay (RC) obtained from the Pacific Ocean. Typically the permeability of the nanno-fossil turbidites in the GME area is 1×10^{-5} mm/s but increases to 1×10^{-3} mm/s in the silty bases. The marls and oozes in the KTF area generally have coarser grain sizes than at GME and have permeabilities around 5×10^{-5} mm/s. Permeability values for the RC samples range from 1×10^{-4} mm/s near the surface to less than 1×10^{-7} mm/s at a sub-bottom depth of 170m. More detailed discussion of the measurements obtained for samples in the KTF and GME area is given in Chapter 4.

The measurement of differential pore pressure gradients in sediment can only be done in situ. Consequently a Pop-Up-Pore-Pressure-Instrument (PUPPI) has been developed which can achieve the required differential pressure resolution for measuring extremely slow rates of flow (Figure 3.ii.2). The PUPPI incorporates a 3 or 4 metre lance which penetrates the sea-floor after the device has fallen through the water column. A pore pressure port near the tip of the lance is connected to a differential pressure transducer and solid state logger which records the difference between the tip pressure and the hydrostatic pressure. A positive pressure pulse is recorded as the probe enters the sediment which decays with

time. The instrument ascends to the surface, leaving the disposable lance and the driving weights in the sea-floor, on an acoustic command from the ship. It is still unclear how long it is necessary to record the pressure decay before the residual pore pressure can be calculated. During a deep water trial some 100 miles NE of the GME area in November 1983, the instrument was left recording for 2 days. The pore pressure was still decaying after this time but the extrapolated residual pore pressure was 0.28 kPa at a depth of 1.4m which indicated an upward pore water velocity of 8 mm/yr (Schultheiss et al, 1984).

The major problem that has arisen with the development of the PUPPI is coping with the variation in strength of various sediment types. If the sediment is too hard then the instrument may not penetrate fully and there is a risk that it will topple over. If the sediment is too soft then the instrument may over penetrate and the mud will cause suction forces which may prevent the recoverable section 'taking off' on release. Although it is possible to trim the PUPPI by using different amounts of ballast and different lengths of probes to compensate for variations in sediment properties this requires a detailed prior knowledge of the sediment and experience with the PUPPI which is now accumulating.

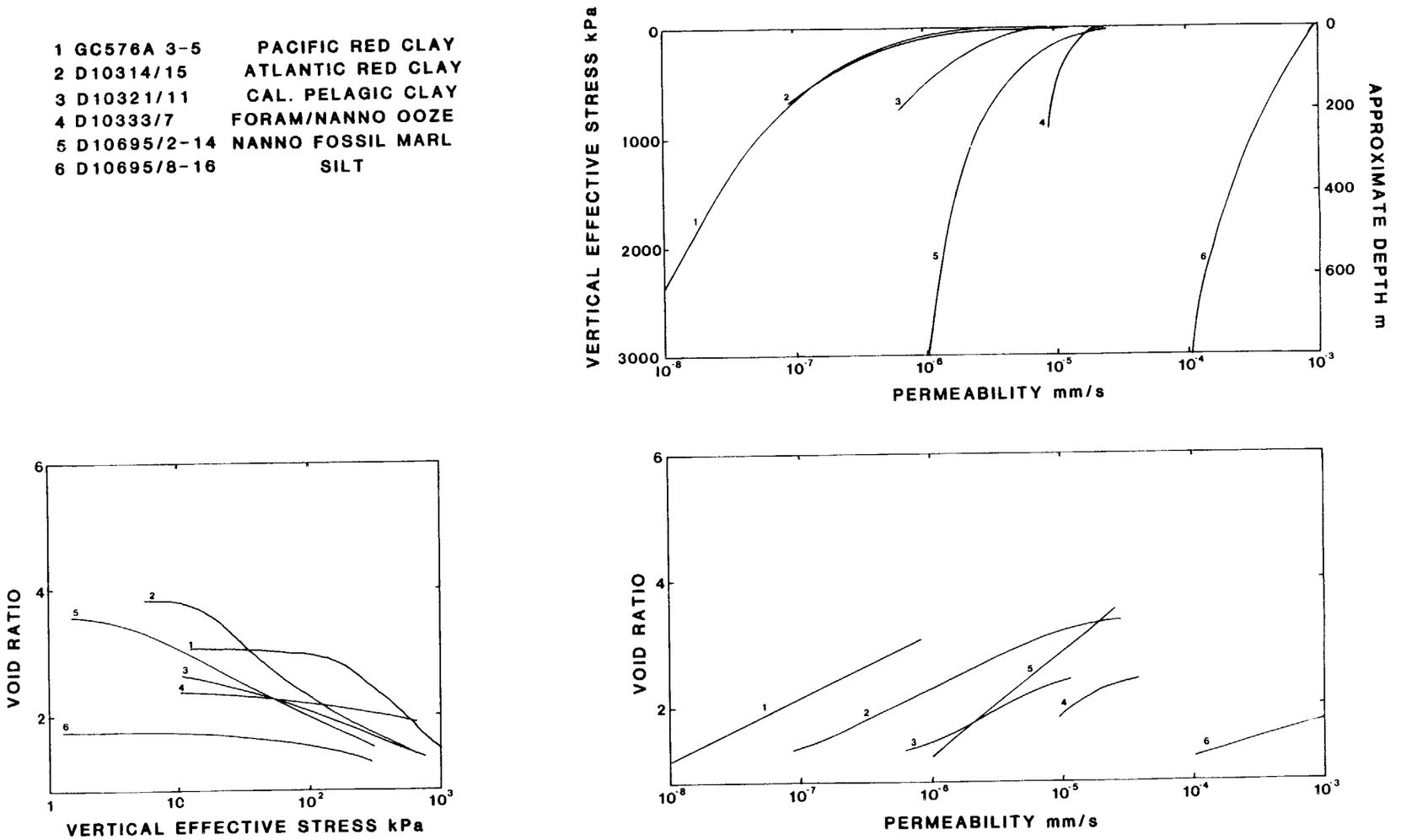

Figure 3.ii.1 A comparison of the consolidation and permeability characteristics of different sediment types.

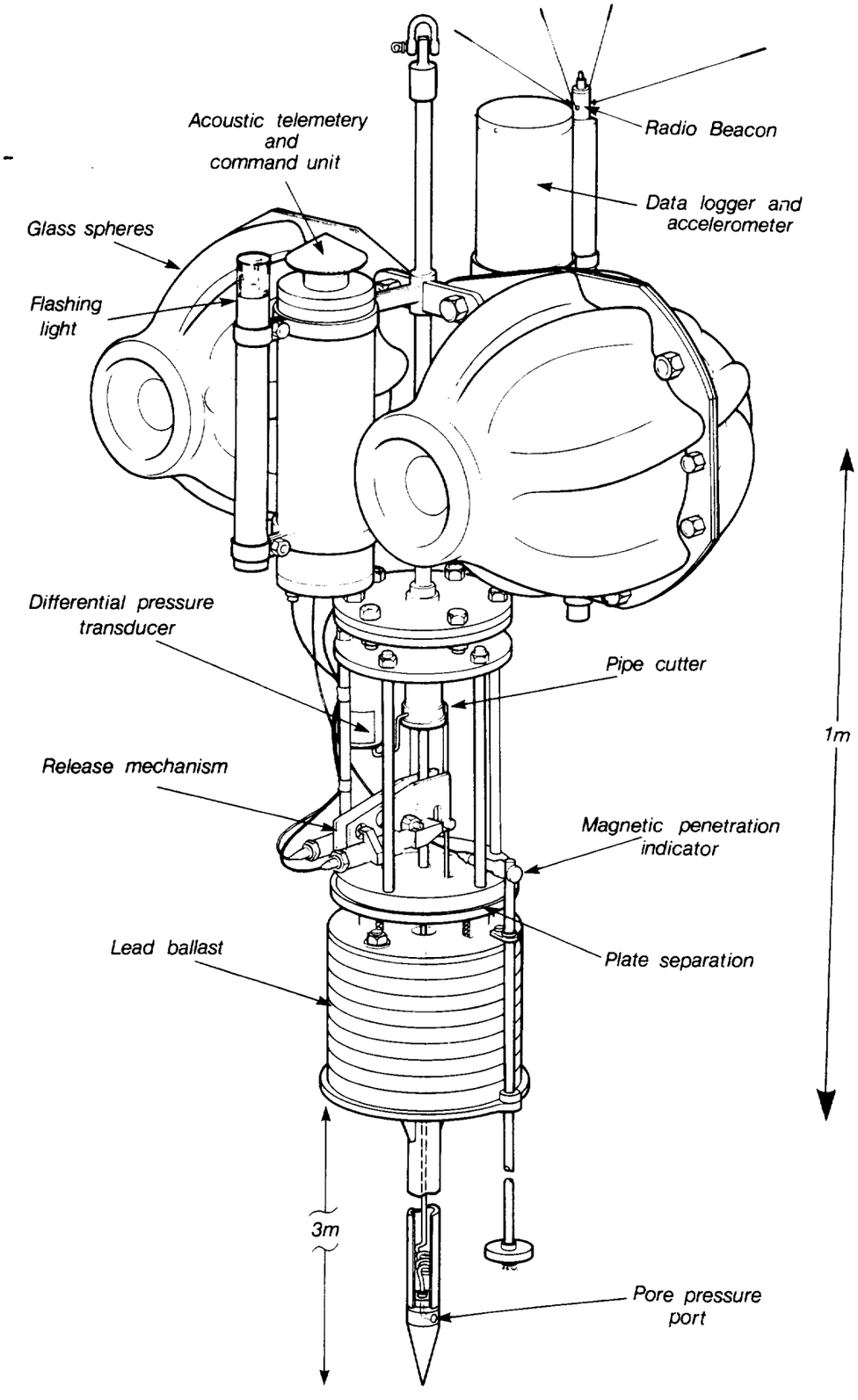

Figure 3.ii.2 Pop-Up-Pore-Pressure-Instrument (PUPPI) designed to measure vertical pore pressure gradients in deep sea sediments.

3.iii Glacial Erratics

The scouring action of a glacier as it flows downhill scrapes rock from the floor and walls of the enclosing valley. This debris becomes frozen into the ice and protrudes in places, so increasing the scouring action of the glacier. In this way, the action of glaciers erodes bedrock to produce a sediment called glacial drift which is characteristically unsorted; it is composed of particles of rock (or glacial erratics) which vary in size from rock flour to large boulders.

Depending upon climatic and geographic conditions, a glacier may terminate on land or at sea. If the termination occurs on land, rock material trapped in the ice is released at the toe of the glacier to produce thick deposits of glacial material called terminal moraines. When a glacier terminates in the sea, the toe moves away from land and is repeatedly broken off to form icebergs. These float oceanwards carrying glacial erratics frozen into them; the process is known to geologists as "ice rafting".

Calculations based upon the densities of rock and ice indicate that icebergs may carry up to 7.5% by volume of rock material before sinking. This being the limiting case, however, concentrations of up to 1% or more are normally cited for glacier ice (Ovenshine, 1966).

Rock material may be continuously released from icebergs, either through their slow melting or in batches, as icebergs roll over and deposit material lying loose on their upper surfaces. Small fragments of ice containing more than 7.5% rock material may calve off larger icebergs and sink before completely melting, so producing a characteristically clustered deposit of erratics on the sea floor (Heezen & Hollister, 1971).

For at least the past three million years, glaciers have been active in many areas around the North Atlantic Ocean. An estimated 200,000 km^3 of glacial drift has been moved from the continents by ice rafting alone (Ruddiman, 1977). During interglacial periods like the present, glacial activity is much reduced. Small icebergs (up to 10m thick) have, nevertheless, been observed as far south as 31°N in the North Atlantic (USNOO, 1968).

Glacial erratics may, therefore, be expected to occur on and within deep sea sediment in the NE Atlantic Ocean. It is also expected that, as the frequency of iceberg sightings falls off to the south, so too should the density of ice-rafted material found on the sea floor. Other variations in the distribution of ice-rafted material are also expected; the main cause being differences in the rate of sedimentation of fine-grain pelagic sediments which ultimately bury any material (like glacial erratics) lying on the sea floor.

In the IOS report, "Guidelines for the selection of sites for disposal of radioactive waste on or beneath the ocean floor" (Searle, 1979), it was recognised that glacial erratics could obstruct the emplacement of waste canisters into the sediment. This project has, therefore, been conducted to collect data that would enable an assessment to be made of:

1. The risk of canister impact with individual boulders; and
2. The southernmost limit of ice rafting in the NE Atlantic Ocean.

The data for this project were collected from dredge hauls containing rock material, sediment cores and sea-floor photographs.

(a) Dredge Hauls. Visits to all the main repositories of dredged rock material in the UK, France, Germany and USA have been made. A total of 288 dredge hauls have been examined from which 121 yielded glacial erratics. Twenty-one of these dredge hauls had been run with excellent control and so accurate data on the distribution of ice rafted material have been collected.

(b) Sediment Cores. A literature survey of 1164 sediment cores revealed 72 containing material identified as glacial erratics. A further, more detailed study of core no. D10333 (taken from the Kings Trough Flank) has produced data covering the variations in ice-rafted input to the deep sea over the past 120,000 years (down to 2m depth in the sediment).

(c) Sea-floor Photographs. Photographs from 176 camera stations have been examined. Thirty-two of these were run with sufficient control to estimate surface distributions of glacial erratics. Ten survey camera stations were run specifically for this project to cover areas of low distributions of glacial erratics where other sampling techniques were unable to cover sufficient ground.

Results

The risk of canister impact is dependent upon two variables: the grain-size of the particles considered hazardous to canister emplacement and the latitude which controls the bulk quantity of material within the sediment.

(a) Grainsize. Ice rafted material can occur on or in deep sea sediments as pebble/boulder material of any size up to 78m diameter. The grainsize distribution of this material has been assessed at a number of sites (Figure 3.iii.1) and can be described by the negative exponential distribution represented by the equation:

$$\text{Log}_{10}X = \text{Log}_{10}M - 0.5D$$

where: M is the intercept of the line of the y axis
D is the grain size (maximum diameter in cm)
X is the cumulative number of particles per sq.km.

In estimating the risk of canister impact, particle size is clearly important. Figure 3.iii.2 shows a curve giving the percentage of ice rafted material to be found in the upper 3cm of sediment with diameters between 2.0 and 10.0cm. This is a cumulative curve from which values for the percentage of ice rafted material up to 10.5cm in diameter may be estimated. This work has been extended to take account of both the varying proportions of ice-rafted material down through the sediment and the larger grain sizes which have not been sampled.

(b) Latitude. As one moves south, away from the source of icebergs in the N. Atlantic there is a fall off in the amount of ice rafted material to be found on and in deep sea sediments. Accurate measurements of ice rafted input have been made at 50°, 42° and 32°N in order to estimate the risk of canister impact down to the southernmost limit of ice rafting which is at about 30°N.

A full description of this project is in preparation (Huggett, 1984).

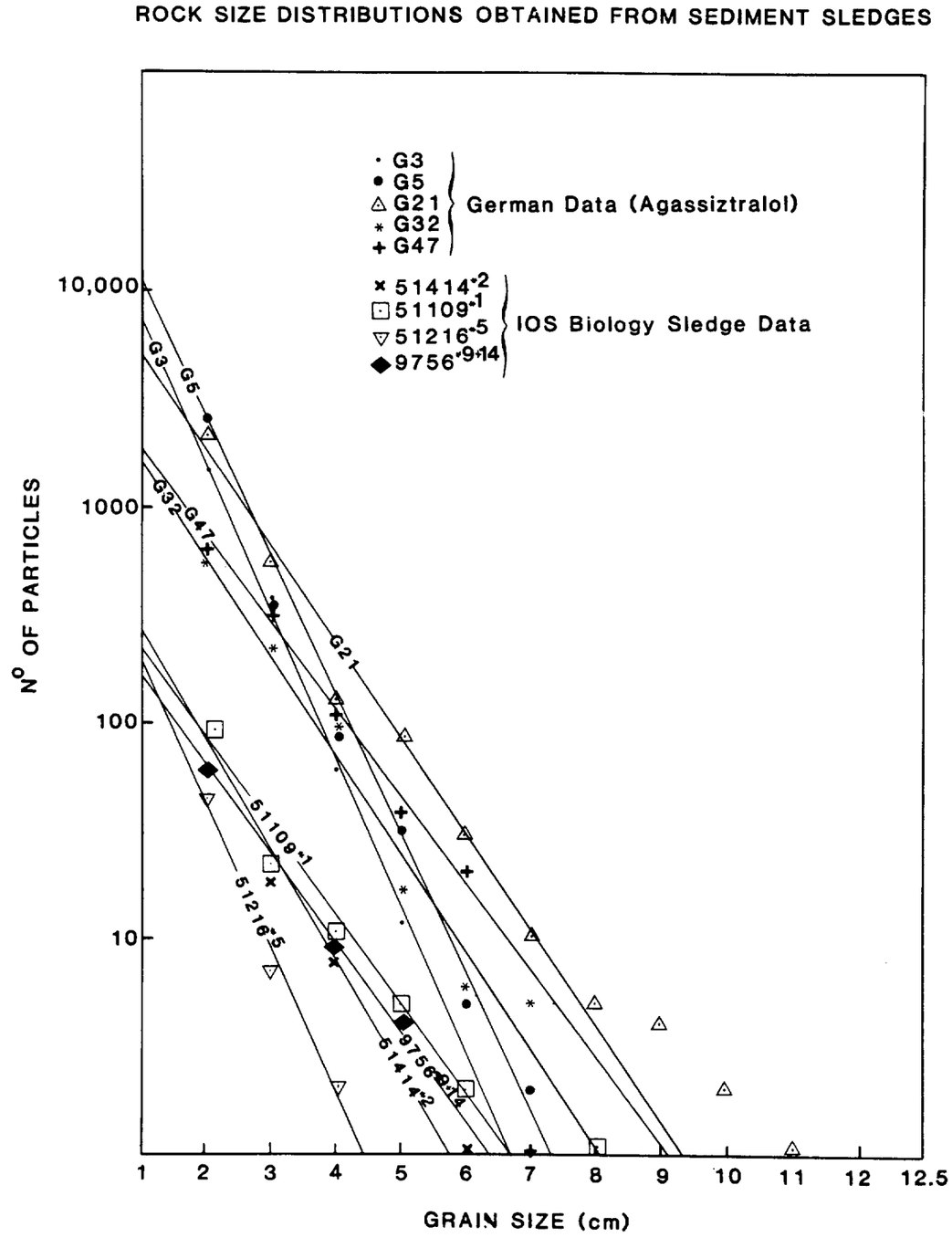

Figure 3.ii.1 Grain size data of Glacial Erratics drawn on log-linear paper for comparison. (NB: data not normalised for areas sampled.)

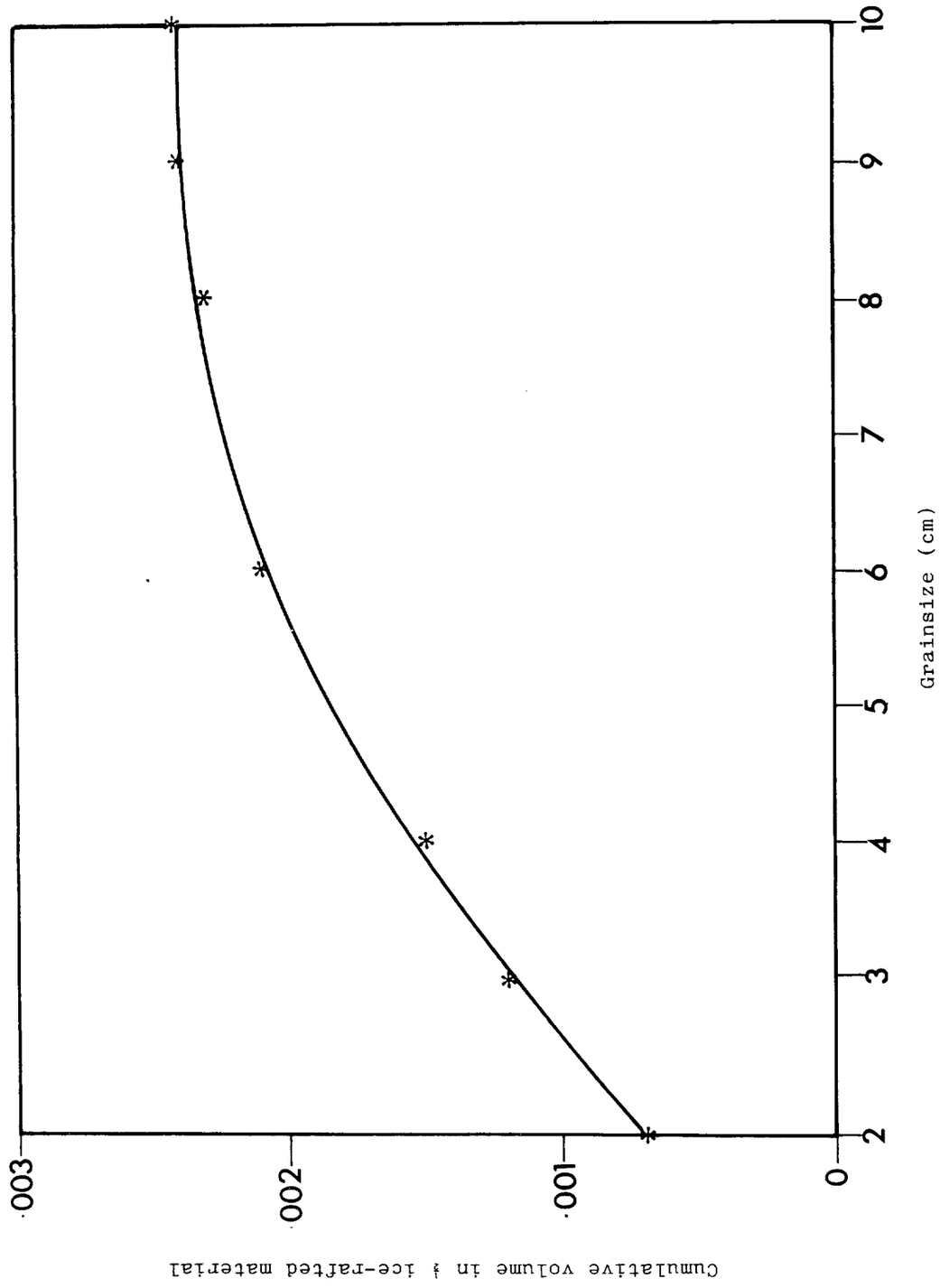

Figure 3.iii.2 Curve showing the cumulative volume of ice-rafted material in the surface sediments at 42°N.

CHAPTER 4

SITE SPECIFIC STUDIES

4.i GREAT METEOR EAST

4.i.a Regional Setting

The Great Meteor East study area (GME) lies between 30.5°N and 32.5°N, 23.0°W and 26.0°W. Five IOS cruises have carried out site assessment studies in the area: Discovery cruises 118, 126, 134 and 144, and Farnella cruise 3/81 (Francis et al., 1981b, 1983, 1984; Schultheiss et al., 1984c; Searle et al., 1982b). The Farnella cruise carried out a GLORIA long-range sidescan and airgun seismic profiling survey, while the others conducted various other seismic profiling surveys (using both airgun and higher resolution sources) and sediment sampling.

The age of the igneous oceanic basement in the area is estimated to be mid-late Cretaceous (about 75 My in the NW, 106 My in the SE corner). It is inferred that this crust is overlain by carbonates, then pelagic clay, and finally turbidites. The latter probably account for most of the uppermost 125m of sediment, but have only been sampled to a maximum of 22m depth. The total sediment thickness ranges from zero to over 2km, but is between 250 and 1250m in most of the area (Figure 4.i.1).

The sea floor west of 24°W is generally flat, representing the distal Madeira Abyssal Plain at a depth of 5440m. The plain is pierced by occasional abyssal hills that rise a few hundred metres above it. These are mostly covered by pelagic sediment, although a few have outcrops of igneous crust. East of 24°W the seabed begins to shoal gradually and here represents the lowermost part of the northwest African continental rise. Studies of this continental rise have shown evidence of strong turbidity current and debris flow activity, including channeling and deposits of coarse sand, east of 24°W (Simm & Kidd, 1984; Kidd et al., 1984a).

Sediments cored from the abyssal plain west of 24°W are calcareous to marly turbidites alternating with pelagic sediments that range from clays, in the severest glacial periods, to marly oozes in the interglacials; Figure 4.i.2 (Weaver &

Kuijpers, 1983). These sediments are generally fine-grained (fine silt to clay), but the basal units of some turbidites contain somewhat coarser silts.

It has been possible to date the pelagic intervals using a combination of oxygen isotope and coccolith stratigraphy (Weaver, 1983). This has shown that there has been continuous sedimentation over most of the area west of 24°W during at least the last 350,000 years (Weaver & Kuijpers, 1983). Only in one core taken near an abyssal hill are two very thin units missing, possibly because of enhanced bottom currents around the hill. It appears that turbidity current input to GME occurs principally during changes from glacial to interglacial or from interglacial to glacial climate (Weaver & Kuijpers, 1983). The overall mean sediment accumulation rate during the last 190,000y has been between 4 and 11cm per thousand years.

The largest basin within GME that is free of abyssal hills lies between 31.2°N and 31.8°N, 24.0°W and 25.0°W. However, high resolution seismic profiling has shown that in this area the sediments are affected by faults spaced about 10km apart (Duin et al., 1984; Searle et al., 1984b). They offset sediments deeper than about 15m, and are thought to be related to differential sediment compaction and dewatering (Searle et al., 1984b). A smaller basin some 20km across near 31.2°N, 25.3°W appears at present to be fault-free.

In addition to the references given above, work at GME by various nations has been reported at the NEA Seabed Working Group (Anderson, 1980, 1981, 1982, 1984) and by the Dutch Geological Survey (Kuijpers, 1982; Duin & Kuijpers, 1983).

4.i.b Chemistry

The information presented in this section of the report derives mainly from study of three cores taken at Discovery station 10554 (Posn: 31°30'N 24°30'W) during RRS Discovery Cruise 129. This station is situated a little to the east of the centre of the Great Meteor East area, and was chosen for its lack of relief so as to minimise the chance of encountering horizontal variability in the sediments. It was intended that the station should be as typical as possible of the study area as a whole.

A preliminary study of piston core material taken in the area by Dutch researchers and by IOS has shown that the pelagic sediments are predominantly calcareous, as would be expected at this depth in the Atlantic. The pelagic material consists of calcareous (biogenic) and detrital material (mainly terrestrial in origin). Minor contributions include a component scavenged from the overlying water column. This scavenging process is of obvious interest in the context of waste disposal. It appears to be redox-related, and elements scavenged in oxidising conditions are remobilised into solution if the redox potential later falls. Accordingly, a high priority has been assigned to studies related to these processes.

Although presently accumulating sediments are carbonate-rich, this has not been true continuously in the past. During cold (glacial) stages the bottom water becomes undersaturated with respect to calcium carbonate (calcite), so that much of this mineral dissolves at the sediment-water interface and is not buried. Consequently, an argillaceous (clay) material is typical of glacial periods, and this contrasts with the more calcareous (marl or ooze) material which accumulates during warmer periods.

Although it is possible to obtain cores near to the GME study area which are almost devoid of turbiditic material (e.g. RGD core 82 PCS 17, Colley et al, 1983), these are by no means typical. Weaver and Kuijpers (1983) demonstrated that pelagic sedimentary accumulation in this area is interrupted sporadically by turbidite units, which possibly originate on the NW African continental margin. Over the past 3×10^5 years the pelagic accumulation rate has averaged 0.5cm per kyr, while the overall accumulation rate is 10cm per kyr because of the turbiditic contribution. Many of the turbidites have relatively high organic carbon contents, sometimes greater than 1% by weight of the sediments. For this reason it was expected that the redox potential at this site could be lower than average for pelagic sites in general. It was also considered possible that the redox state might vary from place to place within the study area, since the relative contribution of turbiditic material is known to be less in the south east of the area. The studies made on RRS Discovery Cruise 129 were not designed to address this latter point, which is among the objectives of a forthcoming cruise, but the results presented below indicate that the sediment at station 10554 was unexpectedly variable in redox state with position. It was also more reducing than had been expected, dissolved oxygen falling rapidly to near zero in the upper few tens of centimeters. The reasons for this behaviour, and its implications in relation to High Level Waste Disposal research, are discussed in succeeding sections.

Station 10554

Two box cores and two Kasten cores were taken at 10554, as well as a series of in situ pore water samples. One of the box cores was devoted entirely to a study of rare earth elements (Dr H. Elderfield, Cambridge University); since this work is reported separately the results from this core are not further considered here. Kasten core 1K, taken some 4 nautical miles to the ENE of the main sampling area proved to be atypical. It contained dissolved oxygen at about 20% of saturation levels at all depths sampled, in contrast to the remaining cores which show values close to zero below 30cm depth. The reason for this difference is not at present clear; further investigation is a prime objective of our future field studies. The discussion below is therefore limited to the cores taken in the main sampling area. The cores showed a prominent green-coloured band at about 40cm depth in the core. This has an organic carbon content of about 1.5% and exhibits sharp contacts at both upper and lower surfaces. Originally, this band was interpreted as a discrete turbidite unit, but later information showed that in fact the green layer is only the lower part of a large turbidite. Figure 4.i.3 shows the depth profiles of ^{230}Th, SiO_2, $CaCO_3$ and Al_2O_3 in boxcore 10554 BX. (Total ^{230}Th is is plotted here rather than ^{230}Th excess because of the mobility of uranium at this site, a feature further discussed below.) The top 0.6m of the core is entirely Holocene, on the evidence that the coccolith Emiliania Huxlleyii is the dominant species. The ^{230}Th (total) data indicate a high surface value, as would be expected from pelagic accumulation, but downward mixing by bioturbation occurs over 15cm or so, to a lower value of 6-7 d.p.m. g^{-1} which characterises the turbidite. Below the base of the green layer a high (total) value of 18.5 d.p.m. g^{-1} is found, again indicating sediment formed under pelagic conditions. The SiO_2, Al_2O_3 and CaO profiles (Figure 4.i.3) are consistent with this interpretation. Because of bioturbation the depth of the top of the turbidite cannot be defined precisely, but the section from 12cm to the base at 51cm appears largely homogenous.

What then is responsible for the difference in appearance of the upper (brown) zone and the lower (green) zone of the turbidite? Considering the oxygen and nitrate pore water profiles (Figure 4.i.4), their relationship to the onset of the green colouration, and the solid phase organic carbon profile (Figure 4.i.5) it is inferred that the colour change represents a downward-moving oxidation front. The rate of movement of this front is controlled, inter alia, by the rate of diffusion of oxygen and nitrate from the bottom water to the front. Thus, the brown

upper section is the part of the turbidite where reactive organic carbon has been combusted and which is now oxic. The linear profiles of oxygen and nitrate indicate that oxidation occurs at a restricted locus of activity at or near the colour change boundary, rather than throughout the sediment thickness above this layer. Initially, it was considered that the colour change might be related directly to the step in organic carbon content (Figure 4.i.5) which occurs at the colour change boundary, but the recent paper by Lyle (1983) demonstrates that such colour changes are often related to redox changes in the lattice iron content of clay minerals. Experimentally, the colour of both parts of the turbidite may be changed reversibly by treatment with oxidising or reducing agents. These observations indicate that, although organic carbon content may influence sediment colour, the redox profile exerts considerable influence on the colour of the sediment by the direct mechanism described by Lyle (1983). Further evidence of a strong redox gradient in the colour-change region of the core is provided in Figure 4.i.5. The step in solid-phase manganese concentration which occurs in the brown zone above the colour interface is caused by migration of manganese in the pore waters from below and precipitation at this point on the rising redox gradient. The pore water manganese profile (Figure 4.i.5) is supplying manganese to the bottom of the solid phase peak in this manner. A second redox-related feature is the slight decrease in CaO of the brown section of the turbidite relative to the green section (Figure 4.i.3). This is believed to be due to carbonate dissolution consequent on the production of CO_2 when organic carbon is oxidised.

A peak in the uranium solid phase concentration occurs in the green band, about 2cm below the colour change (Figure 4.i.5). A similar observation has previously been made in a core from the Cape Verde Abyssal Plain (Colley et al, 1984). As here, the peak was attributed to a post-depositional mobilisation of uranium originally associated with organic matter in response to the progress of an oxidation front; preferential downward migration is caused by fixation deeper in the sediment under reducing conditions (Bonatti, et al, 1971).

The measurements made on uranium in the porewaters (Figure 4.i.6) also depict an active system, although there are discrepancies between core-squeezed samples and in situ sampler measurements. Some of these have been traced to a systematic error in uranium samples taken by the former method (see section 5.iv) and Toole et al, 1984). The in situ profile is enhanced over the seawater value; from the uppermost four points a uranium flux from the sediments to seawater is indicated.

Using Fick's relationship:

$$F = -D \, dC/dZ$$

where F is the flux in g/cm/yr, D is the diffusion coefficient in cm/yr (a value of 30cm/yr is used here; see Li & Gregory, 1974 and Ku et al, 1977) and dC/dZ is the measured gradient, a flux of 1.1 x 10 g cm^{-2} yr^{-1} is estimated. The source of this flux is inferred to be uranium remobilised at the oxidation front. The process involved may be the oxidation of organic matter to which the uranium is bound, the complexation of uranium by ligands formed in the oxidation process or inorganic remobilisation as a direct consequence of the redox change which occurs across the reaction front. At present it is not possible to distinguish between these alternative mechanisms, nor is it possible to define the uranium speciation in the solid or the solution phases of the natural system in any detail. Although considerable progress has been made in the thermodynamics of solution/mineral equilibria (Langmuir, 1978), such work has been concerned with uranium minerals and high laboratory concentrations. These contrast with the laboratory situation; in particular, the effects of organic complexation have not yet been elucidated (Giblin et al, 1981).

The concept of a progressive downward migration of an oxidation front into a turbidite is not steady-state, but implies a continuing readjustment of the redox profile after the emplacement of organic-rich sediment. Initially this turbidite sediment is present at the sediment-water interface, and oxygen from bottom water rapidly raises the redox potential of the uppermost centimeters. This higher redox potential front thus moves downward as reaction proceeds. (This is in contrast to the steady-state behaviour customarily assumed in deep-sea sediments, in which subsurface redox boundaries track upwards to maintain a constant separation from the sediment-water interface.) On this interpretation, it would be predicted that organic-rich turbidites which are exposed at the ocean floor for any length of time subsequent to deposition should exhibit organic carbon removal in their uppermost section due to oxidation. Examination of piston cores taken in the Madeira Abyssal Plain region confirms that this diagenetic phenomenon is commonly found in the upper layers of organic-rich turbidites, and it may be inferred from this that the behaviour described has been a recurrent feature in this area for at least 3 x 10^5 years (Weaver & Kuijpers, 1983).

Model of Labile Carbon Oxidation at CV2 and GME

The concept that an oxidation front can progressively 'burn down' into an organic-rich layer potentially has wide applicability. Any site which has an organic-rich layer at a shallow depth is likely to exhibit this type of subsurface maximum in metabolic activity. The consequences of such behaviour are difficult to predict without a quantitative treatment. One approach is to model the progress of a diagenetic oxidation front into an organic-rich layer by a time-stepped numerical model. The rate of reaction may be computed from the diffusion-limited supply of electron-acceptors. A new diffusion depth is then calculated, and this is used to recalculate the diffusion gradient, and hence the flux, applicable to the next time-step. We have appied a model of this type at another station (Colley et al, 1984); the application of this model to the present results is presented in Table 4.i.1. However, models of this type, although useful, do not provide information on the biological and chemical processes which are active. In the present case, the data are adequate to support a more detailed treatment, which permits conclusions of general applicability to be drawn from a consideration of the data reported here.

Although the depth of the subsurface reaction site is increasing with time, it is possible to show (Table 4.i.1) that the present rate of this process is slow, on the same order as the rate of pelagic sedimentation. Consequently, one may assume that the pore water profiles do not materially differ from the characteristics which they would have if the depth of the reaction site was held fixed. This permits removal of the advective terms from the equations describing the system, and a considerable simplification is thereby attained.

Since at station 10554 oxygen is observed to be reaching the surface of the organic rich layer, the initial assumption is made that both oxic and anoxic processes are active within this layer. On this hypothesis, the upper surface of the layer will be undergoing oxic diagenesis, while at some distance below this an anoxic denitrification layer will exist.

The linear sections of the oxygen and nitrate profiles do not, when extrapolated to the sediment-water interface, intersect at the bottom water values of these reactants (Figures 4.i.8 and 4.i.9). Instead there is an offset, (positive for nitrate, negative for oxygen), the magnitude of which reflects the activity at

the sediment-water interface which must be included in the model. This activity is controlled by solid phase bioturbation of organic carbon as well as the reaction rate constant in the surface layer.

In summary, the model presented here has the following properties:

i. The distributions of oxygen, nitrate and organic-carbon are inter-related. The processes of solid-phase bioturbation, diffusion in solution and reaction are modelled.

ii. Metabolism at the sediment-water interface and at the surface of the high-substrate layer is included.

iii. Reaction according to the Redfield ratio stoichiometry is assumed.

iv. All reactions in the oxic layer are taken to be first-order in organic carbon. This assumption implies that the bacterial community is substrate-limited, a conditions which does not seem unlikely in the relatively lean deep-sea environment (Jahnke et al, 1982b).

v. Porosity (Ø) is assumed constant, and free-solution diffusion coefficients are corrected for tortuosity effects using the relation

$$D_s = D_{soln} / \theta^2 \qquad 1$$

where D_s is the corrected coefficient and θ^2 is assigned the empirically derived value of 1.8. The surface reaction layer, in which organic-carbon arriving at the sediment-water interface is metabolised, is defined by the depth (Z_1) (Figure 4.i.7) at which the processes of bioturbation and metabolism have reduced the pool of non-refractory organic-carbon effectively to zero. Below this depth the reaction term is unimportant, giving linear oxygen and nitrate profiles. Since the slopes (P and F) and the concentration intercepts Z_2 and Z_3 of these straight portions of the profiles are relatively well defined by the data, these parameters were chosen as input data for the model presented here.

The general diagenetic equation given by Berner (1980) may be written:

$$\frac{\partial C_i}{\partial t} = \frac{-\partial F_i}{\partial Z} + \Sigma R_i \qquad 2$$

where C_i is the concentration of component i in terms of mass per unit volume of sediment, F_i is the flux of i in terms of mass per unit area of total sediment per unit time, and R_i is the rate of each reaction involving component i, the units being mass per unit volume of total sediment per unit time.

For a dissolved species in a diffusive system the flux per unit area of sediment (Berner, 1980) is given by Fick's First Law of diffusion:

$$F_i = -\phi D_s \frac{\partial C_i}{\partial Z} \qquad 3$$

where ϕ is the porosity, D_s is the diffusion coefficient in the sediment (equation 1), and C_i is the concentration in units of mass per unit porewater volume. Hence for constant ϕ, at steady state, assuming that only a single removal process operates and that this is first order in C_i (rate constant K_i)

$$\phi D_s \frac{\partial^2 C_i}{\partial Z^2} - K_i C_i = 0 \qquad 4$$

The organic carbon associated with the solid phase is subject to bioturbation. This may be represented by:

$$\text{Biodiffusional flux} = -D_B \frac{\partial [\hat{C}]}{\partial Z} \qquad 5$$

where D_B is a biodiffusion coefficient (Berner, 1980). Assuming a single reaction process, rate R_c and steady-state conditions, we may therefore write, from 2 and 5:

$$-D_B \frac{\partial^2 [\hat{C}]}{\partial Z^2} + R_c = 0 \qquad 6$$

The rate of reaction R is assumed to be first order in $\hat{C}$ so that

$$-D_B \frac{\partial^2 \hat{C}}{\partial Z^2} + K_c [\hat{C}] = 0 \qquad 7$$

(Note that the units of organic-carbon are mass per unit volume of sediment).

The rates of reaction of organic-carbon (R_c), nitrate (R_N) and oxygen (R_O) are related to each other by the stoichiometry of the oxidation reaction. Assuming that the classical Redfield stoichiometry holds, this reaction may be written as:

$$138O_2 + (CH_2O)_{106}(NH_3)_{16}\ H_3PO_4 + 18\ HCO_3^- \rightarrow 124CO_2 + 16NO_3^- + HPO_4^{2-} + 140H_2O$$

So that

$$R_O = \frac{138}{106} R_c \qquad 8$$

$$R_N = \frac{-16}{106} R_c \qquad 9$$

from 4 and 8

$$\phi D_o \frac{\partial^2[O_2]}{\partial Z^2} - \frac{138}{106}\ K_c\ [\hat{C}] = 0 \qquad 10$$

and from 4 and 9

$$\phi D_N \frac{\partial^2[NO_3]}{\partial Z^2} + \frac{16}{106}\ K_c\ [\hat{C}] = 0 \qquad 11$$

The general solution of equations of the form of 7 has the form

$$[C] = Ae^{-\beta z} + Be^{+\beta z} \qquad 12$$

and, since in the present case $[\hat{C}] \rightarrow 0$ as $Z \rightarrow \infty$, the value of B is zero.

Hence,

$$[\hat{C}] = Ae^{-\beta z} \qquad 13$$

and the constants A and β are given by

$$\beta = \left(\frac{K_c}{D_B}\right)^{\frac{1}{2}} \qquad 14$$

and

$$A = [\hat{C}]_o \qquad 15$$

the organic-carbon concentration at Z = 0. Thus $[\hat{C}]$ may be expressed as a function of the reaction rate constant and the biodiffusion coefficient. Substituting for $[\hat{C}]$ in equation 10

$$\phi D_o \frac{\partial^2[O_2]}{\partial Z^2} - \frac{138}{106} K_c A e^{-\beta z} = 0 \qquad 16$$

By definition, $[O_2] = 0$ when $Z = Z_2$. The first differential of the oxygen concentration tends to be a constant value P with increasing depth. Hence, integrating 16:

$$\frac{\partial[O_2]}{\partial Z} = - \frac{138}{106} \frac{Kc}{\phi D_o \beta} A e^{-\beta z} + P \qquad 17$$

and

$$[O_2] = \frac{138}{106} \frac{D_B}{\phi D_o} [\hat{C}]_o e^{-\beta z} + ZP + Q \qquad 18$$

where

$$Q = -Z_2 P \qquad 19$$

An analogous treatment for nitrate gives

$$[NO_3^-] = - \frac{16}{160} \frac{D_B[\hat{C}]_o}{\phi D_N} d^{-\beta z} + ZF - Z_3 F \qquad 20$$

Equations 13, 18 and 20 define the model in the region $O<Z<Z_L$. In order to estimate the total metabolic activity in this zone it is necessary to derive K_c and D_B from the measured oxygen, nitrate and organic carbon profiles. Literature values for the free solution diffusion coefficients are also required.

Equation 13 defines the organic-carbon profile in terms of D_B and K_c. Since the experimental labile organic-carbon profile is not well-defined it was decided to derive K_c by reference to the oxygen and nitrate data. From these data, it is possible to estimate the depth of Z_1 below which the profiles of oxygen and

nitrate are linear. If it is assumed that at this depth the labile organic-carbon content $[\hat{C}]$ has fallen to a value corresponding to $0.01[\hat{C}]_o$ then this effectively defines the layer of surficial metabolic activity. It follows (from 13) that:

$$\beta = -(\ln(0.01))/Z_1 \qquad 21$$

thus fixing the ratio between K_c and D_B (equation 14).

Equations 18 and 20 may be used to derive independent estimates of the product of D_B and $\hat{C}_o$ from the oxygen and nitrate profiles. At station 10554 these estimates differ by about 15%, a very satisfactory agreement in view of the assumptions involved. The mean value was used in the calculation of D_B: a value of $\hat{C}_o$ being chosen to give the best fit to the labile organic-carbon data. This is probably the least satisfactory part of the procedure, since the quality of this data is only fair. However, any error introduced in the choice of $\hat{C}_o$ does not propagate forward to the estimates of metabolic activity, since a corresponding opposing error is produced in the estimate of K_c from D_B using equation 21.

From equations 7 and 13, the rate of consumption of organic-carbon at depth is given by:

$$K_c[\hat{C}]_o \, e^{-\beta z} \qquad 22$$

This may be integrated over the range $0<Z<Z_1$ to give the surficial metabolic rate M:

$$M = \frac{K_c[\hat{C}]_o}{\beta} \, (1 - e^{-\beta z_L}) \qquad 23$$

Within the high carbon layer ($Z>Z_L$) the rate of carbon oxidation is controlled by the rate of supply of oxygen to the layer and the stoichiometry of the oxidation reaction

$$M_L = -\frac{106P}{138} D_o \qquad 24$$

The denitrification within this layer is limited by the supply of nitrate ion. This is derived from two sources, the diffusional supply from the surface and the nitrate produced by the oxidative metabolism within the layer itself. The stoichiometry of the denitrification reaction is:

$$94.4\ NO_3^- + (CH_2O)_{106}(NH_3)_{16}H_3PO_4 \rightarrow 13.6CO_2 + 92.4HCO_3 + 55.2N_2 + 84.8H_2O + HPO_4^{2-}$$

So that

$$M_D = -\frac{106}{94.4} F D_N + \frac{16}{106} M_L$$

gives the rate of carbon oxidation by denitrification processes at the reaction front.

Values of M, M_L and M_D are listed in Table 4.i.2 for station 10554. At station 10552 there is no lower reaction layer, but the value of M at this station may be found using the same procedure as described above for 10554. Because nutrient data points were lost in the upper section of this core, the position can only be estimated from the organic-carbon data as lying in the range 18-22cm. This gives a range of 1.08×10^{-13} to 2.17×10^{-13} moles C sec^{-1} cm^{-2} for the surficial metabolic rate; the value corresponding to Z_1 = 20cm is tabulated. These metabolic rate results are similar to those calculated from the results of Reimers et al, (1984) and Jahnke et al, (1982a) for pelagic sites. Calculated bioturbation coefficients are similar to those previously reported for oxic sediments (e.g. Grundmanis & Murray, 1982; De Master & Cochran, 1982; and Officer & Lynch, 1983).

Model Results

The results obtained from the application of the model at stations 10552 and 10554 are shown in Table 4.i.2, Figure 4.i.8 and Figure 4.i.9. An important aspect of these results is the revelation that the total metabolic activities at the two stations are closely comparable. Indeed, it is possible that the consumption of oxygen at 10552 is slightly higher than at 10554, a finding which is startling in view of the fact that it is the sediment at the latter site which becomes anoxic within the sampled interval. The difference between the stations which causes anoxic conditions to occur is therefore not the total metabolic oxygen demand, but the distribution of this demand with depth in the sediment column. The model results indicate that only a minor proportion (about 30%) of the total respiration at 10554 occurs below the sediment-water interface, but, because of the diffusion-limited supply of oxygen within the sediment column, this small demand imposes a large redox gradient on the system. It becomes clear from these results that the influence of occasional organic-rich depositional events at an otherwise well-

oxygenated site can be profound, and disproportionately larger than would be indicated from a simple consideration of the quantities of organic-carbon involved.

The additional implication to be drawn from the results presented here is that the presence of a discontinuous substrate concentration implies the probability of a discontinuous redox profile. That is not to say that the normal redox succession (Froelich et al, 1979) will not occur, but that it may be highly compressed in the depth dimension. Some sections may occupy quite large sediment depth-intervals while other sections may be compressed into a relatively small interval. Linear nitrate diffusion gradients have been reported in several recent papers; the type III sites of Goloway and Bender (1982) and the data shown in Sawlan & Murray (1983) have this characteristic. Additional references are cited by the latter authors. Organic-carbon profiles have not been published for all these stations. However, the type III sites do possess discontinuous substrate profiles. For Atlantic sediments at least, such substrate distributions may occur quite often. As shown here for station 10554, this phenomenon can exert considerable influence on the overall sediment redox poise, and may also be responsible for the sharp contacts seen at the top of organic-rich layers in otherwise bioturbated cores.

Because the presence of oxygen is known to inhibit denitrification, the idealised profile of Figure 4.i.7 shows nitrate falling to zero at a depth significantly greater than the depth of zero oxygen. Comparison of Figure 4.i.7 with Figure 4.i.9, the 10554 profile, shows that in fact oxygen and nitrate linear profiles extrapolate to zero at almost the same depth. The resolution of the data is inadequate to define the profiles accurately below Z_L, the surface of the high-organic layer, but it is clear that a very steep redox gradient must exist close to the upper surface of the high organic-layer.

It is, of course, possible that the model may not include all significant redox-active species (e.g. iron II) (Reeburgh, 1983; Sørensen, 1982). The upward flux of FeII in solution to the top of the subsurface reaction layer might then remove the downward diffusing oxygen from solution so efficiently that no oxic breakdown of organic-carbon could occur. (The recent report by Lyle (1983) that the brown-green colour transition in pelagic sediments corresponds to the alteration of iron (III) to iron (II) within the clay lattice supports the idea that the redox potential at this point in the profile is close to the iron (III) to iron (II)

transition point). Unfortunately, no porewater iron values were obtained at station 10554, but consideration of the solid phase distribution can provide some indication of the quantitative importance of this species. This would suggest that iron (II) could be of significant importance in electron transport processes and that a detailed model of the lower reaction zone should include iron, but that it is probably not of overwhelming quantitative importance, otherwise very much more diagenetically precipitated iron would be present in the solid phase of the oxic sediment above the reaction front.

The second possible reason for the observed nitrate/oxygen relationship is that denitrification may begin before oxygen is fully exhausted. The assumption made in the initial model, that oxygen must be zero before denitrification starts, is known to be an approximation (Goring, 1968; Cline & Richards, 1972; Cohen, 1978). The observation at station 10554 that Z_3 (the nitrate zero depth) is only very slightly larger than Z_2 (the zero depth for oxygen) appears to support the hypothesis that denitrification can occur below oxygen levels of the order of 10^{-5} M. Clarification of this point would require extremely close-spaced sampling in the region of Z_L.

Summary and Conclusions

The analytical results for the two stations compared show that they exhibit contrasting redox behaviour. At station 10552, on the Cape Verde abyssal plain, the porewater profiles show an oxygenated profile, typical of a slowly accumulated pelagic sediment, with oxygen present over the 0-2m range sampled, nitrate increasing throughout this range and no manganese mobilised within the studied interval. Station 10554, on the Madeira abyssal plain, is found to be very different due to the presence of an organic-rich layer at shallow depth. Porewater oxygen falls to zero at about 35cm, nitrate slightly deeper, and manganese is mobilised below this depth. Little evidence of sulphate reduction is observed, however, and it appears that almost all the redox change in the upper sediment column occurs in two zones, one close to the sediment-water interface and the other near to the top of a green layer of higher organic-carbon content within the sediment.

The solid-phase profiles show that the green layer is closely similar in major element composition and bulk mineralogy to the brown-coloured layer immediately overlying it. The colour and organic-carbon content, and the redistribution of

redox-sensitive elements (Mn, U) are the only major differences observed. It is hypothesised that these two layers together constitute a single distal turbidite. This is supported by thorium-230 compositional data and palaeontological evidence, and an early Holocene age is indicated for the emplacement event.

It is concluded that the organic-carbon content of the original turbidite has 'burned down' by reaction with oxygen diffusing from the overlying seawater. The resulting redox change has turned the upper part of the turbidite from green to brown. The observed oxygen profile supports this concept of 'burning down' by reaction at a subsurface oxidation front, since it is linear with depth as would be expected from the hypothesised source-sink diffusion geometry. The nitrate profile shows a peak value just below the sediment-water interface, but then also falls linearly with depth. This is interpreted as indicating a similar simple diffusion geometry, with denitrification occurring at, or about, the depth of zero oxygen.

In order to provide a more quantitative insight into the processes at work, a diffusion-reaction model capable of accommodating a step-change in organic-carbon has been developed. This analytical model utilises oxygen, nitrate and organic-carbon as input data. Like the finite-difference model of Jahnke et al (1982b), it enables the assumptions on stoichiometry and reaction rate constants, used in this and previous models, to be tested by observing the degree of agreement of the nitrate and oxygen sections of the model at these sites. In general, agreement is good at the level of accuracy achieved. Given higher quality data, such an approach is capable of providing considerably improved measurements of reaction rate constants and of mixing coefficients.

The most important conclusion of the model study, and perhaps the most surprising, is that the overall metabolic intensity at the two contrasting stations studied is closely comparable. The contrasting redox-profiles observed can be attributed almost entirely to the fact that about 30% of the total metabolism at station 10554 takes place at the surface of the organic-rich layer. Because of the restricted access of oxygen to this reaction-layer a dramatic redox swing results. By comparison, at station 10552 where virtually all the respiration occurs close to the sediment-water interface in conditions of plentiful oxygen supply, the whole sediment column remains much more oxic.

It follows from these results that a relatively infrequent input of substrate-rich sediment can have a considerable impact on the redox-state of the host sediment column. Organic-rich layers are not uncommon in pelagic and hemipelagic Atlantic sediments, and not all are formed by turbidites. We predict that as long as the reaction front remains within a metre or less of the sediment-water interface the 'burning down' phenomenon which we describe here may occur. This non-steady-state condition will result in a distorted redox-depth profile, with rapid redox change localised at the sites of reaction in a manner closely similar to that observed at station 10554.

4.i.c Physical Properties of Sediments in the GME Area

A substantial amount of physical properties data has been obtained from the Great Meteor East study area. This has been obtained from cores and records taken on Discovery cruises 118, 126 and 134, and is reported in detail by Schultheiss & Gunn (1984), and Searle et al., (1984). Cores taken on Discovery Cruise 144 are currently being analysed (April 1984). Table 4.i.5 shows the positions and water depth of the cores analysed (KC-Kastenlot Core, PC-Piston Core).

The upper 20 metres of sediment in the GME study area is dominated by a sequence of distal nannofossil turbidites (thicknesses vary between a few centimetres and a few metres). The bases of some of the turbidites contain sands and silts which thin and eventually disappear as the units become more distal (i.e. in the west of the area). Between each turbidite unit a thin pelagic interval of marl or calcareous clay is present and is typically only a few centimetres thick.

Data from two samples is presented here which represent the consolidation and permeability behaviour of the turbidites. Sample D10695/2/14 (Figure 4.i.10) is typical of the bulk of the nannofossil turbidites. It exhibits a high void ratio and has a high compressibility index (change in void ratio per logarithmic cycles of stress) of 1.1. Samples from the same turbidite (b) in core S126/4 exhibit even higher void ratios towards the top (up to 5.2) with a compressibility index of as high as 1.5. At the base of some turbidites (in particular b and f) the silt component increases rapidly. Sample D10695/8/16 (Figure 4.i.11) illustrates the behaviour of a very silty base. The void ratio is below 1 with a compressibility index of only 0.1. To illustrate the change in permeability that occurs within this turbidite sequence the profile for core D10695 has been constructed from the available data (Figure 4.i.12). It should be noted that the

permeability in the silty bases can be over two orders of magnitude higher than in the bulk of the turbidite unit.

To investigate the continuity of the turbidites and their silty bases correlations between 3.5 kHz records and four piston cores in the GME area have been made.

The 3.5 kHz records in the GME area are dominated by continuous parallel reflectors over most of the area. To enable the reflectors to be identified, the four piston cores were acoustically logged before being split. Compressional wave velocities (V) were measured at intervals along the core, using a 1 MHz pulse technique and were corrected to ambient pressure and temperature. Bulk density (ρ) measurements were taken at selected intervals along the cores after they were split. Acoustic impedance (ρV) profiles have been produced and compared with the 3.5 kHz records (Searle et al, 1984). These profiles are dominated by sharp impedance contrasts at the turbidite bases (caused by the coarser grain sizes, giving higher bulk densities and velocities) which correlate with the major reflectors on the 3.5 kHz records. Consequently, it is possible in an area such as GME to map the thickness and extent of the major turbidites from the 3.5 kHz records hence eliminating the necessity to take large numbers of cores.

4.i.d Heat Flow Data in the GME Area

Five heat flow stations were occupied in the Great Meteor East area: station 10318 on Discovery Cruise 118, stations S126/3 and S126/5 on Discovery/Shackleton Cruise 126 and stations 10972 and 10983 on Discovery Cruise 144. The data from the latter two stations, obtained in February 1984, are still being analysed. The data from the three former stations are discussed fully in Noel (1984a,b).

Station 10318 was on the western extremity of the Madeira Abyssal Plain while stations S126/3 and S126/5 were in the central Madeira Abyssal Plain. These three stations record remarkably linear temperature profiles at a total of 10 penetrations. This may be evidence for a low rate of pore water movement. It is interesting to note that on younger crust to the northwest, at station 10674, the results suggested pore water velocities of up to 112 cm/y.

During cruise 144 attention was focussed on an area within GME where a network of 3.5 kHz surveys have revealed fault-like structures in the sediments. Using

acoustic navigation, two heat flow surveys were run across a selected fault resulting in a total of 23 dips, one of which was within a few hundred metres of the fault plane. It is hoped, from an analysis of the sediment temperature data, to determine whether the fault structures are preferred paths of porewater migration through the sediment. This work is being carried out at Sheffield University under contract to the DoE.

Table 4.i.1 Diffusion limited numerical model used to estimate rate of movement of organic reaction front (Colley, et al., 1984)

Assumptions:

Pelagic accumulation rate	0.5 cm kyr^{-1}
Model timestep	0.1 kyr
Turbidite organic-carbon	1.5%
Sediment dry density	0.5 gcm^{-3}
Porosity	0.7
Diffusion coefficient	1.5×10^{-5} cm^{-2} sec^{-1}
Bottom Water O_2	2.56×10^{-4} molar
Surface O_2 consumption offset	46×10^{-4} molar

Results:

Time to reach present oxidation front depth	9.0 kyr
Pelagic accumulation since turbidite arrival	4.55 cm
Depth of turbidite oxidised	30.75 cm
Present rate of downward front movement	2 cm kyr^{-1}

Table 4.i.2 Input data and best-fit output results for the oxygen-nitrate-organic-carbon diagenetic model.

ANALYTICAL DATA	10552	10554	UNITS
Oxygen profile linear slope	-3.03×10^{-10}	-5.79×10^{-9}	moles cm^{-4}
Oxygen linear depth intercept	597.8	37.5	cm
Bottom-water oxygen	2.56×10^{-7}	2.56×10^{-7}	moles cm^{-3}
Nitrate profile linear slope	3.02×10^{-11}	-1.024×10^{-9}	moles cm^{-4}
Nitrate linear depth intercept	-1470	37.9	cm
Bottom-water nitrate	2.8×10^{-8}	2.8×10^{-8}	moles cm^{-3}
MODEL RESULTS			
Surficial organic carbon (O_2)	8.45×10^{-5}	7.3×10^{-5}	moles cm^{-3}
Surficial organic carbon (NO_3^-)	9.58×10^{-5}	10.5×10^{-5}	moles cm^{-3}
Surface layer rate constant (K)	1.25×10^{-9}	10^{-9}	sec^{-1}
Surface layer bioturbation coefficient (D)	5×10^{-9}	3×10^{-9}	$cm^2 sec^{-1}$
Deep layer rate constant (K)	-	1.1×10^{-11}	sec^{-1}
Denitrification rate constant (K_D)	-	3.21×10^{-6}	sec^{-1}
Integrated surficial metabolism Z<Z	4.89×10^{-13}	2.91×10^{-13}	moles $cm^{-2} sec^{-1}$
Integrated deep oxic metabolism $Z<Z_L$	-	0.33×10^{-13}	moles $cm^{-2} sec^{-1}$
Integrated denitrification rate	-	0.09×10^{-13}	moles $cm^{-2} sec^{-1}$
Total metabolic rate	4.89×10^{-13}	3.33×10^{-13}	moles $cm^{-2} sec^{-1}$

Note: Free solution diffusion coefficients assumed for O_2 1.5×10^{-5} cm^2 sec^{-1} for nitrate 9×10^{-6} cm^2 sec^{-1}. Porosity assumed 0.7

Table 4.i.3 Compositional Data for Core 10554#5BX (31°29.9'N, 24°26.1'W: 5370m)

Depth Interval cm	Major element data, % wt											Trace element data, ppm										
	SiO_2	Al_2O_3	Fe_2O_{3T}	MnO	MgO	CaO	K_2O	TiO_2	P_2O_5	Cl	LOI	Total	Rb	Sr	Y	Zr	Nb	Ni	Co	V	Cr	Cu	ZN
0-1	24.99	9.66	3.64	0.15	1.57	27.50	1.27	0.36	0.12	2.23	30.68	99.94	58	881	16	109	11	46	22	83	69	58	61
8-9	34.61	14.08	5.54	0.16	1.86	15.85	1.56	0.54	0.11	2.17	23.00	97.31	77	576	21	126	15	60	18	105	113	52	78
16-17.5	39.26	15.92	6.23	0.20	2.09	12.20	1.84	0.63	0.13	2.44	19.82	98.32	88	486	22	143	18	66	17	117	132	50	88
20-22	39.64	16.20	6.17	0.20	2.21	10.29	1.81	0.64	0.12	2.52	18.60	95.88	89	432	21	144	17	67	19	119	136	49	85
26-27	38.54	15.69	5.99	0.19	2.15	12.75	1.73	0.62	0.13	2.26	20.74	98.53	86	493	22	138	16	71	23	118	134	51	83
28-31	36.12	14.74	5.32	0.02	2.01	13.06	1.73	0.57	0.13	2.31	23.92	97.62	82	471	20	134	17	67	24	115	131	47	81
31-32	33.63	13.77	4.80	0.02	2.00	15.51	1.65	0.53	0.13	3.08	25.75	97.84	84	571	17	130	17	59	16	198	115	74	79
34-36	34.13	13.90	4.86	0.03	2.00	15.79	1.73	0.55	0.13	2.99	24.93	98.05	86	587	19	130	15	64	18	105	114	49	77
45-47	32.65	13.49	4.67	0.01	1.90	17.44	1.74	0.52	0.13	2.69	25.33	97.88	82	651	18	120	13	68	22	103	109	50	74
51.5-53.5	21.22	6.78	2.68	0.03	1.54	34.51	1.20	0.36	0.15	2.30	32.73	101.20	46	1063	15	112	12	26	15	75	39	59	55

Table 4.i.4 Compositional Data for Core 10554#11K (31°27.'N, 24°.8'W: 5370m)

Depth interval cm	Major element data, % wt (dry basis)												Trace element data, ppm										
	SiO_2	Al_2O_3	Fe_2O_{3T}	MnO	MgO	CaO	K_2O	TiO_2	P_2O_5	LOI	Total	NaCl*	Rb	Sr	Y	Zr	Nb	Ni	Co	V	Cr	Cu	Zn
5-7	19.47	6.54	2.80	0.05	1.60	32.40	1.27	0.37	0.21	33.88	98.59	4.04	54	1096	18	96	12	32	12	71	45	65	68
15-17	19.06	6.65	2.83	0.05	1.62	31.70	1.30	0.37	0.21	33.99	97.78	4.03	55	1047	17	95	10	34	12	76	47	56	58
25-27	29.24	12.34	4.97	0.13	1.77	22.20	1.39	0.54	0.22	24.37	97.17	3.14	69	711	19	99	13	52	17	92	101	50	71
35-37	39.40	16.53	6.37	0.19	2.24	11.12	1.58	0.72	0.20	18.40	96.79	4.06	91	458	26	133	18	65	19	122	141	52	91
45-47	33.86	14.47	5.12	0.04	2.08	14.37	1.75	0.63	0.20	24.65	97.17	4.77	90	542	19	133	16	67	17	108	120	49	81
55-57	29.98	12.58	4.70	0.02	1.87	17.37	1.69	0.57	0.20	27.53	96.51	4.51	83	658	17	124	14	69	24	102	106	51	76
65-67	18.23	5.96	2.71	0.05	1.41	34.79	1.15	0.43	0.22	33.46	98.41	3.59											
75-77	20.01	6.57	3.83	0.06	1.92	30.20	1.25	0.65	0.28	34.18	98.95	4.62	45	1012	18	139	21	32	17	99	40	57	59
95-97	19.64	6.56	4.12	0.07	2.05	31.13	1.21	0.70	0.31	32.14	97.93	5.27	45	1026	16	139	23	32	18	92	39	43	58
115-117	19.28	6.53	3.89	0.08	1.98	31.98	1.21	0.68	0.30	32.55	98.48	4.82	43	1055	19	137	23	31	18	82	38	54	58
145-147	19.77	6.67	3.95	0.08	2.06	31.78	1.15	0.71	0.33	32.07	98.57	4.57	41	1029	16	141	25	30	16	84	40	57	56
175-177	20.03	6.85	3.96	0.09	2.10	31.96	1.15	0.72	0.33	31.88	99.07	4.46	43	1066	17	144	29	32	19	84	40	55	57
205-207	19.93	6.76	3.97	0.08	2.05	31.95	1.22	0.71	0.32	31.75	98.74	4.42	44	1051	17	139	26	31	18	86	40	56	57
225-227	20.28	6.78	4.09	0.08	2.06	31.23	1.20	0.71	0.32	31.48	98.23	4.32	42	1043	18	140	26	32	19	85	39	41	56
245-247	20.09	6.81	3.94	0.08	2.03	31.65	1.22	0.72	0.33	31.54	98.41	4.15	42	1068	18	149	28	34	18	170	40	139	58
265-267	19.72	6.81	3.87	0.09	1.92	31.34	1.23	0.70	0.32	31.59	97.59	4.34	43	1064	17	147	29	33	17	99	41	59	59
295-297	19.69	6.71	3.84	0.09	1.93	31.93	1.21	0.68	0.30	31.71	98.09	4.12	45	1110	17	149	28	35	18	98	43	61	60
325-327	19.24	6.51	3.62	0.09	1.83	33.28	1.18	0.64	0.28	32.38	99.05	4.15	46	1129	16	139	23	35	19	89	41	59	58
345-347	18.32	6.25	3.51	0.08	1.82	33.33	1.19	0.60	0.26	33.00	98.37	4.12	42	1080	17	125	20	31	17	83	37	52	56

Table 4.i.5. Cores from GME on which physical property measurements have been made

Core	Water Depth m	Latitude	Longitude
D10321 (KC)	4978	31°04'.8N	25°49'.3W
D10325 (KC)	5407	30°22'.9N	24°05'.8W
D10688 (PC)	5428	32°03'.0N	24°12'.1W
D10695 (PC)	5433	31°23'.7N	24°46'.3W
D10698 (PC)	5433	31°38'.2N	24°49'.8W
D10699 (PC)	5433	30°43'.8N	24°29'.0W
S126/2 (KC)	5466	31°32'.2N	24°50'.5W
S126/4 (KC)	5446	31°31'.7N	24°25'.3W
S126/15 (KC)	5330	30°22'.0N	23°35'.0W

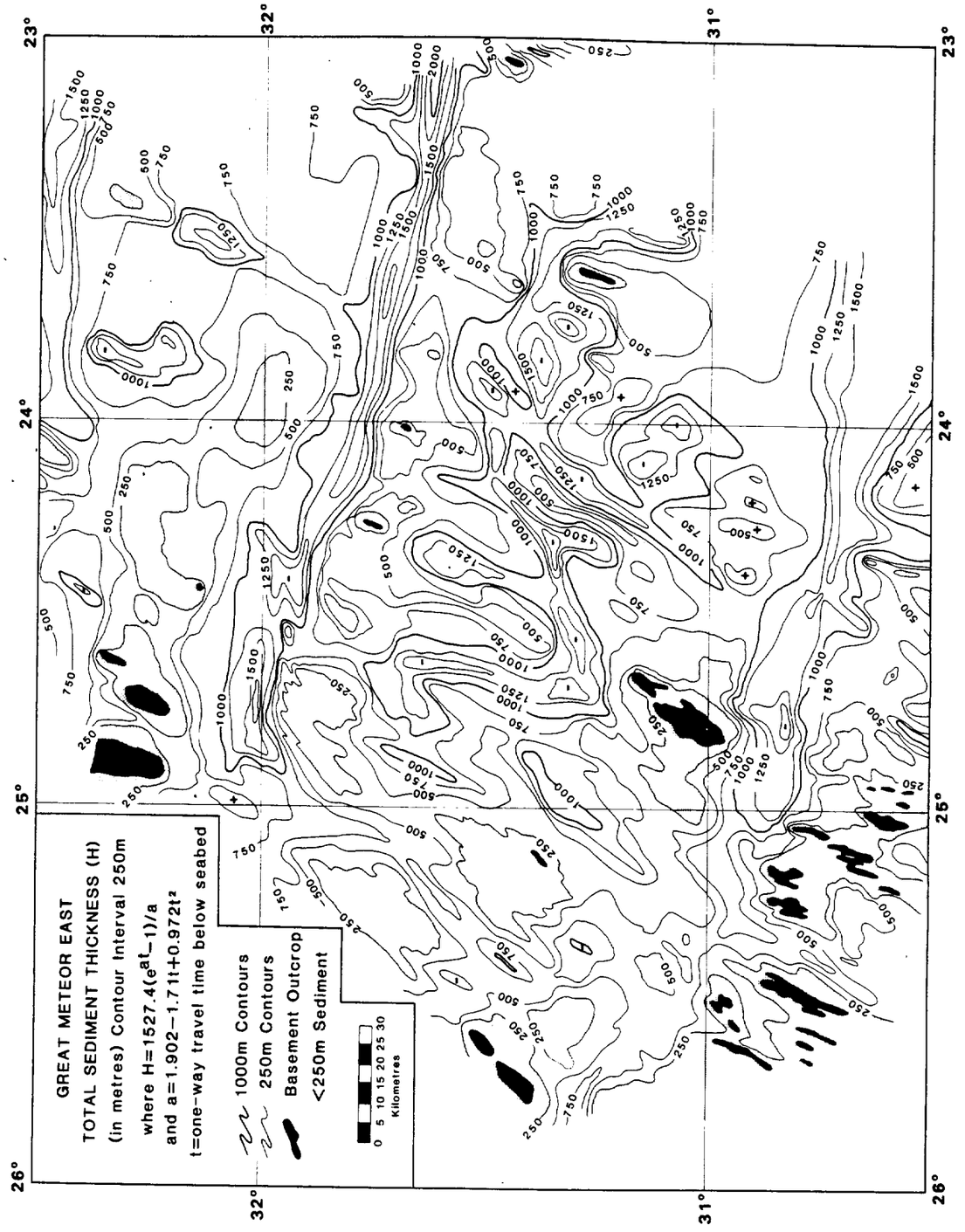
GREAT METEOR EAST
TOTAL SEDIMENT THICKNESS (H)
(in metres) Contour Interval 250m
where H=1527.4(e^at−1)/a
and a=1.902−1.71t+0.972t²
t=one-way travel time below seabed
1000m Contours
250m Contours
Basement Outcrop
<250m Sediment
0 5 10 15 20 25 30
Kilometres
23°
24°
25°
26°
32°
31°

Figure 4.i.1

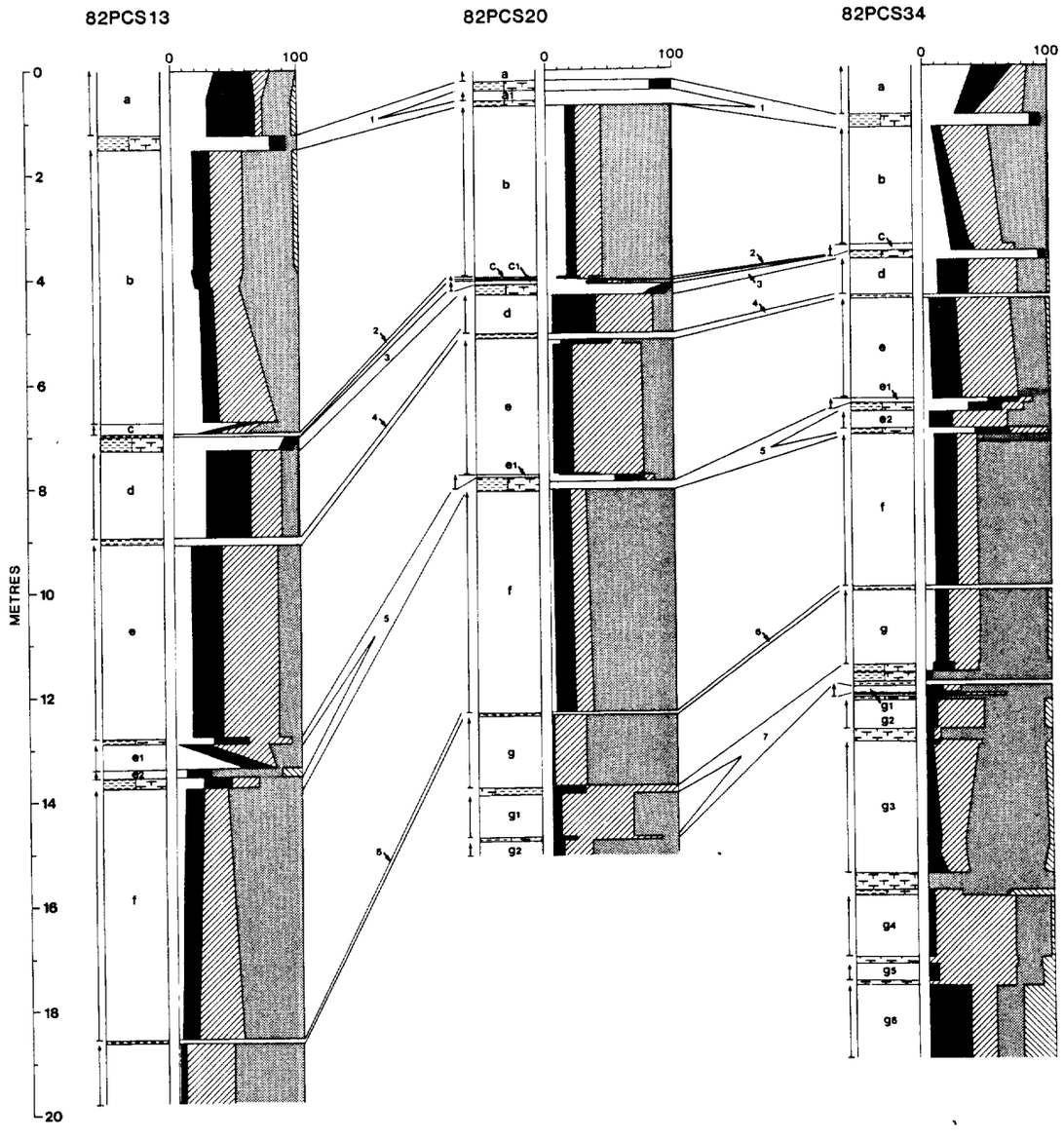

Figure 4.i.2 Lithology and age of recent sediments from GME. For each core, the left-hand column gives the lithology. Blank, lettered units are turbidites, each one deposited essentially instantaneously. Intervals with ornamentation are pelagic units, the ornamentation indicating the lithology, from clay (horizontal dashes) to ooze (brick wall symbol). The right-hand column for each core shows the relative abundances of different coccolith species, which change markedly at glacial stage boundaries. The stages identified by oxygen isotope variations are numbered. (The base of stage 7 is 247,000 years before present.) From Weaver & Kuijpers (1983).

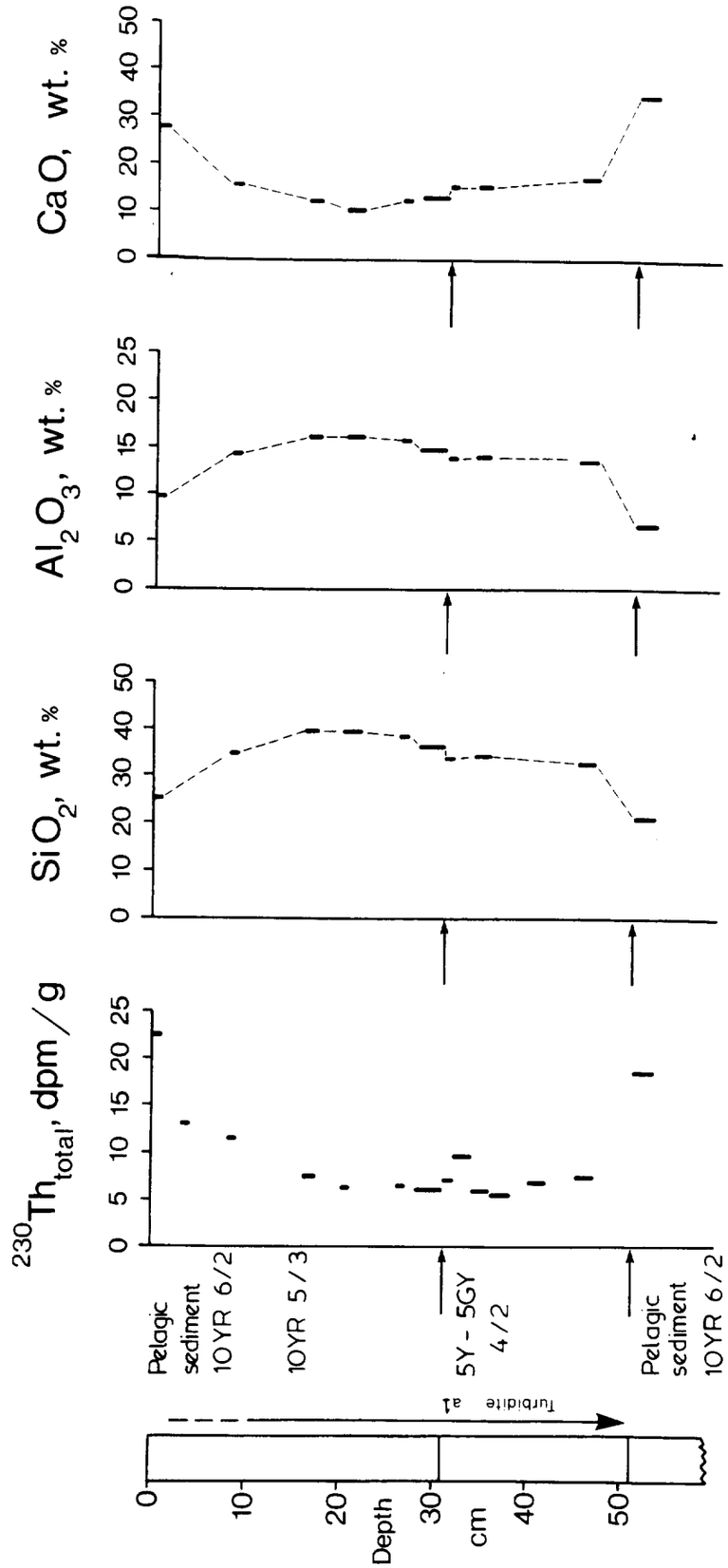
$^{230}Th_{total}$, dpm / g
SiO_2, wt. %
Al_2O_3, wt. %
CaO, wt. %
0 5 10 15 20 25
0 10 20 30 40 50
0 5 10 15 20 25
0 10 20 30 40 50
Pelagic sediment 10YR 6/2
10YR 5/3
5Y - 5GY 4/2
Pelagic sediment 10YR 6/2
Turbidite a1
Depth cm
0
10
20
30
40
50

Figure 4.i.3

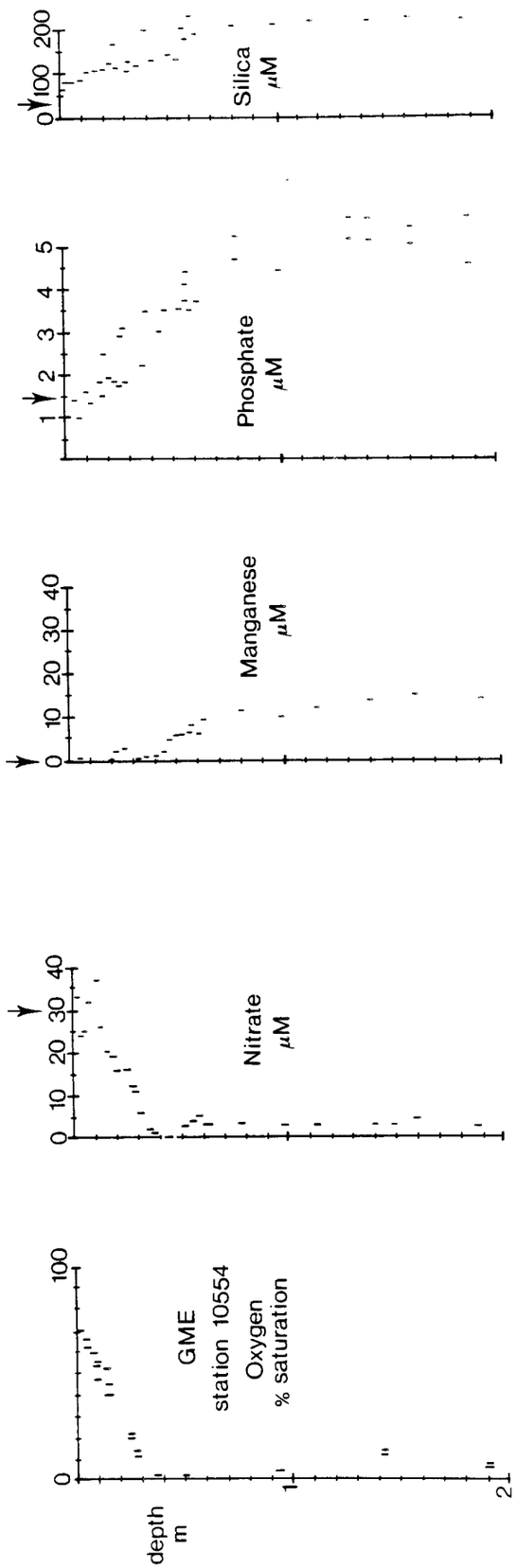

Figure 4.1.4 Porewater data for Station 10554.

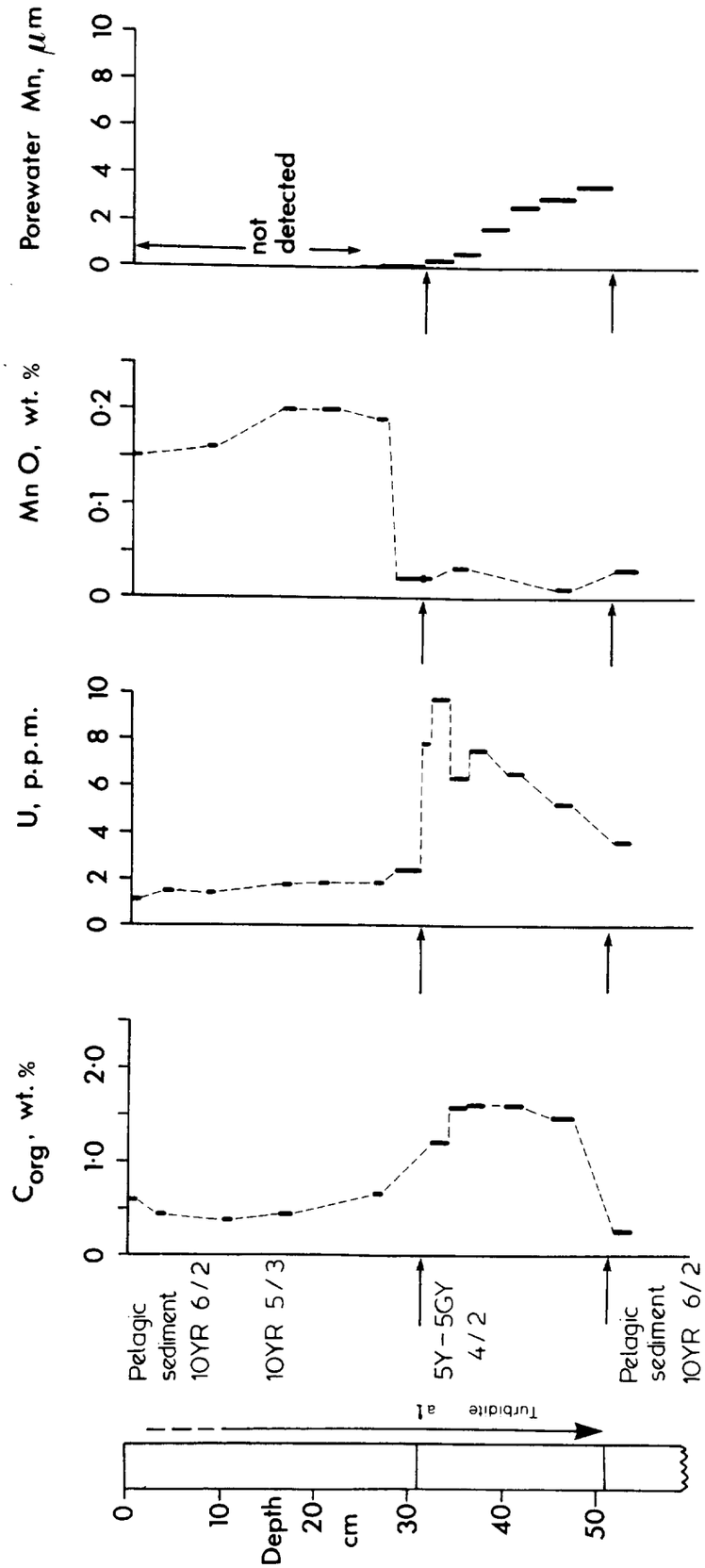

Figure 4.1.5 Core 10554 BX

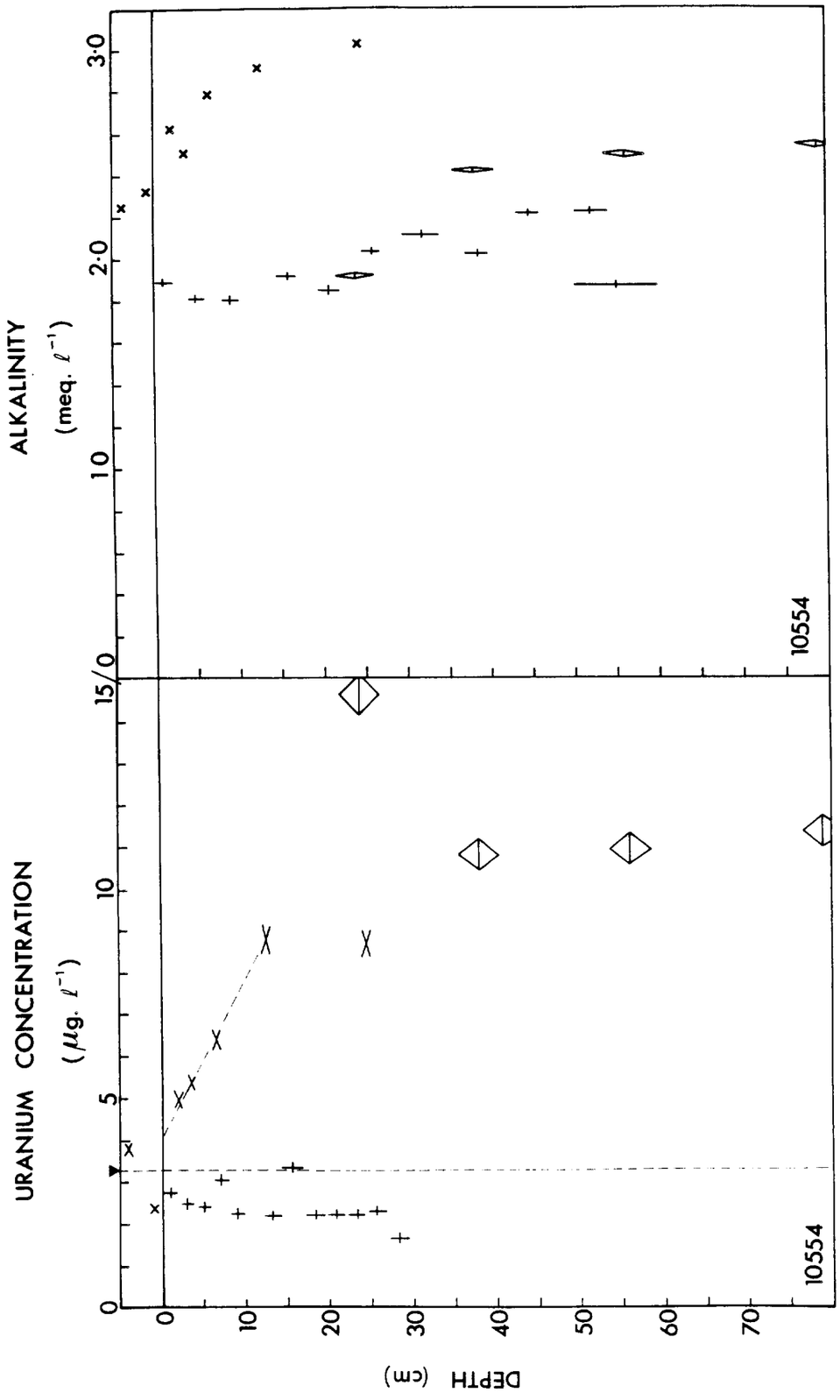

Figure 4.i.6 Porewater data for 10554

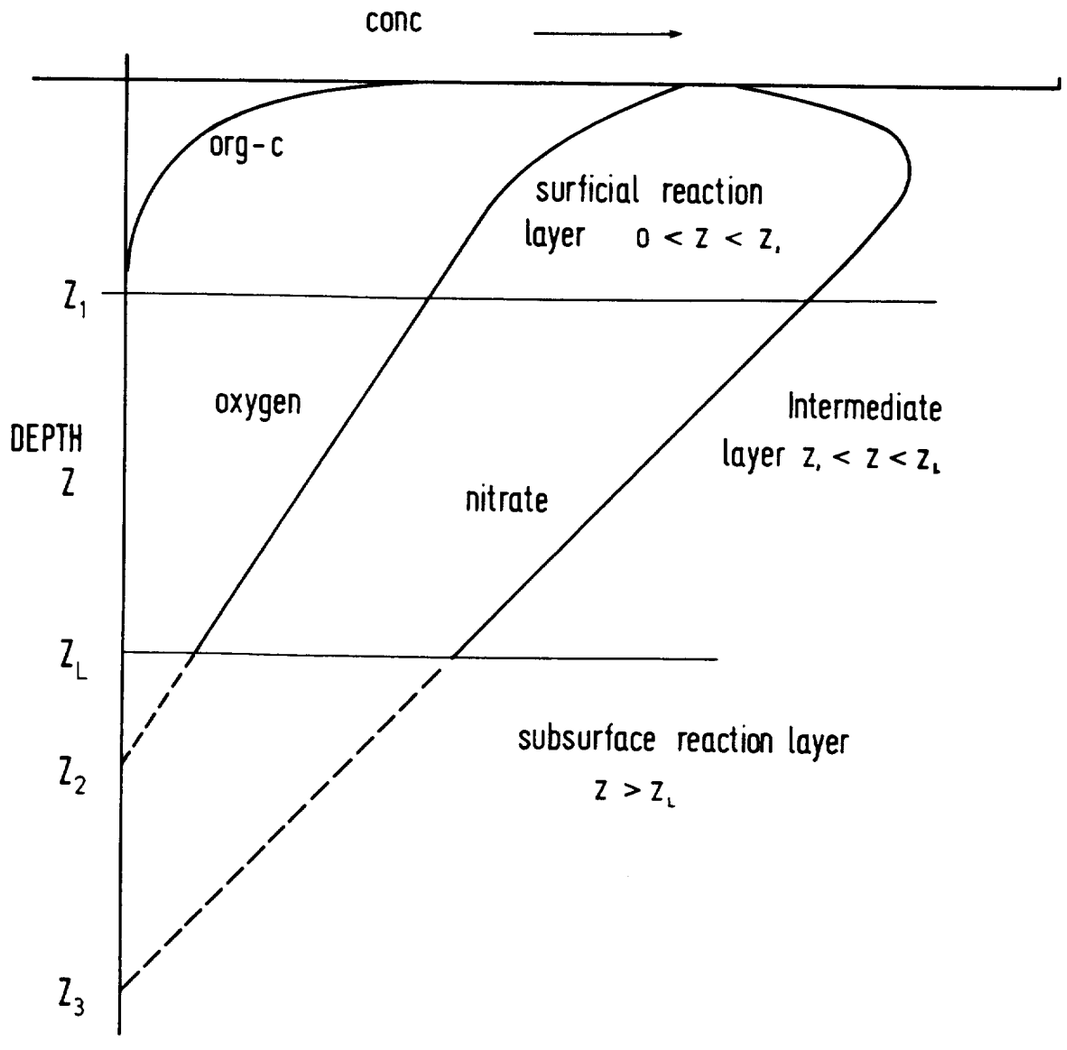

Figure 4.i.7 Schematic of model profiles for organic-carbon, oxygen and nitrate. The model is roled for intervals $O<Z<Z_L$. Below Z_L the organic layer breakdown rates for the processes of oxidation and denitrification are estimated from the oxygen and nitrate fluxes through Z_L (see text).

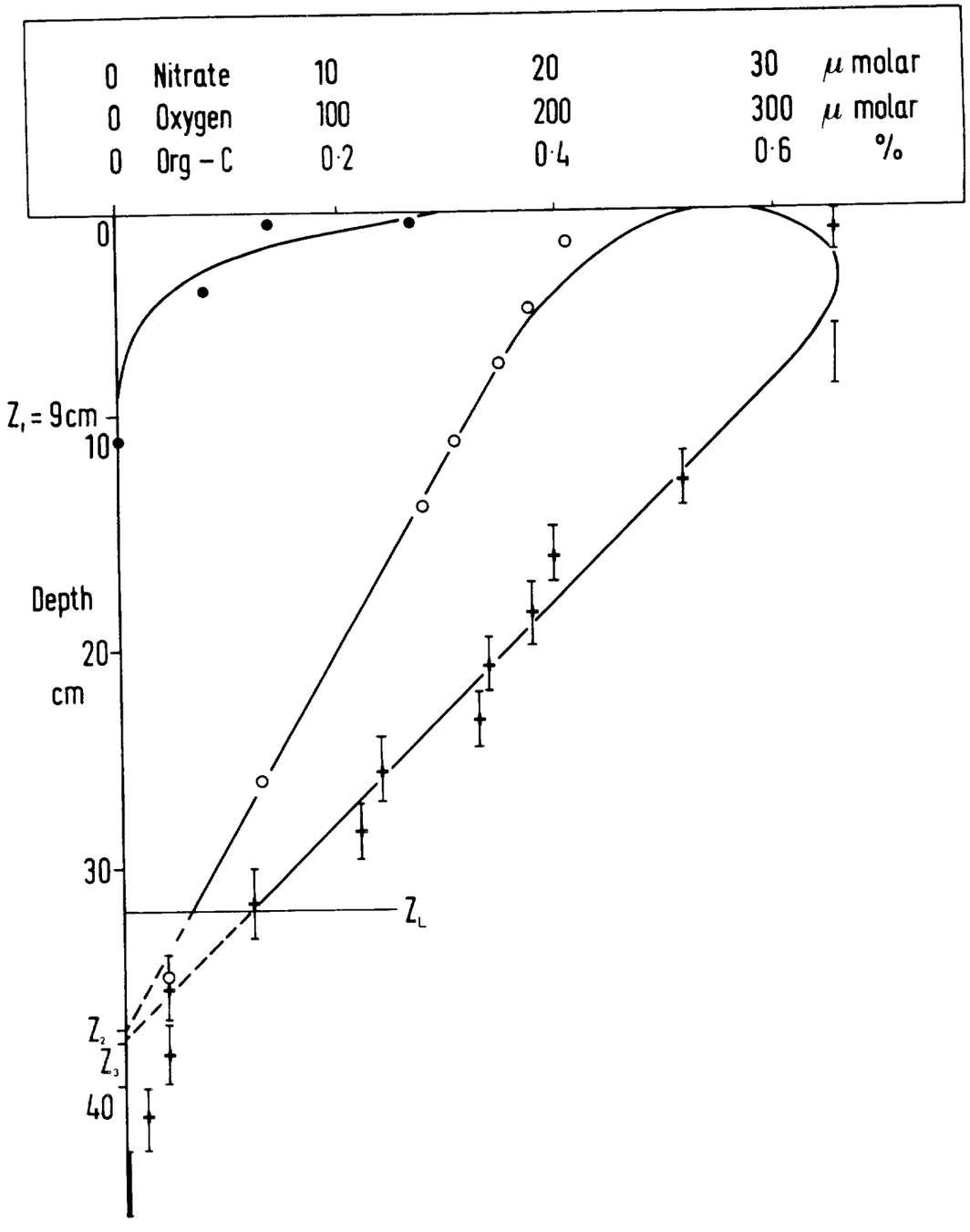

Figure 4.i.8 Fit up model to oxygen, nitrate and labile organic-carbon data for station 10554.

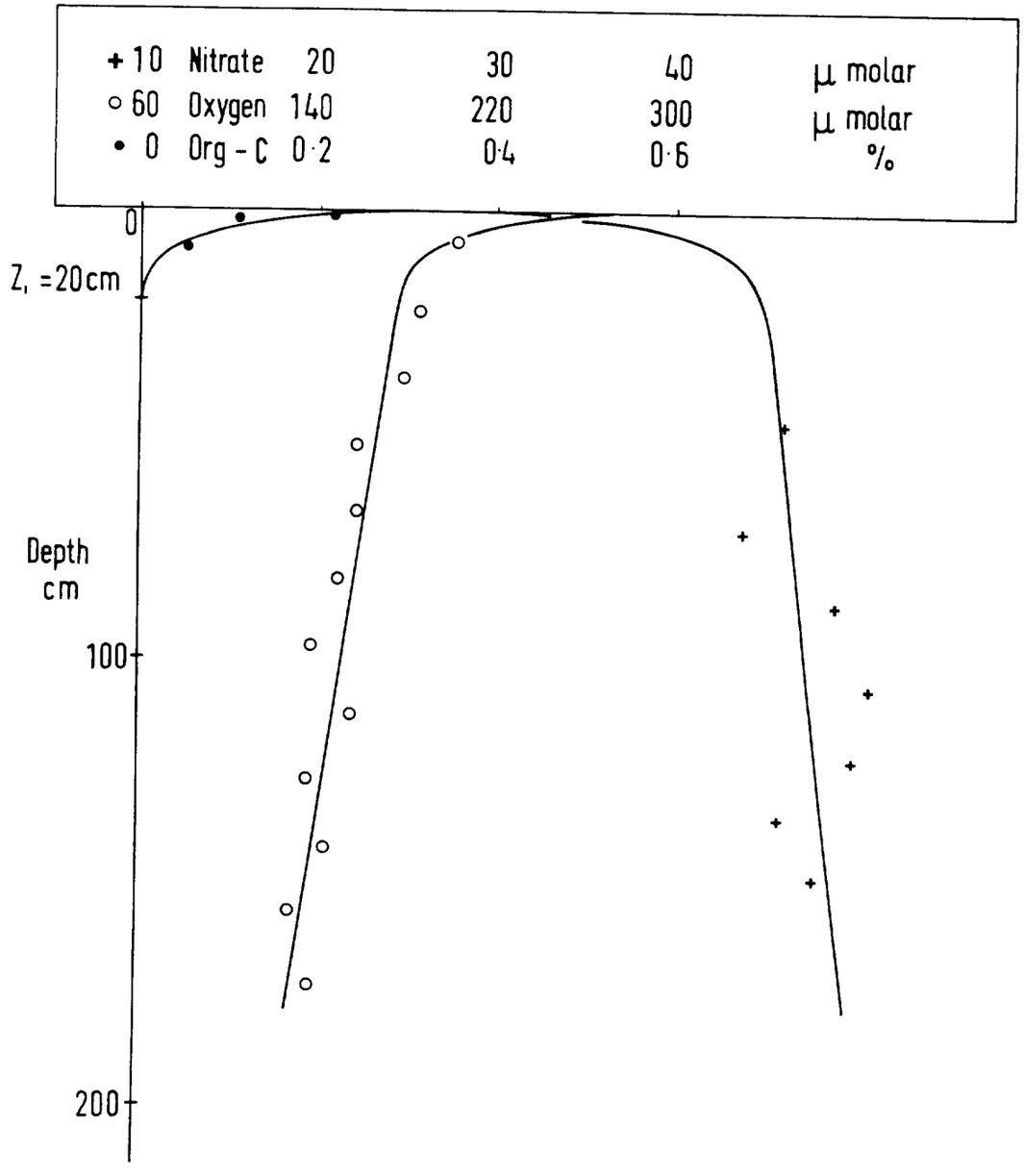

Figure 4.i.9 Model C_{org} and porewater oxygen and nitrate data for core 10552#2K (Wilson et al., 1984).

SAMPLE : D10695/2/14
SUB-BOTTOM DEPTH : 1.68m
ORIENTATION : VERTICAL
SEDIMENT TYPE : NANNO MARL

Initial void ratio e_o - - - - 3.554

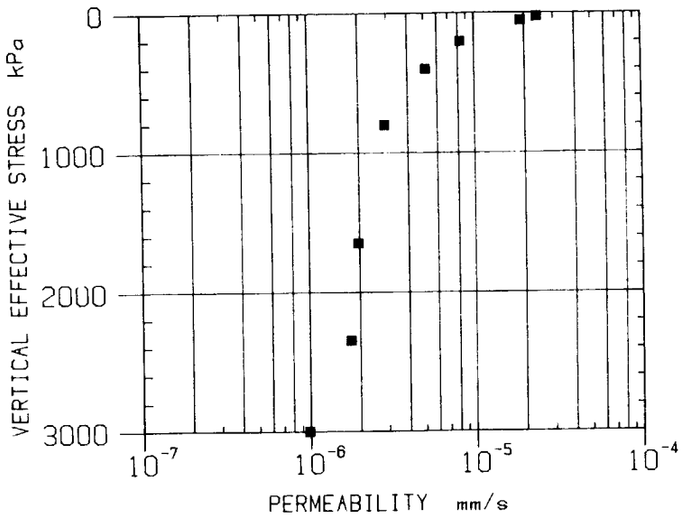

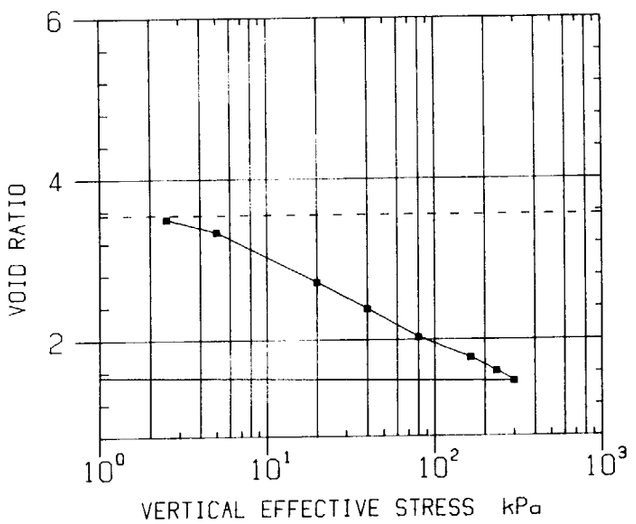

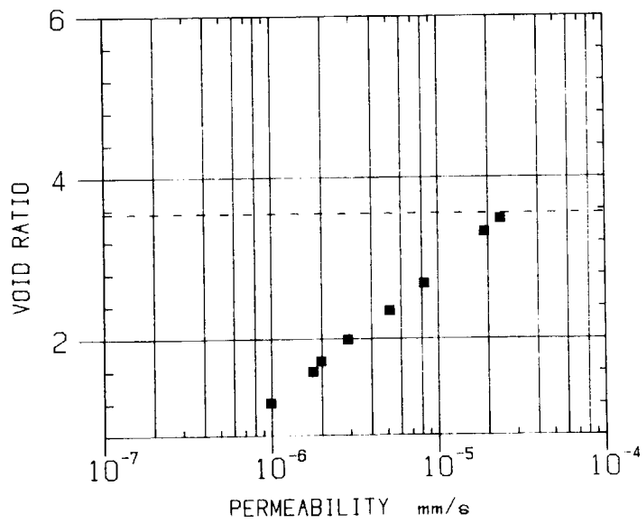

Figure 4.i.10 Consolidation and permeability data for nannofossil marl (turbidite) in the GME area.

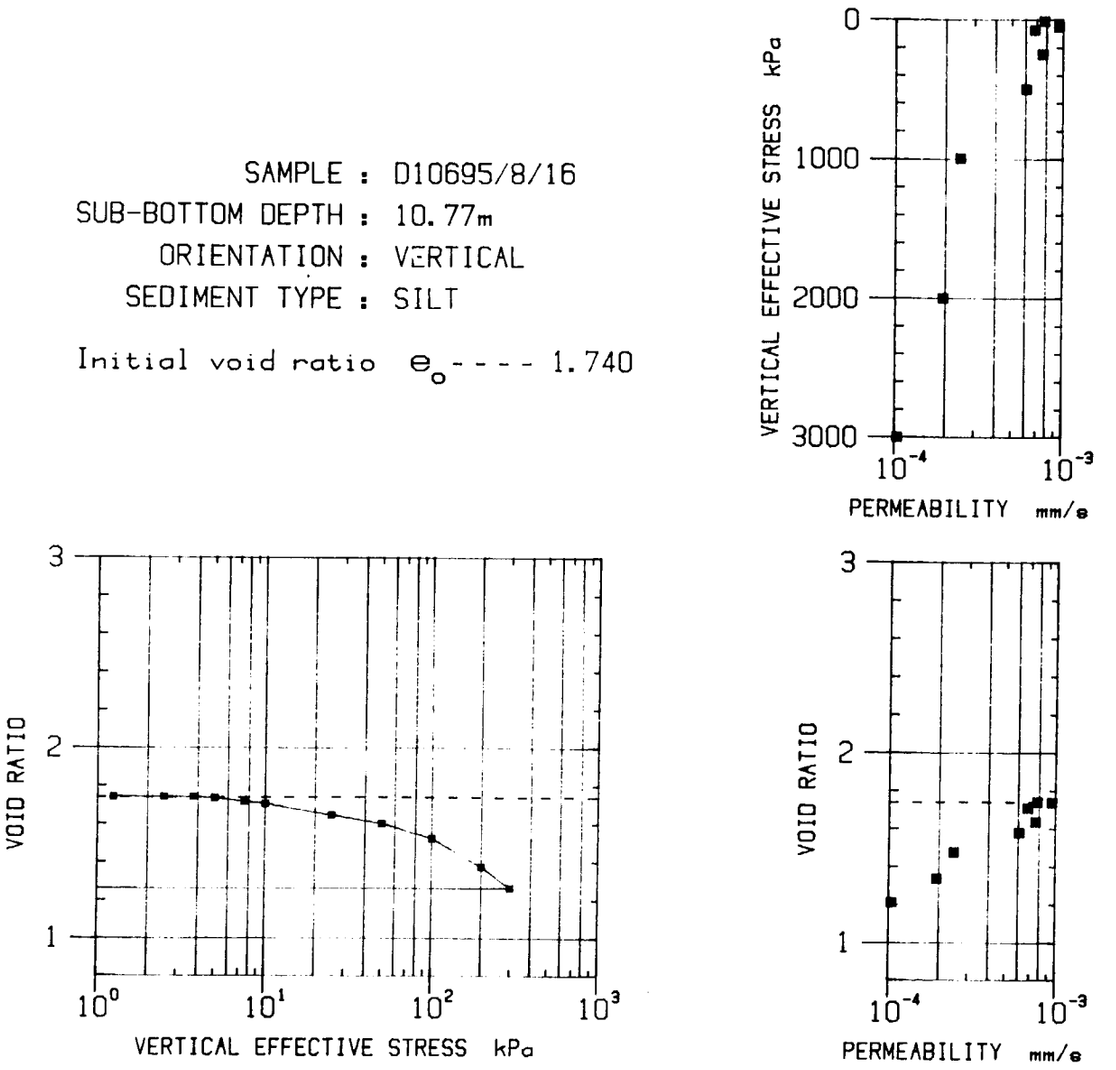

Figure 4.i.11 Consolidation and permeability data for a silt at the base of a turbidite in the GME area.

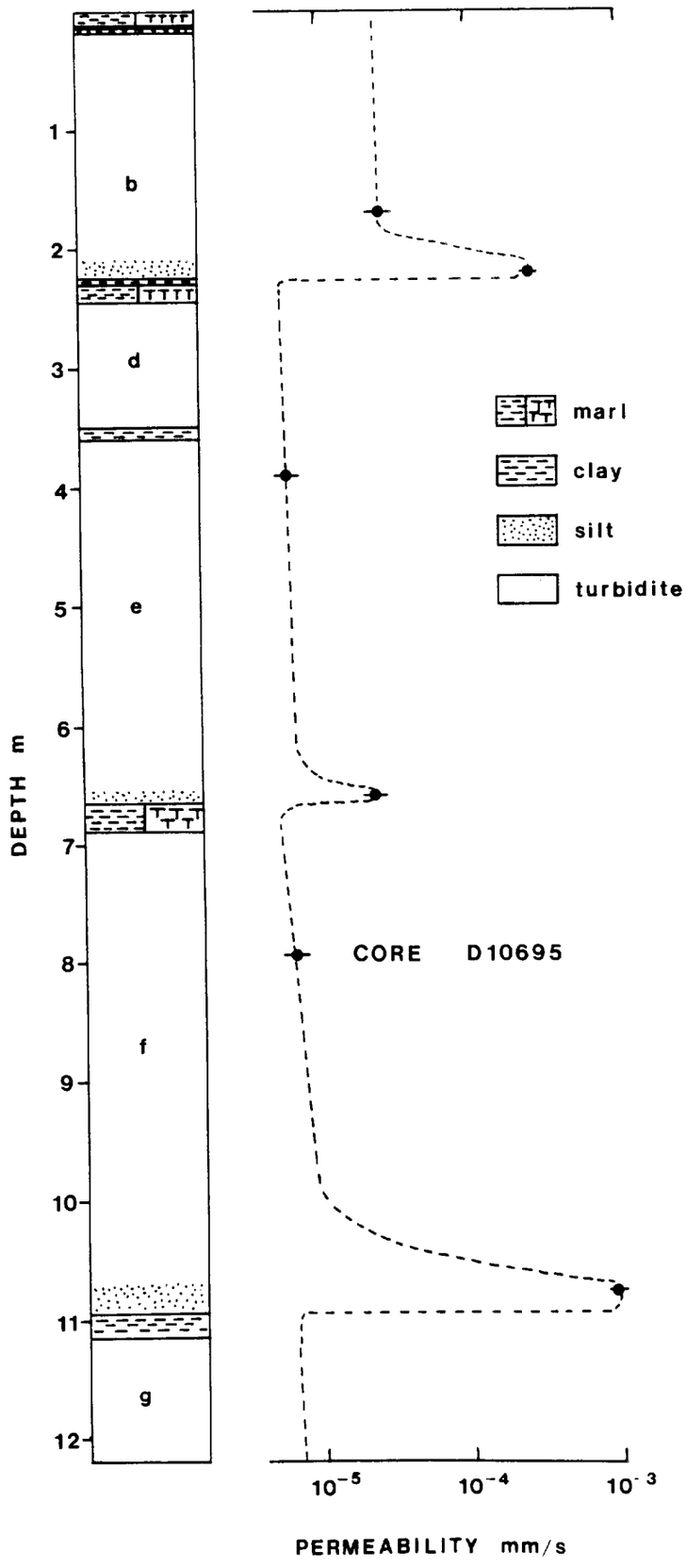

Figure 4.i.12 Permeability profile for a sequence of distal turbidites with silty bases in the GME area (Core D10695).

4.ii KINGS TROUGH FLANK

4.ii.a Regional Setting

The KTF study area is located on the lower eastern flank of the Mid-Atlantic Ridge some 300 miles northeast of the Azores. There is a general regional slope to the south-east upon which are superimposed a series of sub-parallel ridges and intervening low areas bounded by scarps aligned in an approximate 010° direction. Water depths range from less than 2000 metres to more than 4300 metres but generally are between 3500 and 4000 metres (Figure 4.ii.2). The topography to a large extent mirrors the morphology of the acoustic (igneous) basement that was generated at the Mid-Atlantic Ridge. The area was chosen in 1979 because its apparently extensive sediment cover, half to one kilometre thick, offered an opportunity to study the suitability of pelagic carbonate sequences as a disposal medium.

Kidd et al., (1983) summarised the results of studies undertaken following visits by four research cruises to the area up to the end of 1982. Subsequently a further RRS Discovery cruise has been mounted there (Francis et al., 1984) and drilling has taken place from D.V. Glomar Challenger on the northern edge of the study area (Kidd, Ruddiman et al., 1983; Kidd, 1984). Dredge sampling suggested that the study area is located on oceanic crust of predominantly Eocene age (Kidd et al., 1982) and this was confirmed by the recent drilling (Kidd, 1984) which also allowed calibration of a magnetic anomaly in the area. Analysis of the magnetic profiling data suggests that at least one minor transform fault disrupts the igneous basement in an east-west direction.

KTF is bounded on three sides by unusual bathymetric features which have been much discussed because of their implications for the tectonic history of the North-east Atlantic Ocean. To the north is the Kings Trough tectonic complex of anomalously deep troughs and ridges now believed to result from rifting of a hot-spot ridge about 30 million years ago and its later subsidence (Kidd, Ruddiman et al., 1983). The Azores Biscay Rise to the southeast is also thought to be an extinct hotspot trace but one which pre-dated that at Kings Trough (Whitmarsh et al., 1982). The Azores Platform to the southwest is the present day site of the active Mid-Atlantic Ridge/Azores Fracture Zone triple junction (Searle, 1977). Despite this tectonic setting our studies indicate that no major tectonic upheavals have occurred in the area since the middle Miocene, i.e. in the last 11 to 15 million years.

What is still not clear, however, is whether any local tectonic movements, such as small-scale adjustments on basement-controlled faults, have occurred in the recent geological history of the area. An analysis of intraplate seismicity in the Atlantic Ocean identified four earthquake events in this general region over the historical period 1913-1979 with magnitudes >4.5 (Lilwall, 1982). One of these occurred near the western end of the Kings Trough complex but none was recorded from KTF itself.

The area has remained above the regional carbonate compensation depth for all of its 40-60 million year geologic history and thus the sediment column above oceanic basement is dominated by pelagic carbonate sequences. Sediment thicknesses, as detected from seismic reflection profiling (Figure 4.ii.1), vary greatly across the study area. They are thickest, reaching 1200 metres thick, in a 40km wide basin in the southeast, but are between 300 and 900 metres over most of the remaining area and become nil where igneous basement crops out on the flanks and summits of the hills. As well as outcropping igneous rock, outcrops of older consolidated carbonate rock occur on the seismic profiles at topographic scarps that appear fault-controlled.

Drilling results at DSDP Site 608 show that the only major change in sediment character that has occurred in the last 30 million years was due to the onset of glacial-interglacial cycles 2.4 million years ago. Because of the stiffness of the uppermost sediments, our sediment cores are limited to 10 metres penetration. The cyclic climatic changes cause them to display alternations of carbonate oozes and marls. The marls are produced during glacial intervals when clay, silt and rock fragments (erratics) are added to the sediment from melting ice. Deposition rates average 2.5 to 3 cm/1000 years but are around 2.0 cm/1000 years in the pre-glacial drilled section.

Studies of sediment stability in the area have concentrated upon the uppermost few tens of metres of the sediment column (representing the last one million years or so) using 2 kHz, 3.5 kHz and 10 kHz profiling records. A variety of echo types are observed and horizontal variability is evidently marked. Eliminating, in the first instance, those areas of hills and scarps occurring at a spacing of about 10 to 30km, and the slopes around hills, as areas of likely sediment disturbance, it was found that areas of relatively smooth sea-floor (< 10m relief) are available at KTF. Even these, however, sometimes displayed anomalous echo types that suggested sediment instability.

Only a few examples of sediment disturbance had been found in the twelve gravity and piston cores recovered up until the end of 1982 (Figure 4.ii.2). The cores, recovered from a variety of environments, are well-correlated across the area using an integrated high resolution stratigraphy based upon coccolith, foraminiferal, oxygen isotope, lithologic and paleomagnetic analyses (Weaver, 1983a) (Figures 4.ii.3, 4.ii.4). Slumps, sandy turbidites and minor hiatuses do occur in the cores but these appear to be local phenomena.

The station work carried out at KTF subsequently was aimed at resolving the apparent discrepancy between the picture of great horizontal variability provided by the geophysical data and the long-range similarity of the cored sequences. In particular, we needed to identify the causes of anomalous echo-character in the vicinity of the areas of relatively smooth relief. Figure 4.ii.2 shows the additional station work conducted. Much analysis of the recovered samples and data remains to be done but the additional 3.5 kHz profiling suggests that anomalous echo character may be confined to the margins of the 'smooth' areas and preliminary results of coring and camera studies indicate that current winnowing and erosion of sediments cannot be discounted in the area. Localised sediment slumping near steep slopes and concentration of current activity also near slopes seem to combine to produce unusual bedforms and variable sediment sequences at the margins of the 'smooth' areas.

Upon completion of analyses on the Discovery 134 samples and data the so-called 'smooth' areas may remain attractive sites for further investigation. However, the difficulties of corer penetration encountered at KTF and the long-term predictability of the deeper drilled sections may already argue against shallow penetrometer disposal but in favour of drilled disposal in such ridge-flank carbonate sequences.

4.ii.b Chemistry

The KTF area was revisited during RRS Discovery Cruise 135 (Wilson et al, 1984) to obtain porewater and sediment samples. Porewater samples were obtained successfully using the Mk II in situ sampler at station 10702 (42°04'.6N 23°30'.1W), and 161cm (10702 2K) and 301cm (10702 8K) long Kastenlot cores were recovered at the same site, the latter in a water depth of 3551m. The proximity of the site to 82PCS01 (previously cored) makes it possible to provide a precise geological

control. Detailed biostratigraphic (planktonic foraminifera and coccoliths), oxygen-isotope (^{18}O) and calcimetric analyses have been performed on core 82PCS01 (Kidd et al, 1983). Integration of this data has enabled the identification in this core of four glacial and interglacial phases during the last 150,000y, the last interglacial being further subdivided into three discrete isotope stages. (Kidd et al, 1983). This stratigraphy provides a useful framework for geochemical interpretation.

Sedimentology and Coring Artefacts at Station 10702

The sedimentary successions in cores 10702 2K and 10702 8K are closely comparable with that in 82PCS01, consisting of very pale orange to white intervals of carbonate ooze, interbedded with yellowish brown marly oozes and marls. Clay-rich intervals correlated broadly with glacial periods, possibly due to a greater input of terrigenous non-carbonate material associated with ice-rafting and increased erosion of the continental shelves during glacial periods (Ruddiman & McIntyre, 1976). This is particularly important near Kings Trough as the polar front lay just to the north during glacial maxima (McIntyre et al, 1972).

Lithostratigraphic correlation of the two Kastenlot cores with piston core 82PCS01 (Figure 4.ii.3) demonstrates that the former are severely attenuated. Burrow cross-sections (principally of the ichnogenera Planolites and Chondrites) are severely compressed in the horizontal in the Kastenlot cores, indicating that attenuation is a result of coring, and not a consequence of lateral depositional variation. Detailed correlation of individual bedding planes (Figure 4.ii.3) enables a comparison to be made of bed thickness, and demonstrates that in core 10702 8K marly intervals are reduced by up to 50% of their thicknesses in 82PCS01. Beds of the firmer carbonate ooze, however, are more than 95% of their original thicknesses. Core 10702 2K is less attenuated, with marls more than 70% and oozes up to 100% of their original thicknesses. This difference may be attributed to the heavier weight of the longer barrel corer.

Attenuation of sedimentary successions is a well-known problem with narrow-diameter gravity corers (Richards, 1961; Weaver & Schultheiss, 1983) but has not been widely recognised in Kastenlot cores, which have a 15cm cross-section. Attenuation during coring is believed to result from lateral flow of sediment during penetration of the corer into the sediment (P.J. Schultheiss, personal communication,

1984) and should not have caused appreciable lateral movement of porewater or mixing of lithologies.

Since the amount of attenuation varies between cores, it is only possible to compare directly depth versus concentration (e.g. porewater) profiles if compressional effects are removed. This was accomplished by normalising the thickness and depth of each bed to that of the corresponding interval in core 82PCS01 (Table 4.ii.1), which displays no evidence of deformation. The validity of this technique is supported by marked improvement in the correspondence of porewater profiles obtained from the in situ sampler and depth-normalised Kastenlot cores.

Porewater Chemistry at Site 10702

Methods

The nutrients silicate, phosphate and nitrate were determined colorimetrically using a continuous flow analyser. The precision of the analyses for all three methods was 1%. (Hydes 1984). The metals were determined by flameless atomic absorption spectroscopy. Manganese was determined by direct injection of samples diluted with 5% nitric acid into the graphite furnace atomiser (GFA). Nickel, copper and cadmium were extracted as their dithiocarbamate complexes into Freon, back extracted into nitric acid and determined by GFA (Chapman et al, 1983).

Results

Nutrients

The general picture of nutrient distributions seen at site 10702 (Table 4.ii.2, Figure 4.ii.6) is similar to that seen at the MANOP site C in the eastern equatorial Pacific (Jahnke et al, 1982a), which is also characterised by carbonate rich sediments.

Silicate

Marine sediment pore waters are universally enriched in dissolved silicate compared to the overlying water column. The extent of the enrichment and the shape of the concentration profile with respect to depth depends on the composition of

the sediment, the sedimentation rate and the degree of biologically induced mixing at the sediment/water interface. The smoothness of the observed profiles, and the correspondence of observed concentrations at similar depths with what should be similar sites, can be used as a criterion of how successful sampling has been (Bischoff et al, 1970) and how similar the sites are. The profiles plotted in Figure 4.ii.6 from three sample sets obtained at Station 10702 agree well. This indicates that (a) the recalculated sample depths produce a coherent silicate distribution for the three sets, (b) the material at the three sites is similar, and (c) no major problems have occurred with the sampling techniques.

Phosphate

The average phosphate concentration in both cores is 3.0 μM, with a range from 1.7 μM at the top of core 8K to 4.3 μM at 168cm depth in core 2K. This range of concentrations does not reflect a clear trend in phosphate concentrations with depth, and there is some scatter of observed concentrations around the mean concentration. All observed concentrations are higher than that of bottom water (1.3 μM). The results of Jahnke et al (1982a) indicate that sampling artefacts induce changes in observed phosphate concentrations. At site C results obtained by in situ (harpoon) pore water sampling are about 25% higher than those from pore waters sampled from cores. This is probably related to pressure changes in parallel to those which occur within the carbonate system (e.g. Toole et al, 1984). Such a large effect as this is not seen in other types of sediments. All but one of the sets of samples collected by Jahnke et al (1982a) at their siliceous ooze site S by in situ sampling agree quite well with the core results. The exception is one site where the in situ results are actually lower than in the other sets. Jahnke et al (1982a) also point out that, in both in situ and non-in situ data, they consistently observe that the level of phosphate in the sample closest to the interface is lower than that in bottom water. They calculate that the actual occurrence of such a gradient of phosphate into the sediment is highly unlikely as the corresponding accumulation of phosphate in the solid phase is not seen.

In the light of the results of Jahnke et al (1982a) it would appear likely that the phosphate values obtained at station 10702 do not represent in situ conditions. True values may be some 20% or so higher. In contrast to their results the topmost sample in both cores contains more phosphate than bottom water. However, this is probably due to the greater depth of these samples, 8 and 10cm as opposed to the 0-1cm interval from which the Jahnke et al (1982a) top sample came.

The results do, however, suggest that during the aerobic mineralisation of organic material in the upper layer of the sediment phosphate is released along with nitrate. If one assumes a Redfield ratio for the organic matter being metabolised in the upper layer of the sediment, then nitrate and phosphate should be released in a molar ratio of 16 to 1 (Froelich et al, 1979). For core 10702 2K nitrate and phosphate increase in a ratio of 12:1 between bottom water and the first pore water sample at 8cm depth. In contrast, for core 8K the ratio is 72:1. This higher ratio results from the low level of phosphate in the 10cm sample from core 8K. The phosphate profile from core 8K looks the most coherent of the two sets of data from station 10702, showing less scatter than the 2K results. This however may represent a more complete degree of equilibration with the conditions that produce phosphate loss than occurred in core 2K before pore water sampling.

Nitrate

In the top 20cm of sediment the nitrate data from the two cores 10702 2K and 8K and the in situ pore water sampler all show a rapid increase in nitrate concentrations corresponding to the rapid decrease in dissolved oxygen measured in samples from the in situ pore water sampler. When the oxygen decrease is compared to the increase in nitrate, a ratio of 8.6 is predicted by the equation:

$$(CH_2O)_{106}(NH_3)_{16}(H_3PO_4) + 138O_2 = 106\ CO_2 + 16HNO_3 + H_3PO_4 + 122\ H_2O$$

(Redfield organic composition)

The oxygen to nitrate ratios are 8.0, 6.1, 5.8 for cores 2K and 8K and the PWS respectively. This agreement is better than for the nitrate/phosphate ratio and indicates that the quality of these data is more consistent. Below 20cm depth to 2m there is an offset between the results from the two cores. Both sets do, however, show a consistent trend to decrease with depth. Interestingly the offset between data sets from closely spaced stations is also seen in the results from MANOP site C (Jahnke et al, 1982).

Metals

Concentration profiles for manganese, nickel, copper and cadmium in pore waters from site 10702 are presented in Figure 4.ii.7.

Manganese

Both cores 2K and 8K become sufficiently anoxic for manganese to be mobilised within the pore waters at 140cm and 95cm depth respectively. This discrepancy between the positions of the manganese oxidation horizons is, as with the offset between the nitrate profiles, reflected in the MANOP site C results. This raises the question of whether this degree of lateral inhomogeneity is a universal phenomenon or peculiar to such carbonate-rich sites. It is only seen clearly in the redox sensitive components of the pore water. Major differences in the sediment solid phase can be ruled out as silica profiles in the two 10702 cores are similar. Differing rates of ventilation of pore waters to overlying waters by burrowing animals can also be dismissed as this would also effect the silica profiles (Schink et al, 1975). The offset could be produced by a minor component, which is mostly likely to be the organic carbon content of the sediment. It is difficult to envisage, however, how the organic carbon content could be different at the two sites without there being corresponding differences in the solid phase composition of the sediment. One possibility is that differences in the ecological settings at the two sites produce animal communities which at site 8K are able to bury organic matter deeper in the sediment than at site 2K, without having a significant effect on the silicate profile. Further work is currently being undertaken to clarify these problems.

Nickel

As has been observed previously, the nickel profile closely resembles that of manganese (Klinkhammer et al, 1982). This is consistent with the incorporation of nickel into mixed manganese oxide phases, as discussed by Hem (1978).

Copper

The copper distribution is also similar in shape to those observed previously (Sawlan & Murray, 1983). Diagenetic processes in the topmost layer of the sediment release copper from solid phases, into which it has been scavenged from the water column as particles have settled to the sea bed. At this site the manganese oxidation horizon would appear to act as a sink for this copper released from the sediment surface layer. Copper incorporated into manganese oxide phases at this horizon appears to be released into solution upon reduction of the manganese oxides

at depth in the sediment. The question which arises from these observations is that of the chemical form of copper in solution in these pore waters. Copper tends to be very strongly adsorbed by solid phases as is evidenced by its scavenging by particles in the water column, but a change in speciation may give rise to its mobility in pore waters.

Cadmium

Measurements of dissolved cadmium concentrations in pore waters have only been reported previously by Klinkhammer et al (1982), who made measurements at the MANOP siliceous and carbonate ooze sites. At both sites little variation in cadmium concentration was seen with increasing depth in the sediment. Cadmium concentrations were approximately twice those seen in bottom waters. Our results from around 100cm depth in both cores from site 10702 correspond to those observed at their site C by Klinkhammer et al (1982). This suggests that we do not have a serious contamination problem.

The shape of the cadmium profiles we observed are, in contrast to MANOP site C, similar to those observed for copper. Rapid release of cadmium from particulate material arriving at the seafloor is consistent with its relatively rapid regeneration in the water column, in parallel to the release of phosphate from the softer parts of decaying organisms. (In contrast to the case for copper, there is, as yet, no evidence from studies of cadmium in the water column to suggest that it may be enriched in sediment surface layers.) In parallel to copper and nickel, cadmium is probably incorporated into mixed manganese oxide phases at the manganese oxidation boundary and is then released from these oxides as conditions become more reducing with deeper burial.

Uranium and thorium isotopic analysis of 10702 8K

Uranium and thorium analyses have been carried out on sixteen samples from core 10702 8K. The analyses are tabulated in Table 4.ii.3. Figure 4.ii.8 shows a plot of ^{230}Th excess versus depth measurements corrected for the preferential compression within the marl and clay horizons which occurred on penetration of the Kastenlot corer. This plot yields an average accumulation rate of 2.61 cm/10^3 years. The points are distributed on either side of the line, suggesting that sediment accumulation has not been constant over this period (approximately 150,000

years, using corrected measurements). Also shown on Figure 4.ii.8 are the approximate boundaries for the oxygen isotope stages, transposed from oxygen isotope determinations made on the piston core 82PCS01 (Kidd et al, in press).

Comparison of the calculated water column supply of ^{230}Th for this water depth with the sediment inventory of ^{230}Th excess, shows that the sediment contains between 106% (uncorrected depths) and 140% (corrected for differential compaction) of the water column ^{230}Th production. Both of these values are high compared with average values of 68% for the depth range 3400-4600m and 96% for the depth range 2000-3400m (Kadko, 1980).

Table 4.ii.3 compares ages for the boundaries between selected oxygen isotope stages determined by Pisias & Moore (1981) with those calculated from the accumulation rate found in 10702 8K and isotope data from 82PCS01. There is good agreement for the 1/2, 4/5 and 5/6 boundaries.

Table 4.ii.4 uses the thickness of selected identified stages, together with their durations (after Pisias & Moore, 1981) to calculate average accumulation rates within each stage. It can be seen that the main glacial interval (2-4) is represented by a period of high sedimentation, compared with stage 1, probablly due to increased input from ice-rafted debris and the transport of river-borne material across the shelf to deeper waters. These accumulation rates compare well with those calculated from other piston cores studied by the IOS Marine Geophysics Group taken in the same area. The intercept of 1.2dpm/g ^{230}Th excess indicates that the terrigenous material supplied to this area is out of radioactive equilibrium. Scott (1968) found a concentration of 0.5dpm/g for twelve $<20\,\mu m$ fraction samples, and Bacon and Rosholt (1982) found an intercept of 1.1 ± 0.7dpm/g for the terrigenous component of core GPC-5 from the Bermuda Rise. The positive correlation of age-corrected ^{230}Th excess and ^{232}Th (expressed on a carbonate free basis) is unexpected in view of the oxygen isotope data, which indicate that clay-rich (and therefore ^{232}Th-rich) glacial sediments represent periods of faster accumulation. It would be expected that ^{230}Th excess concentrations should be lower at these horizons. The data appear to suggest that the terrigenous clay material supplied during colder periods performs as a more efficient water column scavenger of ^{230}Th than during interglacials, and that a positive correlation of age-corrected ^{230}Th excess and ^{232}Th is developed. Plots of Th and U versus $CaCO_3$ indicated that the clay fraction of the sediment contains 2.53ppm U and

13.9 ppm Th, and there does not appear to have been any post-depositional relocation of U (Figure 4.ii.9).

Mineralogy

Preliminary mineralogical analyses by X-ray diffraction (XRD) indicate that sediments in the Kings Trough Flank area are composed essentially of biogenic calcite with varying proportions of detrital quartz and clay minerals, principally illite, smectite and chlorite. Fragments of basaltic pumice and shards of volcanic glass are common in some samples. Stratigraphic analysis of the mineralogical data is currently being undertaken in an attempt to differentiate between glacial and interglacial sediments using mineralogical criteria.

Sediment Geochemistry

Twenty-three samples from core 10702 8K were analysed for major (Si, Ti, Al, Fe, Mn, Mg, Ca, K and P) and eleven trace-element (Cl, V, Cr, Co, Ni, Cu, Zn, Rb, Sr, Y, Zr) by X-ray fluorescence (Table 4.ii.6) using standard IOS laboratory techniques. Chlorine data were utilised to recalculate analyses on a salt-free basis assuming stoichiometric concentrations in NaCl. Analyses were also compared on a carbonate-free basis (CFB) by assuming all Ca occurs as $CaCO_3$. This assumption was confirmed by the close correspondence between recalculated carbonate-contents and those obtained independently by 'LECO' carbon analyser.

Major Element Data

The distributions of the principal major-elements (excluding Ti and P) are shown in Figure 4.ii.10. With the exception of Ca, all major elements display higher concentrations in sediments deposited during glacial, compared with those deposited during interglacial, times.

Calcium varies inversely with the other elements. These trends reflect the higher carbonate contents of interglacial sediments, and when expressed on a CFB most elements show no systematic variation. Notable exceptions are Mn and K.

The distribution of manganese (Figure 4.ii.10) corresponds least well with the other elements, displaying a steady decline in concentration from the base of

the analysed section (around 4m) to 1m below the sediment/water interface. Above this, there is a marked peak in concentration at 40cm below the sediment surface with Mn concentrations up to four times their background value. The increase in solid-phase Mn begins at the point where Mn concentrations in the pore water falls below 1 μ molar. This indicates that Mn is mobilised at depths under reducing conditions which permits its migration into the upper oxic layer, here it is precipitated as an oxyhydroxide (Bender 1971; Froelich et al, 1979).

When expressed on a CFB, the Mn distribution is more complex. The peak at 40cm depth remains well defined, but comparable enrichments occur at 340, 240 and 10cm depth. Furthermore, CFB Mn concentrations are generally higher in carbonate-rich (interglacial) sediments. This suggests that Mn is located principally in a discrete hydrogenous (authigenic) phase. The good correlation between other elements, when expressed on a CFB, indicates that these are controlled primarily by the alumino-silicate (clay) component.

The distribution on a CFB of K is relatively uniform except for a major increase at 250cm (Figure 4.ii.10). This peak does not correlate with any trends shown by other major elements and is probably related to a change in the mineralogy of the alumino-silicate phase.

Small changes in the composition of the alumino-silicate phase are not well-displayed by the CFB data but become more apparent if elements are compared with aluminium. The distributions of Si, Ti and K were examined when normalised to Al (Figure 4.ii.11). These elements were selected because they are known to be associated dominantly with alumino-silicate minerals. It is apparent that glacial sediments contain a higher proportion of Si and Ti while K remains fairly constant except for the peak at 250cm (also recorded by the CFB plot).

The higher Si and Ti ratios in glacial sediments may be attributed to a higher proportion of detrital clay minerals, principally illite, since illites may be enriched in these elements relative to smectite (Weaver & Pollard, 1973). On a smaller scale, minor fluctuations within glacial and interglacial intervals indicate that Si and Ti covary in glacial sediments, but are inversely correlated in interglacial parts of the succession (Figure 4.ii.11). This suggests that quartz content only becomes a significant control on geochemical variation during interglacial times.

These hypotheses are currently being tested by detailed mineralogical analysis.

Trace Elements

Concentrations of trace-elements determined by XRF are given in Table 4.ii.6. The distributions of additional trace-elements and the REE are currently being determined by Inductively Coupled Plasma (ICP) techniques.

Preliminary analysis of the trace element trends indicate that Sr covaries with Ca and is located principally in biogenic calcite. Vanadium, Cr and Rb covary with K. Cobalt and Ni correlate well with Mn and are probably controlled by the same diagenetic processes. Both Y and Zr, and to a lesser extent Cu and Zn, are apparently enriched in the non-carbonate fraction of carbonate-rich sediments, although this requires confirmation by ICP analysis.

All trace elements except Sr are enriched at the same level as the peak in the CFB K data. This coincides with a marly horizon within an otherwise pure carbonate succession (Figure 4.ii.11), and suggests that a very atypical alumino-silicate phase is controlling the geochemistry at this level. The nature of this phase or phases is currently under investigation.

Conclusions

1. The thicknesses of sedimentary units may be reduced by up to 50% in Kastenlot cores when compared with corresponding intervals in piston cores from the same site. Attenuation is a function of corer weight and the competence of each sedimentary interval.

2. The distribution of pore water nutrients at station 10702 is similar to that at MANOP site C in the eastern equatorial Pacific. Silicate is strongly enriched at depth. Phosphate shows no clear trends but absolute values are probably 20% too low because of a pressure related sampling artefact. Nitrate varies inversely with oxygen, being released by the oxidation of organic matter in the uppermost 50cm of sediment.

3. Porewater Mn and Ni are enriched below 1m indicating suboxic conditions at depth. Copper and Cd are strongly enriched in porewaters because of rapid

mobilisation from the solid phase during burial. Depletion in porewater Cu and Cd at 50cm depth is related to incorporation by Mn-oxides.

4. The ^{230}Th excess data yield an average accumulation rate of 2.61cm 10^{-3} y. The ages of isotope stage boundaries are in good agreement with published values. Radiochemical analyses indicate that the terrigenous component is out of radioactive equilibrium. A positive correlation of age-corrected ^{230}Th excess and ^{232}Th suggests that clays supplied during glacial periods act as more efficient water-column scavengers of ^{230}Th than inter-glacial clays. There is no evidence of diagenetic remobilisation of U.

5. Interglacial sediments are carbonate-rich, glacial sediments contain higher proportions of alumino-silicates. Consequently, solid-phase geochemical variation is dominated by the inverse correlation between Ca and the other major elements. Manganese and, to a lesser extent, Ni and Co, have been fixed in the oxic part of the sediment column after being remobilised and diffusing upwards from the suboxic environment below. Other elements do not display redox-related distributions but may be indicative of the fluctuating provenance of detrital phases.

4.ii.c Physical Properties of the Sediments in the KTF Area

A limited amount of physical properties data has been obtained from the Kings Trough Flank study area. This has been obtained from the single Kastenlot core D10333 (15cm square section) taken on Discovery Cruise 118 in the southern part of the area.

The consolidation and permeability characteristics of sediments composed predominantly of calcium carbonate microfossil debris have been studied relatively little compared with those of clay-rich sediments. Bryant et al, (1974), using consolidation data from a range of sediments, provided a clear discussion on the type of information that can be obtained from consolidation tests. It was concluded that fine-grained carbonate muds consolidate in a similar way to non-carbonate silty clays. The only difference observed was that under equal loads older carbonate sediments do not consolidate to as low a final void ratio as non-carbonate sediments. Miller & Richards (1969) observed marked differences in the void ratio/pressure relationships obtained from a laboratory consolidation test and from

a sedimentation-compressed computation on a short core of calcareous ooze. They concluded that laboratory consolidation tests on carbonate oozes should be interpreted with caution for geological and engineering purposes.

Six samples from core D10333 have been tested. Sample D10333/7 taken at a sub-bottom depth of 76cm is used to illustrate their behaviour. The consolidation test is similar to that commonly used (Lambe & Whitman, 1979) except that the sample (75mm in diameter, 20mm in height) is subjected to a back pressure of 700kPa to ensure complete saturation. Following each incremental load, the permeability is measured assuming Darcian behaviour by applying a small hydraulic gradient and measuring the volume flow of water through the sample (Lambe & Whitman, 1979).

Figure 4.ii.12 shows the results from sample D10333/7. The void ratio/vertical effective stress (e log P) shows no obvious preconsolidation pressure, hence it is assumed to be normally consolidated. The slope of the e log p curve during the latter stages of the test defines the compression index, C, which in this case is 0.37. The compression index was found to vary between 0.2 and 0.63 in core D10333 depending on the carbonate content (higher values of C_c are obtained for lower carbonate values). These values are similar to data obtained by Buchan et al. (1971) on comparable North Atlantic sediments. The permeability/void ratio curve gives a permeability index (change in void ratio per logarithmic cycle of permeability) of 1.39. The extrapolated permeability at the initial void ratio (e_o = 2.431) is 3 x 10^{-5} mm/s. The low value of C_c and the high value of the permeability index compared with other deep-sea sediments means that there is likely to be only a relatively small decrease in permeability with increasing depths as shown by the effective stress/permeability curve. For comparison purposes it is worth noting that 'red clays' have permeabilities around 2 x 10^{-7} mm/s at similar void ratios.

It is concluded, therefore, from the very limited data available that the surficial sediments in the KTF study area are probably normally consolidated (i.e. they exhibit no evidence of large-scale erosion or large excess pore pressures) and they have relatively high values of permeability ($\sim 10^{-5}$ mm/s). If confirmed by further sampling the higher values of permeability might make sediments of this type somewhat less attractive than deep sea clays as host media for shallow burial options of high-level radioactive wastes.

The sediments in the Kings Trough Flank area were continuously cored to basement at Site 608 on Leg 94 of the Deep Sea Drilling Project in July 1983 (Kidd et al., 1983). The consolidation and permeability characteristics of some of these deeper samples are currently (April 1984) being measured in the Wormley laboratory.

4.ii.d Heat Flow Data in the KTF Area

Two heat flow stations were occupied in the Kings Trough Flank area: station 10335 on Discovery Cruise 118 and station 10662 on Discovery Cruise 134. The first station gave three full penetrations, one of which disclosed a marked non-linearity in the sediment temperature profile (Figure 4.ii.13) which could imply upward porewater movement. When the data are modelled using conduction-convection theory the suggested velocity is 52 cm y^{-1}. The ten measurements at station 10662 also showed consistent evidence for non-linear sediment temperature profiles along an $\sim$5nm transect. However, in this case the implied upward advection was only $\sim$10 cm y^{-1}. Both stations may have recorded water movements which form part of a more regional scale pore water convection pattern.

Detailed discussion of these and other heat flow stations in the Northeast Atlantic is contained in Noel (1984a,b).

Table 4.ii.1 Sample depths in Kasten cores from station 10702 recalculated using data from piston core PCS8201

Isotope Stage	Sample depth 10702#2K		10702#8K	
1	7-9	(7-9)	0-2	(0-2)
	22-24	(22-24)	4-6	(4-6)
			8-10	(8-10)
			15-17	(15-17)
2	35-37	(40-42)	25-27	(25-27)
	60-62	(74-76)	30-32	(33-37)
	76-78	(94-96)	35-37	(42-44)
			45-47	(74-76)
			55-57	(86-88)
			75-77	(111-113)
			78-80	(114-116)
3	95-97	(138-140)	95-97	(136-138)
	115-117	(145-147)	98-100	(139-141)
			105-107	(147-149)
4	135-137	(167-169)	118-120	(164-166)
	152-154	(184-186)	125-127	(175-178)
5			147-147	(202-204)
			165-167	(227-229)
			171-173	(234-236)
			175-177	(238-240)
			185-187	(249-251)
			205-207	(271-273)
			207-209	(273-275)
			225-227	(291-293)
			245-247	(313-315)
			265-267	(336-338)
6			275-277	(352-256)
			282-284	(366-368)
			296-297	(384-386)

Depth in centimetres below sediment surface. Converted depths in parentheses. Isotope stage boundaries after Shackleton in Kidd et al. 1984.

Table 4.ii.2 Porewater geochemistry at Station 10702

Sample	Depth cm	Element						
		O_2	SiO_2	PO_4	NO_3	Mn	Ni	Cu	Cd
		% Saturation	μM			ηM			
In Situ	Bottom Water	85	31		22.3				
	0	66	27		23.9				
	3		127		34.3				
	4.5	37.5	96		35.3				
	7.5	28.8	149		38.5				
	13.5	22.5	184		37.8				
	25.5	18.8	191		36 0				
10702#2K	8		168	3.1	42.5	0.07	3	67	6.5
	23		191	3.5	31.3	0.09	52	21	3.2
	41		256	2.6	30.5	0.03	7	10	2.8
	75		292		28.8	0.03	8	6	1.6
	95		347	2.9	42.0	0.16	23	6	1.7
	139		339	2.8	33.5	0.24	9	11	1.4
	146		367	3.1	30.0	2.3	12	39	2.5
	168		354	4.8	29.0	4.5	15	37	2.9
	185		384	3.2	21.5	5.5	26	28	2.3
10702#8K	10		200	1.7	49.6	0.10	nd	55	3.0
	74		336	2.5	33.1	0.07	4	28	2.3
	115		389	2.8	21.8	3.3	6	25	1.6
	140		389	3.2	20.0	8.6	23	25	1.7
	165		354	3.2	14.8	11.2	42	31	2.0
	202		354	3.5	15.7	15.0	86	40	5.7
	235		287	2.4	45.2				
	273		363	3.0	19.1	19.9	100	39	5.5
	313		363	3.2		24.8	104	18	3.1
	367		359	2.4	36.5	25.2	109	25	2.7

Depths in Kasten cores corrected for attenuation during sampling by normalisation to 82PCS01

Table 4.ii.3 Radiochemical data for core 10702#8K

Original Sample Depth,cm	Corrected Sample Depth,cm	U ppm	Th ppm	Th/U	$\frac{^{230}Th}{^{232}Th}$ Activity Ratio	$\frac{^{234}U}{^{238}U}$ Activity Ratio	^{230}Th dpm/g	^{234}U dpm/g	$^{230}Th_{excess}$ dpm/g
10702#8K									
0-2	0-2	0.34±0.01	1.32±0.06	3.88±0.21	15.5 ±0.6	1.05±0.05	4.98±0.09	0.27±0.01	4.71±0.09
8-10	8-10	0.39±0.02	1.50±0.06	3.85±0.25	15.8 ±0.05	1.14±0.07	5.38±0.08	0.33±0.01	5.05±0.08
30-32	33-37	1.30±0.05	6.43±0.32	4.95±0.32	3.82±0.17	0.99±0.04	5.97±0.24	0.96±0.03	5.01±0.24
55-57	86-88	1.21±0.04	7.22±0.32	5.97±0.33	3.80±0.13	0.93±0.04	6.60±0.24	0.84±0.03	5.82±0.24
75-77	111-113	0.93±0.03	5.92±0.29	6.37±0.37	3.94±0.17	0.92±0.04	5.66±0.21	0.64±0.02	5.02±0.21
105-107	147-149	0.64±0.02	3.82±0.11	5.97±0.25	3.73±0.10	0.93±0.05	3.46±0.07	0.45±0.02	3.01±0.07
125-127	175-178	0.73±0.03	4.28±0.20	5.86±0.36	4.39±0.17	0.97±0.05	4.56±0.16	0.53±0.02	4.03±0.16
135-137	190-193	1.10±0.03	6.22±0.18	5.65±0.22	3.57±0.08	0.93±0.03	5.39±0.12	0.76±0.02	4.63±0.12
145-147	202-204	0.86±0.03	4.62±0.23	5.37±0.33	3.82±0.15	0.87±0.04	4.28±0.16	0.56±0.02	3.72±0.16
165-167	227-229	0.36±0.02	1.63±0.06	4.53±0.31	6.22±0.23	0.94±0.06	2.47±0.05	0.25±0.01	2.22±0.05
185-187	249-251	0.52±0.03	2.83±0.16	5.44±0.44	5.24±0.27	0.97±0.07	3.60±0.14	0.38±0.02	3.22±0.14
205-207	270-272	0.24±0.04	1.20±0.04	5.00±0.45	6.87±0.22	1.12±0.10	1.99±0.03	0.20±0.01	1.79±0.03
225-227	291-293	0.38±0.02	1.94±0.09	5.11±0.36	5.17±0.24	0.99±0.06	2.44±0.07	0.28±0.01	2.16±0.07
245-247	313-315	0.23±0.01	1.14±0.09	4.96±0.45	6.20±0.50	1.09±0.09	1.72±0.07	0.19±0.01	1.53±0.07
265-267	336-338	0.31±0.02	1.79±0.07	5.77±0.44	4.88±0.18	1.00±0.08	2.13±0.06	0.23±0.01	1.90±0.06
295-297	384-386	0.76±0.03	4.07±0.25	5.36±0.39	2.00±0.10	0.82±0.05	1.98±0.11	0.47±0.02	1.51±0.11

Table 4.ii.4

Oxygen Isotope Stage boundary	Boundary age, kyr	Boundary age, kyr for 10702#8K
1/2	11	9.6
4/5	73	76.6
5/6	127	130.3

Ages of oxygen isotope boundaries for 10702#8K compared with stage boundaries from Pisias & Moore (1981).

Table 4.ii.5

Oxygen Isotope Stage (Pisias & Moore, 1981)	Accumulation rate per stage cm/10^3yrs
1	2.3
2 - 4	2.7
5	2.6

Accumulation rates for isotope stages, 1, 2 - 4 and 5 for 10702#8K (Isotope stage boundaries transposed from 82PCS01).

Table 4.ii.6 Solid phase compositional data for core 10702#8K

Core 10702#8K (42°4.52'N, 23°30.11'W: 3551 m)

Depth Interval cm	Major Element Data, % wt (dry basis)													Trace Element Data, ppm								
	SiO_2	Al_2O_3	Fe_2O_{3T}	MnO	MgO	CaO	K_2O	TiO_2	P_2O_5	LOI	Total	Cl	C_{org}	Rb	Sr	Y	Zr	Ni	Co	V	Cr	Cu	Zn
0-2	3.72	1.21	0.44	0.047	0.51	49.49	0.20	0.06	0.14	43.40	99.22	2.71	0.30	13	1439	9	44	9	8	19	11	23	14
4-6	3.76	1.17	0.44	0.047	0.44	50.03	0.18	0.05	0.15	42.90	99.17	2.43	0.26	13	1422	8	40	9	8	20	10	23	13
8-10	4.12	1.28	0.49	0.051	0.49	49.53	0.26	0.06	0.15	42.79	99.22	1.95	-	14	1379	8	40	10	8	20	10	25	14
15-17	4.82	1.39	0.61	0.051	0.53	48.77	0.03	0.08	0.06	42.18	98.79	2.04	0.19	16	1359	9	40	11	8	23	11	28	16
25-27	14.75	3.76	1.66	0.089	1.30	40.01	0.78	0.21	0.08	36.05	98.69	1.91	-	32	1063	11	67	21	13	43	24	40	31
33-37	23.13	5.80	2.57	0.171	1.76	32.71	1.22	0.35	0.17	30.90	98.78	1.80	0.17	47	825	18	93	42	17	60	34	49	50
42-44	22.16	6.11	2.65	0.216	1.56	32.46	1.25	0.33	0.08	32.03	98.85	1.98	0.31	53	885	19	79	46	27	64	35	59	57
74-76	29.19	6.69	3.11	0.127	2.23	25.58	1.50	0.39	0.08	26.99	96.16	1.59	0.29	60	608	17	97	40	28	69	40	55	55
86-88	26.77	7.49	3.42	0.074	1.61	28.74	1.60	0.40	0.19	28.41	98.70	2.08	0.27	69	778	19	92	37	16	77	43	54	62
111-113	21.43	5.88	2.74	0.031	1.51	33.46	1.22	0.31	0.17	32.13	99.88	1.96	0.24	52	905	17	78	26	12	61	39	37	51
136-138	14.64	4.10	1.78	0.030	1.16	39.49	0.85	0.20	0.06	36.16	98.47	1.88	0.18	41	1091	12	59	21	10	50	29	31	36
147-149	14.78	4.01	1.65	0.034	1.21	39.34	0.81	0.19	0.16	35.68	97.86	1.63	-	35	1087	11	59	15	9	43	28	33	30
175-178	14.70	4.52	1.98	0.044	0.96	39.62	0.85	0.23	0.07	35.83	98.80	1.80	0.21	40	1147	14	68	21	12	51	31	42	39
202-204	17.20	5.06	2.20	0.041	1.09	37.54	0.58	0.26	0.06	34.58	98.61	1.87	0.19	26	1213	11	50	11	6	31	17	19	23
227-229	5.28	1.56	0.62	0.041	0.51	47.82	0.35	0.07	0.05	41.87	98.17	1.82	-	17	1364	12	39	9	5	22	12	28	17
238-240	3.61	1.06	0.39	0.047	0.41	50.00	0.20	0.05	0.05	42.92	98.74	1.92	0.14	13	1430	9	44	6	5	32	9	9	13
249-251	8.10	2.54	1.11	0.045	0.70	45.97	0.84	0.13	0.06	39.77	99.26	1.54	-	49	1157	17	75	26	11	54	34	59	44
271-273	3.94	1.00	0.36	0.043	0.37	49.75	0.39	0.04	0.06	43.12	99.07	1.89	0.17	19	1360	12	54	8	5	22	12	26	19
291-293	5.70	1.70	0.69	0.053	0.53	47.93	0.21	0.08	0.06	41.43	98.38	2.38	0.14	12	1375	7	36	6	3	17	9	11	14
313-315	3.65	1.02	0.34	0.053	0.43	49.79	0.17	0.04	0.06	43.10	98.65	2.12	0.15	12	1359	8	34	5	3	15	9	14	11
336-338	4.23	1.35	0.54	0.074	0.47	49.10	0.29	0.06	0.06	42.36	98.53	1.86	0.14	13	1356	10	50	9	9	19	11	47	21
352-356	8.79	2.64	1.16	0.072	0.70	44.80	0.50	0.14	0.06	39.25	98.11	1.83	-	26	1227	12	66	13	9	32	20	36	27
384-386	15.26	4.33	1.91	0.086	1.03	38.74	1.15	0.23	0.07	35.61	98.42	1.61	0.35	40	1105	14	73	26	16	53	29	37	48

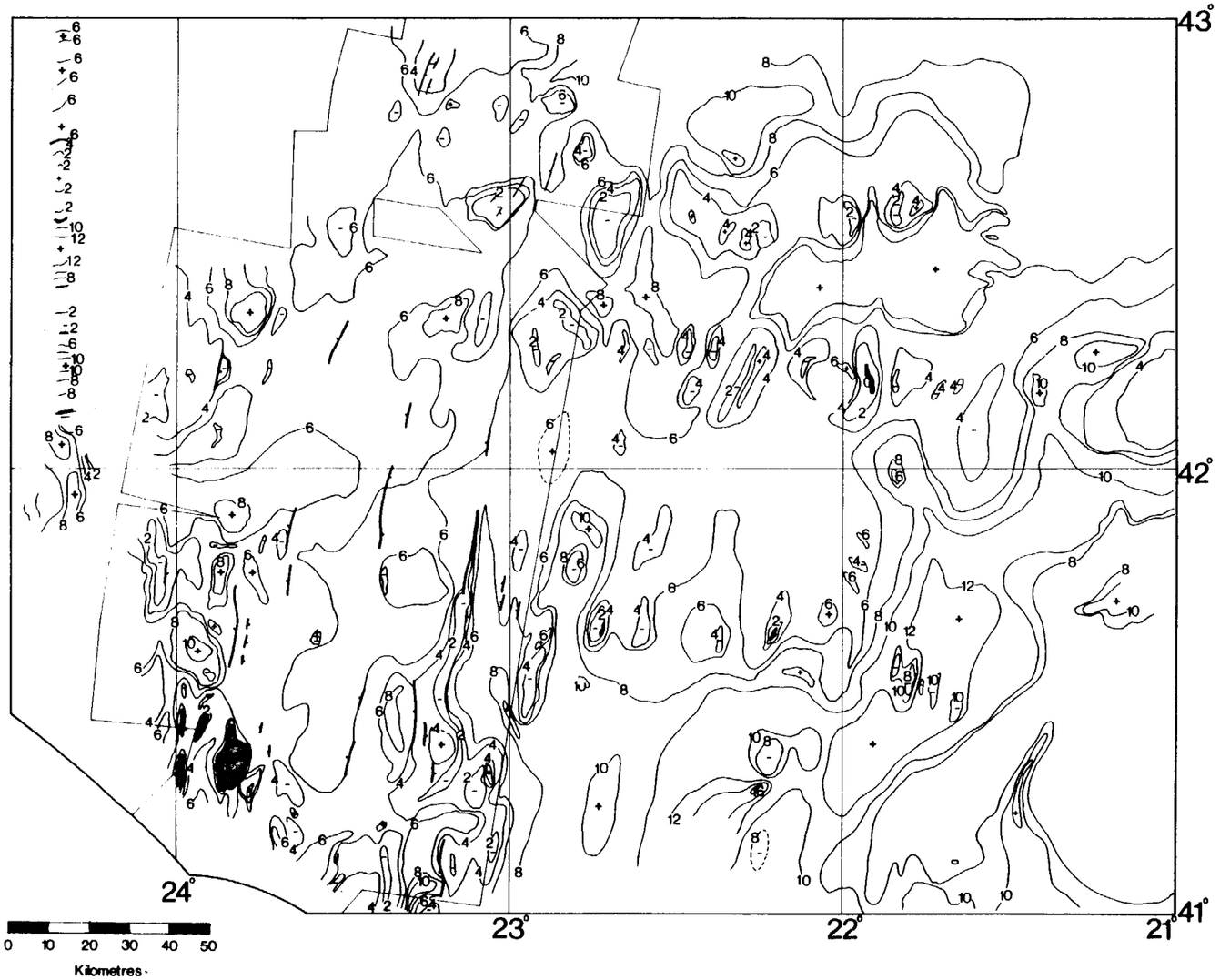

Figure 4.ii.1 Sediment thickness on the KTF study area: isopachs are in 200 m s intervals uncorrected two-way travel time; thin box outline shows GLORIA coverage; faults are indicated from the sonograph interpretation; rock outcrop is black.

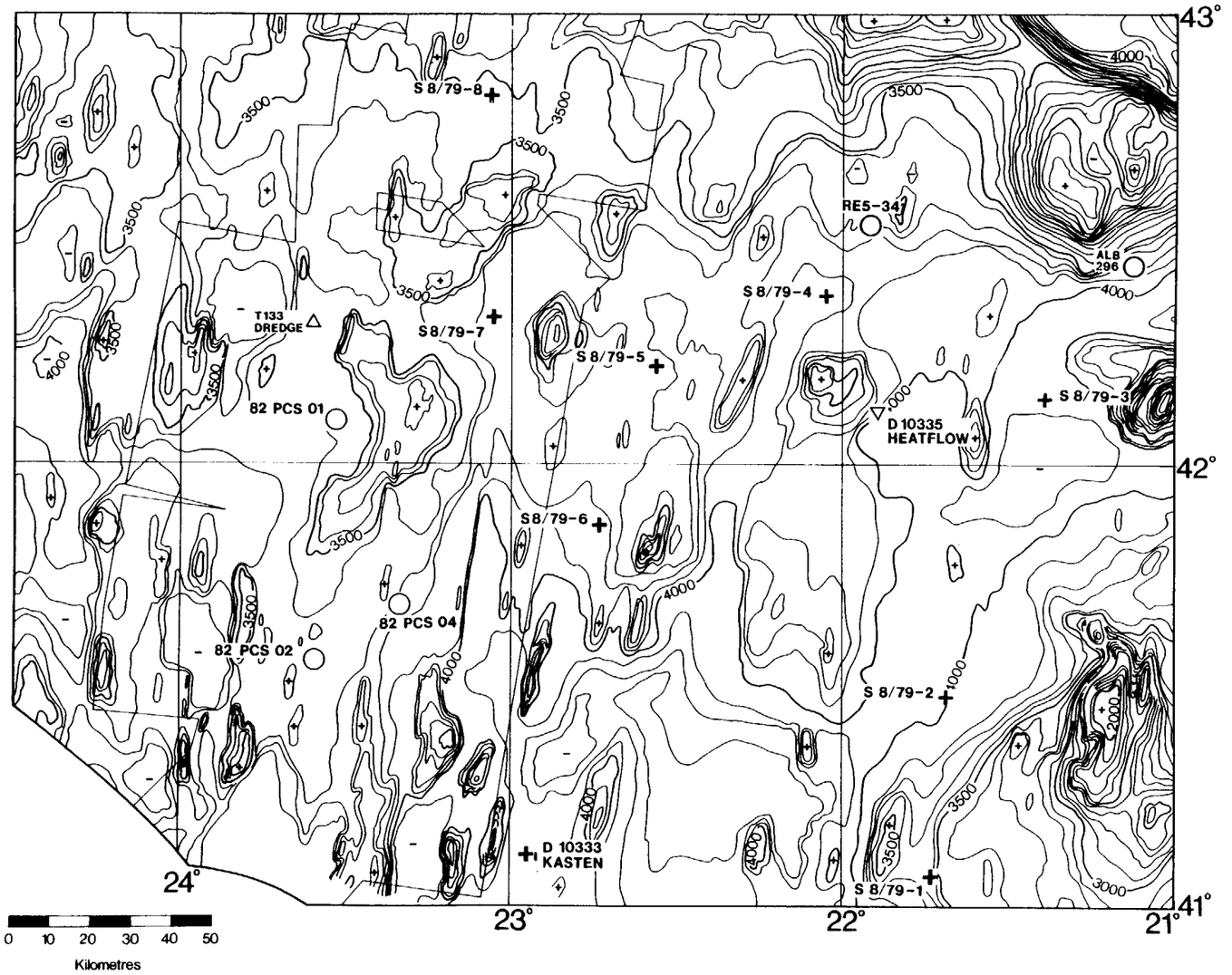

Figure 4.11.2 Location of sampling and heat-flow station referred to in this report. Box outline locates GLORIA coverage, circles are piston cores, crosses are gravity cores, the triangle is the dredge station and the inverted triangle is the heat-flow station.

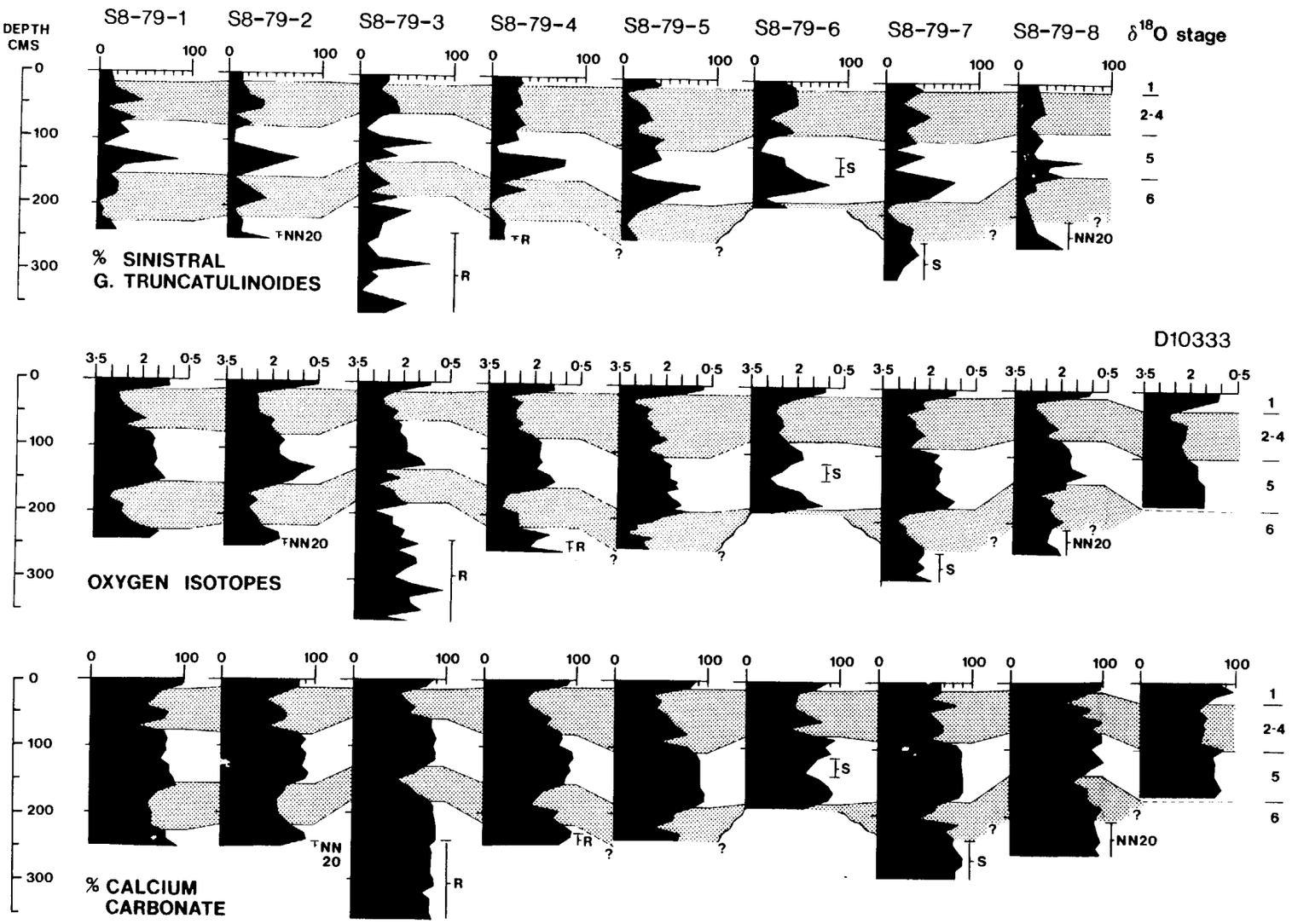

Figure 4.ii.3 Correlation of KTF gravity cores: percentage abundance of the sinistrally-coiled foraminifera Globorotalia truncatulinoides; oxygen isotope measurements, and percentage calcium carbonate. Stippled areas represent glacial intervals; S - slump unit; R - repenetrated unit, NN20 - stratigraphically older units below hiatuses.

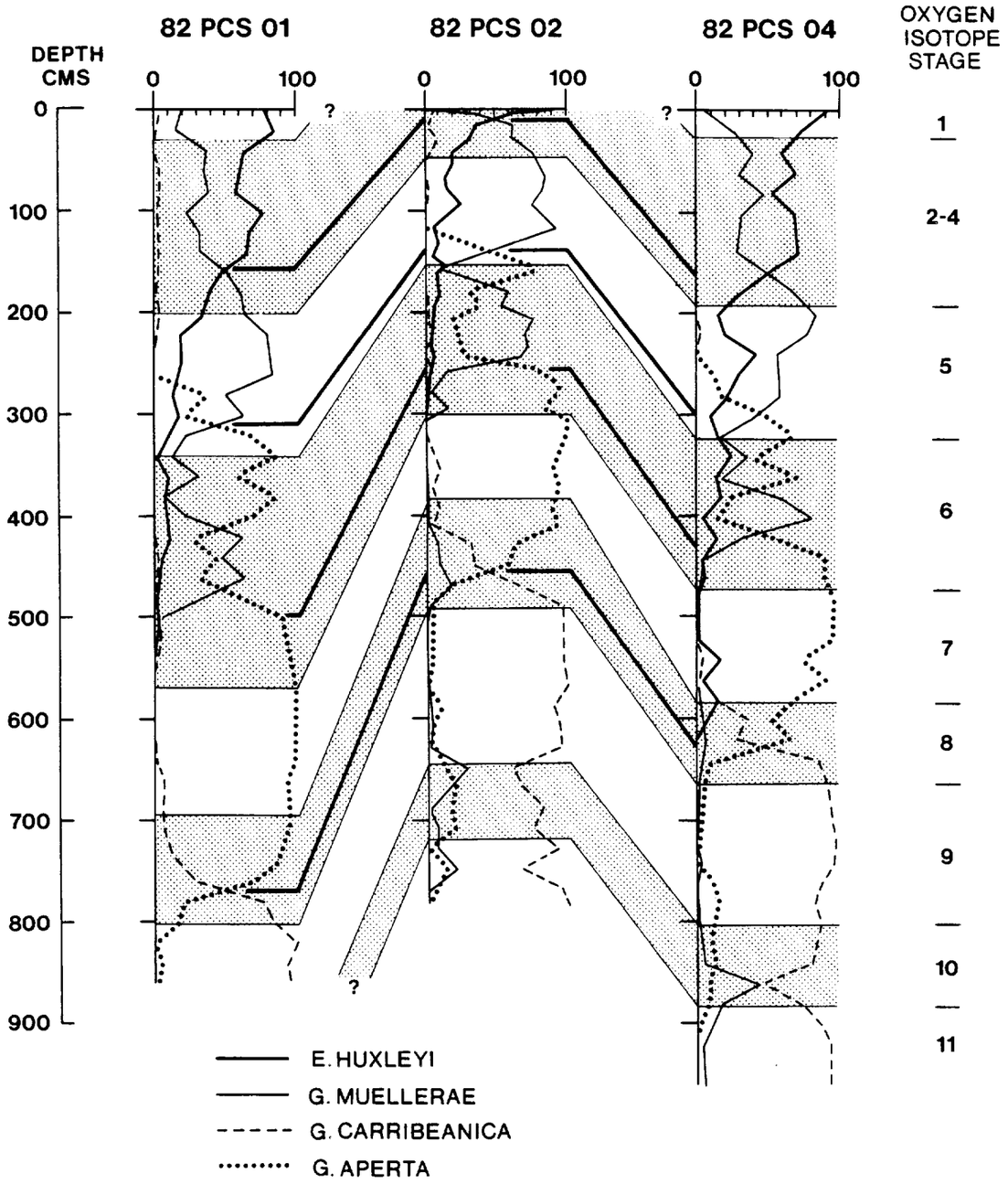

Figure 4.ii.4 Correlation of KTF piston cores: percentage abundance of stratigraphically useful coccoliths in the piston cores; stippled areas represent glacial intervals; correlation lines are thickened.

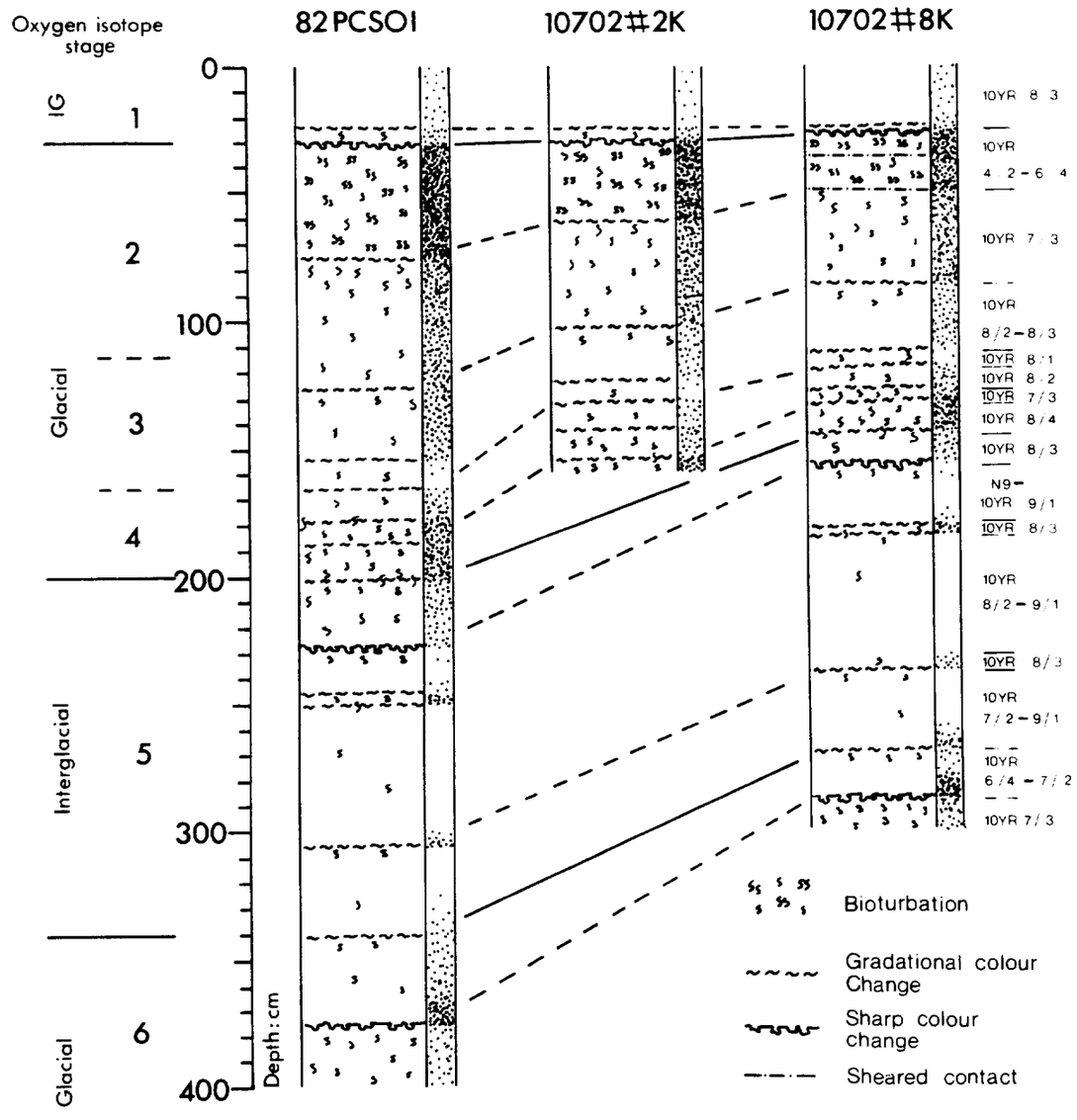

Figure 4.ii.5 Stratigraphic comparisons between closely-spaced cores studied.

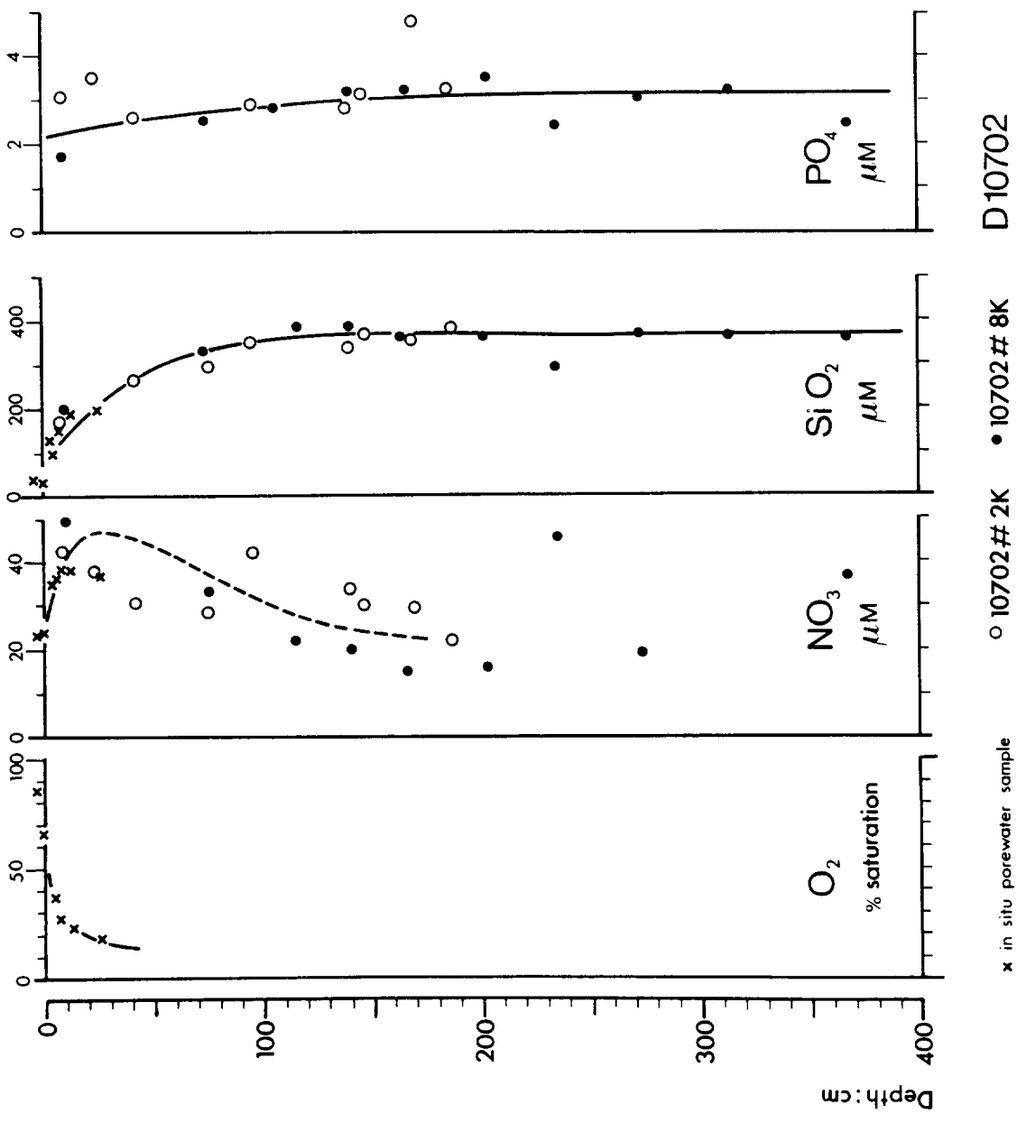

Figure 4.ii.6 Porewater profiles.

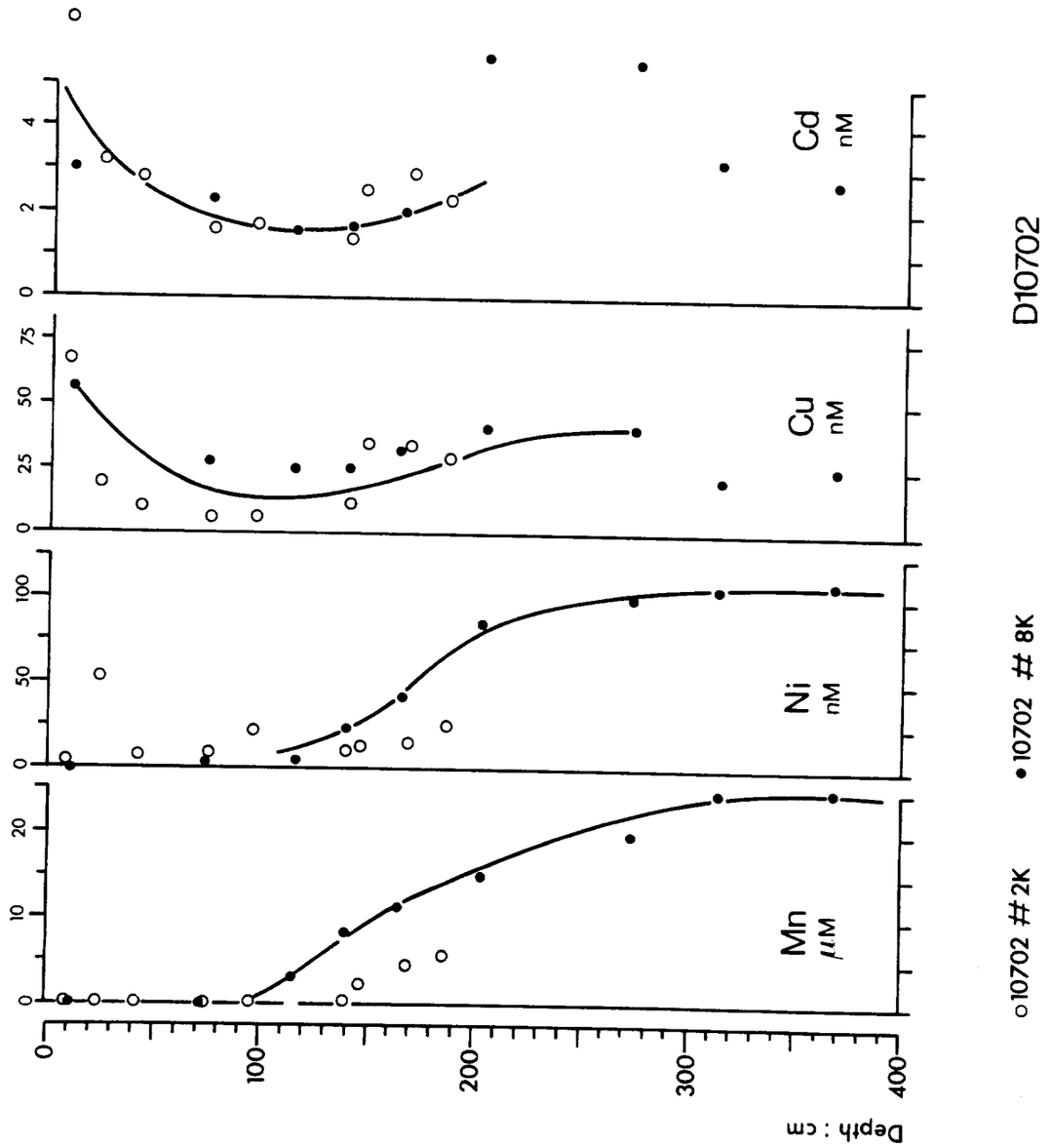

Figure 4.ii.7 Trace element porewater profiles.

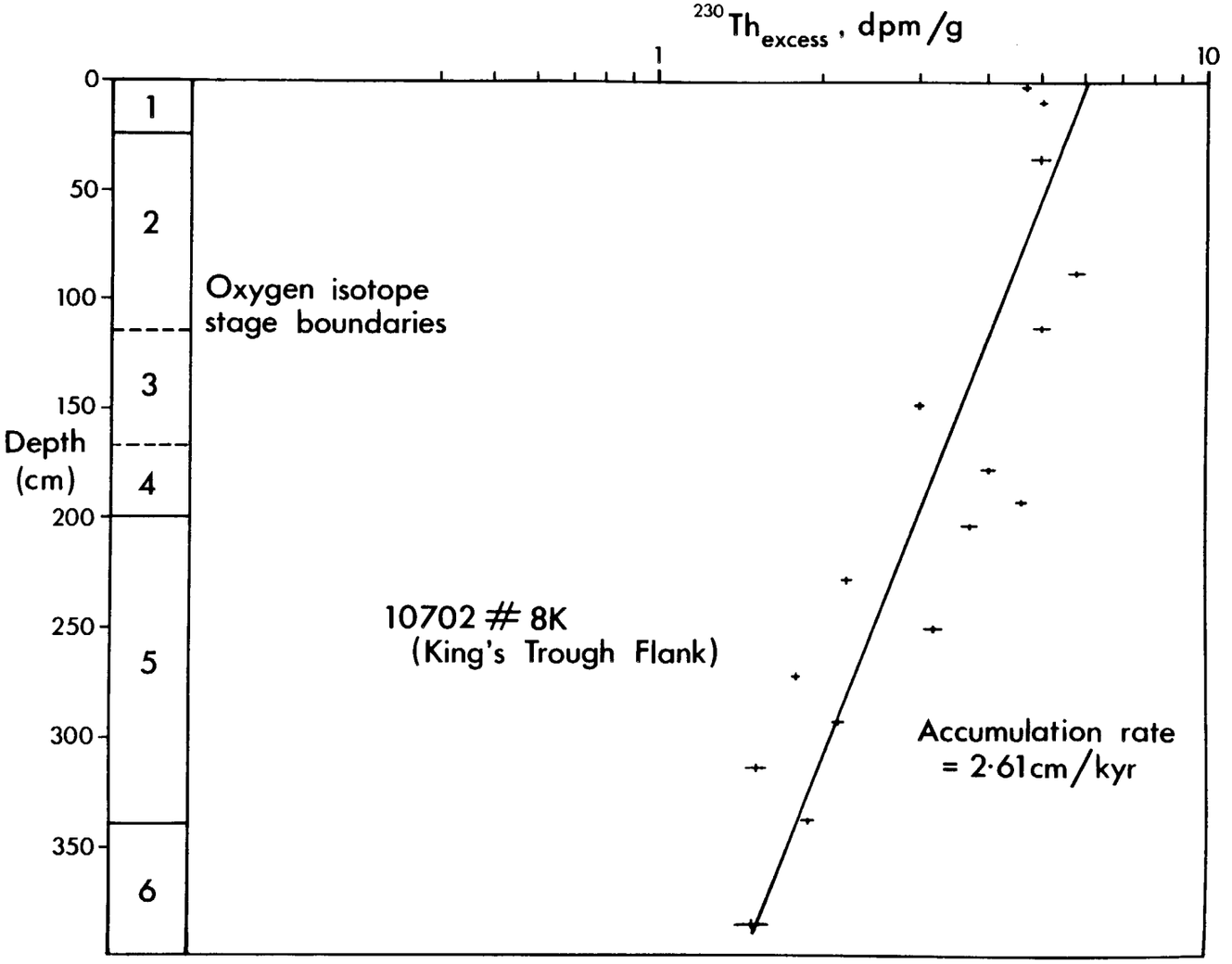

Figure 4.ii.8 $^{230}Th_{excess}$ concentration/depth profile.

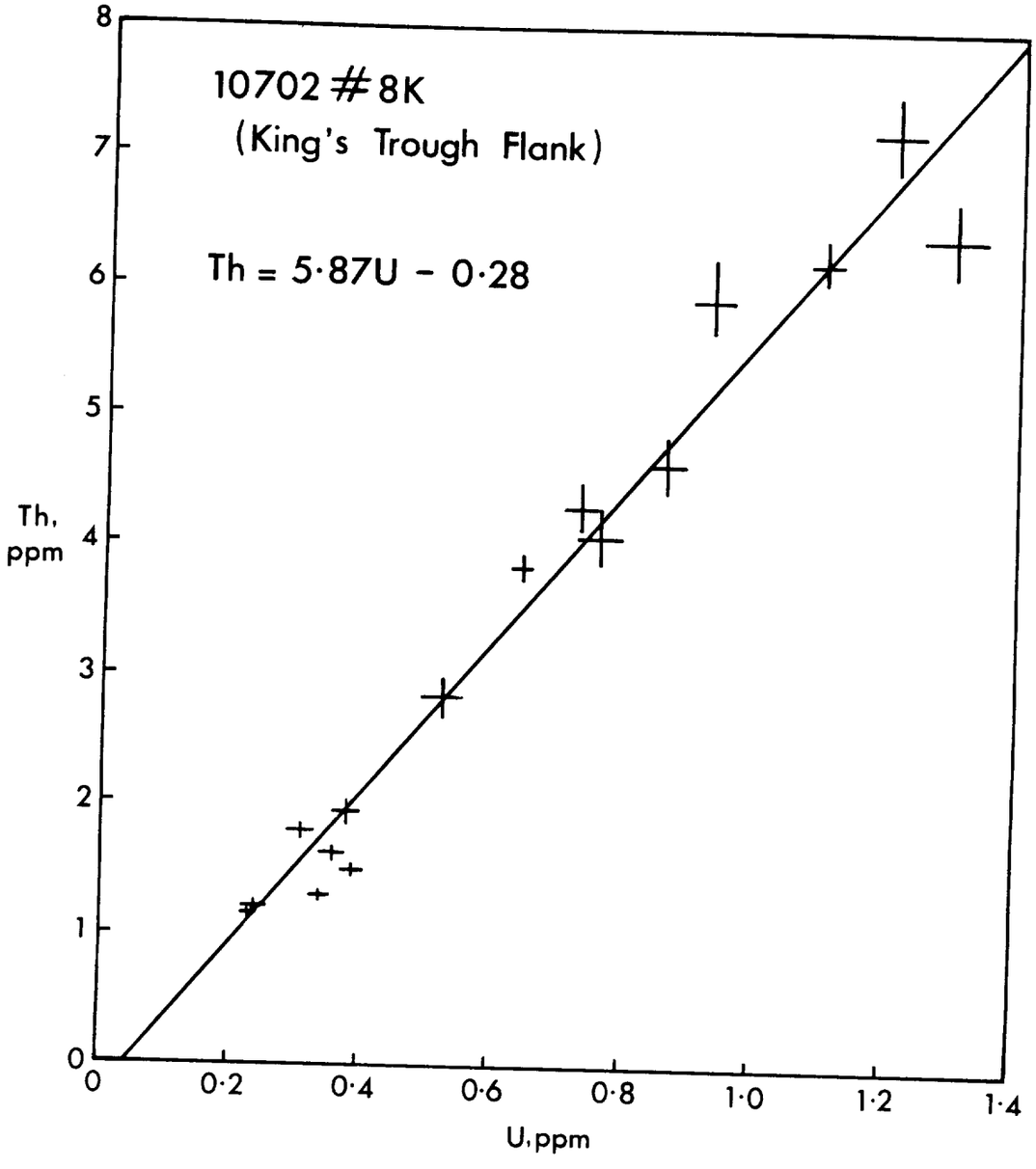

Figure 4.ii.9 Correlation between Th and U in core 10702#8K.

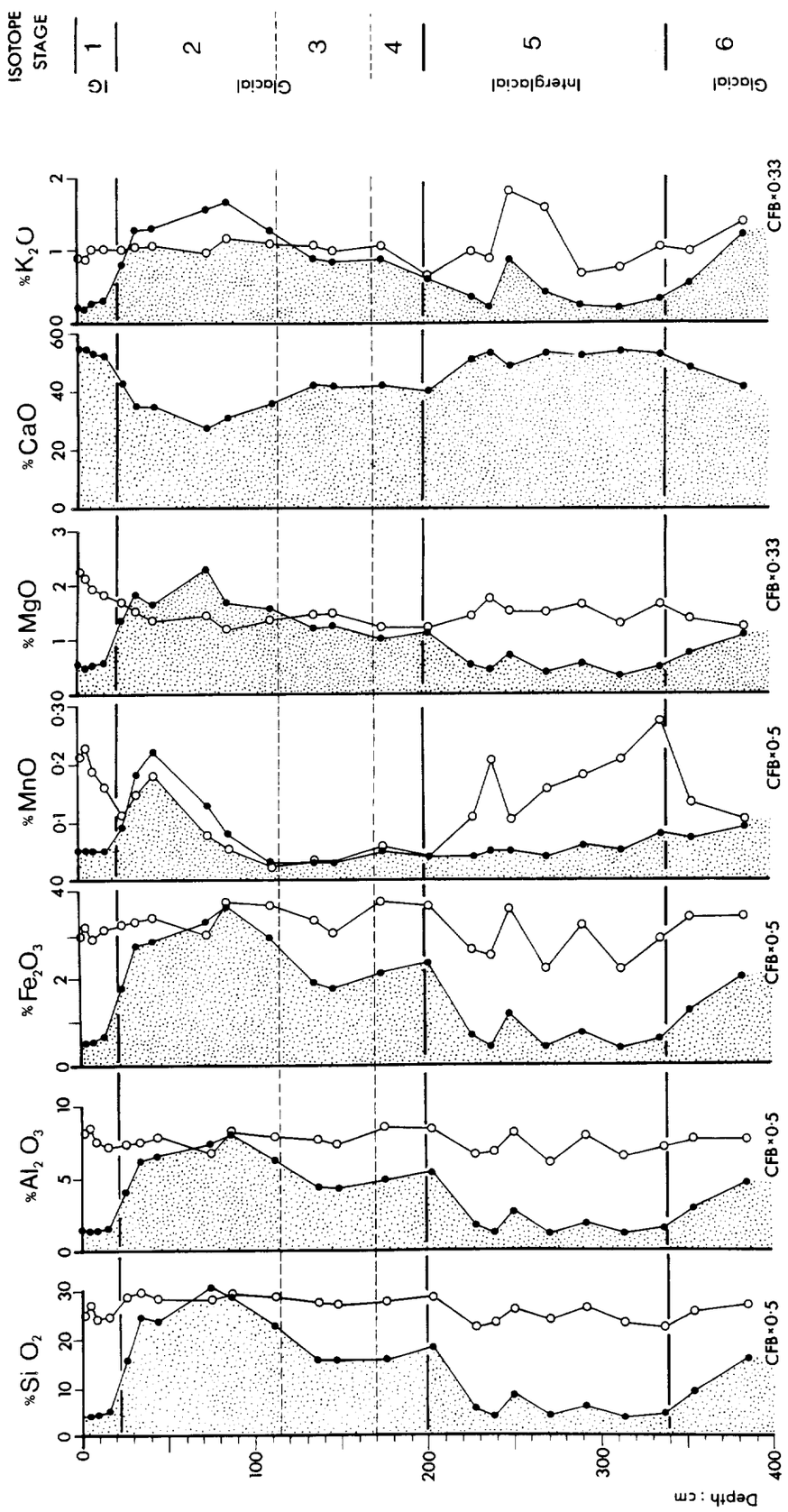

Figure 4.ii.10 Major element concentration/depth profiles for core 10702#8K

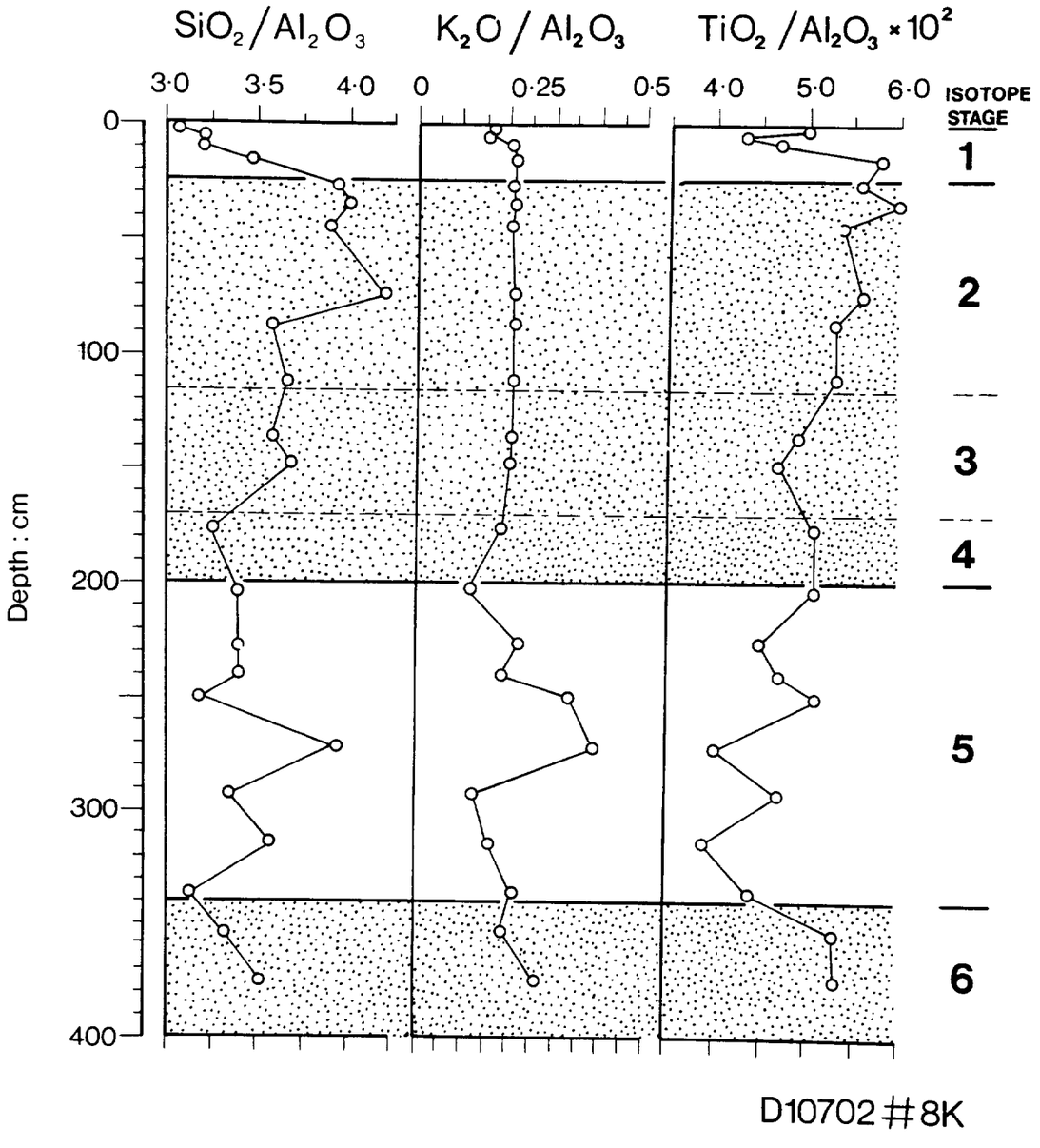

Figure 4.ii.11 Profiles of SiO_2, K_2O and TiO_2 normalised to Al_2O_3.

SAMPLE : D10333/7
SUB-BOTTOM DEPTH : 0.76m
ORIENTATION : VERTICAL
SEDIMENT TYPE : FORAM NANNO MARL

Initial void ratio e_o - - - - 2.431

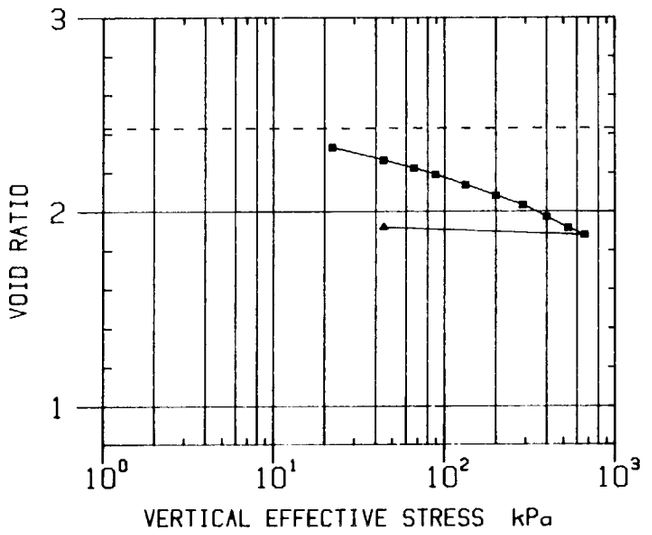

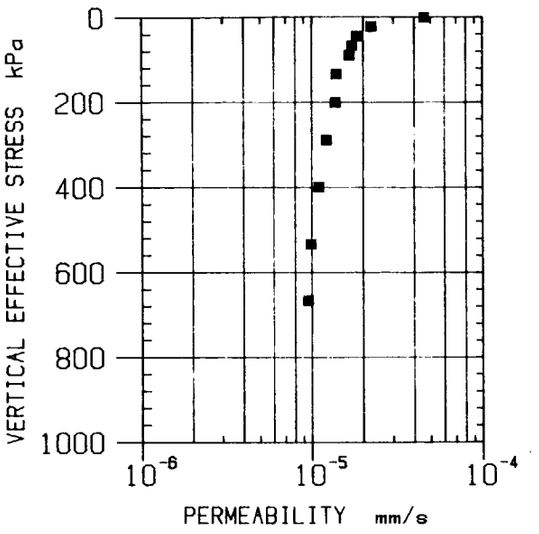

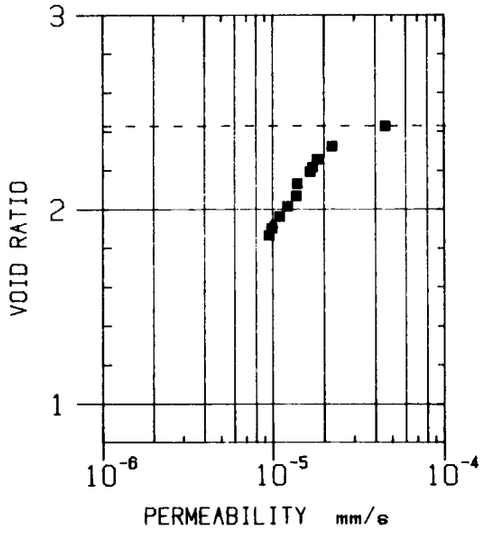

Figure 4.ii.12 Permeability results of a consolidation test on a marl sample, D10333/7, from the KTF area.

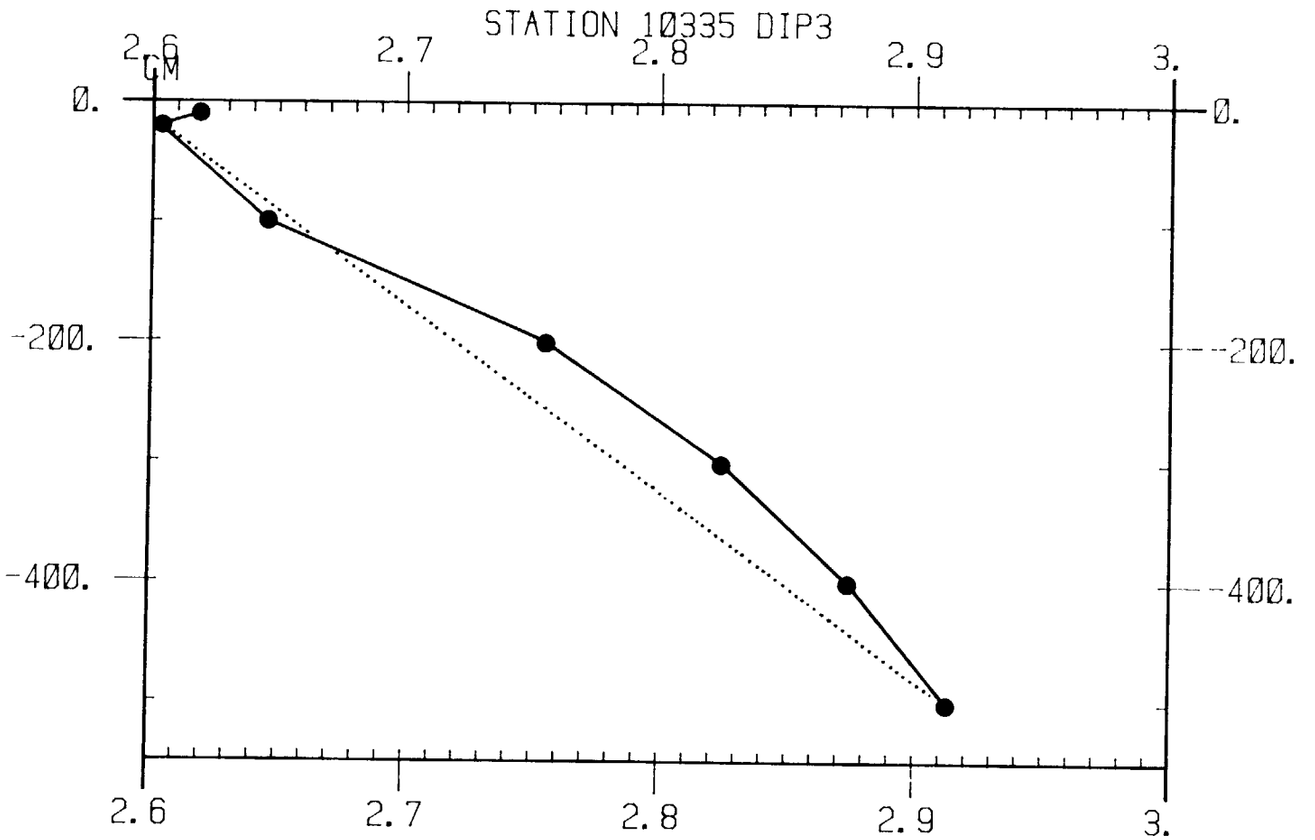

Figure 4.ii.13 Sediment temperature profile at Station 10335/dip 3 in the KTF area, which might indicate upward advection of porewater at 52 cm/yr.

4.iii NARES ABYSSAL PLAIN

4.iii.a Regional Setting

IOS geological involvement in Nares Abyssal Plain has been almost entirely confined to the GLORIA and seismic profiling surveys carried out during Farnella cruise 8, 1982. In addition, a very limited amount of 2 kHz profiling was undertaken during the predominantly chemical cruise Discovery 108. The GLORIA and profiling data have been largely worked up by our US colleagues in the Seabed Working Group, though we have kept a watching brief and have offered comments at various stages. The interpretation is still going on, but a fairly detailed interim report has been produced by Tucholke et al. (1983). Tucholke (1980) has discussed some physical properties of the sediments. Other work by the SWG (principally USA, Canada and Netherlands) is summarised in Nuclear Energy Agency (1984), Auffret et al, (1984a) and Anderson (1984).

Nares Abyssal Plain lies mainly between 22°N and 24°N. At its western end it is linked to the Hatteras Abyssal Plain via Vema Gap at 67.5°W; to the east it runs into the abyssal hills on the lower flank of the Mid-Atlantic Ridge near 60°W. The surface of the plain lies between 5800 and 5900m.

Sediment thickness ranges from about 75m to over 525m, although there are also occasional outcrops of basement in the rare abyssal hills. The majority of the sediment is horizontally bedded and acoustically laminated on seismic records, suggesting that it consists predominantly of turbidites.

3.5 kHz profiles show echo characters ranging from flat, continuous, well-defined sub-bottom reflectors (probably turbidites) to poorly laminated or acoustically transparent bottoms (probably pelagic sediment overlying basement highs).

The 3.5 kHz records show considerable echo focussing (which suggests the presence of very small-scale surface relief), but so far little faulting has been recognised (in contrast to GME).

The GLORIA data show fairly extensive patterns of lineations of a type not observed elsewhere. Our preliminary interpretation is that these reflect sediment transport pathways and facies variations, and this has received limited support from sampling.

However, there is as yet insufficient detailed sampling and geophysical work for a definitive interpretation.

Cored sediments are brown or grey lutites with low calcium carbonate content, although some cores contain layers of coccolith or foram ooze. The lutites are of both pelagic and turbiditic origin, the latter grading from clay to fine silt. The cored sediments appear to be horizontally quite heterogenous on a horizontal scale of 10km or so, and closely-spaced geophysical surveys and sampling are now being undertaken to attempt to understand this variability.

4.iii.b Chemistry

While there is now a reasonable geophysical data base for Nares Abyssal Plain sediments, there is less geochemical information. Chester et al (1973) drew attention to the fact that the elements Mn, Ni and Co were enriched in some (but not all) upper sediments in the south-west area of the North Atlantic relative to a North Atlantic clay average. It was concluded that the enrichments approximated the composition of manganese nodules, and probably were derived from seawater. Addy (1979) examined the rare earth element (REE) contents and patterns of nodules and micronodules from the abyssal hills in the area of the Nares Fracture and Deep Fracture Valleys. From the REE systematics he concluded that these elements in the nodules probably had a seawater origin, although the situation was more complex as regards micronodules. Differences were also found in the contents of Mn, Fe, Ni, Co and Cu of nodules and micronodules co-existing in the same cores (Addy, 1978). Addy (1979) also demonstrated that the red clays which contained micronodules and nodules were enriched in REE, Mn, Fe, Ni and Co relative to the grey clays which had a low ferromanganese phase content.

Similarly, little pore-water data has been published for this region. Addy, Presley and Ewing (1976) report dissolved and solid phase manganese profiles for a single, oxidising site on the north wall of the Puerto Rico trench. They conclude that the observed distributions at this site are due to post-depositional diagenetic remobilisation of a labile, hydrogenous fraction of the manganese at depths greater than 2 metres. Sayles (1979) gives major element data for stations further south, but does not include data on redox-sensitive species. The present paper, therefore, presents the first detailed report on the redox status of the interstitial waters of the Nares Abyssal Plain and in the light of this information discusses the depositional and post-depositional histories of sediments of this area.

Porewaters

In order to interpret the observed solid phase composition profiles, it is important to evaluate the extent of post-depositional mobilisation and migration. For many of the elements of interest, this is a function of the redox potential of the sedimentary environment.

Porewater composition analyses indicate that the sediments sampled are intermediate in redox status between the most oxidising sediments (e.g. Grundmanis & Murray, 1982) at which no reduction is observed, and the much more intensely reducing conditions typical of equatorial and other areas of high productivity (e.g Froelich et al, 1979). In particular, the low levels of dissolved manganese observed (except in core 10164#1K), indicate that active diagenetic remobilisation of this element is not proceeding at present in most of the intervals sampled. From this, it is possible to conclude that the wide variations in manganese content of the solid phase originate either from depositional variations, or from periods of more intense reduction in the past. The latter hypothesis is unlikely. In order to produce the observed profiles, the sediment column would need to have become almost totally anoxic at some time within the last 100,000 years or so. All manganese peaks would then be generated as diagenetic relicts of previous shallow 'stands' of the redox boundary as it migrated downwards towards its presently observed position. It is difficult to visualise such a very strongly reducing profile in this abyssal plain environment. Consequently, it is concluded that the solid phase manganese distribution is predominantly depositional in origin at these sites: exceptions to this are found within the 30-40cm depth interval in core 10164#1K and 140-170cm interval in core 10163#1K (Figure 4.iii.3). In both these intervals, high solid phase manganese values are measured close to the depth at which manganese begins to increase in the pore waters, and these two features are therefore probably diagenetic.

The iodide/iodate couple is an indicator of the redox state of pore waters. Reduction is calculated to take place over the narrow range pE = 10 to 10.7, which means that the couple indicates the depth at which this pE occurs very precisely, though the system is useful over a very limited dynamic range (Wong & Brewer, 1977). For this reason, it would be expected that reduction would take place over a very restricted depth interval (eg Core 10164#1K, Figure 4.iii.2). This behaviour is in fact observed at stations 10164 and 10165, but a more complex

pattern is shown at stations 10163 and 10170 (see Figure 4.iii.2), and it seems possible that these cores are poised at a rather higher pE value than the range indicated above, and further that a strong redox gradient is absent at both these stations. The normally accepted pattern of organic diagenesis in slowly accumulating sediments yields concentration profiles in a characteristic sequence and with a characteristic shape. Because the most intense diagenetic activity is found at the sediment-water interface, the slopes of the concentration profiles are normally greatest near this interface; conversely, slopes approach zero as depth in the sediment increases (Froelich et al, 1979). This simple conceptual model, although consonant with the broad majority of the observations, is inadequate to explain certain features observed in our pore water profiles. For instance, in core 10164#1K the slopes of the silicate, manganese, total iodine and alkalinity profiles do not approach zero with increasing depth but tend to constant positive values: cf Figure 4.iii.2 which compares this core with the more typical 10163 profiles. These observations cannot be reconciled with a simple diagenetic model based on the concept of a constant, slow sedimentary accumulation. Instead, it is necessary to postulate that a relatively recent catastrophic event may have occurred at this site. If such an event had resulted in the burial of organic-rich material at or below 2 metres depth, then profiles of the observed shape could be generated.

In order to test this hypothesis, the fluxes implied by the observed gradients were calculated for the four species mentioned (Table 4.iii.2). Assuming simple one-dimensional diffusion, the minimum time to approximate a steady-state linear profile is given by $Dt/l^2=0.45$, where D is the diffusion coefficient, t is time and l is the diffusion distance (Crank,1956). This gives minimum diffusion times on the order of 400 years for manganese (II) and 140 years for iodine. As the calculated fluxes given in Table 4.iii.2 are quite small relative to the total quantities of material present, the linear gradients could thereafter be maintained for considerable periods by mobilising the solid phase. For instance, the dissolved manganese gradient of core 10164#K could be maintained by the mobilisation of a quantity of solid phase manganese equivalent to the content of a 3cm thick layer of sediment every thousand years.

Similar conclusions can be drawn for other diffusing species in this core. It is thus clear that the pore water profiles at this site support the hypothesis that sedimentation has been sporadic and catastrophic, rather than continuous and gentle. Similar, but less dramatic, episodes may have occurred in some sections of other cores sampled. These conclusions are in agreement with the ^{230}Th data (see next section).

Sediment Accumulation Rates and $^{230}Th_{excess}$ data

It has been remarked by Shipley (1978) and Keller & Lambert (1979) that there is a paucity of sediment accumulation rate data for the Nares Abyssal Plain, and in this study radiometric data for the $^{230}Th_{excess}$ method were gathered in parallel with the elemental data for this suite of cores. This method is based on the phenomenon of constant production of ^{230}Th by decay of ^{234}U in the water column, and its subsequent rapid removal and incorporation into the sediments. The customary procedure is to estimate a mean accumulation rate for the sediment column by measuring the decay of unsupported ^{230}Th ($^{230}Th_{excess}$) with depth (Ku, 1976; Goldberg & Bruland, 1974). By convention $^{230}Th_{excess}$ equals the total ^{230}Th specific activity measured minus the corresponding ^{234}U specific activity. If the rate of sediment accumulation has been constant in time, then:

$$\ln A = \ln A_{\circ} - \lambda . z/s$$

where A is the $^{230}Th_{excess}$ specific activity at depth z, $A_{\circ}$ is the sediment interface value of $^{230}Th_{excess}$, λ is the decay constant for ^{230}Th and s is the sediment accumulation rate. Figure 4.iii.4 illustrates plots of the data from the four box cores treated in this fashion, with mean sediment accumulation rates obtained from the slopes of the best-fit lines. (No rate can be estimated for core 10165#2BX because grey clay with low $^{230}Th_{excess}$ values is observed below 20cm, and this core will be discussed later along with the Kasten cores. Although a thin lens of grey clay is also observed in core 10163#3BX, a regression line has been drawn in this case because the influence on the full core section is minor.) For core 10164#5BX, $^{231}Pa_{excess}$ data are available (Table 4.iii.10). These may be treated similarly to $^{230}Th_{excess}$ data and yield an independent (if less accurate because of lower activity levels) estimate of accumulation of $0.42cm/10^3$ yr which compares with the value of $0.49cm/10^3$ yr from the $^{230}Th_{excess}$ method.

The process of bioturbation is commonly observed in the uppermost few centimeters of sediment in deep sea deposits (Turekian et al, 1978), even in some slowly accumulating clays (Cochran & Krishnaswami, 1980). This feature is not observed within the resolution of the data here and has been ignored in the calculation of mean rates. These three box cores yielding sedimentation rates are interpreted as having been formed under pelagic conditions, and are referred to subsequently as slowly accumulated brown clay.

It should be noted that the accumulation rates obtained (0.49 - 1.02 cm/10^3 yr) are higher than those estimated by Shipley (1978) for the brown clay in this area since mid-Cretaceous time (0.1 - 0.3 cm/10^3 yr). They translate, however, to clay fluxes of 0.3 - 0.7 g/cm^2/10^3 yr, which are not unusually high values for Atlantic sediments in the past 100,000 years (Turekian, 1965; Bacon, 1983). Shipley (1978) observed that brown clay always overlay the uppermost grey unit in the cores he studied, and used his long-term accumulation rates to estimate that turbidity current activity (as revealed by the presence of grey clay units) had not been active for 300,000 years in the area. If the higher recent accumulation rates determined here are also applicable to the abyssal hills in the area of the Fracture Valleys where most of his cores were taken, they suggest that 300,000 years will be an overestimate. Specifically, a grey silt layer is found within 12cm of the surface in core 10163#3BX, a depth corresponding to an age of only 15,000 years.

$^{230}Th_{excess}$ data obtained for the two Kasten cores are illustrated in Figure 4.iii.5. The section 29-71cm in core 10163#6K yields a rate of 0.51/10^3 yr and like the three box cores above is interpreted as slowly accumulated brown clay. Nevertheless as with the case of box core 10165#2BX, no plausible sedimentation rate can be derived for most of the Kasten core sections because low and erratic $^{230}Th_{excess}$ values are observed. The $^{230}Th_{excess}$ method has little power when lateral movement and consequent sediment mixing has occurred. First, low $^{230}Th_{excess}$ values are expected when a sediment section moves, is mixed and redeposited; and second, rapidly accumulated sediment from shallower water will have low $^{230}Th_{excess}$ levels even before it is moved and introduced to greater depth. The interpretation of the grey clay units as turbidites leads to an expectation of low specific activities, and this is in accord with observation in the sections 150-200cm in core 10163#6K and 50-160cm in core 10164#1K.

A further useful aspect of $^{230}Th_{excess}$ data is that a comparison may be made of the sediment inventory of $^{230}Th_{excess}$ activity with that anticipated by supply from the overlying water column. ^{230}Th has one of the shortest water residence times known (Bacon & Anderson, 1982) and the consensus opinion is that it does not tend to move out of the ocean basin in which it is formed (Bacon & Rosholt, 1982). In view of calculations made later in this paper to estimate the fluxes of various elements removed from the water column to the sediments, it is of interest to make this sediment/water column comparison for $^{230}Th_{excess}$. The comparison

is in Table 4.iii.3, where the water column supply is calculated from the uranium content and $^{234}U/^{238}U$ activity ratio of sea water (3.3 µg/ℓ and 1.14 respectively, Ku et al, 1977) and the sediment column inventory evaluated from the expression (Krishnaswami et al, 1971):

$$\Sigma = \frac{p.s.A_o}{\lambda}$$

where Σ is the $^{230}Th_{excess}$ inventory per cm^2, p is the in situ dry sediment density (measured for the slowly accumulated brown clay as $0.65 g/cm^3$), s is the mean sediment accumulation rate, A_o is the interface (regression line intercept) $^{230}Th_{excess}$ specific activity and λ is the ^{230}Th decay constant. It is evident from Table 4.iii.3 that there is marked shortfall, around 40%, in the sediment inventory. Kadko (1980) found a deficit of 28% for 28 cores from the literature taken in water depths, between 4600 and 5800m, but attributed at least part of this to the effects of surficial sediment mixing on his model calculations. The reasons for the shortfall here are unclear, but the consistency for all three box cores suggest that the sediments are systematically failing to record the $^{230}Th_{excess}$ production of the full water column depth.

Geochemical and mineralogical characterisation

This discussion is based on 62 sediment subsamples taken from four box cores and two Kastenlot cores obtained on four stations. Alternate layers of grey and reddish-brown clay were described in all cores taken at water depths greater than 5700m (Table 4.iii.1) the grey clays generally forming graded silty units 10-80cm thick with coarse, sharp bases. The cores lacking grey silty interbeds were taken at shallower water depth; on a small topographic high (core 10164#5BX: 55cm homogenous brown clay in 5613m) and above the carbonate compensation depth on the northern flank of the Puerto Rico Trench outer ridge (core 10170#1BX: 60cm of yellowish grey marls and brown clay in 5520m).

These observations are in agreement with those of Shipley (1978), who concluded that the brown and grey clays are ultimately derived from the same source but that the grey clays represent distal turbidites (containing more silt-sized material) and the brown clays represent slow pelagic deposition. In this study, the following classification of sediment types has been adopted as a result of both core description and analytical data:

1. Homogenous brown clays, subdivided into:
   (a) metal-rich or slowly accumulated brown clays,
   (b) metal-poor brown clays.

2. Grey clays with some silt-sized material.

3. Assorted minor lithologies, predominantly laminated and mottled clays and predominantly red/brown/orange in colour.

The first two major lithologies mentioned above account for 46 out of a total of 62 analyses, whereas minor lithologies such as orange and tan clays, laminated clays and yellowish marls, account for 16 analyses. Although the grey clays (18 analyses) are very heterogenous as a group (see Table 4.iii.4), this variability is coherent in the sense that it can be explained in terms of co-variance of well correlated variables (see Table 4.iii.5). The minor lithologies are included in the overall mean of Table 4.iii.4 even though, as a group, they lack both chemical homogeneity and statistical coherence.

It is only in conjunction with $^{230}Th_{excess}$ data that it is possible to subdivide the homogenous brown clays (28 analyses) into 1(a), slowly accumulated brown clays (16 analyses) with clear enrichment in metals generally regarded (e.g. reviews by Chester & Aston, 1976; Murray & Brewer, 1977) as hydrogenous (Mn, Cu, Ni and Co) and 1(b) brown clays (12 analyses) with little or no enrichment in hydrogenous metals, i.e. metal-poor deep sea clays with no evidence for slow, pelagic deposition ($<1cm/10^3$ yr) yet exhibiting no evidence of turbidite characteristics.

In general, the variations in mineralogy between brown and grey clays support the suggestion of Shipley (1978) that colour differences are not reflected in a primary way in mineralogy. XRD mineralogical scans on the same samples used for XRF analysis have revealed a marked but variable enrichment of calcite and quartz contents in the grey clays (up to 9% calcite and 15% quartz contents) compared with homogenous brown clays (<2% calcite and <8% quartz). Nevertheless, there appears to be little systematic difference in clay mineralogy between the brown and grey layers, as observed by Addy (1978) and Shipley (1978).

The major significant difference between slowly accumulated brown clays, metal-poor brown clays and grey clays are best summarised by correlation matrices for

each group which identify the main controls on co-variance amongst the major and trace element data base (see Table 4.iii.5). Chemical variation between groups can then be accounted for by changes in the relative importance of five cluster groups which are as follows:

i. Ni, Co, Cu and MnO - micronodules are evident in the samples exhibiting this association; (both slowly accumulated and metal-poor brown clays).

ii. Al_2O_3, Zn, V and Fe_2O_3T - these elements are partly related to the Fe-rich hydrogenous component in slowly accumulated brown clays, and partly associated with impurities in kaolinite and/or chlorite in grey clays. They are excluded from the carbonate phase, and from metal-poor clays.

iii. K_2O, Rb and Cr - these elements are associated with illite (the dominant clay mineral phase in all groups). Cr may be associated with illite and chlorite in grey clays, but is excluded from illite in slowly accumulated brown clays.

iv. Sr, CO_2, organic C and CaO - here the association is with biogenic calcite, found mainly in grey clays.

v. SiO_2, Zr and Nb - these elements are associated with the quartz variation in grey clays.

These five groups of well correlated elements have been interpreted (see Table 4.iii.5) in terms of mineralogical control, i.e. good positive correlations between pairs of elements are taken to imply a process such as solid solution or an association due to inclusions or coatings, whereas negative correlations imply an exclusion or dilution effect. If the major and trace element data base were recalculated on a salt-free, carbonate-free basis, the conclusions drawn from correlation matrices would no longer be valid, due to the removal of a major source of variance ($CaCO_3$) and the discrimination between slowly accumulated brown clays and grey clays would become statistically significant (at the 1σ level) only for organic carbon, Rb and the hydrogenous metals, Mn, Ni, Cu and Co.

In comparing the metal-rich brown clays (type 1(a)) with the grey clays (Table 4.iii.4), it is apparent that the metal-poor homogenous brown clays and the assor-

ted minor lithologies are intermediate in composition between the two end members (pelagic clays and turbidites) in most respects apart from carbonate content. This overall enrichment in preserved biogenic calcite in grey clays is consistent with an initial rapid deposition and burial of biogenic material and subsequent transportation from shallower water sites to the Nares Abyssal Plain by turbidity currents. A comparison of the group mean compositions in Table 4.iii.4 shows that slowly accumulated brown clays differ from metal-poor brown clays in having generally higher average contents of MnO, Ni, Cu and Co, but significantly lower contents of K_2O, Rb and Cr. These differences can be explained if the metal-poor brown clays result from either an in situ mixing of compositionally distinct end members (i.e., pelagic clays and turbidites) or a chemical fractionation related to transport and settling of particles during a waning current regime. The latter hypothesis is supported by the grain size and mineralogical variation from grey silty clays through laminated clays to homogenous brown clays, which is observed in vertical succession in certain cores (10163#6K and 10164#1K).

The average grey clay composition as presented in Table 4.iii.4 bears certain similarities to an average shale composition (Wedepohl, 1968) which is itself representative of near-shore type sediments. However, the SiO_2/Al_2O_3 ratio is much lower in the grey clays here (2.96) than Wedepohl's average shale (3.52) and there appears to be some enrichment in $Fe_2O_{3_T}$, MgO, TiO_2, Co, V and Zn, even when account is made for quartz dilution. It must be stressed that the grey clays are very heterogenous as a group and that their range of variation (apart from SiO_2, MgO, Rb, Sr, Y, V and Zn) encompasses average shale composition. The average mineral composition of shales (Wedepohl, 1971) shows much more quartz and feldspar than any Nares grey clays (see Table 4.iii.6), whilst the proportion of kaolinite is much greater in all the Nares sediments than average shale and also most North Atlantic sediments (Griffin et al, 1968; Windom, 1976).

Since the metal-poor brown clays are intermediate in composition between slowly accumulated brown clays and grey clays, we can assume that they probably result from intermediate and limited up-take of hydrogenous metals onto an illite dominated detrital matrix. This detrital assemblage shows evidence of grain size and mineral fractionation away from rapidly accumulated grey clay - the coarsest fraction of the silty grey clays appears enriched in quartz and has a clay mineralogy dominated by illite and chlorite. An enhancement of kaolinite in the slowly accumulated brown clays (relative to average shale) reflects either the finest grained

fraction of transported near-shore sediment, or alternatively may reflect a greater proportion of windborne dust derived from the NE Trade Winds (Delany et al, 1967). Under no condition, however, can the trace element abundance pattern of the NE Trades aeolian dust (Chester & Johnson, 1971) explain the hydrogenous element enrichment of the slowly accumulated brown clays in the Nares Abyssal Plain.

In conclusion, the slower the rate of sedimentation for a particular core section, the greater is the uptake of hydrogenous metals and the greater is the relative proportion of kaolinite in the bulk mineralogy. Thus there is an association between fine grained kaolinite and micronodules in the more pelagic of the Nares Abyssal Plain brown clays. The rate of accumulation for the metal-poor brown clays must be slow enough to ensure almost complete decomposition of organic material within the sediment whilst being fast enough to limit the growth of micronodules and coatings rich in hydrogenous metals. The more rapidly deposited grey clays lack micronodules and are comparable in terms of chemical composition to near-shore sediments - thus the grey clays represent a sporadic, detrital input of sedimentation which can be mixed in variable proportions with a pelagic component to produce the sections observed.

A model for metal accumulation in the slowly-accumulated brown clay

As discussed in the previous section, a comparison of the metal contents of the sediments with the $^{230}Th_{excess}$ data suggests an association between the elements Mn, Co, Ni and Cu and $^{230}Th_{excess}$ levels in the homogenous brown clay sediment types. Where the $^{230}Th_{excess}$ specific activities are high in the pelagic brown clay sections (indicating slow accumulation rates), high concentrations of those elements are also found. The converse also holds, for example in core 10163#6K between 80 and 100cm, where the homogenous brown clay has low $^{230}Th_{excess}$ values, these transition element contents are not greatly enriched over shale values (Figures 4.iii.3. and 4.iii.5.). The fact that low contents of the redox sensitive element manganese are observed in the pore waters of the box core sections with high metal contents is taken as evidence that diagenesis is not the primary cause of enrichment. It has been remarked previously that $^{230}Th_{excess}$ is considered to be supplied to the sediment entirely by scavenging from the water column, so it appears reasonable to expect a similar source for the transition element enrichment. This expectation prompts examination of the fluxes of the transition elements in the four instances where the radiometric data yield reasonable accumulation rates (29-71cm in 10163#6K, and the box cores 10163#3BX, 10164#5BX and 10170#1BX).

In Figure 4.iii.6 the metal data have been averaged over the same core section intervals for which $^{230}Th_{excess}$ mean accumulation rates have been estimated, and their mean fluxes plotted against the total accumulation fluxes for the same intervals. This procedure is similar to a model developed by Turekian (1965) for the case where all or part of the trace element content of a sediment is added at a rate independent of the clay accumulation rate (in fact Turekian did not find any case to utilise this model but suggested that $^{230}Th_{excess}$ might approximate to it). Here it is used to evaluate the concept that the transition element content is a function of a constant hydrogenous flux superimposed on a variable detrital flux of constant composition:

$$\Sigma F = F_H + k.s$$

where ΣF is the total mean flux of the element, F_H is the hydrogenous flux of the element, s is the total mean sediment flux and k is the concentration of the element in the detrital phase. The regression line data in Figure 4.iii.6 therefor allow evaluation of both the hydrogenous flux and of the detrital phase content (Table 4.iii.7). These values are averages over the sampled area of the Nares Abyssal Plain over a period of around 100,000 years. The linearity of the plots supports the assumption that the composition of the hydrogenous flux is constant over the area. Secondary factors not taken into account are the differences in water column depth and the indications from the box cores that there is a deficit in the $^{230}Th_{excess}$ sediment inventories relative to water column supply.

The approach taken above is similar in concept, though different in approach, to other work with a similar theme of a constant hydrogenous flux superimposed on a detrital matrix of constant composition. Among these are the "trace element veil" concept for the world ocean as described by Wedepohl (1960) and further developed and criticised by Turekian (1965, 1967), the "constant flux model" developed for Pacific sediments by Krishnaswami (1976) and the "constant water column supply model" of Bacon & Rosholt (1982) invoked for a site on the Bermuda Rise. There appear to be few other estimates of hydrogenous flux deduced from sediments. It is clear from Table 4.iii.7 that there is only a modest agreement between the magnitudes of the fluxes obtained and literature values. Nevertheless, there does appear to be a tendency for the fluxes to decrease in the order observed here, i.e. Fe > Mn > Cu > Ni > Co > Zn $\sim$ V.

Recent work on the trace element content of seawater with low-contamination analytical procedures have reduced estimates of the absolute concentrations of most of the elements just discussed. As a consequence of these more accurate data an improved understanding of the element water column relationships with the major nutrients phosphate and silica has been established (Bruland, 1980, Boyle et al, 1981). Copper exhibits additional complexities in behaviour due to deep water scavenging and a regeneration into bottom water from diagenesis at shallow depth in sediments (Boyle et al, 1977, 1981). Manganese is believed to be scavenged from the dissolved to the particulate phase throughout the water column (Klinkhammer & Bender, 1980; Landing & Bruland, 1980) and a similar behaviour has been proposed for cobalt (Knauer et al, 1982). While the relative importance of these different water column geochemistries may well vary from area to area of the ocean and vary the magnitude of the different fluxes, it appears that these variations do not dramatically alter the sequence observed. It is also noteworthy that the hydrogenous flux values determined for the north-east Atlantic are higher than those obtained for the Pacific by Krishnaswami (1976) from a widely-spaced selection of cores.

Following the suggestion of Chester et al (1973) that sediment enrichments in this area approximate to the composition of manganese nodules, a further comparison of the model-derived hydrogenous fluxes (Figure 4.iii.6 and Table 4.iii.7) can be made with authigenic ferromanganese phases (nodules and micronodules) from the area of the Nares Fracture Valleys (Addy, 1979). Figure 4.iii.7a illustrates the result of this comparison, using mean values obtained from Addy's (1979) data. In order to display all the information simultaneously it has been necessary to normalise the data against average shale. The plot for the hydrogenous flux has as its fixed point the same Mn enrichment factor (around 200) as that of the two micronodules selected. It is evident that the plots for nodules, micronodules and the hydrogenous flux are generally of the same order of size and sequence except for Cu. A perfect agreement is not expected, as Moore et al (1981), for example, have demonstrated that the top and bottom of a single nodule and its co-existing sediment can all have markedly different relative enrichments of Fe, Mn and cogeners. Addy (1978) has also shown from a comparison of complementary nodules and micronodules that differences usually exist. The best agreement in Figure 4.iii.7a is between the mean of two of Addy's (1979) separated micronodule fractions which were selected because they show the same Mn/Fe ratio as the hydrogenous flux. This might be expected as the slowly accumulated brown clays, which

were the dominant sediment type used in the model to derive the hydrogenous flux, do themselves contain micronodules. Thus the same pattern of relative enrichment over shale values is also evident in Figure 4.iii.7a for the means of the slowly accumulated (or metal-rich) clay type (Table 4.iii.4).

The model also provides values for the detrital matrix on which the hydrogenous flux is superimposed. As can be seen from Table 4.iii.7, these estimates are in close agreement with the mean grey clay composition listed in Table 4.iii.4 except for manganese where diagenetic remobilisation is a known problem. This further supports the idea already discussed of a similar source, close in composition to average shale (Wedepohl, 1968), for both the brown clay and the grey clay types. The estimated detrital values also compare well with other data, from different methods, from the Bermuda Rise (Bacon & Rosholt, 1982) and the North Atlantic (Chester & Messiha-Hanna, 1970). In Figure 4.iii.7b the means of the slowly accumulated brown clay, the metal-poor brown clay and the grey clay (Table 4.iii.4) are plotted on a similar basis to Figure 4.iii.7a along with the model detrital matrix data. This illustrates the points just made concerning the similarity to average shale, and the effect of the superimposed hydrogenous flux on the two types of brown clay already identified.

Conclusions

This investigation of six cores from five sites produces a more detailed appreciation of the geochemistry of the near surface (up to 2m) sediments of the Nares Abyssal Plain, as revealed by the sediment record and associated pore waters. Together with previous work it illustrates a complex geochemical situation apparently controlled by sedimentation processes.

In line with Shipley's (1978) observations, grey silty clay turbidites were observed only in cores taken from water depths greater than 5700m. Despite the marked colour difference, comprehensive major element and mineralogical data here confirm the similarity noted by Shipley between those grey clays and the pelagic brown clay also commonly observed.

The major modifications introduced here to Shipley's (1978) representation are that:

i. Over a 10^5 year time scale the $^{230}Th_{excess}$ data indicate a higher rate of pelagic sediment accumulation than previously estimated, but consistent with other Atlantic clay accumulation values.

ii. A grey clay unit found within a decimetre or so of the surface in a box core from the eastern end of the Plain demonstrates that turbidity currents have been active until much more recently (on the order of 10^4 years) than shown by previous work (10^5 years).

iii. Besides the two types of sediment already referred to, there are other sediment types which have brown as the main colour but which do not appear to be pelagic.

Interstitial water analyses reveal that the pore water condition is very mildly reducing. In general mobilisation of the redox sensitive element manganese into pore solution is not observed in the top 0.5-1m, and this is interpreted as evidence that no diagenetic migration of elements in this zone is occurring. An exception was observed in one core (10164#1K), and here it has been possible to model the data on the assumption of relatively recent burial of organic material at depth. It is found that profiles similar to those found could have been established in only a few hundred years in these circumstances, and thereafter maintained as oxidation proceeded.

A strong association has been demonstrated in the brown clays between the $^{230}Th_{excess}$ data and the hydrogenous suite of elements. In those cases where the $^{230}Th_{excess}$ data are consistent with slow sediment accumulation, clear enrichments of Mn, Co, Ni and Cu, and less marked enrichments of V, Fe and Zn are found. These enrichments are not found in the grey clay sections and are less in brown clays with low and erratic $^{230}Th_{excess}$ values. On the basis of this observation a model has been applied to the area of the Nares Abyssal Plain which allows estimation of the hydrogenous fluxes of these metals and of their detrital clay matrix concentrations. The values of the hydrogenous fluxes follow a pattern broadly similar to that found in previous studies, but it is clear that the absolute flux values exhibit considerable geographical variation. The detrital concentrations agree well with the means of the grey clay analyses and are close to shale values.

Table 4.iii.1 Details of cores collected

Core	Type	Latitude (N)	Longitude (W)	Depth (Corr.m)	Percentage of grey clay
10163#3BX	Box	23°41.3'	59°40.9'	5933	31
10163#6K	Kasten	23°43.5'	59°41.7'	5947	20
10164#1K	Kasten	26°14.0'	60°20.7'	6221	62
10164#5BX	Box	26°04.9'	60°24.7'	5613	0
10165#2BX	Box	23°43.8'	61°29.4'	5900	40
10169#4K	Kasten	23°44.8'	65°13.0'	5835	91
10170#1BX	Box	21°43.6'	65°30.5'	5520	0

Table 4.iii.2 Calculated diffusive fluxes in the interstitial waters of core 10164#1K.

	Manganese	Alkalinity	Total Iodine	Silicate
Concentration gradient (μmoles cm^{-1})	0.0016	.0025	3.6×10^{-6}	.0013
Effective diffusion coefficient (cm^2 sec^{-1})*	1.3×10^{-6}	3×10^{-6}	5.2×10^{-6}	3.3×10^{-6}
Flux (μmoles cm^{-2} sec^{-1})	2.1×10^{-9}	7.5×10^{-9}	1.9×10^{-11}	4.4×10^{-9}
Time to steady state (yrs) +	110	48	28	43

* Silicate value from FANNING and PILSON (1974). Other values from LI and GREGORY (1974). Assumed temperature 0°C and $\alpha\theta^{-2} = 0.55$.

\+ Minimum values as assumption is made that linear portion does not extend below samples interval. Criterion for steady state $Dt\,\ell^{-2} > 0.45$ (CRANK, 1956).

Table 4.iii.3 Comparison of $^{230}Th_{excess}$ water column production with sediment column inventory.

Core	Corrected Water Depth (m)	Steady State Water Column Production (P d.p.m./cm^2)	Calculated Sediment Column Inventory* (Σ d.p.m./cm^2)	$\frac{\Sigma}{P}$
10163#3BX	5933	1600	940	0.59
10164#5BX	5613	1500	910	0.61
10170#1BX	5520	1500	1000	0.67

* Calculated with an *in situ* dry sediment density of 0.65 g/cm^3 (measured).

Table 4.iii.4 Average major and trace element composition of bulk sediment samples (this study) compared with average shale composition (WEDEPOHL, 1968).

	Nares Abyssal Plain sediments: overall mean of 62 Analyses		Slowly accumulated brown clays. Group mean N = 16		Metal-poor brown clays Group mean N = 12		Assorted minor Lithologies Group mean N = 19		Grey clays Group Mean N = 15		Average Shale Wedepohl (1968)
SiO_2	50.61	(2.25)	50.06	(0.57)	51.06	(1.39)	50.12	(2.35)	51.44	(3.38)	58.61
Al_2O_3	17.88	(1.12)	18.61	(0.72)	18.12	(0.74)	17.64	(0.98)	17.64	(1.44)	16.63
$Fe\ O_T$ ‡	7.85	(9.65)	8.15	(0.14)	8.14	(0.43)	7.83	(0.49)	7.35	(0.95)	6.89
MnO	0.35	(0.20)	0.53	(0.14)	0.29	(0.10)	0.34	(0.17)	0.10*	(0.04)	0.11
MgO	3.17	(0.26)	3.03	(0.13)	3.23	(0.25)	3.12	(0.26)	3.29	(0.28)	2.60
CaO	1.91	(1.59)	1.07	(0.28)	1.26	(0.37)	2.28	(2.26)	2.84	(1.36)	2.21
K_2O	3.55	(0.34)	3.33	(0.14)	3.66	(0.20)	3.57	(0.40)	3.68	(0.42)	3.61
TiO_2	0.82	(0.22)	0.81		0.82		0.81		0.89		0.77
P_2O_5	0.17	(0.00)	0.17		0.18		0.17		-		0.16
NaCl	2.41	(0.38)	2.69		2.81		2.04		1.85		0.92
Na_2O	1.45	(0.17)	1.55		1.50		1.40		1.40		2.10
LOI†	9.33	(1.42)	9.22		8.64		9.48		9.79		
TOTAL	99.42	(2.13)	99.37		99.98		99.40		100.27		
CO_2	1.40	(1.10)	0.64	(0.40)	0.84	(0.40)	1.57		2.23	(1.20)	1.3
Org.C	0.27	(0.17)	0.17	(0.10)	0.16	(0.13)	0.28		0.42	(0.14)	
Rb	157	(13)	146	(3)	161	(6)	158	(14)	162	(17)	140
Sr	155	(19)	152	(12)	139	(14)	165	(64)	158	(35)	300
Y	31	(2)	32		30		32		31		41
Zr	135	(15)	130	(10)	135	(13)	133	(12)	142	(22)	160
Nb	17	(2)	17		18		17		17		18
Ni	78	(24)	107	(29)	79	(16)	69	(15)	56	(10)	68
Co	38	(17)	59	(13)	39	(14)	32	(10)	24	(4)	19
V	165	(12)	170	(9)	170	(7)	166	(8)	155	(17)	130
Cr	96	(6)	92	(3)	100	(3)	99	(5)	94	(8)	90
Cu	77	(15)	122	(20)	76	(2)	65	(22)	45	(20)	45
Zn	126	(9)	132	(4)	128	(4)	125	(7)	117	(12)	95

Nares samples are grouped into three main classes according to colour and inferred accumulation rate; N is total number of samples assigned to each group, and figures in brackets are standard deviations of the mean. * indicates 3 high values excluded from mean. Units: SiO_2 - Org C, % wt; Rb - Zn, ppm (dry basis). † LOI - loss on ignition (1000°C). ‡ Fe_2O_{3T} - all Fe expressed as Fe(III).

Table 4.iii.5 Summary of correlation coefficients calculated for pairs of chemical variables in overall database, slowly accumulated brown clays (1a) metal-poor brown clays (1b) and grey clays (2).

	Correlation Coefficients:				Interpretation and Comments
	Overall 62 x 27 matrix	(1a) 16 x 16 matrix	(1b) 12 x 12 matrix	(2) 15 x 15 matrix	
Ni Co	0.94	0.81	0.94	-	
Ni Cu	0.89	0.72	0.87	(0.23)	
Cu Co	0.87	0.72	0.72	-	Controlled by variations in hydrogenous component: enriched in slowly accumulated brown clays, affected by Mn diagenesis.
MnO Ni	(0.53)	0.93	(0.66)	(0.02)	1
Ni Sr	(0.06)	0.72	0.89	(-0.37)	
MnO V	(0.41)	0.71	(-0.33)	(0.31)	
MnO Zn	(0.44)	0.67	(-0.04)	(0.31)	
Al_2O_3 V	0.88	0.84	-	0.95	
Al_2O_3 Zn	0.88	0.82	-	0.96	Controlled by variations in kaolinite + associated impurities (Fe-rich): partly associated with hydrogenous component, partly associated with heterogenous grey clays.
Zn V	0.86	0.86	(0.02)	0.96	
Fe_2O_3 Zn	0.85	(0.48)	(0.55)	0.93	2
Fe_2O_3 Al O	0.83	(0.54)	-	0.92	
Fe_2O_3 V	0.82	0.69	(0.27)	0.93	
K_2O Rb	0.93	(0.29)	(0.52)	0.97	Controlled by variations in illite: enriched in grey silty clays, excluded from slowly accumulated brown clays.
Rb Cr	(0.56)	(0.01)	(0.15)	0.94	3a
K_2O Cr	(0.53)	-0.67	(0.55)	0.93	
Al_2O_3 Cr	(0.35)	0.74	-	0.92	Controlled by variations in impurities common to chlorite and kaolinite, mostly in grey clays.
Fe_2O_3 Cr	(0.55)	(0.18)	(0.52)	0 97	3b
Zn Cr	(0.40)	(0.47)	(0.22)	0.96	
CO_2 Sr	0.74	(0.27)	-	0.80	Controlled by variations in calcite in grey clays
CaO CO_2	(0.44)	-	-	-	4
CaO Org	0.71	-	-	0.75*	
SiO_2 Zr	(0.54)	(0.1)	-	0.83	Controlled by variation in quartz and zircon content in grey clays.
Zr Nb	(0.55)	-	-	-	5

Footnote: All positive, highly significant correlations are quoted from each separately established matrix. Values in brackets are only weakly significant ($r < 0.66$) and absent values are due to limitations in numbers of variables in each particular matrix.

* indicates r value from 20 x 20 matrix on station 10164 data alone.

Table 4.iii.6 Mineralogical composition of Nares Abyssal Plain sediments (1) compared with composition of average shale (2) aeolian dust (3 and 4) and North Atlantic deep-sea sediments (5)

	1	2	3	4	5
Illite	40 - 55	45 - 55	37	54	48
Quartz	< 5 - 15	20	10	-	13
Feldspar	1 - 5	10 - 15	-	-	-
Chlorite	0 - 10	14	9	13	9
Kaolinite	15 - 30		29	28	17
Smectite	0 - 10	-	-	<5	14
Calcite	0 - 10	3	14	-	-
$\frac{K+C^*}{I}$	0.28	0.6 - 1.2	1.0	0.76	0.54

Footnote:

1. Range of 62 bulk XRD scans (this study)
2. American and European shales (WEDEPOHL, 1971)
3. N.E. Trade wind dust, Barbados (DELANY, et al., 1967)
4. N.E. Trade wind dust, Barbados (GLACCUM, 1978)
5. (GRIFFIN et al., 1968; WINDOM, 1976)

All values quoted as either average composition or total range of percent weight abundance.

*K+C/I is ratio of kaolinite plus chlorite to illite.

Table 4.iii.7 Comparison of estimated (i) pelagic brown clay detrital compositions and (ii) hydrogenous fluxes, of V, Mn, Fe, Co, Ni, Cu and Zn.

(i) Detrital compositions (p.p.m. by weight)

Element	Nares A.P. Brown clay	Nares A.P. Grey clay[a]	Bermuda Rise (GPC-5)[b]	North Atlantic average[c]	Pacific[d]	Average Shale[e]
V	157± 11	157	-	-	-	130
Mn	570±360	770	600±300	582	2087	850
Fe($\times 10^{-3}$)	49.2±1.2	51.8	51±3	-	38 43	48
Co	24± 13	27	23±2	12	31 - 48	19
Ni	63± 15	60	66±4	63	51 - 92	68
Cu	50± 10	52	36±9	67	169 - 224	45
Zn	114± 6	118	124±7	-	-	95

(ii) Hydrogenous fluxes ($\mu g/cm^2 . 10^3$ yr)

Element	Nares Abyssal Plain	Northwest Atlantic (Gulf Stream)[b]	Caribbean[f]	Pacific[d]
V	6± 2	-	-	-
Mn	1300± 50	4300±1100	-	500
Fe	2600±200	-	-	800
Co	13± 2	7.2±5.7	7.4	5
Ni	17± 2	46± 16	10.7	10
Cu	26± 2	76± 26	18,2	8
Zn	7± 1	17± 20	-	-

a. Table X, this work
b. BACON and ROSHOLT (1982)
c. CHESTER and MESSIHA-HANNA (1970)
d. KRISHNASWAMI (1976)
e. WEDEPOHL (1968)
f. Turekian (1965)

Note: uncertainties quoted are derived from one standard deviation of the regression line slopes and intercepts.

TABLE 4.iii.8

Interstitial Water Analysis: List of Results

Table 4.iii.8

10165 # SG

Depth cm	Si µm	PO_4 µm	NO_3 µm	ΣIodine µm	Iodine µm	Iodate µm	Manganese µm
0 - 2	117	4	23	0.56	0.22	0.34	-
2 - 4	122	8	23	0.46	0.06	0.40	0.5
4 - 7	138	7	26	0.61	0.12	0.49	0.6
7 - 9	132	4	26	0.59	0.07	0.52	0.7
9 -11	-	5	22	0.68	-	-	1.4
11-13	117	5	19	0.61	0.05	0.56	0.8
13-15	113	5	22	0.76	0.15	0.61	0.8
15-17	119	2	23	0.74	0.07	0.67	1.4
17-19	121	5	22	0.74	0.04	0.70	0.9
19-21	117	5	24	0.79	0.37	0.41	0.9
21-23	123	5	22	0.84	0.15	0.70	-
25-27	123	5	24	0.96	0.14	0.82	0.4
31-33	-	4	25	0.96	0.35	0.61	0.7
35-37	130	4	24	1.02	0.21	0.82	0.5
43-45	138	5	11	0.98	0.32	0.65	1.0
47-49	160	1	-	0.56	0.50	0.06	16.6
53-55	103	5	13	0.60	0.56	0.04	-

Note: Nutrient data on this core obtained from stored samples at shore laboratory.

Table 4.iii.8 (continued)

Depth cm	ΣIodine µm	Iodine µm	Iodate µm	Manganese µm
10163#3BX				
0 - 3	0.39	0.22	0.17	1.0
3 - 6	0.38	0.25	0.12	1.6
6 - 9	0.36	0.21	0.15	0.5
9 - 12	0.39	0.27	0.12	1.1
12 - 15	0.36	0.25	0.11	0.6
15 - 18	0.48	0.36	0.12	1.2
18 - 21	0.48	0.36	0.11	0.7
21 - 24	-	-	-	0.6
24 - 27	0.55	0.41	0.14	0.6
27 - 30	0.60	0.48	0.12	1.1
30 - 33	0.33	0.18	0.15	-
33 - 36	0.39	0.27	0.12	-
36 - 39	0.24	0.10	0.13	-
39 - 42	0.28	0.02	0.25	-
42 - 45	0.38	0.09	0.30	1.0
45 - 48	0.42	0.17	0.25	1.2
48 - 51	0.35	0.19	0.17	2.3
51 - 54	0.35	0.07	0.28	0.6
54 - 57	0.33	0.16	0.17	0.5
10163#3K				
11 - 18	0.52	-	-	-
18 - 25	0.49	0.44	0.05	-
46 - 53	-	-	-	-
53 - 60	-	-	-	0.3
83 - 90	0.52	0.33	0.20	0.8
93 - 100	0.60	0.53	0.09	0.8
123 - 130	0.52	0.26	0.25	0.7
143 - 150	0.66	0.51	0.15	1.2
10164#5BX				
0 - 3	-	-	-	0.1
3 - 6	0.39	0.13	0.27	0.2
6 - 9	-	-	0.30	0.1
9 - 12	0.31	0.03	0.28	0.1
12 - 15	-	-	0.27	0.3
15 - 18	-	-	-	0.3
18 - 21	-	-	-	-
21 - 24	0.40	0.08	0.32	0.3
24 - 27	0.24	0.04	0.20	0.1
27 - 30	0.24	-	-	0.1
30 - 33	-	-	0.18	-
33 - 36	0.31	0.23	0.08	0.2
36 - 39	-	-	-	-

Table 4.iii.8 (continued)

Depth cm	ΣIodine µm	Iodine µm	Iodate µm	Manganese µm
10164#5BX(continued)				
39 - 42	0.35	-	-	0.5
42 - 45	0.31	0.31	0.0	0.3
45 - 48	0.30	-	-	0.6
48 - 51	-	-	-	0.4
10164#1K				
23 - 29	0.56	0.21	0.36	8.5
35 - 42	-	-	-	9.1
48 - 55	0.42	0.34	0.08	13.1
61 - 67	0.46	0.46	0.00	23.1
90 - 96	0.48	0.48	0.00	63.1
124 - 131	0.71	0.71	0.00	117.3
137 - 143	0.72	0.72	0.00	140.2
161 - 168	0.77	0.77	0.00	156.9
168 - 174	0.80	0.80	0.00	183.3
181 - 187	0.81	0.78	0.04	211.8
10165#2BX				
0 - 2	0.55	0.15	0.40	0.2
2 - 5	0.45	0.06	0.39	0.3
5 - 8	0.33	-	-	0.1
8 - 11	0.50	0.15	0.36	0.2
11 - 14	0.54	0.12	0.42	0.3
14 - 17	0.56	0.16	0.40	0.3
17 - 20	0.61	0.15	0.46	0.3
20 - 23	0.56	0.13	0.43	0.1
23 - 26	0.78	0.20	0.58	0.1
26 - 29	0.48	-	-	-
29 - 32	0.68	0.16	0.52	0.2
32 - 35	0.73	0.14	0.59	-
35 - 38	0.86	0.17	0.69	0.5
38 - 41	0.85	0.11	0.74	0.5
41 - 44	0.74	0.11	0.62	0.6
44 - 47	0.72	0.44	0.29	0.5
47 - 50	0.81	0.61	0.20	0.1

Table 4.iii.8 (continued)

Depth cm	ΣIodine µm	Iodine µm	Iodate µm	Manganese µm
10170#1BX				
0 - 0.5	1.03	0.53	0.50	0.1
0.5 - 1	0.74	0.30	0.45	0.2
1 - 2	0.65	0.30	0.35	0.1
3 - 4	0.56	0.20	0.36	0.6
6 - 7	0.58	0.22	0.36	0.1
8 - 9	0.56	0.18	0.38	0.8
10 - 11	0.76	0.48	0.28	0.7
11 - 12	0.61	0.14	0.47	0.3
13 - 14	0.61	0.15	0.45	1.1
15 - 16	0.77	0.27	0.50	1.3

Table 4.iii.9

Sediment analysis for major and minor elements: List of Results

(Note: Fe_2O_3 : All Fe expressed as Fe (111) LOI : Loss on ignition at 1000°C. Org.C : organic carbon).

Table 4.iii.9

Sediment type	Depth Interval cm	Major element data, % wt. dry basis														Trace element data, ppm dry basis										
		SiO_2	Al_2O_3	Fe_2O_{3T}	MnO	MgO	CaO	K_2O	TiO_2	P_2O_5	NaCl	Na_2O	LOI	Total	CO_2	Org.C	Rb	Sr	Y	Zr	Nb	Ni	Co	V	Cr	Cu	Zn
		10163#3BX: Water depth 5933m																								
1b	0-2	50.04	17.16	7.31	0.31	3.27	1.23	3.30	0.77	0.20	7.12	1.36	10.94	103.2	-	-	160	147	28	141	17	88	46	172	96	97	118
1b	4-6	53.33	18.11	7.78	0.31	3.17	1.29	3.58	0.81	0.21	3.20	1.70	7.78	101.28	-	-	159	138	30	146	21	88	42	174	99	87	129
1b	8-10	52.03	18.82	8.02	0.28	3.22	1.25	3.83	0.85	0.22	2.50	1.58	8.33	100.94	-	-	160	137	32	146	20	86	40	175	100	83	129
3	16-18	52.75	18.07	7.27	0.27	3.23	2.65	3.59	0.82	0.19	1.62	1.44	8.56	100.47	-	-	155	170	32	146	20	86	37	165	96	69	124
2	18-20	53.06	18.34	7.72	0.20	3.22	1.74	3.82	0.85	0.20	1.68	1.46	7.94	100.24	-	-	164	137	33	152	19	82	25	164	97	64	124
3	20-22	51.61	19.21	8.47	0.29	3.06	1.08	3.43	0.85	0.22	2.61	1.37	8.77	100.96	-	-	153	143	32	153	18	85	55	182	98	96	131
1a	30-32	51.23	19.37	8.18	0.47	3.08	0.98	3.23	0.83	0.19	2.94	1.55	8.68	100.74	-	-	148	150	29	144	17	103	51	175	96	121	135
1a	40-42	49.83	18.93	8.15	0.53	2.93	0.93	3.22	0.83	0.20	3.06	1.54	8.91	99.06	-	-	145	150	34	143	19	105	52	175	92	123	139
1a	50-52	49.87	19.12	8.10	0.56	2.94	0.91	3.23	0.83	0.20	2.91	1.64	9.88	100.20	-	-	145	148	32	144	18	119	52	175	93	127	134
1a	61-64	50.50	19.16	8.23	0.48	2.95	0.89	3.25	0.81	0.19	2.74	1.54	9.48	100.17	-	-	151	145	32	146	17	103	51	176	96	118	132
1b	66-69	50.90	19.37	8.41	0.38	3.02	0.82	3.41	0.84	0.20	2.55	1.43	9.13	100.45	-	-	157	138	30	160	21	92	42	179	99	102	130
		10164#5BX: Water depth 5613m																								
1a	0-1	49.37	18.19	8.16	0.62	2.95	1.27	3.42	0.83	0.18	2.25	1.42	9.29	98.60	0.66	0.29	147	158	32	142	17	129	72	172	99	128	130
1a	10-12	49.43	17.93	8.15	0.64	2.88	1.90	3.33	0.80	0.17	2.45	1.50	9.13	98.53	1.68	0.08	145	185	35	123	16	127	69	168	89	130	131
1a	20-22	49.72	18.20	8.07	0.65	2.97	1.12	3.29	0.81	0.15	2.43	1.50	9.08	09.16	0.50	0.09	147	152	35	128	19	128	81	171	90	144	132
1a	30-32	49.98	18.54	8.19	0.67	2.97	0.77	3.34	0.84	0.19	2.26	1.44	8.94	98.16	0.37	0.14	142	162	33	123	17	132	71	166	88	143	132
1a	36-38	49.80	18.32	8.23	0.66	2.90	0.77	3.35	0.83	0.16	2.39	1.54	9.28	98.22	0.68	0.06	145	149	37	128	18	124	76	175	92	141	135

Table 4.iii.9 (continued)

Sediment type	Depth Interval cm	Major element Data, % wt. dry basis														Trace Element Data, ppm. dry basis										
		SiO_2	Al_2O_3	Fe_2O_{3T}	MnO	MgO	CaO	K_2O	TiO_2	P_2O_5	NaCl	Na_2O	LOI	Total	CO_2	Org.C	Rb	Sr	Y	Zr	Nb	Ni	Co	V	Cr	Cu	Zn
		10164#1K: Water depth 6221m																								
1b	26-28	49.09	17.51	9.11	0.35	2.79	0.85	3.71	1.53	0.82	0.15	2.25	9.59	96.75	0.43	0.13	166	120	32	141	19	56	21	157	102	43	132
3	32-34	49.58	18.01	8.11	0.32	2.81	0.83	3.81	1.58	0.83	0.16	2.19	9.45	97.68	0.44	0.16	169	126	34	143	20	56	24	162	105	37	125
3	38-40	52.49	16.59	7.58	0.48	2.56	0.99	3.57	1.64	0.84	0.15	1.99	9.04	97.92	0.42	0.33	163	120	32	139	18	58	22	167	106	36	122
3	44-46	50.91	16.99	8.49	0.30	2.78	0.86	3.79	1.65	0.84	0.16	1.97	8.71	97.45	0.58	0.25	161	132	31	160	21	56	23	158	99	81	123
3	50-52	48.06	17.55	7.99	0.12	3.10	1.10	4.00	1.19	0.81	0.15	2.33	10.08	96.48	0.82	0.37	174	118	33	135	19	51	22	163	98	37	127
2	55-57	49.32	17.89	8.21	0.06	3.10	1.15	4.15	1.15	0.81	0.14	2.04	9,53	97.55	0.97	0.32	177	120	33	137	21	50	20	162	98	27	125
2	65-67	50.08	18.39	7.81	0.07	3.52	2.11	4.13	1.02	0.81	0.13	2.19	10.17	100.43	1.68	0.47	180	139	34	137	19	52	20	170	100	65	127
2	84-86	48.97	17.96	7.35	0.09	3.64	3.90	3.75	0.80	0.78	0.14	2.95	11.87	102.20	2.56	0.64	172	183	29	139	17	52	20	156	96	42	118
2	104-106	48.20	16.84	7.00	0.10	2.90	3.90	3.60	0.88	0.77	0.13	2.43	12.27	99.02	3.11	0.44	165	177	30	135	16	47	20	151	92	39	114
2	124-126	52.52	15.85	6.25	0.10	3.24	4.41	3.27	1.28	0.51	0.13	2.11	11.25	100.92	3.78	0.67	148	182	32	156	18	48	23	142	84	34	104
2	135-137	62.08	12.75	4.38	0.06	2.55	4.16	2.44	1.98	0.72	0.13	1.73	9.14	102.12	3.78	0.44	107	170	30	211	18	68	30	102	68	25	80
2	144-146	50.39	17.85	7.70	0.11	3.48	1.23	3.99	1.19	0.79	0.14	2.29	9.62	98.78	1.02	0.30	169	121	30	135	16	57	27	171	98	101	123
2	164-166	52.61	16.76	7.28	0.10	2.96	1.28	3.65	1.29	0.90	0.15	2.02	9.47	98.47	1.28	0.46	163	120	33	160	18	64	31	155	98	32	121
1a	184-186	50.00	16.89	8.09	0.20	3.16	1.28	3.67	1.37	0.78	0.15	2.64	10.36	98.59	1.30	0.33	150	132	29	135	16	67	35	149	86	58	122
1a	196-198	49.23	17.53	7.80	0.24	2.95	0.99	3.49	1.37	0.81	0.15	2.75	10.45	97.76	0.49	0.21	147	135	29	137	17	68	50	148	93	127	123

Table 4.iii.9 (continued)

Sediment type	Depth Interval cm	Major element data, % wt. dry basis															Trace element data, ppm. dry basis										
		SiO_2	Al_2O_3	Fe_2O_{3T}	MnO	MgO	Cao	K_2O	TiO_2	P_2O_5	NaCl	Na_2O	LOI	Total	CO_2	Org.C	Rb	Sr	Y	Zr	Nb	Ni	Co	V	Cr	Cu	Zn
		10165#2BX: Water depth 5900m																									
1b	0-1	49.13	17.82	7.80	0.27	3.80	1.19	3.46	0.78	0.13	3.41	1.20	10.20	99.19	0.74	0.46	155	131	28	132	18	73	35	165	95	72	125
3	9-11	50.28	18.04	7.80	0.26	3.60	1.23	3.74	0.82	0.17	1.79	1.44	8.76	97.93	0.92	0.26	164	134	31	138	20	68	32	167	100	66	129
3	19-21	50.94	18.32	7.45	0.32	3.59	2.50	3.87	0.83	0.16	1.87	1.45	9.21	100.51	1.44	0.29	164	153	31	137	20	59	25	156	95	56	125
2	30-32	49.53	16.83	7.54	0.15	3.48	4.60	3.47	0.75	0.14	2.10	1.15	11.56	101.30	4.83	-	156	226	29	139	29	51	29	148	85	37	117
2	40-42	48.39	17.11	7.60	0.11	3.53	5.12	3.49	0.77	0.15	1.68	1.18	10.80	99,93	2.20	-	156	217	30	133	16	51	21	149	94	31	112
		10170#1BX: Water depth 5520m																									
3	0-1	48.36	16.71	7.49	0.27	3.24	2.36	3.23	0.79	0.19	4.21	1.40	11.47	99.72	3.00	0.05 0.12	143	166	27	127	15	73	34	162	100	84	118
3	10-12	44.19	15.28	6.75	0.27	2.83	9.10	2.47	0.68	0.18	2.30	1.00	14.37	99.42	4.27	0.96 0.94	129	360	28	122	15	70	37	146	90	78	110
3	20-22	45.78	16.36	7.12	0.28	2.86	7.38	2.82	0.71	0.17	2.10	1.04	12.72	99.34	4.67	0.53 0.48	135	303	27	128	15	77	40	155	95	81	115
3	30-32	48.46	17.20	7.74	0.34	3.07	4.05	3.30	0.76	0.16	2.01	1.22	10.15	98.46	2.32	0.34	143	216	30	136	17	88	43	170	111	87	123
3	40-42	49.48	17.20	7.86	0.45	3.28	1.97	3.55	0.79	0.17	2.36	1.36	8.83	97.30	1.12	0.19	147	161	30	134	16	104	50	169	109	98	128
1b	50-52	50.69	17.25	7.89	0.37	3.45	1.90	3.81	0.80	0.18	3.19	1.60	8.32	98.35	1.49	0.08	152	162	36	133	17	97	52	165	102	91	129
1b	60-62	51.58	17.16	7.86	0.37	3.51	1.99	3.60	0.76	0.15	2.24	1.73	8.56	99.51	1.36	0.16	153	168	32	133	16	109	73	160	99	87	128

Table 4.iii.10

Radiochemical Analysis: List of Results

(Note: quoted uncertainties are derived from one-sigma counting statistics).

Table 4.iii.10

Depth cm	U ppm	Th ppm	Th/U	$\frac{^{234}U}{^{238}U}$ Activity Ratio	$\frac{^{230}Th}{^{232}Th}$ Activity Ratio	^{230}Th dpm/g	^{234}U dpm/g	$^{230}Th_{excess}$ dpm/g
10163#6K								
8-10	2.74±0.10	16.2±0.7	5.9±0.3	0.91±0.04	1.77±0.05	7.0 ±0.3	1.87±0.07	5.10±0.31
29-31	2.39±0.08	16.9±0.6	7.1±0.4	1.01±0.04	5.00±0.09	20.6 ±0.7	1.80±0.06	18.8 ±0.7
39-41	2.26±0.08	15.1±0.5	6.7±0.3	0.89±0.04	4.60±0.08	16.9 ±0.5	1.51±0.06	15.3 ±0.5
49-51	2.19±0.07	15.0±0.4	6.8±0.3	0.96±0.04	3.34±0.08	12.2 ±0.3	1.57±0.05	10.6 ±0.3
59-61	2.38±0.06	15.3±0.5	6.4±0.3	0.87±0.03	3.68±0.09	13.6 ±0.3	1.55±0.04	12.1 ±0.3
69-71	2.30±0.05	14.5±0.8	6.3±0.4	0.87±0.04	2.82±0.09	10.0 ±0.5	1.47±0.06	8.5 ±0.5
79-81	2.38±0.06	15.6±1.5	6.5±0.6	0.82±0.02	0.75±0.05	2.85±0.28	1.46±0.04	1.39±0.28
109-111	2.39±0.07	14.2±0.9	5.9±0.4	0.88±0.03	0.68±0.03	2.35±0.15	1.57±0.05	0.76±0.16
119-121	2.48±0.10	16.2±0.7	6.5±0.4	0.87±0.04	0.67±0.02	2.66±0.12	1.61±0.07	1.04±0.14
139-141	2.47±0.06	12.1±0.6	4.9±0.3	0.85±0.02	0.78±0.03	2.30±0.11	1.56±0.04	0.74±0.12
169-171	2.45±0.09	15.7±0.7	6.4±0.4	0.88±0.04	0.66±0.02	2.51±0.13	1.60±0.06	0.91±0.14
10163#3BX								
0-2	2.26±0.07	18.2±0.9	8.0±0.5	0.96±0.04	5.2 ±0.1	22.8 ±1.0	1.63±0.05	21.1 ±1.0
8-10	2.40±0.09	14.8±0.7	6.2±0.4	1.02±0.05	4.4 ±0.1	15.8 ±0.7	1.83±0.07	14.0 ±0.7
18-20	2.68±0.11	15.2±0.7	5.7±0.3	0.95±0.04	2.36±0.06	8.7 ±0.7	1.91±0.08	6.8 ±0.7
30-32	2.32±0.07	16.0±0.8	6.9±0.4	0.92±0.03	3.6 ±0.1	14.1 ±0.6	1.60±0.05	12.5 ±0.6
40-42	2.96±0.11	16.7±0.9	5.7±0.4	0.89±0.04	3.8 ±0.1	15.6 ±0.8	1.97±0.08	13.6 ±0.8
50-52	2.73±0.05	18.6±0.9	6.8±0.3	0.92±0.02	3.5 ±0.1	15.9 ±0.7	1.89±0.04	14.0 ±0.7
66-69	2.55±0.06	12.1±0.6	4.8±0.2	0.92±0.03	2.46±0.08	7.3 ±0.3	1.75±0.04	5.5 ±0.3

Table 4.iii.10 (continued)

Depth cm	U ppm	Th ppm	Th/U	$\frac{^{234}U}{^{238}U}$ Activity Ratio	$\frac{^{230}Th}{^{232}Th}$ Activity Ratio	^{230}Th dpm/g	^{234}U dpm/g	$^{230}Th_{excess}$ dpm/g
10164#1K								
26-28	2.36±0.08	13.2±0.9	5.6±0.4	0.94±0.04	1.19±0.06	3.81±0.26	1.66±0.06	2.15±0.27
32-34	2.37±0.08	15.7±0.7	6.6±0.4	0.93±0.04	0.96±0.04	3.66±0.17	1.64±0.06	2.02±0.18
38-40	2.49±0.09	14.8±0.6	5.9±0.3	0.92±0.04	1.03±0.03	3.72±0.14	1.71±0.06	2.01±0.15
44-46	2.54±0.06	12.3±0.3	4.8±0.2	0.95±0.03	1.23±0.03	3.66±0.09	1.81±0.04	1.85±0.10
50-52	2.48±0.11	14.8±0.7	6.0±0.4	0.96±0.05	1.51±0.05	5.45±0.24	1.78±0.08	3.67±0.25
55-57	2.72±0.09	15.4±0.8	5.7±0.3	0.84±0.04	1.09±0.05	4.06±0.21	1.70±0.06	2.36±0.22
65-67	3.31±0.08	13.8±0.6	4.2±0.2	0.94±0.03	1.03±0.03	3.45±0.14	2.34±0.06	1.13±0.15
84-86	4.00±0.09	14.1±0.4	3.5±0.1	0.95±0.02	1.01±0.02	3.46±0.10	2.85±0.06	0.61±0.11
104-106	2.87±0.10	13.7±0.7	4.8±0.3	0.98±0.04	1.01±0.04	3.37±0.17	2.12±0.07	1.25±0.18
124-126	3.18±0.09	11.6±0.4	3.6±0.2	0.91±0.03	1.00±0.03	2.83±0.11	2.16±0.06	0.67±0.13
135-137	2.87±0.07	9.58±0.28	3.3±0.1	1.06±0.03	1.19±0.03	2.78±0.08	2.27±0.07	0.51±0.11
144-146	2.87±0.10	14.8±0.6	5.2±0.3	0.99±0.04	1.36±0.03	4.89±0.18	2.13±0.07	2.76±0.19
164-166	2.81±0.07	13.2±0.4	4.7±0.2	0.88±0.03	1.60±0.04	5.11±0.14	1.84±0.05	3.27±0.15
184-186	2.19±0.07	14.4±0.7	6.6±0.4	0.95±0.04	4.07±0.12	14.2 ±0.6	1.56±0.05	12.6 ±0.6
196-198	2.21±0.05	10.7±0.3	4.8±0.2	0.90±0.03	3.05±0.06	7.97±0.18	1.47±0.04	6.50±0.18

Table 4.iii.10(continued)

Depth cm	U ppm	Th ppm	Th/U	$\frac{^{234}U}{^{238}U}$ Activity Ratio	$\frac{^{230}Th}{^{232}Th}$ Activity Ratio	^{230}Th dpm/g	^{234}U dpm/g	$^{230}Th_{excess}$ dpm/g	$^{231}Pa_{excess}$ dpm/g
10164#5BX									
0-1	2.59±0.09	17.6±0.6	6.8±0.3	0.90±0.04	6.66±0.13	28.4±0.8	1.73±0.06	26.7 ±0.8	1.07±0.11
10-12	2.54±0.07	14.6±0.8	5.7±0.4	0.97±0.03	6.61±0.21	23.5±1.1	1.84±0.05	21.7 ±1.1	0.76±0.08
20-22	2.37±0.07	14.8±0.8	6.2±0.4	0.93±0.03	5.05±0.16	18.2±0.9	1.65±0.05	16.6 ±0.9	0.44±0.06
30-32	2.60±0.06	17.1±0.4	6.6±0.2	0.88±0.03	3.95±0.07	16.4±0.4	1.71±0.04	14.7 ±0.4	0.36±0.08
36-38	2.57±0.07	18.4±0.06	7.2±0.3	0.91±0.03	3.42±0.06	15.3±0.5	1.76±0.05	13.5 ±0.5	0.14±0.05
10165#2BX									
0-1	2.30±0.07	16.3±0.7	7.1±0.4	1.06±0.04	4.40±0.12	17.4±0.6	1.82±0.06	15.6 ±0.6	
9-11	2.54±0.10	14.4±0.6	5.7±0.3	0.96±0.05	3.30±0.09	11.5±0.4	1.82±0.07	9.7 ±0.4	
19-21	2.64±0.07	14.5±0.6	5.5±0.3	0.91±0.03	1.34±0.05	4.73±0.20	1.80±0.05	2.93±0.21	
30-32	2.31±0.07	13.8±0.4	6.0±0.3	0.90±0.03	1.44±0.04	4.82±0.14	1.56±0.05	3.26±0.15	
40-42	2.32±0.06	13.2±0.6	5.7±0.3	0.92±0.03	1.28±0.05	4.11±0.18	1.60±0.04	2.51±0.18	
10170#1BX									
0-1	2.24±0.08	13.8±0.4	6.2±0.3	0.93±0.04	5.18±0.12	17.4±0.4	1.56±0.06	15.8 ±0.4	
10-12	2.02±0.06	12.0±0.3	5.9±0.2	0.97±0.03	5.08±0.11	14.8±0.3	1.47±0.04	13.3 ±0.3	
20-22	2.04±0.06	12.0±0.4	5.9±0.3	0.95±0.04	4.17±0.11	12.1±0.3	1.45±0.05	10.7 ±0.3	
30-32	2.32±0.06	13.2±0.4	5.7±0.2	0.97±0.03	3.62±0.08	11.6±0.3	1.69±0.05	9.9 ±0.3	
40-42	2.39±0.06	13.7±0.5	5.7±0.3	0.92±0.03	3.39±0.09	11.3±0.3	1.64±0.04	9.7 ±0.3	
50-52	2.28±0.07	12.8±0.4	5.6±0.2	0.93±0.04	3.40±0.08	10.6±0.3	1.59±0.03	9.0 ±0.3	
60-62	2.17±0.06	14.6±0.4	6.7±0.3	0.94±0.03	2.98±0.06	10.6±0.2	1.52±0.04	9.1 ±0.2	

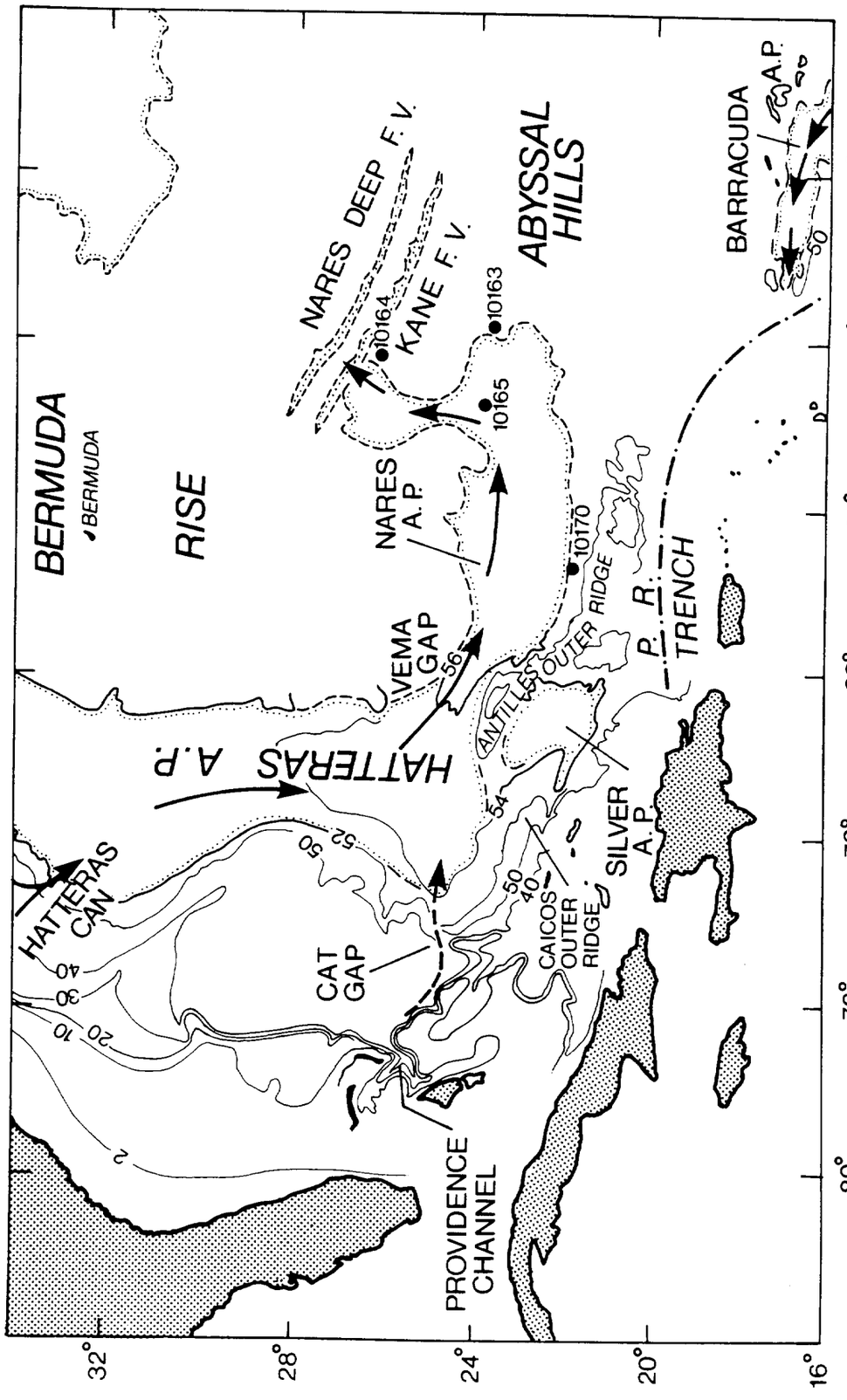

Figure 4.iii.1 A representation of the Nares Abyssal Plain and environs, showing coring stations and inferred turbidity current dispersal paths (after TUCHOLKE, 1980). (Reproduced by kind permission of Dr. B. E. Tucholke and the American Institute of Physics.)

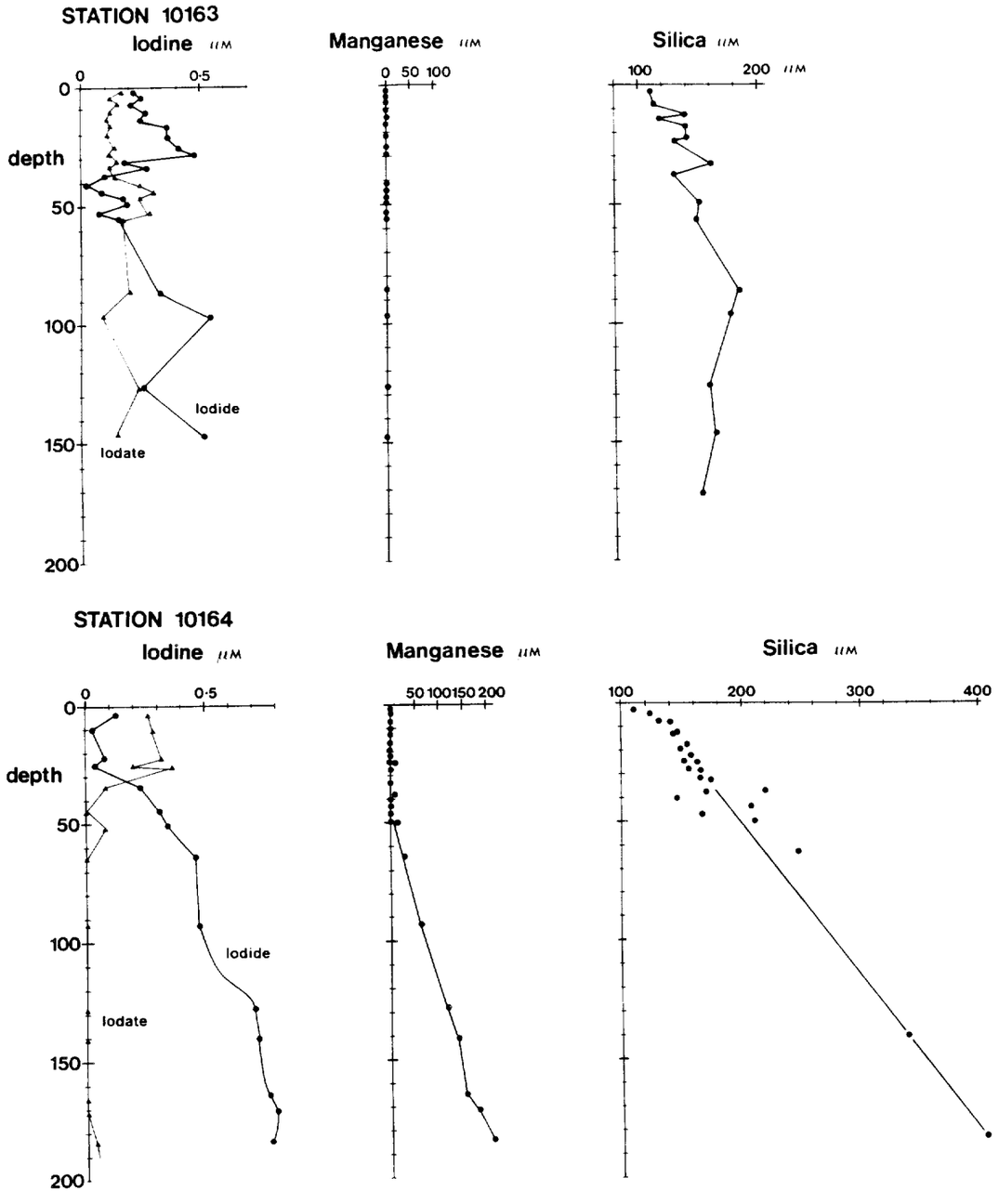

Figure 4.iii.2 Concentration/depth profiles of the interstitial water contents of iodine, manganese and silica at Stations 10163 and 10164. The profiles are composites from both box and Kasten cores recovered at these stations.

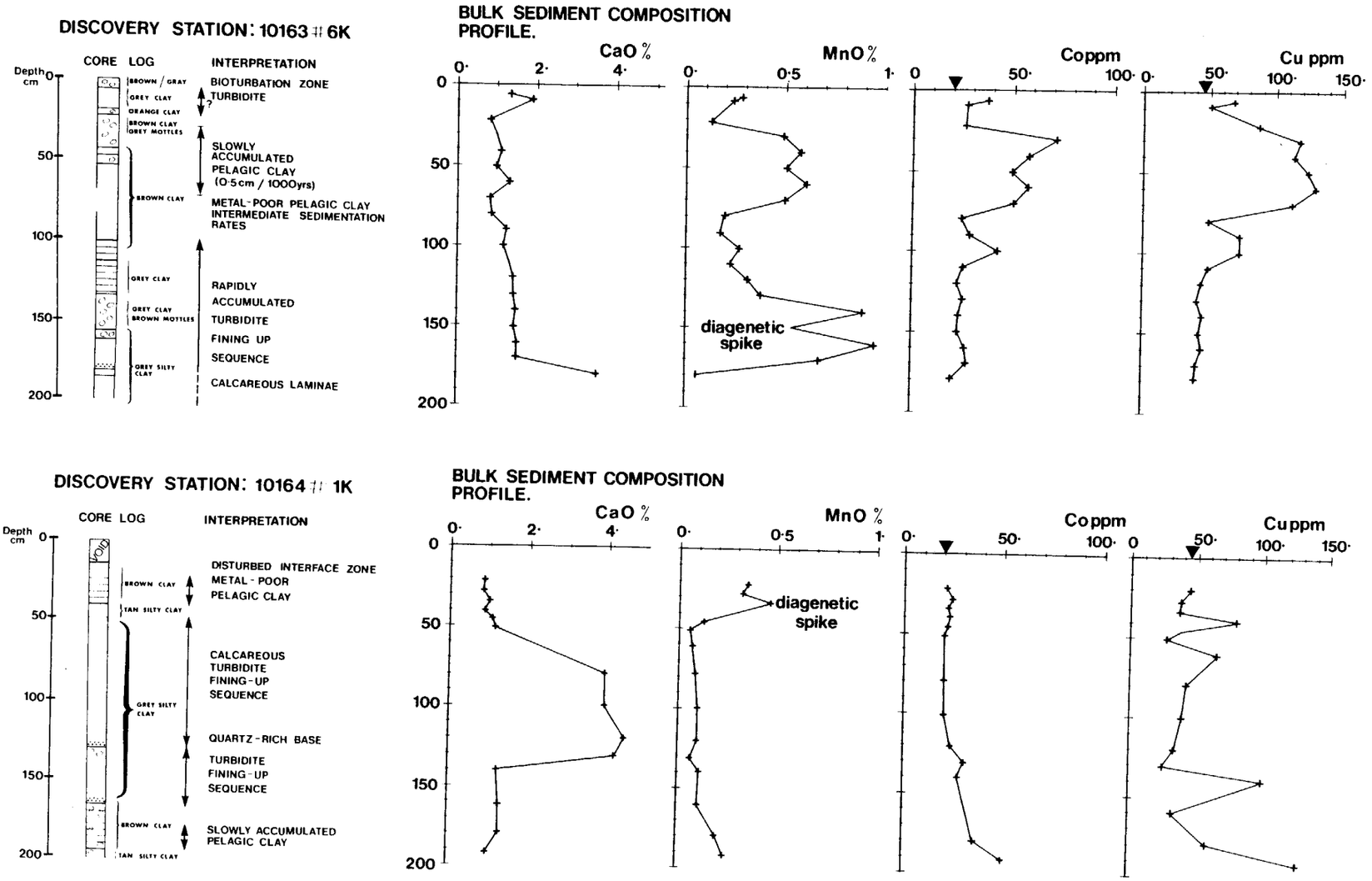

Figure 4.iii.3 Descriptive core logs and solid phase concentration/depth profiles for CaO, MnO, Co and Cu in cores 10163#6K and 10164#1K. The triangles indicate the values of Co and Cu typical of shale (WEDEPOHL, 1968).

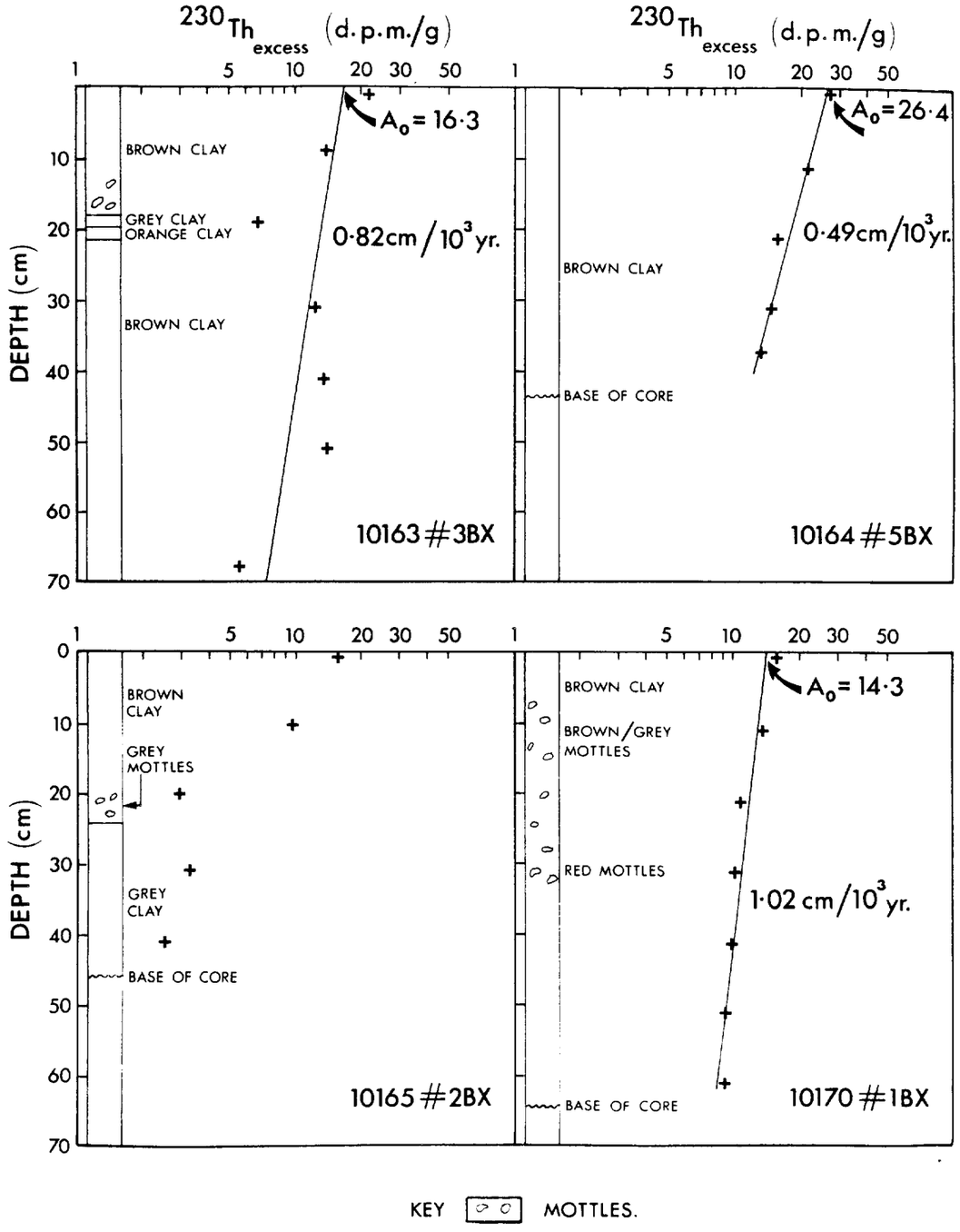

Figure 4.iii.4 Core descriptions and $^{230}Th_{excess}$ data versus depth for the four box cores studied. The surface intercept (A_o) and sediment accumulation rates derived from the best-fit lines are also shown.

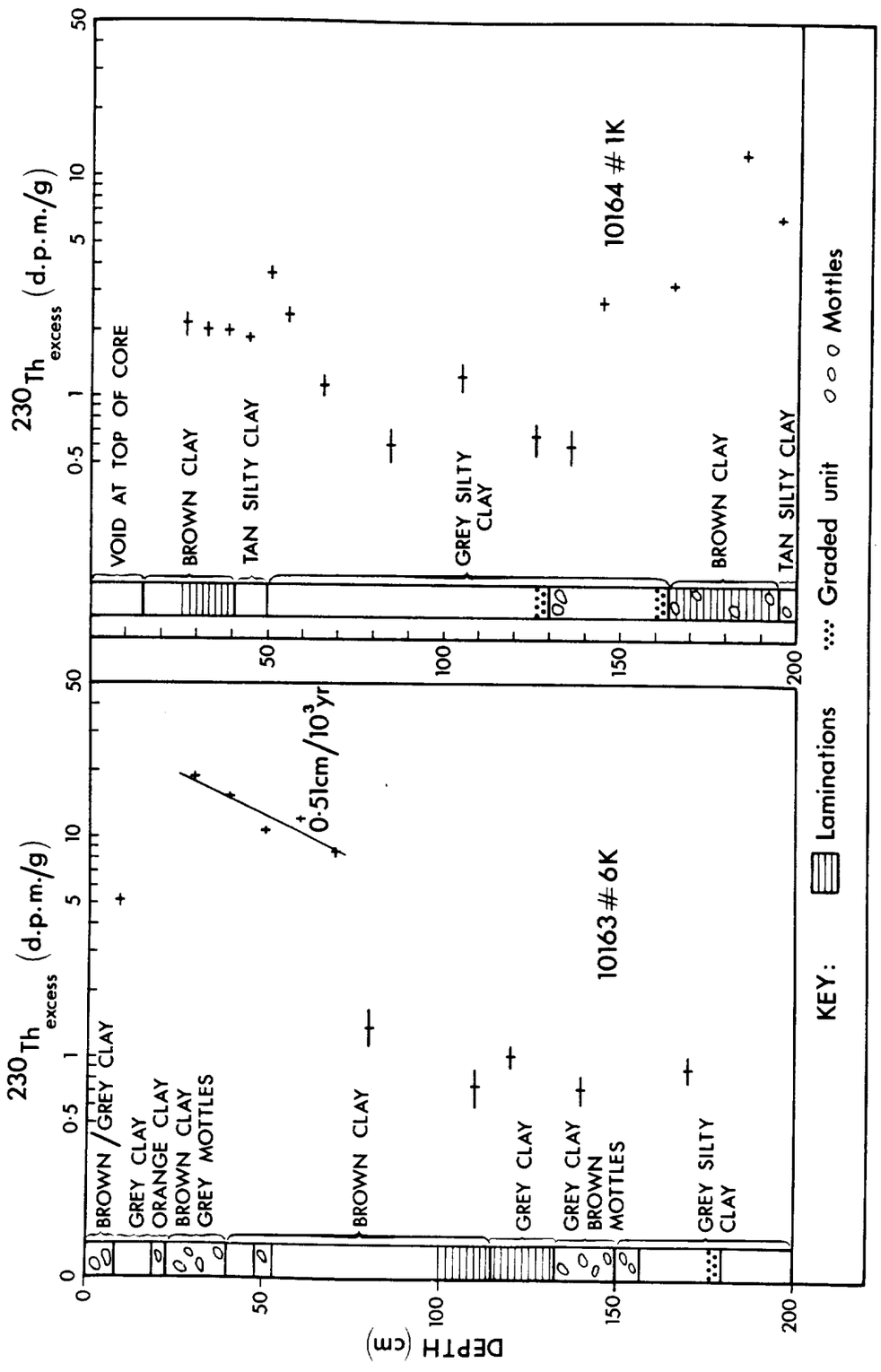

Figure 4.iii.5 Core descriptions and $^{230}Th_{excess}$ data versus depth for Kasten cores 10163#6K and 10164#1K. A sediment accumulation rate can be derived only for a short portion of core 10163#6K as shown.

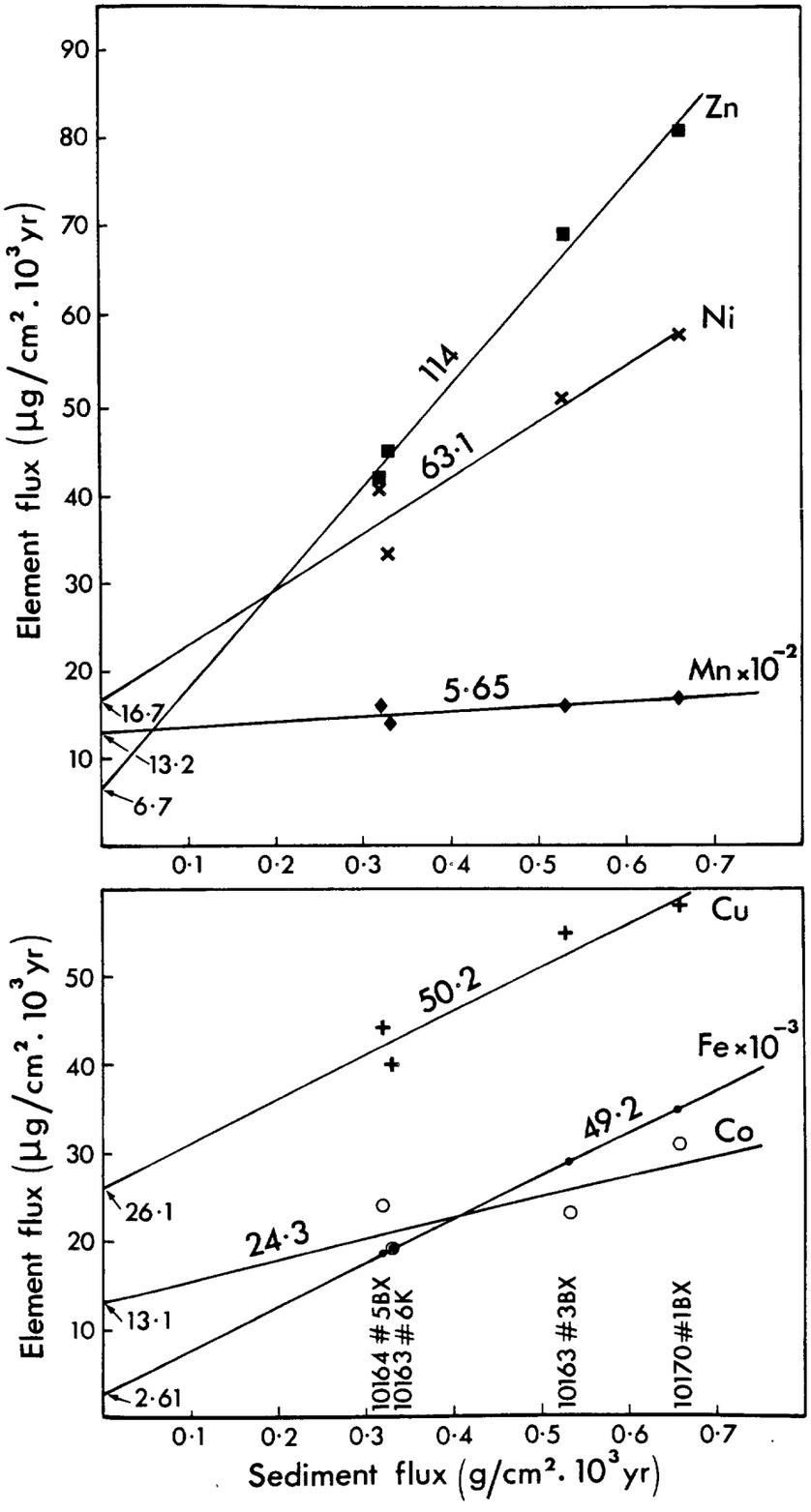

Figure 4.iii.6 Regression lines of the fluxes of the elements Mn, Fe, Co, Ni, Cu and Zn on the total mean sediment fluxes derived from the sediment accumulation rates of cores 10164#5BX, 10163#6K, 10163 #3BX and 10170 #1BX. The slope values, corresponding to the detrital matrix content of the element, and the intercept values, corresponding to the hydrogenous flux of the element, are also shown (see text, Section 4). (A similar treatment can be made for vanadium on a different scale).

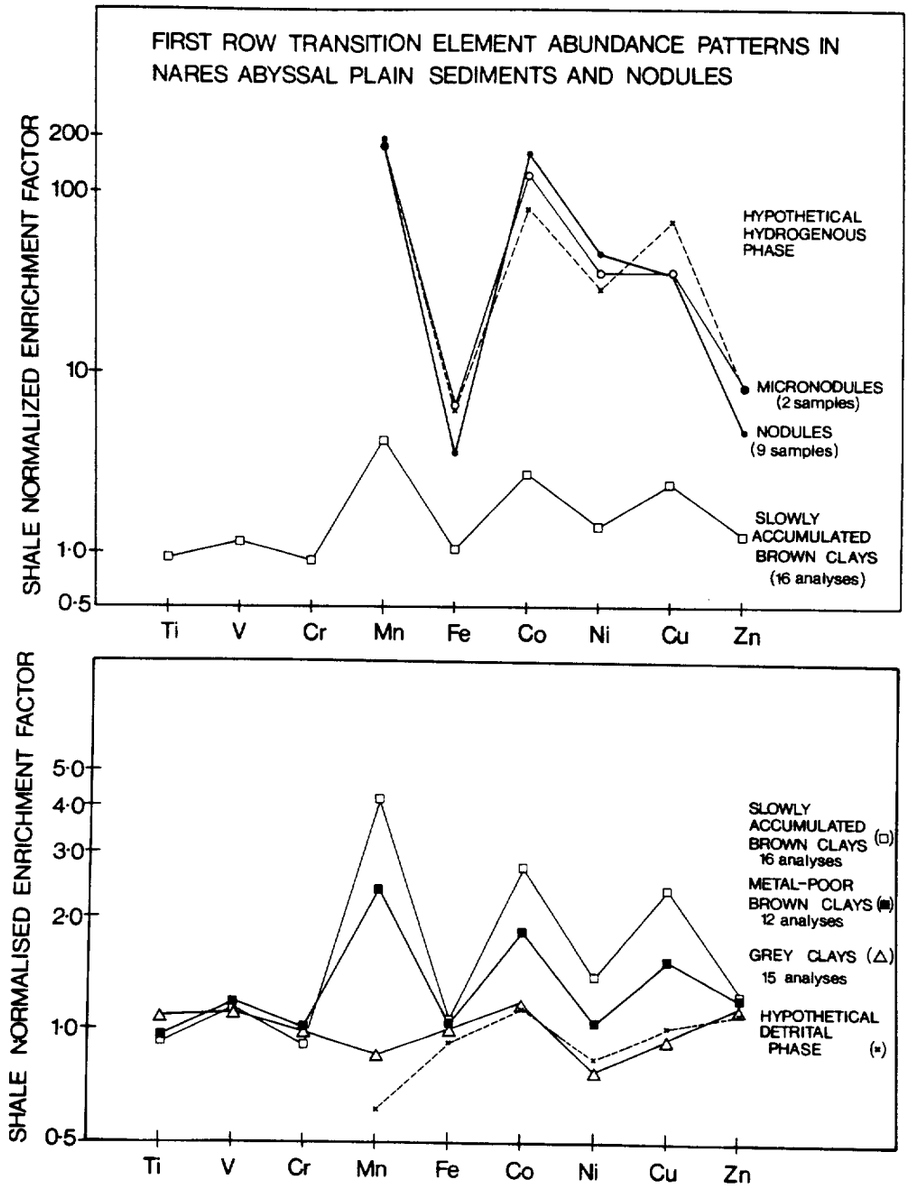

Figure 4.iii.7 7a (upper): Shale normalised enrichment factors for some first row transition elements in the derived hydrogenous phase, in nodules and micronodules from the Nares Abyssal Plain area (ADDY, 1979), and in the slowly-accumulated brown clay. The Mn enrichment factor of the micronodules has been used as the fixed point for the hydrogenous phase plot.

7b (lower): The mean values of the various types of sediment identified (Table 4.iii.4) and the derived detrital phase, normalised against shale and plotted for some first row transition elements. The similarity of the derived phase, the grey clays and shale is apparent, as is the effect of the superimposed hydrogenous flux on the brown clay composition

4.iv CAPE VERDE ABYSSAL PLAIN

4.iv.a Regional Setting

The Cape Verde Abyssal Plain was studied by IOS during Farnella cruise 4, using GLORIA and seismic reflection profiling. The results have been reported by Kidd & Searle (1984). This followed an earlier reconnaissance carried out by 2.2 kHz profiler during Discovery cruise 118 (McGiveron, 1981). The majority of the work in the area has been carried out at the CV1 location (near 25°N, 25°W) by the French, and has been reported in Anderson (1980, 1981, 1982, 1984), Nuclear Energy Agency (1984) and Auffret et al (1984a,b).

CV1 was originally thought to be on a distal abyssal plain, but SEABEAM, coring and GLORIA studies all revealed considerable evidence of energetic sediment transport, coarse-sediment deposition, and possibly channelling. The sea bed is 4850m deep and slopes westward at 1.2%. It now seems that the location would be more properly viewed as part of the lower continental rise, and sediment transport processes there may be too energetic and too inhomogenous for it to be a prime site for waste disposal, at least with shallow emplacement.

The Discovery and Farnella cruises were designed in part to seek a more distal abyssal plain setting west of CV1. However, it was found that strongly developed sediment lineations persist as far west as 28°W-29°W, by which point there are numerous abyssal hills so that no extensive flat sea floor could be found there. Although the precise nature of the sediment lineations seen by GLORIA has not been proved here, by analogy with similar features elsewhere we interpret them as indicative of relatively high-energy bed-transport, possibly accompanied by local sand deposition and erosion. It seems unlikely that there is any extensive distal abyssal plain in this region.

4.iv.b Chemistry

CV1 Area

Only one core from the CV1 area was investigated, core 10399#7K which was collected on RRS Discovery Cruise 125 in 1982 (Thomson et al, 1982). This was a 2m Kastenlot core collected more or less in the centre of the CV1 area (25°16'N,25°26'W: 5235m).

Data collection on this core was well advanced before it was appreciated that it represented a repenetration sequence of the type occasionally seeem with the Kastenlot corer (Weaver & Schultheiss, 1983). The core is probably good to 86cm depth (Tables 4.iv.1 and 4.iv.2): from 70-85cm a sand layer is present and this appears to have terminated the corer's penetration. The remainder of the core (89-126cm) seems to represent two repenetrations of the overlying pelagic carbonate marl with an incomplete stratigraphy. The compositional data for this core is collated as Table 4.iv.2 and the radiometric data as Table 4.iv.2, but no further interpretation seems warranted.

CV2 Area

On RRS Discovery cruise 129 in 1982 (Wilson et al, 1982), station 10552 was devoted to intensive geochemical sampling on the most westerly plateau of the area. Successful deployments were made with the IOS box corer and a 2m Kastenlot corer to obtain sediment samples from which porewaters were obtained by squeezing. The IOS Mark II porewater sampler was used to obtain porewaters in situ.

Sediment and Porewater Sampling in the CV2 Area on "RRS Discovery" Cruise 129

Identification	Latitude	Longitude	Water Depth (m)	Sampling
10552#2	19°23.1'N	29°53.6'W	4683	2 metre Kastenlot core.
10552#7	19°24.5'N	29°52.7'W	4735	Pore water sampler (IOS Mark II).
10552#9	19°27.3'N	29°53.6'W	4655	41cm box core.
10552#11	19°21.2'N	29°52.5'W	4745	Pore water sampler (IOS Mark II).

Porewaters

Figure 4.iv.1 is a composite of data obtained from porewaters squeezed from corer sediment and from porewaters collected in situ at station 10552. The data are tabulated as Table 4.iv.3.

It is evident that the porewaters at this site are well oxygenated: extrapolation of the data trend of the dissolved oxygen profile suggests in fact that they may remain oxic to at least 10m. This observation is that expected of pelagic accumulation where the incoming flux of organic carbon is remineralised extensively at shallow depth in the sediment, with only a refractory C_{org} component being buried and further oxidation only taking place slowly (Müller & Mangini, 1980; Grundmanis & Murray, 1982). As a result of the availability of oxygen, denitrification does not occur, and a slight increase is seen in nitrate concentration with depth due to nitrification as a result of the slow remineralisation of more refractory organic carbon by oxygen. This process has been modelled at this site (Wilson et al, 1984), and Figure 4.iv.2 shows the fit of the model to the data for the longer core, 10552#2K. The total metabolic rate of C_{org} in the sediment column is 1.08×10^{-13} moles. $cm^2.sec^{-1}$ (Wilson et al, 1984). Also as a consequence of oxic conditions, no remobilisation of the redox-sensitive metal manganese is observed, and dissolved manganese remains below detection limits at all depths.

$^{230}Th_{excess}$ data and sediment accumulation rates

Radiochemical measurements for the $^{230}Th_{excess}$ method were carried out on three cores from CV2: the box and Kastenlot cores from RRS Discovery station 10552, and a CNEXO Kullenberg core KSO6 collected during the French SEABED cruise to this area. Fourteen analyses spaced over 180cm depth were made for the IOS cores and 6 on samples from near the top of core KSO6. Micropalaeontological studies of the coccolith component of these cores were also carried out by Dr P.P.E. Weaver (IOS). The radiochemical data for the alpha emitting isotopes of uranium and thorium are tabulated as Tables 4.iv.4, 4.iv.5 and 4.iv.6, and the $^{230}Th_{excess}$ plot for the IOS cores is presented in Figure 4.iv.3 and for the KSO6 core in Figure 4.iv.4.

Figure 4.iv.3 shows that the IOS box and Kastenlot $^{230}Th_{excess}$ data together suggest a layer of approximately similar $^{230}Th_{excess}$ activity some 35cm thick, underlain by a zone of regular decrease in $^{230}Th_{excess}$ from which a mean accumulation rate of $0.42cm.kyr^{-1}$ may be estimated. Because 35cm is much greater than the surface mixed layer thickness commonly observed (7-13cm: Cochran & Krishnaswami, 1980), it is not believed that the 35cm depth has a biological origin or is a true mixed layer. Figure 4.iv.5 shows a plot of the $^{230}Th/^{232}Th$ activity ratio versus depth for the station 10552 cores. This plot has better linearity than Figure 4.iv.3

and indicates a mean accumulation rate of 0.48cm.kyr^{-1}. The $^{230}Th/^{232}Th$ activity ratio plot is, in effect, similar to a $^{230}Th_{excess}$ plot expressed on a carbonate-free basis, and in general is not favoured (Ku, 1976). In the present case, the Th (^{232}Th) content of the sediment is inversely correlated with calcium carbonate content, with a clay end-member content (i.e. zero carbonate) of 14.7 ppm Th. It therefore appears that authigenic ^{230}Th is more closely associated with ^{232}Th (or clay) than is customarily the case (Ku, 1976). As the clay/carbonate variations in these cores are a function in different climatic regimes of first, the clay and carbonate input fluxes, and second of carbonate dissolution by undersaturated bottom water at these depths, this aspect is difficult to resolve fully.

Similar low but variable mean accumulation rates are derived from the biological marker horizons shown on Figure 4.iv.3 for the station 10552 cores, 0.32 and 0.41 cm.kyr^{-1}, and with the average rate of 0.36cm.kyr^{-1} obtained from $^{230}Th_{excess}$ measurements and micropaleontological investigations on core KS06. All these rates are somewhat lower than the values of 0.5 and 0.7cm.kyr^{-1} for a single box core (KG40) from the area measured by Mauviel et al (1982). As their data were based on proxy radiometric methods, a clay/carbonate effect similar to that observed at station 10552 may be present.

A calculation may be made to compare the sediment inventory of $^{230}Th_{excess}$ with the unique value expected from supply by the overlying water column. The sediment inventory amounts to between 60 and 70% of the water column supply for cores 10552 #2K and KS06, depending on the assumptions made. A recent review (Kadko, 1980) found a mean value of 72% of potential water column supply in 28 cores from between 4600 and 5800m water depth. It therefore does not appear that substantial sections of the studied cores are missing, despite the low and variable accumulation rates found.

Geochemical characterisation

Sediment analyses were performed by XRF on fused discs for major elements (SiO_2, Al_2O_3, Fe_2O_3, MnO, MgO, CaO, K_2O, TiO_2 and P_2O_5) and on pressed powder pellets for minor elements (Rb, Sr, Y, Zr, Nb, Co, V, Cr, Cu and Zn). Nineteen analyses were made on core 10552#2K, 4 analyses on core 10552#9BX, and 22 analyses on core KS06, as listed in Tables 4.iv.7, 4.iv.8 and 4.iv.9 respectively.

The most striking feature of the concentration/depth profiles of core 10552 #2K (which also applies to the other two cores) is that two main profile shapes are found. One shape is that typical of the aluminosilicate elements; the other is its mirror image and is exhibited only by CaO and Sr. The first shape is exhibited by Al_2O_3, SiO_2, Fe_2O_3, MgO, K_2O and TiO_2 of the major elements, V, Zr, Zn, Y and Cr of the trace elements, and U and Th (Table 4.iv.4). The two shapes are exemplified by Figures 4.iv.6 and 4.iv.7 for a major (Al_2O_3) and trace (Cr) element on the one hand and by figure 4.iv.8 for CaO on the other. The profiles are therefore consistent with a simple two-component mixing of biogenic calcium carbonate with a clay or aluminosilicate fraction of uniform composition. The variations in calcium carbonate content are expected to be climatically controlled, with a variable carbonate input flux and differing degrees of carbonate dissolution in the sediments by undersaturated bottom water at low accumulation rate. Of the elements measured here, only the chemically-related Sr shows an association with $CaCO_3$. As a consequence of the two component-system, good direct correlations are found between the concentrations of the detrital elements associated with clays, and good inverse correlations with CaO. The detrital elements also exhibit constant level concentration/depth profiles when expressed on a $CaCO_3$-free basis, e.g. Figure 4.iv.9 for Al_2O_3(carbonate free).

In studies of other sediments on this project a fraction of the elements Fe, Mn, Co, Ni and Cu have been shown to be enriched over clay or shale levels due to the hydrogenous or authigenic component of sedimentation which is markedly enriched in these elements. In the CV2 case it has not been possible to make good estimates of the magnitude or flux of this component, which must be present at such low accumulation rates, because of the variable sediment composition. The concentration depth profiles of these elements in core 10552 #2K are broadly similar to those of the alumino-silicate elements, and therefore correlate directly with Al_2O_3, although not with such good linearity as the elements mentioned above. As the porewater data indicated that the sediments are well oxygenated, no migration of the redox sensitive elements is anticipated. Specifically, no Mn^{2+} was found in solution, and no solid phase peaks characteristic of MnO_x immobilisation are observed. It has been found in previous work in oxic sediments (Carpenter et al, 1984) that the hydrogenous component correlates well with $^{230}Th_{excess}$ specific activity, as might be expected since both are derived from some water column scavenging process. The observations here that there is a direct correlation of the hydrogenous component with Al_2O_3, and that the $^{230}Th/^{232}Th$ activity ratio

plot with depth has a better linearity than the $^{230}Th_{excess}$ plot, suggest that both the hydrogenous component and the $^{230}Th_{excess}$ are associated with clay in this case.

As a consequence of the oxic nature of these sediments, the C_{org} values are generally low, 0.05 - 0.36wt.%, with the highest values observed near the sediment/water interface. This is the expected observation in such slowly-accumulated oxic sediments as discussed in the consideration of the porewater data.

The rare-earth elements (REE) were analysed on 8 samples from core 10552#2K (Table 4.iv.10), to investigate possible changes in provenance or diagenetic variation within the sediment. Analyses were performed by Inductively Coupled Plasma (ICP) at Kings College London. Absolute concentrations of the REE vary between 0.3 and 0.8x those of average shale (Haskin & Haskin, 1966) and the REE co-vary with Y (Table 4.iv.5), having a closely comparable distribution to Al.

When normalised to shale (Piper, 1974), the REE distributions are flat (Figure 4.iv.10) with no evidence of anomalous behaviour by the redox sensitive REE (Ce and Eu), or fractionation between the light and heavy end-members. The absence of fractionation supports evidence from the other geochemical data above that the sediments remained oxic throughout their history, and indicates that a detrital aluminiosilicate phase is the major control on the REE with little or no contribution from authigenic phases.

Conclusions

All the porewater data from the 10552 cores are consistent with a well-oxygenated sediment at steady-state. This is a consequence of the low overall sediment accumulation rate, below the threshold value for the onset of anoxia in pelagic sediment columns. It is concluded from the radiometric and palaeontological data that pelagic accumulation at a low rate between 0.35 and 0.5cm.kyr^{-1} is dominant in the studied cores. No evidence of turbidites was found, and the $^{230}Th_{excess}$ inventory suggests that no substantial loss of material has occurred in the past 450kyr. Despite this, however, both the $^{230}Th_{excess}$ and palaeontological data indicate that accumulation has not been regular in time.

The compositional data of these sediments are consistent with a simple two-component system of biogenic carbonate and detrital clay. An unquantified hydrogenous component is also present as shown by elevated levels of Mn, Co, Ni and Zn, and like $^{230}Th_{excess}$ this component appears loosely correlated with the clay content rather than the carbonate content. It is suggested that this is caused by climatically controlled variations in carbonate and clay fluxes, and carbonate dissolution by undersaturated bottom water at these low accumulation rates. No post-depositional migration of redox-sensitive metals, and low C_{org} values, are observed as expected from a fully oxic sediment section.

Flat REE profiles are observed, suggesting that the aluminosilicate phase is the major control on REE with little authigenic contribution.

Table 4.iv.1 Compositional Data for Core 10399

Core 10399#7K (25°16'N, 25°26'W; 5235m

Depth Interval cm	Major element data, % wt. (dry basis)												Trace element data, ppm									
	SiO_2	Al_2O_3	Fe_2O_{3T}	MnO	MgO	Cao	K_2O	TiO_2	P_2O_5	LOI	Total	NaCl*	C_{org}	Rb	Sr	Y	Zr	Nb	Ni	Co	V	Cr	Cu	Zn
0-1	24.37	7.54	2.99	0.12	1.54	30.76	0.33	0.33	0.16	30.70	98.84	2.89		53	930	20	122	9	41	22	67	47	62	56
4-5	19.15	5.89	2.32	0.10	1.23	36.29	0.12	0.23	0.12	33.46	98.91	2.79		41	1033	14	97	5	33	20	61	38	50	46
9-10	25.67	7.95	3.09	0.13	1.62	30.05	0.42	0.32	0.15	29.55	99.95	2.79		46	944	18	109	8	44	21	68	44	53	55
10-12	25.51	7.79	3.02	0.12	1.58	29.21	0.36	0.32	0.13	30.84	98.88	2.70		48	934	19	102	9	65	19	70	46	60	62
14-16	24.84	7.49	2.87	0.13	1.65	30.32	0.32	0.28	0.15	30.80	98.85	2.46		52	903	22	113	9	50	22	74	47	59	61
18-20	28.50	7.47	2.85	0.12	1.65	28.15	0.49	0.33	0.16	28.61	98.33	2.43		50	839	24	125	8	53	18	69	46	59	57
23-25	36.45	10.64	4.60	0.08	2.01	20.10	1.07	0.53	0.19	22.48	98.14	1.90		62	633	30	156	13	41	28	98	58	73	73
29-31	27.08	8.01	3.25	0.13	1.58	28.81	0.45	0.36	0.15	28.71	98.52	2.13		54	855	23	121	7	41	24	76	43	59	57
33-35	42.53	12.84	5.47	0.22	2.28	14.23	1.75	0.66	0.18	18.01	98.17	2.15		86	504	30	179	20	67	34	121	67	94	87
40-42	41.37	12.87	5.42	0.24	2.31	14.81	1.70	0.67	0.16	18.49	98.04	1.65		84	511	32	177	21	72	35	121	67	87	87
42-44	39.51	12.22	5.25	0.25	2.23	16.87	1.53	0.62	0.19	19.90	98.57	1.83		80	361	31	167	16	69	33	114	65	82	84
47-49	36.94	11.18	4.65	0.19	2.09	18.89	1.15	0.55	0.16	21.55	97.35	2.24		73	591	26	157	16	62	31	106	63	70	77
55-57	37.53	12.00	4.78	0.14	2.30	17.88	1.18	0.53	0.14	21.39	97.87	2.18		78	623	24	138	14	60	22	102	75	58	83
66-68	39.30	9.14	3.36	0.11	1.97	20.55	0.97	0.42	0.14	22.11	98.07	2.46		62	607	22	155	9	41	15	73	57	41	63
70-72	46.10	7.21	2.36	0.10	1.57	19.95	1.23	0.37	0.14	19.75	98.78	2.33		53	485	18	198	8	27	10	53	39	27	45
86-88	46.40	5.96	1.80	0.10	1.24	20.76	1.07	0.33	0.13	19.77	99.56	2.52		43	492	16	239	6	23	11	45	38	21	37
93-95	22.55	6.89	2.69	0.10	1.40	32.58	0.17	0.27	0.14	31.55	98.34	2.97		42	848	16	95	6	33	16	55	35	44	48
99-101	42.52	13.14	5.42	0.25	1.77	13.90	1.82	0.67	0.16	16.87	96.52	2.05		85	495	33	182	26	68	33	120	67	94	88
105-107	20.05	6.14	2.40	0.11	1.88	35.58	0.16	0.24	0.12	33.02	99.70	2.35		41	1031	14	94	5	34	20	62	39	53	47
123-125	35.44	10.19	4.33	0.11	1.39	21.19	1.09	0.49	0.15	23.41	97.79	2.02		68	671	29	150	14	40	35	94	54	71	70

Table 4.iv.2 Radiometric Data for Core 10399

Depth cm	U ppm	Th ppm	Th/U	$\frac{^{234}U}{^{238}U}$ Activity Ratio	$\frac{^{230}Th}{^{232}Th}$ Activity Ratio	^{234}U dpm/g	^{230}Th dpm/g	$^{230}Th_{excess}$ dpm/g
10399#7K								
4-5	1.06 ± 0.30	5.7±0.2	5.2 ± 0.2	1.07±0.04	17.5 ±0.5	0.85±0.02	23.5 ±0.5	22.6 ±0.5
10-11	1.05 ± 0.04	5.7±0.2	5.4 ± 0.3	1.08±0.05	10.3 ±0.3	0.85±0.03	14.3 ±0.4	13.4 ±0.4
25	1.60 ± 0.05	9.0±0.2	5.6 ± 0.3	1.05±0.04	10.4 ±0.2	1.26±0.04	22.6 ±0.5	21.3 ±0.5
33-35	2.04 ± 0.07	11.4±0.6	5.6 ± 0.3	1.01±0.04	7.7 ±0.2	1.54±0.05	21.2 ±0.9	19.6 ±0.9
45	1.93 ± 0.06	10.1±0.4	5.2 ± 0.3	0.93±0.03	6.5 ±0.2	1.34±0.04	15.9 ±0.5	14.5 ±0.5
55-57	1.79 ± 0.04	10.4±0.3	5.8 ± 0.2	1.01±0.03	3.19±0.07	1.35±0.03	8.1 ±0.2	6.7 ±0.2
65	1.64 ± 0.05	6.9±0.2	4.2 ± 0.2	1.08±0.04	3.51±0.09	1.32±0.04	5.8 ±0.2	4.5 ±0.2
70-72	1.62 ± 0.04	5.5±0.2	3.38±0.16	0.97±0.03	1.62±0.06	1.18±0.03	2.15±0.18	0.97±0.08
77-79	1.84 ± 0.05	5.2±0.1	2.82±0.13	1.00±0.04	1.36±0.05	1.37±0.04	1.71±0.06	0.34±0.07
85	2.10 ± 0.06	5.5±0.2	2.62±0.13	0.94±0.03	1.33±0.06	1.48±0.04	1.77±0.07	0.29±0.08
89-91	1.08 ± 0.04	5.6±0.2	5.2 ± 0.2	1.02±0.04	17.0 ±0.4	0.82±0.03	23.0 ±0.5	22.2 ±0.5
95-97	1.62 ± 0.06	9.0±0.3	5.6 ± 0.3	0.98±0.05	9.0 ±0.3	1.19±0.05	20.7 ±0.6	19.5 ±0.6
105	1.01 ± 0.03	5.1±0.2	5.0 ± 0.2	0.99±0.04	17.5 ±0.5	0.74±0.03	21.4 ±0.4	20.7 ±0.4
111-113	1.20 ± 0.03	6.4±0.3	5.3 ± 0.2	1.06±0.03	9.5 ±0.3	0.95±0.02	14.9 ±0.4	13.9 ±0.4
117-119	1.52 ± 0.04	7.1±0.3	4.7 ± 0.2	1.08±0.03	9.0 ±0.2	1.23±0.03	15.5 ±0.4	14.3 ±0.4
123-125	1.72 ± 0.04	8.7±0.4	5.1 ± 0.3	0.99±0.03	11.2 ±0.3	1.28±0.03	23.8 ±0.9	22.5 ±0.9

Table 4.iv.3 Porewater data for Station 10552

Position		Sample ID	cm Depth	µM SiO_2	µM PO_4	µM NO_3	meq l^{-1} Alk	µM Mn	nM Ni	nM Cu	nM Cd	µM O_2
19°27.3'N 29°53.6'W	Core 9B	Bottom W		47.4	1.7	-						
		055	0- 2.5	61	1.1	35			21	144	3.8	
		056	2.5- 5	65	1.0	42			17	78	3.0	
		057	5- 7.5	75	1.1	50			33	43	3.1	
		058	7.5-10	75	1.2	34		0.26	19	24	2.4	
		059	10-12.5	75	1.1	36			45	35	2.6	
		060	12.5-15	87	1.3	34			21	17	8.2	
		061	15-17.5	87	1.3	34			17	11	2.6	
		062	17.5-20	79	1.1	35			14	13	2.5	
		063	20-24	84	1.1	35			13	10	3.1	
		064	24-28	89	1.1	43			11	15	2.5	
		065	28-32	90	1.1	27			13	17	2.4	
		066	32-27	88	1.1	31			11	15	2.2	
19°24.5'N 29°52.7'W	P.W.S. MkII Cast 7	0C	Bot W	53	0.7	-						296
		1C	0	49	0.5	-						285
		2C	3	69	0.7	-						188
		3C	4.5	48	0.6	-						-
		4C	7.5	68	0.5	-						193
		5C	13.5	79	1.1	-						150
		6C	25.5	89	1.3	-						138
		7C	41.5	79	0.6							110
19°21.2'N 29°52.0'W	P.W.S. MkII Cast 11	0C	Bot W	49	0.7							
		1C	0	50	0.6							
		2C	3	68	1.0							
		3C	4.5	50	0.7							
		4C	7.5	74	0.7							
		5C	13.5	76	1.2							
		6C	25.5	90	4.6							
		7C	41.5	97	1.2							

Table 4.iv.3 Porewater data for Station 10552 (continued)

Position	Sample ID	cm Depth	µM SiO_2	µM PO_4	µM NO_3	meq l^{-1} Alk	µM Mn	nM Ni	nM Cu	nM Cd	µM O_2
19°23.1'N 29°53.6'W Core 2K	Bottom		47.4	1.7	-						
	044	11	89	1.4	48	1.99		21	18	5.1	
	045	29	91	1.3	27	1.81	0.28	18	12	2.3	
	046	47	103	1.4	46	1.91		13	11	2.8	
	047	60	113	1.4	36	2.03		12	10	1.7	
	048	71	115	1.6	43	2.09	0.28	19	30	2.3	
	049	87	118	1.7	49	2.11		17	8	1.6	
	050	106	122	1.6	51	2.09		44	14	2.2	
	051	122	111	1.4	50	1.90		43	8	1.4	
	052	135	126	1.9	46	2.36	0.54	82	9	1.6	
	053	148	110	1.1	48	2.12		71	14	1.6	
	054	166	118	1.3	60	2.09		17	7	2.2	

Table 4.iv.4 Radiometric data for core 10552#2K

Depth cm	U ppm	Th ppm	Th/U	$\frac{^{230}Th}{^{232}Th}$ Activity Ratio	$\frac{^{234}U}{^{238}U}$ Activity Ratio	^{230}Th dpm/g	^{234}U dpm/g	$^{230}Th_{excess}$ dpm/g
10552#2K								
0-2	1.02+	4.1 ±0.2	-	15.1 ±0.6	-	15.1 ±0.5	0.75+	14.3 ±0.5
21-23	1.02±0.04	5.7 ±0.3	5.6±0.3	8.6 ±0.3	0.98±0.05	13.3 ±0.4	0.75±0.03	12.6 ±0.4
36-38	1.20±0.04	5.1 ±0.3	5.0±0.4	7.9 ±0.4	1.01±0.05	9.9 ±0.4	0.76±0.03	9.1 ±0.4
41-43	1.45±0.04	7.6 ±0.3	5.2±0.3	7.3 ±0.2	1.03±0.04	13.4 ±0.4	1.11±0.03	12.3 ±0.4
51-53	1.00±0.05	5.5 ±0.2	5.5±0.3	6.9 ±0.2	1.08±0.07	9.2 ±0.2	0.81±0.04	8.4 ±0.2
66-68	0.72+	4.24±0.22	-	5.3 ±0.3	-	5.5 ±0.2	0.62+	4.9 ±0.2
86-88	1.17±0.05	7.0 ±0.3	5.9±0.4	3.08±0.11	1.04±0.05	5.2 ±0.2	0.91±0.04	4.3 ±0.3
126-128	1.49±0.04	8.2 ±0.3	5.5±0.3	1.58±0.05	0.95±0.03	3.13±0.11	1.06±0.03	2.07±0.11
146-148	0.99+	6.8 ±0.2	-	0.86±0.02	-	1.42±0.04	0.66+	0.76±0.04
175-177	0.71±0.03	4.1 ±0.2	5.7±0.4	0.57±0.04	0.90±0.04	0.56±0.04	0.48±0.02	0.09±0.04

+ Estimated values

Table 4.iv.5 Radiometric data for core 10552#9BX

Sample Depth cm	U ppm	Th ppm	Th/U	$\frac{^{234}U}{^{238}U}$ Activity Ratio	$\frac{^{230}Th}{^{234}Th}$ Activity Ratio	^{234}U dpm/g	^{230}Th dpm/g	$^{230}Th_{excess}$ dpm/g
10552#9BX								
0- 1.25	0.56+	3.06±0.09	5.46±0.33	-	15.6±0.04	0.54+	11.6±0.2	11.1±0.2
3.8- 5.1	0.84±0.03	4.30±0.20	5.11±0.30	0.94±0.05	14.1±0.6	0.59±0.02	14.7±0.02	14.1±0.4
11.5-12.5	0.87+	2.49±0.13	2.74±0.15	-	18.0±0.8	0.65+	10.9±0.3	10.2±0.3
18.5-19.5	0.91±0.02	5.10±0.21	5.60±0.26	1.04±0.26	10.2±0.3	0.7 ±0.02	12.7±0.4	12.0±0.4

+ Estimated value

Table 4.iv.6 Radiometric data for core KS06

Sample Depth cm	U ppm	Th ppm	Th/U	$\frac{^{230}Th}{^{232}Th}$ Activity Ratio	$\frac{^{234}U}{^{238}U}$ Activity Ratio	^{230}Th dpm/g	^{234}U dpm/g	$^{230}Th_{excess}$ dpm/g
KS06								
0-5	0.64±0.02	3.48±0.12	5.4 ± 0.3	16.9 ±0.5	1.10±0.05	14.3 ±0.3	0.52±0.02	13.8 ±0.3
63-68	1.51±0.06	8.2 ±0.3	5.4 ± 0.3	3.01±0.09	0.99±0.05	6.0 ±0.2	1.12±0.04	4.88±0.20
91-96	0.90±0.03	5.3 ±0.2	5.8 ± 0.3	1.73±0.07	1.07±0.04	2.21±0.08	0.72±0.02	1.49±0.08
101-106	2.03±0.05	12.5 ±0.5	6.2 ± 0.3	1.36±0.05	0.90±0.03	4.15±0.17	1.37±0.03	2.78±0.17
178-183	1.69±0.05	9.7 ±0.2	5.8 ± 0.2	0.65±0.01	0.94±0.03	1.53±0.04	1.19±0.03	0.33±0.05
211-216	1.96±0.07	10.3 ±0.3	5.2 ± 0.2	0.53±0.01	0.87±0.04	1.32±0.04	1.27±0.05	0.05±0.06

Table 4.iv.7 Compositional data for core 10552#2K

Core 10552#2K (19°23'N, 29$42'W; 4683m)

Depth Interval cm	Major Element Data, % wt. (dry basis)													Trace Element Data, ppm									
	SiO_2	Al_2O_3	Fe_2O_{3T}	MnO	MgO	Cao	K_2O	Na_2O	TiO_2	P_2O_5	LOI	Total	NaCl	Corg	Rb	Sr	Y	Zr	Nb	Ni	Co	V	Cr	Cu	Zn
0-2	13.86	4.38	1.92	0.06	1.08	40.53	0.71	0.43	0.24	0.18	36.09	98.91	2.99	0.24	34	1030	16	58	2	20	13	52	29	42	39
6-8	9.02	2.85	1.20	0.05	0.72	44.78	0.43	0.36	0.16	0.16	39.16	98.51	3.16		22	1047	12	39	2	15	10	35	21	32	29
11.5-12.5	8.30	2.65	1.11	0.04	0.66	45.82	0.46	0.33	0.15	0.16	39.66	98.91	3.19	0.19	21	1046	12	41	<2	13	10	33	19	29	27
15.5-16.5	19.39	3.99	1.71	0.05	0.92	41.50	0.60	0.57	0.22	0.17	36.31	98.96	3.05		28	1008	14	58	4	21	13	47	27	35	34
21-23	19.26	5.70	2.50	0.09	1.14	35.99	0.88	0.80	0.37	0.18	32.81	99.19	2.11	0.09	39	915	21	77	8	28	14	59	33	42	42
36-38	18.80	5.72	2.44	0.08	1.10	35.59	0.96	0.94	0.32	0.19	32.68	98.13	2.36		40	902	19	76	6	30	16	62	35	43	44
41-43	29.65	8.90	3.91	0.13	1.61	25.95	1.39	1.40	0.52	0.22	25.78	98.71	1.54	0.11	59	700	24	128	15	45	22	88	49	64	62
51-53	18.20	5.59	2.50	0.09	1.17	36.77	0.91	0.89	0.32	0.19	33.08	99.02	2.18		38	861	18	82	6	31	16	60	35	46	43
66-68	14.74	4.58	2.00	0.07	0.90	39.67	0.70	0.50	0.26	0.17	35.36	99.36	2.35	0.18	31	957	16	68	4	22	14	49	28	39	36
76-78	24.50	7.43	3.19	0.10	1.25	30.86	1.15	1.12	0.42	0.20	29.27	99.74	1.87		47	805	23	109	9	34	17	70	42	51	51
86-88	23.56	7.41	3.30	0.13	1.38	31.45	1.15	1.03	0.41	0.20	29.74	98.98	1.60		49	802	24	109	8	40	18	72	42	47	53
98-100	32.51	10.33	4.41	0.15	1.72	21.92	1.52	1.59	0.58	0.23	22.97	97 45	1.43	0.16	65	629	27	142	14	51	22	96	54	66	67
116-118	16.18	5.04	2.18	0.07	1.07	38.19	0.76	0.58	0.28	0.18	34.35	99.28	2.50		34	949	18	70	5	27	14	50	30	37	39
126-128	29.20	8.81	3.78	0.12	1.57	25.41	1.43	1.46	0.50	0.21	26.03	97.65	1.45	0.22	58	729	25	133	14	46	20	80	47	60	60
136-138	22.40	6.81	2.90	0.10	1.22	32.98	1.02	0.87	0.38	0.21	30.72	98.95	1.97		43	954	24	106	8	42	18	64	38	50	49
146-148	23.99	7.10	3.07	0.11	1.23	31.29	1.15	0.87	0.41	0.21	30.08	98.81	1.82	0.07	49	920	25	110	12	47	20	72	41	52	55
156-158	33.57	10.55	4.42	0.16	1.76	22.22	1.72	1.65	0.59	0.29	23.07	99.31	1.52		69	634	31	148	15	65	25	94	54	58	72
166-168	18.87	6.04	2.53	0.09	1.03	36.04	0.92	0.87	0.32	0.19	32.78	98.97	1.99		39	881	21	86	8	35	17	58	33	35	45
175-177	13.04	4.25	1.79	0.07	0.89	41.17	0.69	0.49	0.22	0.20	36.43	98.66	2.19	0.05	30	979	15	59	5	26	15	42	25	29	37

Table 4.iv.8 Compositional data for core 10552#9BX

Core 10552#9BX (19°27'N 29°54'W; 4655m)

Depth Interval cm	Major Element Data, % wt. (dry basis)													Trace Element Data, ppm									
	SiO_2	Al_2O_3	Fe_2O_{3T}	MnO	MgO	CaO	K_2O	TiO_2	P_2O_5	LOI	Total	NaCl	$CaCo_3$	C_{org}	Rb	Sr	Y	Zr	Ni	Co	V	Cr	Cu	Zn
0-1.25	12.06	3.42	1.28	0.04	0.84	39.19	0.04	0.11	0.10	39.19	96.27	5.60	75.67	0.36	26	1001	10	45	15	7	42	22	29	32
3.8-5.1	12.31	3.73	1.35	0.04	0.86	33.96	0.07	0.12	0.10	38.41	95.95	2.88	-	-	33	1003	17	58	18	12	50	29	37	36
7.5-8.5	15.66	4.71	1.74	0.06	0.98	36.66	0.08	0.17	0.11	36.50	96.67	3.11	-	-	24	1003	13	42	15	11	37	22	33	30
18.5-19.5	18.67	5.42	2.02	0.07	0.95	35.76	0.16	0.21	0.11	34.23	97.60	2.64	67.58	0.26	33	920	20	72	22	15	55	30	36	38

Table 4.iv.9 Compositional Data for Core KS06

Core KS06 (19°25'35"N, 29°49'50"W: 4830m)

Depth Interval cm	Major Element Data, % wt. (dry basis)											Trace Element Data, ppm										
	SiO_2	Al_2O_3	Fe_2O_{3T}	Mno	MgO	CaO	K_2O	TiO_2	P_2O_5	LOI	Total	NaCl	Rb	Sr	Y	Zr	Nb	Ni	Co	V	Cr	Cu	Zn
0.00-0.5	11.80	3.49	1.45	0.06	0.83	43.45	0.00	0.12	0.10	38.09	101.33	1.94	25	1091	10	72	<2	20	13	40	24	38	35
0.63-0.68	31.75	9.51	3.98	0.15	1.68	25.17	0.87	0.46	0.13	25.39	101.19	2.10	62	712	27	153	19	50	22	89	52	62	65
0.91-0.96	19.16	5.52	2.17	0.08	1.12	36.82	0.21	0.23	0.11	33.32	100.83	2.10	39	981	19	103	7	32	15	56	31	42	44
1.01-1.06	42.20	12.69	5.33	0.19	2.10	14.76	1.69	0.68	0.14	18.29	100.17	2.10	86	487	28	202	25	68	27	118	66	87	87
1.78-1.83	34.83	10.79	4.37	0.16	1.80	21.74	1.20	0.53	0.15	23.00	100.52	1.94	71	613	28	163	15	64	25	101	57	69	69
2.11-2.16	38.42	11.87	4.89	0.15	1.91	18.38	1.53	0.61	0.15	20.67	100.61	2.02	77	532	29	176	19	62	24	108	62	69	78
2.71-2.76	41.78	12.97	5.99	0.19	2.10	14.55	1.69	0.70	0.16	17.88	99.89	1.97	93	428	36	205	21	80	33	125	72	87	93
4.25-4.30	19.81	6.11	2.36	0.01	1.12	35.96	0.26	0.24	0.10	32.68	100.46	1.71	40	1004	19	102	10	38	17	55	34	44	46
5.08-5.13	15.55	4.63	4.63	0.07	0.89	40.15	0.10	0.17	0.10	35.54	100.72	1.71	31	1048	16	88	4	26	14	45	28	37	37
6.14-6.19	23.98	7.59	2.98	0.11	1.27	32.25	0.43	0.33	0.08	30.22	100.94	1.71	49	802	20	130	17	40	19	67	41	60	55
6.72-6.77	13.92	4.20	1.55	0.06	0.83	41.81	0.10	0.15	0.09	36.81	101.20	1.68	28	1081	14	78	4	25	13	40	24	35	34
7.12-7.17	5.66	1.67	0.64	0.04	0.47	48.48	0.00	0.04	0.08	41.65	100.42	1.71	15	1165	11	50	<2	10	10	19	17	19	21
7.85-7.90	28.06	8.80	3.40	0.14	1.58	26.46	0.94	0.41	0.13	29.07	100.56	1.56	47	837	21	117	12	41	22	64	38	60	54
8.78-8.83	27.36	8.34	3.27	0.15	1.46	34.15	0.59	0.36	0.14	23.92	101.30	1.56	67	831	30	160	13	60	27	90	53	74	70
9.22-9.27	12.03	3.63	1.40	0.07	0.76	43.89	0.04	0.11	0.09	37.33	100.98	1.63	25	1140	15	74	4	25	15	34	21	30	32
10.14-10.19	30.21	9.25	3.73	0.15	1.59	22.88	1.27	0.43	0.13	29.98	101.41	1.79	44	774	19	116	9	38	19	58	33	37	50
10.43-10.48	23.28	7.18	2.79	0.10	1.26	29.54	0.58	0.31	0.11	34.47	101.41	1.79	30	954	15	81	6	25	14	40	23	26	36
10.93-10.98	19.35	5.94	2.22	0.08	1.21	45.13	0.11	0.22	0.12	24.99	101.07	1.71	58	1093	28	131	9	59	29	75	45	64	62
11.35-11.40	12.09	3.91	1.46	0.08	0.84	40.85	0.07	0.13	0.11	38.39	99.64	1.71	50	837	26	143	13	58	29	86	50	64	65
11.47-11.52	24.59	7.70	2.94	0.13	1.46	31.49	0.80	0.32	0.14	29.72	101.55	2.25	23	1095	14	63	<2	23	15	33	19	39	34
11.60-11.65	54.44	17.63	7.28	0.32	2.99	1.13	3.18	1.00	0.24	9.21	101.14	2.35	115	160	49	236	28	113	47	148	85	101	118
11.85-11.90	54.27	17.44	7.25	0.32	2.89	1.39	3.03	0.98	0.23	9.41	100.93	2.35	117	152	50	239	30	119	46	151	86	102	119

Table 4.iv.10 10552#2K Rare-Earth Element Data

Sample	Element											
	La	Ce	Pr	Nd	Sm	Eu	Gd	Dy	Ho	Er	Yb	Lu
6 - 8	12.90	23.40	2.90	11.70	2.33	0.58	2.15	1.89	0.38	1.15	0.97	0.15
15 - 16	17.40	32.00	4.01	16.60	3.19	0.77	2.94	2.56	0.52	1.46	1.19	0.19
36 - 38	21.80	43.10	5.07	20.50	3.90	0.94	3.65	3.13	0.64	1.71	1.51	0.24
66 - 68	18.80	35.80	4.30	17.40	3.40	0.82	3.14	2.68	0.55	1.49	1.38	0.21
76 - 78	27.50	54.90	6.25	25.00	4.89	1.16	4.32	3.69	0.75	2.04	1.88	0.28
98 - 100	33.80	72.90	7.71	30.60	5.91	1.42	5.25	4.45	0.89	2.48	2.28	0.35
116 - 118	20.60	38.50	4.65	19.00	3.73	0.89	3.45	2.99	0.61	1.66	1.46	0.23
166 - 168	22.40	44.00	5.25	21.40	4.19	0.99	3.83	3.30	0.67	1.80	1.62	0.24

Sample depths in centimetres below the sediment/water interface

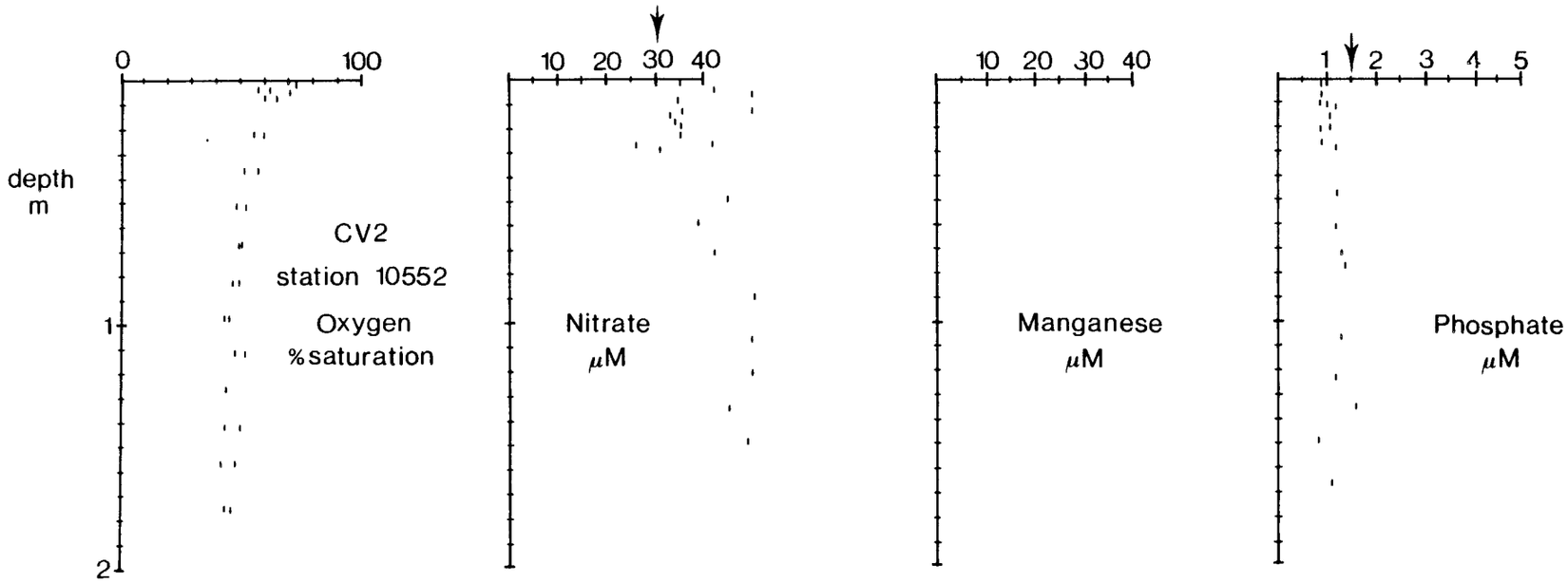

Figure 4.iv.1 Composite porewater data profiles for station 10552.

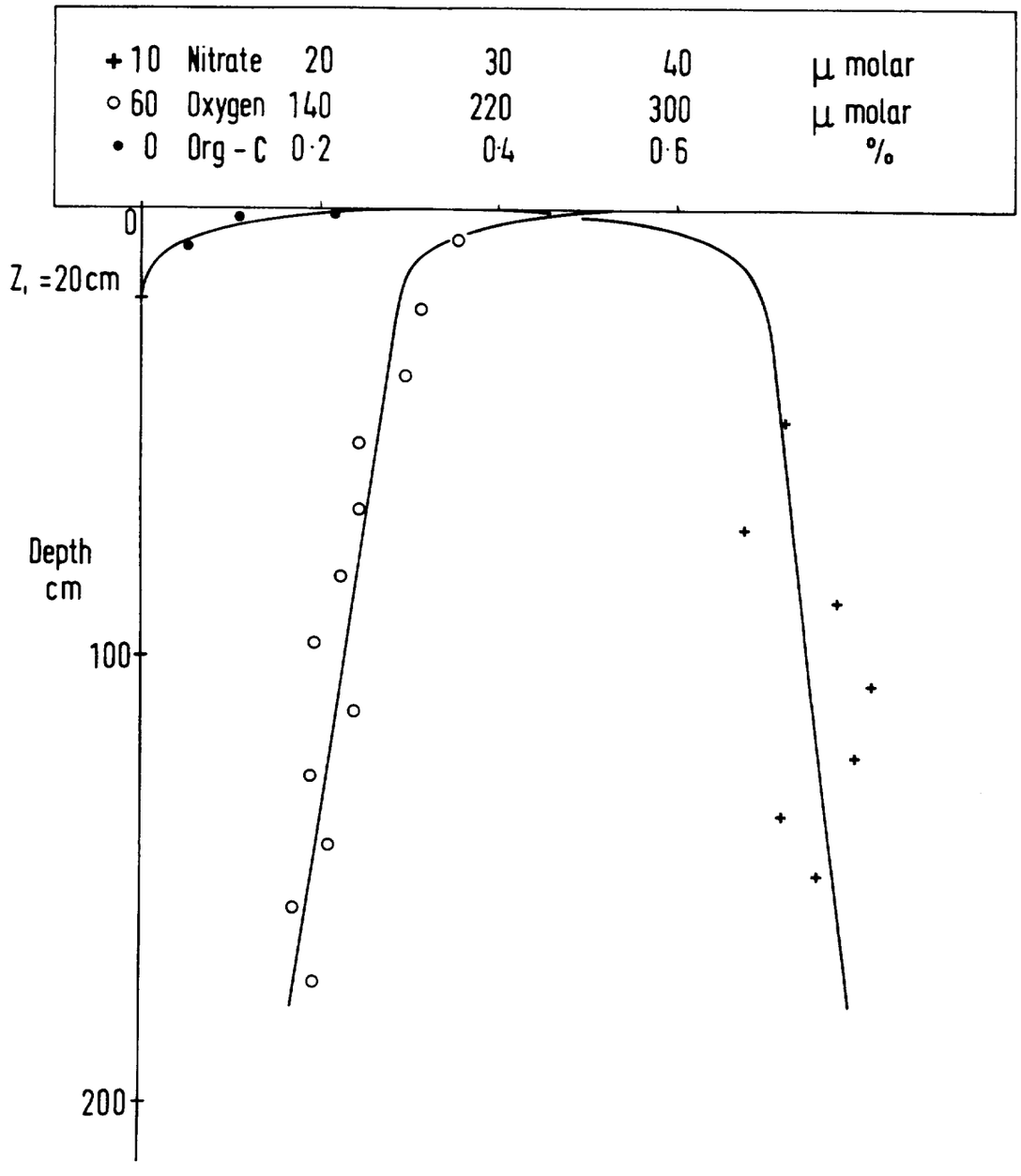

Figure 4.iv.2 Fit of model of oxygen, nitrate and labile organic-carbon data for station 10552. Labile organic-carbon is derived by averaging all values below depth Z and subtracting from the values above this depth.

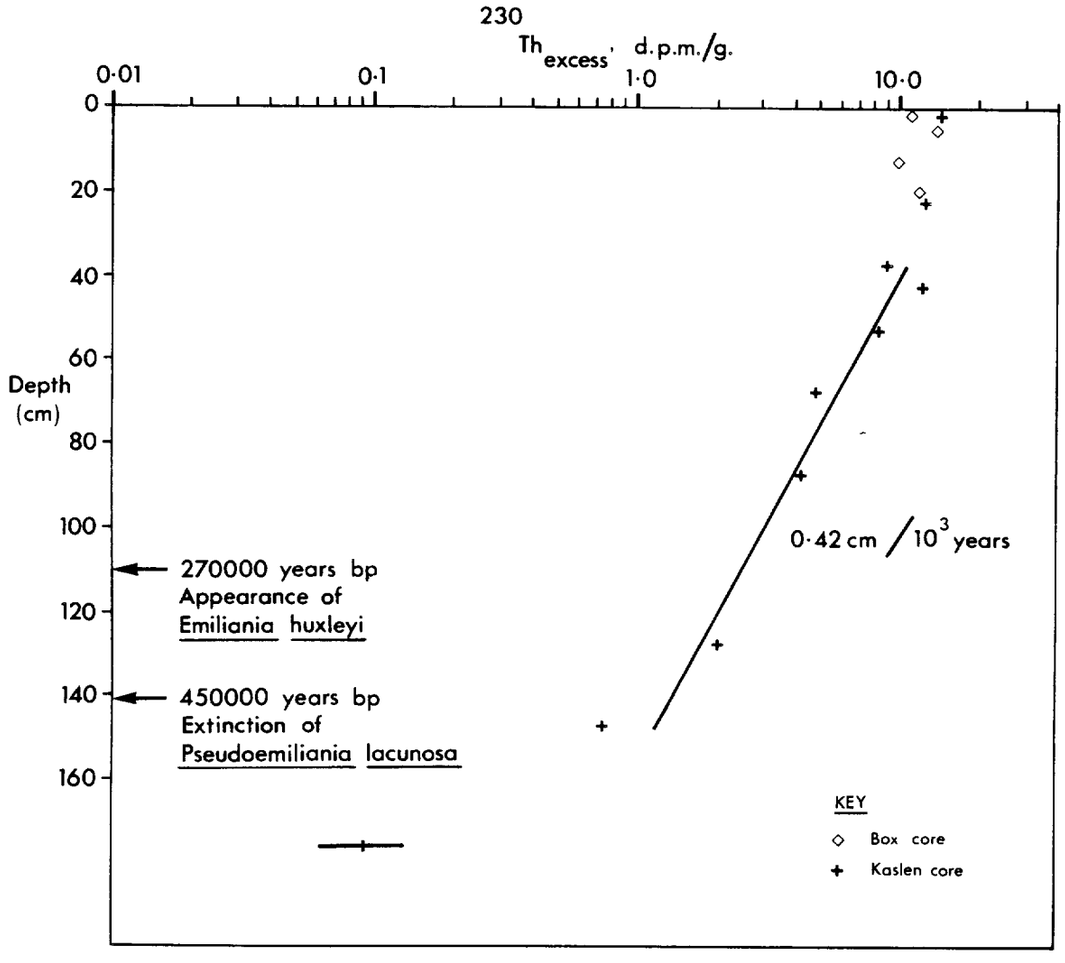

Figure 4.iv.3 $^{230}Th_{excess}$ data for station 10552 cores.

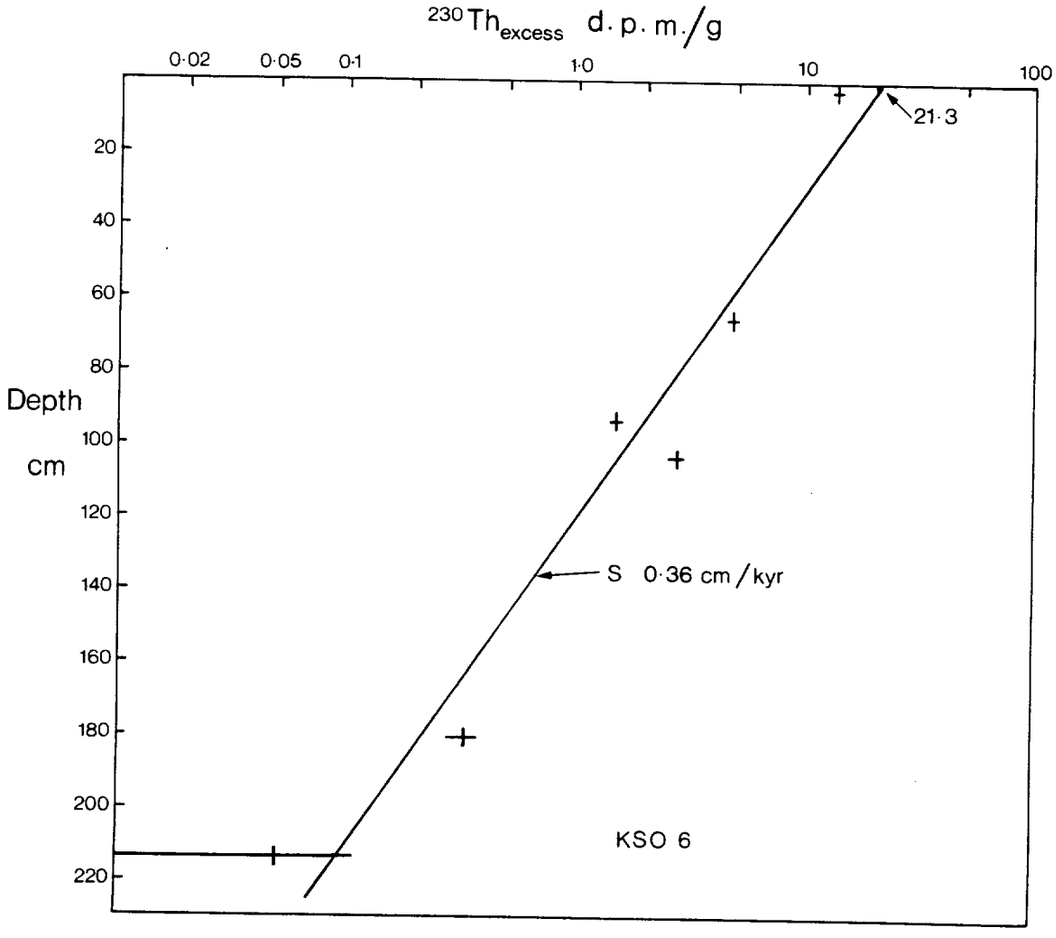

Figure 4.iv.4 $^{230}Th_{excess}$ data for core KS06.

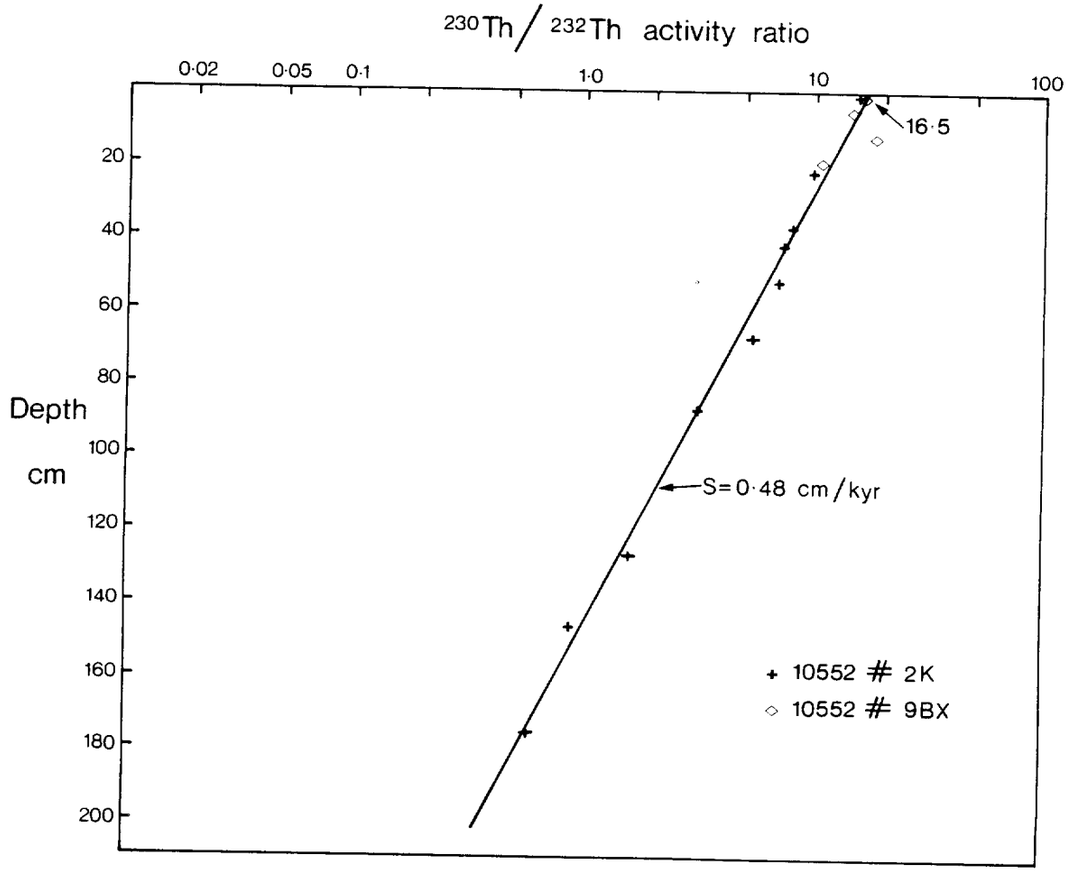

Figure 4.iv.5 $^{230}Th/^{232}Th$ activity ratio plot for station 10552 cores.

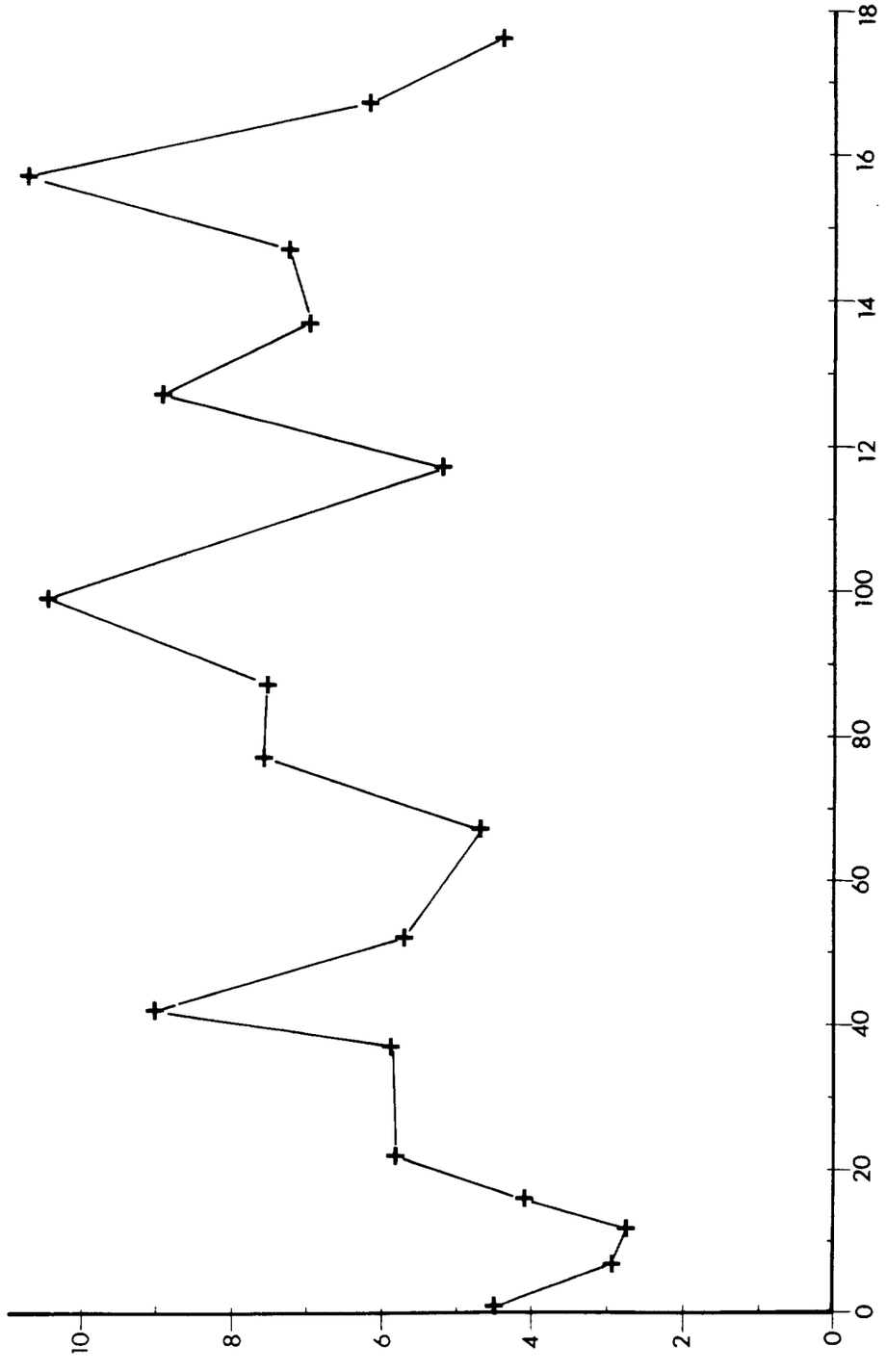

Figure 4.iv.6 Concentration-depth profile of Al_2O_3 in core 10552#2K.

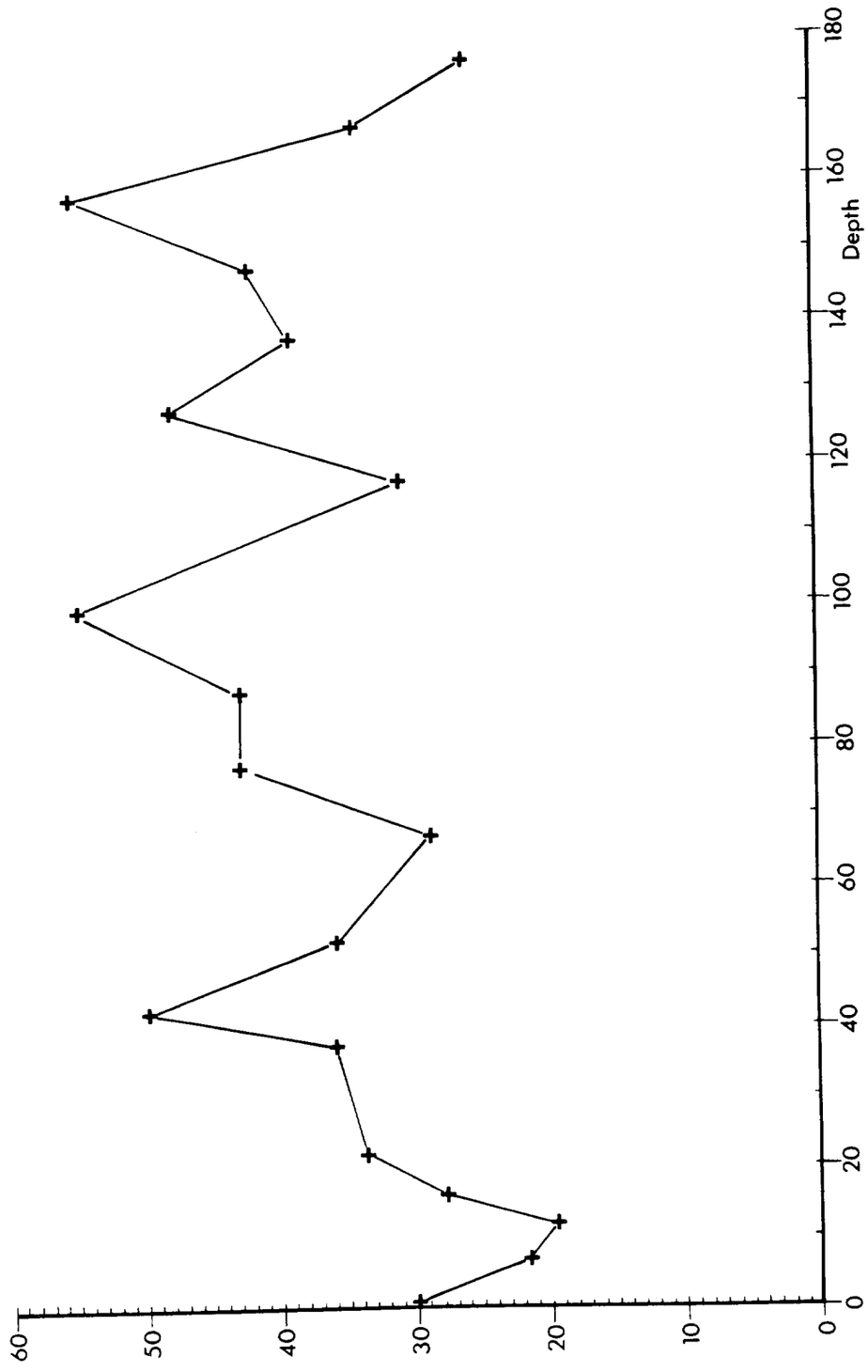

Figure 4.iv.7 Concentration-depth profile of Cr in core 10552#2K.

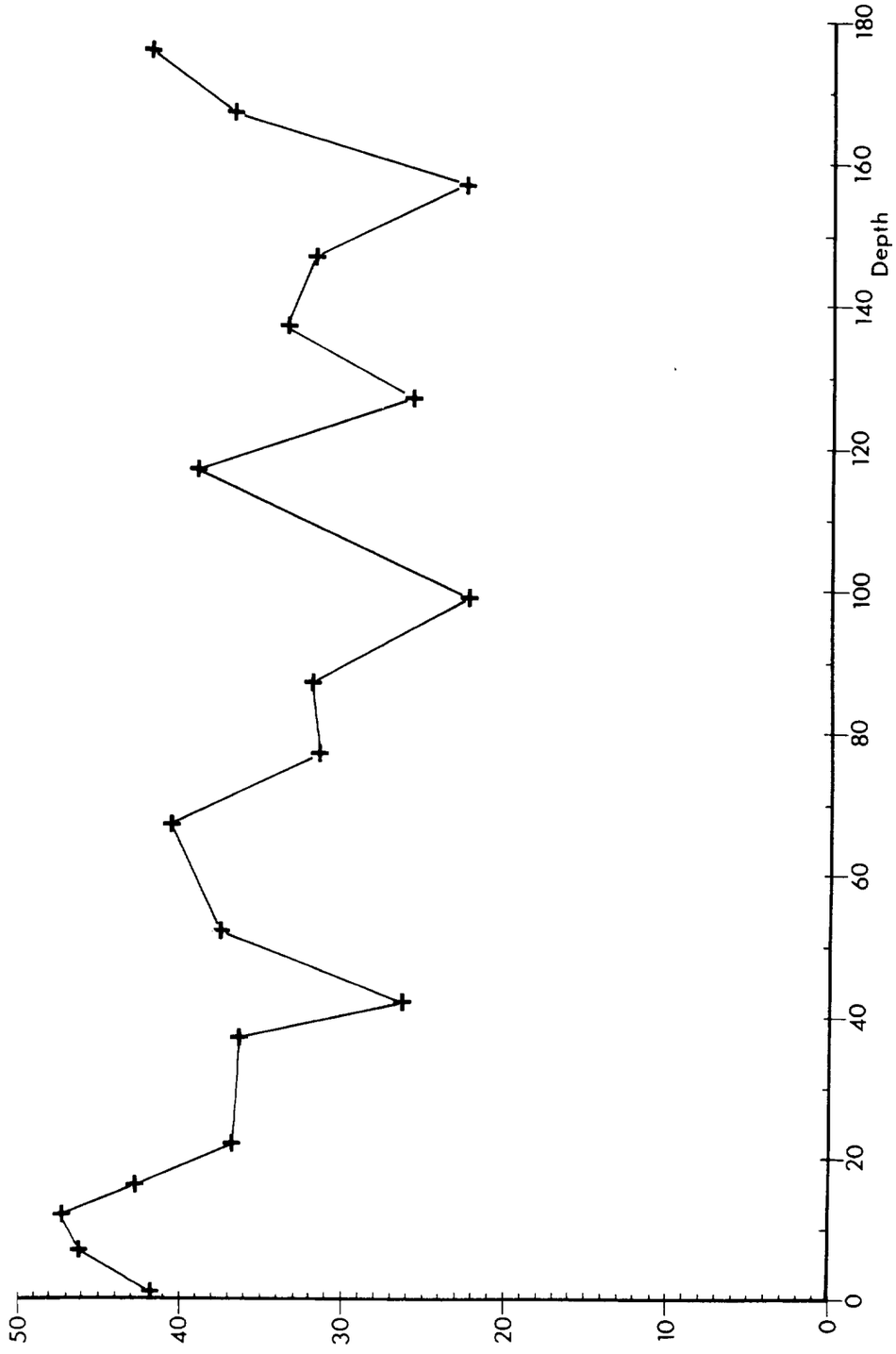

Figure 4.iv.8 Concentration-depth profile of CaO in core 10552#2K.

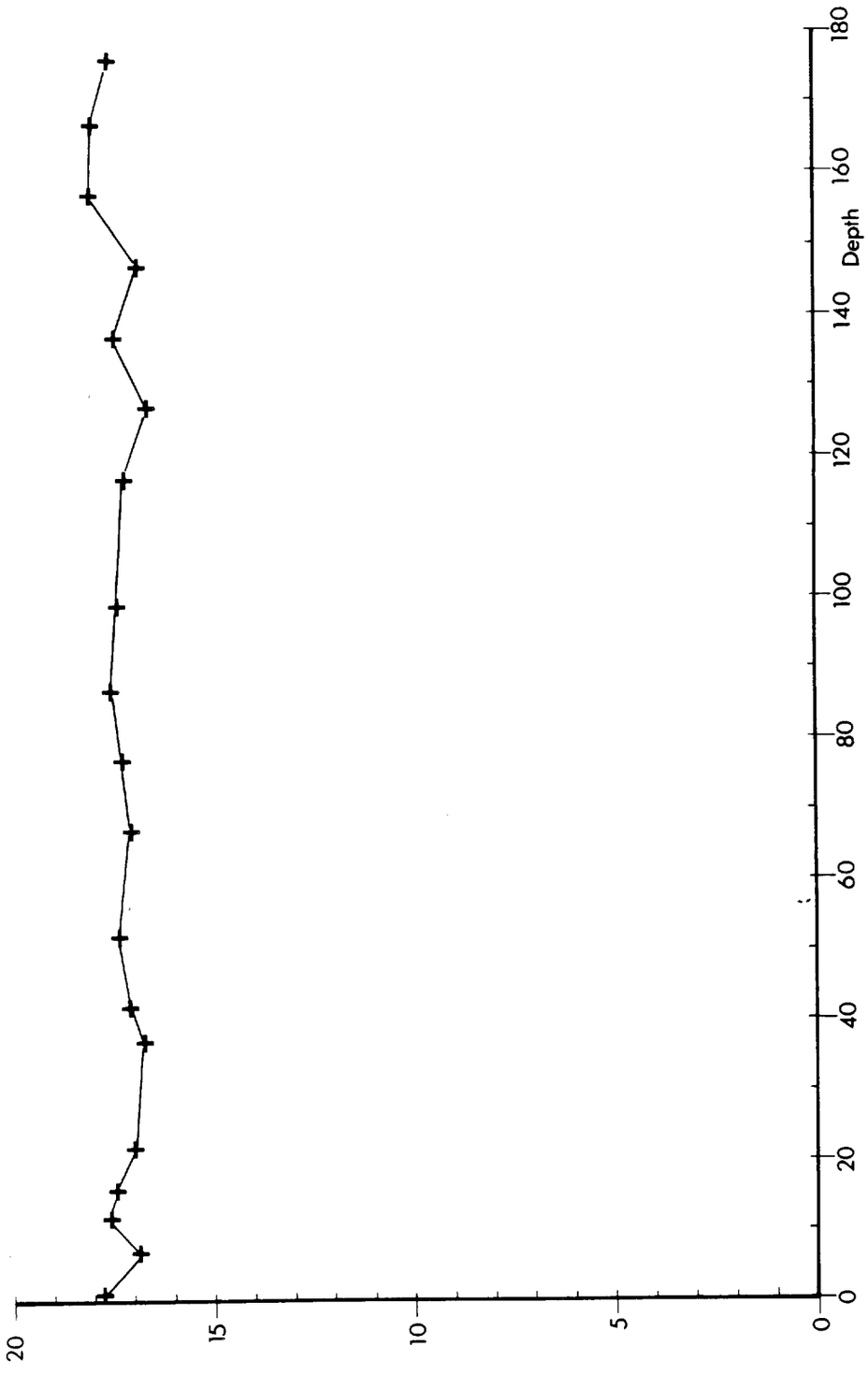

Figure 4.iv.9 Concentration of Al_2O_3 expressed on a carbonate-free basis, core 10552#2K.

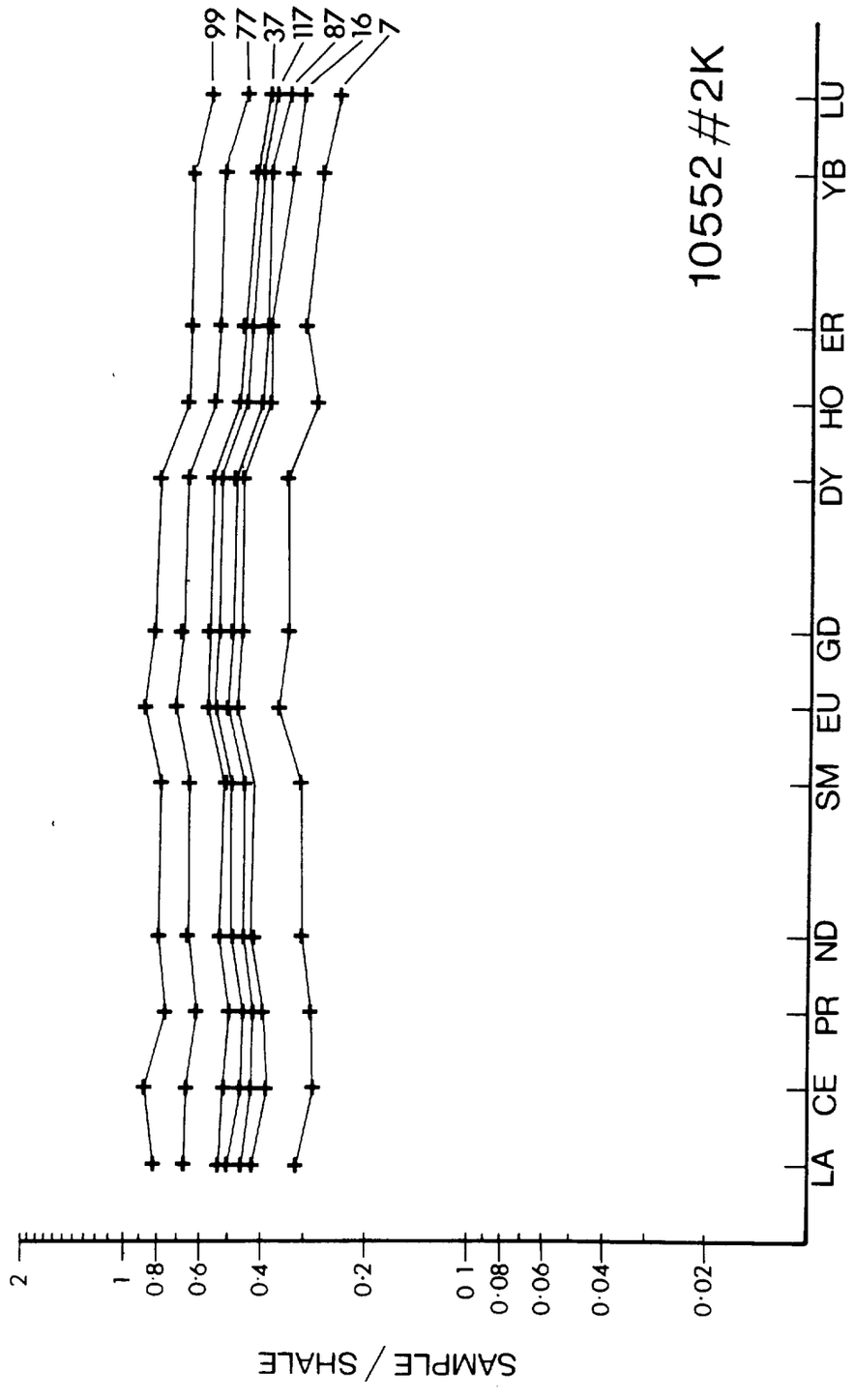

Figure 4.iv.10 Ree distribution normalised to shale for various depths of core 10552#2K.

CHAPTER 5

PROCESSES

5.i THE BENTHIC BOUNDARY LAYER

5.i.a Contract Objectives

The benthic boundary layer (BBL), adjacent to the seabed and varying from 10-100m in thickness, is caused by friction between the moving ocean water and the stationary ocean bottom. Within this layer turbulent mixing is sufficiently strong that properties such as density (and by analogy a radionuclide source term or tracer) are rendered uniform in the vertical. Above it the ocean water density decreases with increasing height and vertical mixing is strongly inhibited.

The contractual obligation has been to examine processes within the benthic boundary layer by direct measurement and to construct models and theories for them. The emphasis of the investigations has been placed on studying those processes relevant to radionuclide dispersal in order that realistic predictive models can be developed.

5.i.b Numerical Modelling Techniques

The complexity of flow and turbulence within the BBL demands the use of modelling techniques in which finite difference forms of the Navier-Stokes equations are integrated numerically. Simplified versions have been employed to study steady uniform flow of a stratified fluid over a smooth boundary which gives rise to a steady BBL (Richards, 1982). This proved a stepping-stone to a (much) more complex model (Richards, 1984a) in which the flow varies both in space and time. Such variation, which is characteristic of the deep ocean, required the use of the very fast and powerful CRAY computer.

5.i.c Observational Programme

Measurements within and above the benthic boundary layer have been made at three sites in the deep Eastern Atlantic all within water depths of between 4500 and

5300m; their locations are shown on Figure 5.i.1. The first site was on the Madeira abyssal plain in a flat area with isolated small abyssal hills about 400m high. The third site was 150 miles west of Madeira on a gently sloping part of the lower continental rise. The second site was in Discovery Gap, a narrow and rugged channel in the East Azores Fracture Zone which communicates between the deepest levels of the Madeira and Iberian Abyssal Plains. The varying topographic nature of these sites ensures that benthic boundary layer and dispersion characteristics are quite different.

Flow was measured using moored self-recording current meters in groups of about 20 at heights between 1m and 1000m above the sea bed. The duration of these measurements was between 3 months and 1 year. Currents were also measured by acoustic tracking of a cluster of between 5 and 10 neutrally buoyant floats: these floats follow the water at a fixed depth and were deployed 100-300 metres above the bottom. Such observations require the presence of the ship nearby and hence were limited to 10 to 20 days at each site. In addition to the flow measurements temperatures are routinely recorded by current meters. Additional observations were made by lowering a platinum resistance thermometer on a conducting wire from the ship. The latter measurements yielded profiles of temperature with depth often revealing the benthic boundary layer in a direct manner.

The extent and scope of the experimental program is summarised in the accompanying table. The resources brought to bear on each experiment are considerable and their cost has been shared by NERC and DOE.

5.i.d Experimental Results from the Madeira Abyssal Plain

Twenty lowered temperature profiles were made within a circle of 50km radius: the bottom mixed layer had a thickness between 20 and 120m (Saunders, 1983a,b). The numerical modelling suggests that this variation is brought about by weak convergences and divergences in the flow which respectively thicken or thin the BBL (Richards, 1984a). Where the flow is strongly divergent the BBL may become very thin and sharp boundaries or benthic fronts are produced. Such fronts, the oceanic counterparts of atmospheric fronts, are found in the temperature records and tilt at a mean angle of 10° to the horizontal (Thorpe, 1983). Fronts may sweep up water in contact with the sea floor on one side and eject the water at a height of 50-200m on the other. The frequency and efficiency of this process which is potentially important for radionuclide dispersal is not yet determined.

Near bottom currents contain three major components: tides, inertial oscillations and low frequency currents. The low frequency component has periods of between 20 and 100 days and a root mean square magnitude of 2.5 cm/s, see Figure 5.i.2. Mapping the flow at a level 10m above the sea floor, see Figure 5.i.3, reveals eddy like motions with a scale of about 50km in the horizontal. These periods and scales are correctly reproduced in the numerical model.

Mixing of a tracer in the horizontal direction has been estimated within the BBL from the current meter data, from the dispersion of the cluster of floats and from the numerical model calculations. For separations between 1 and 20km, the square of the separation of a pair of particles is found to double in 10-15 days. On average, particles initially 0.5km apart spread to 20km in about one half a year; the average concentration falls by a factor of $(^{20}/0.5)^2$ or 1600 in this time. Tracer mixing at scales greater than the eddies shown in Figure 5.i.3 has also been estimated from the current measurements yielding diffusivities of $10^6 cm^2 s^{-1}$. A cloud of tracer of diameter 100km thus halves its concentration in about 40 days. It is encouraging that the numerical models gives generally quite similar results (Richards, 1984b).

5.i.e Experimental Results from Discovery Gap

Detailed bathymetric surveys have revealed Discovery Gap as a valley about 150km in length with axis lying in the direction 060°, see Figure 5.i.4. The sill which lies on the section AA' near a depth of 4700m is approximately 500m above the abyssal plains north and south of the Gap and 500m below the level of East Azores Fracture Zone (Saunders, 1984).

Year-long current measurements made at a section of the channel which is only about 10km wide reveals quite steady and persistent flow from the Madeira to the Iberian basins. Water with (potential) temperature lower than 2.05°C occupies the deepest levels, see Figure 5.i.5, and has a flux estimate of $0.2 \pm 0.05 \times 10^6 m^3 s^{-1}$. This discharge spreads out east and north of the Gap exit where it is warmed by geothermal heating from the seabed and also by mixing with the overlying warm water. By assuming the abyssal water temperature there does not change with time, a value of $2 cm^2 s^{-1}$ is derived for the downward diffusivity of heat within the water column. This value is similar to that found from larger channels in the Western Atlantic (Hogg et al, 1982; Whitehead et al, 1982).

If a tracer was rapidly mixed up within the BBL to a height of 50m, and if the layer then separated from the bottom and diffused vertically at the rate suggested, namely $2cm^2s^{-1}$, within one half a year the layer thickness would have grown to only 150m, producing a dilution of a factor of only 3. These calculations illustrate the anisotropy of vertical (x 3) and horizontal (x 1600) dispersion.

Table 5.i.1 Details of BBL experimental programme

Site 1 Madeira Abyssal Plain

Location 33°N 22°W: with depth 5300m approximately.
No. of moorings deployed 7. No. of current meters 21. Duration 7 months.
No. of neutrally buoyant floats launched 12.
No. of lowered profiles within radius of 50km 20.
RRS Discovery Cruises 114, 117, 122.

Site 2 Discovery Gap

Location 37°N 16°W: water depth 4700m approximately.
No. of moorings deployed 8. No. of current meters 12. Duration 11 months.
No. of neutrally buoyant floats launched 10.
No. of lowered profiles within region 25.
RRS Discovery Cruises 130, 138.

Site 3 Madeira Continental Rise

Location 33°N 20°W: water depth 4500m approximately.
No. of moorings deployed 7. No. of current meters 20. Duration 3 months.
No. of neutrally buoyant floats launched 10.
No. of lowered profiles within 50km radius 20.
RRS Discovery Cruises 136, 139, 141.

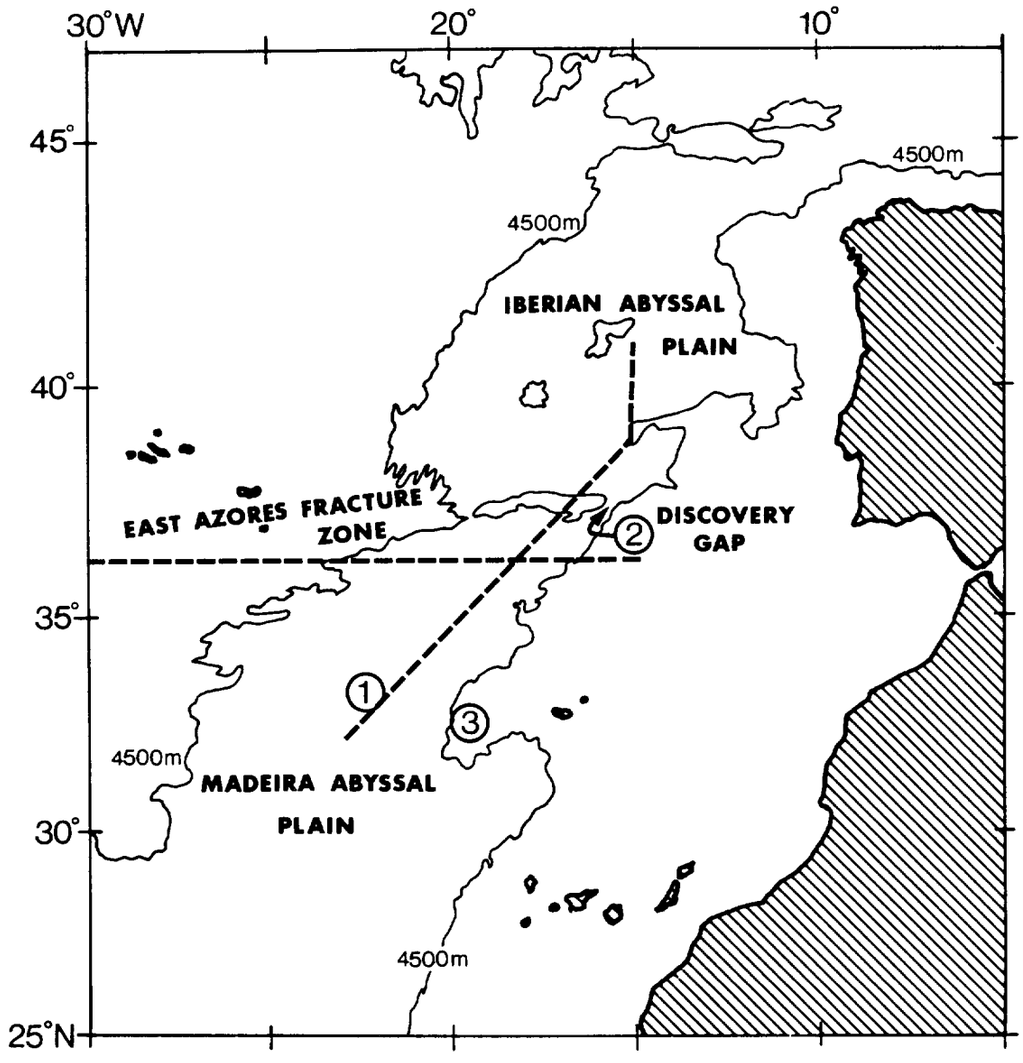

Figure 5.i.1 The location of experiments carried out to investigate processes within the benthic boundary layer.

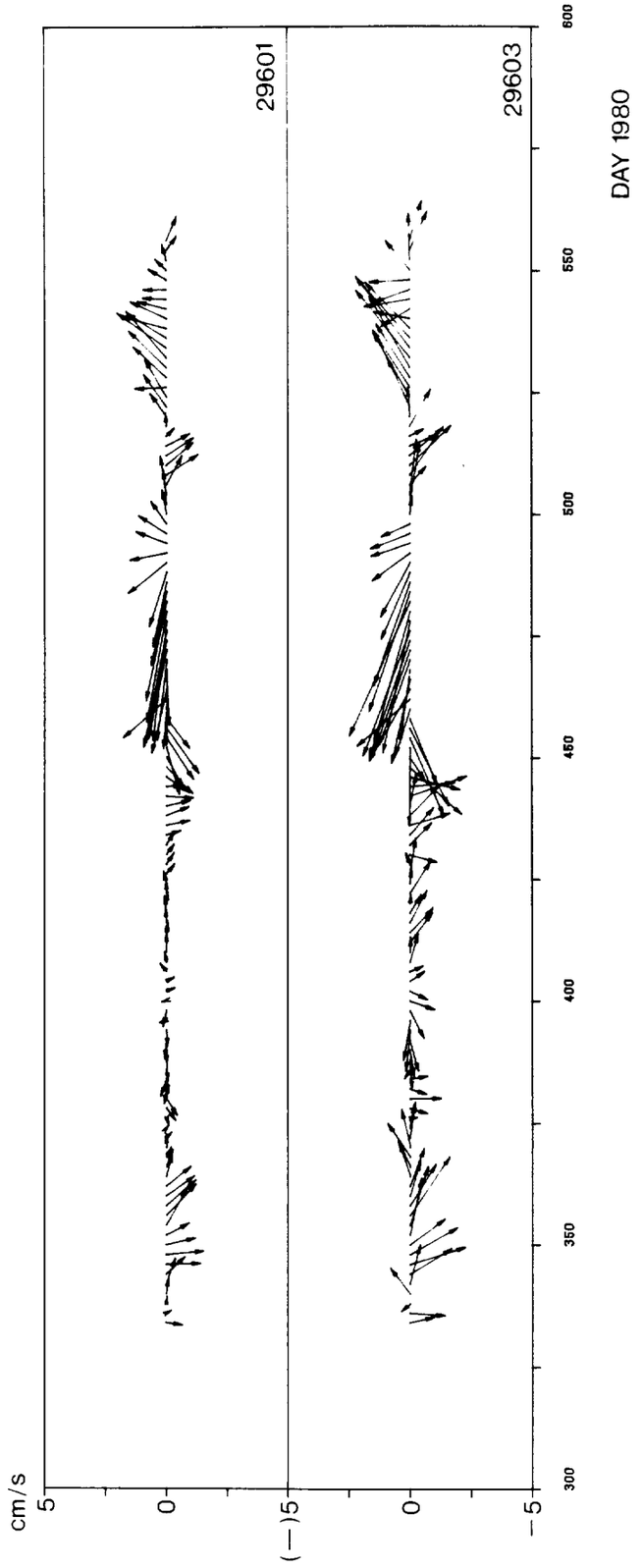

Figure 5.i.2 Currents measured 600m (upper) and 10m (lower) above the seabed on the Madeira abyssal plain. Tides and inertial currents have been filtered out.

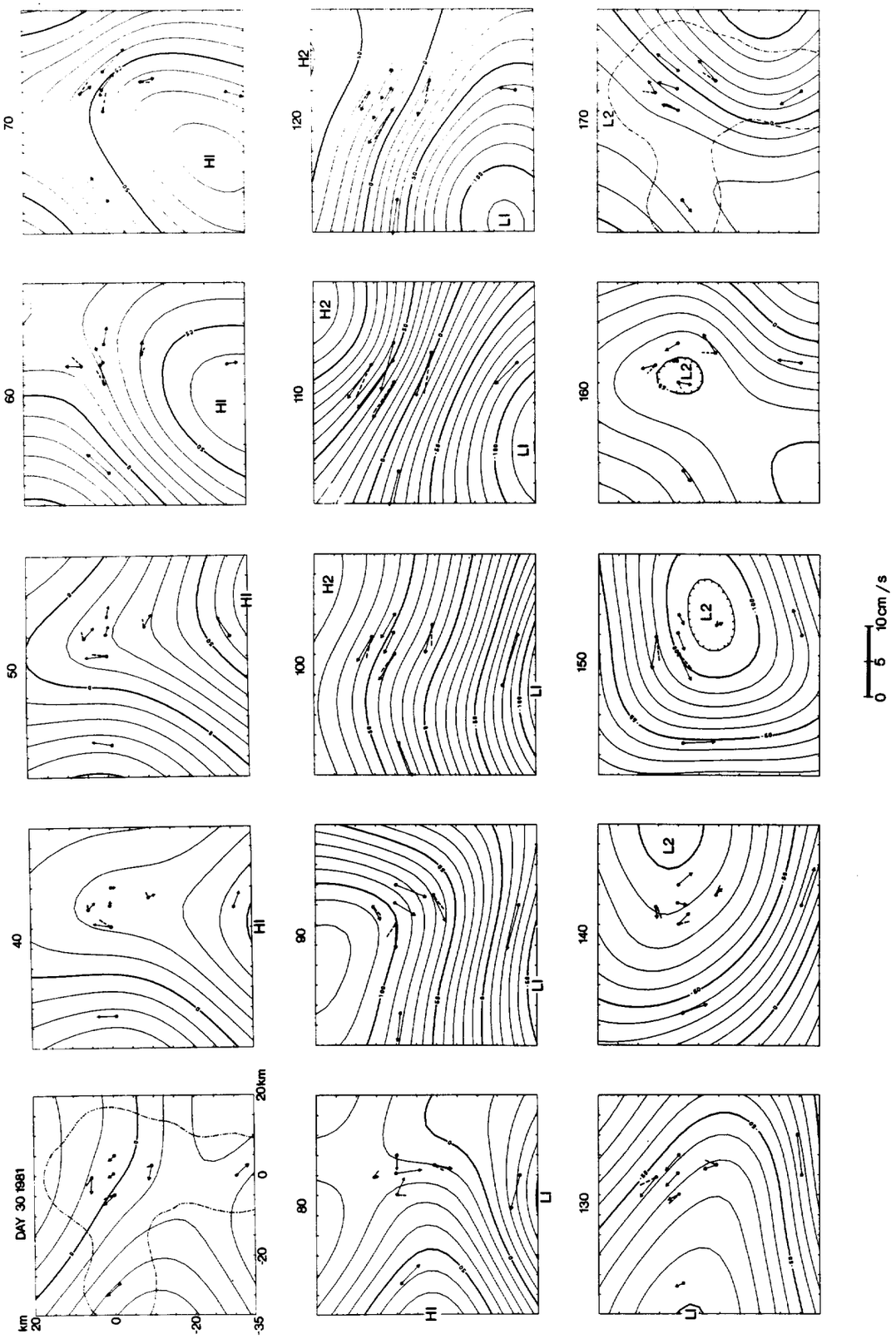

Figure 5.i.3 Maps of the currents measured 10m above the sea bed at 10 day intervals. (Arrows are the observations.)

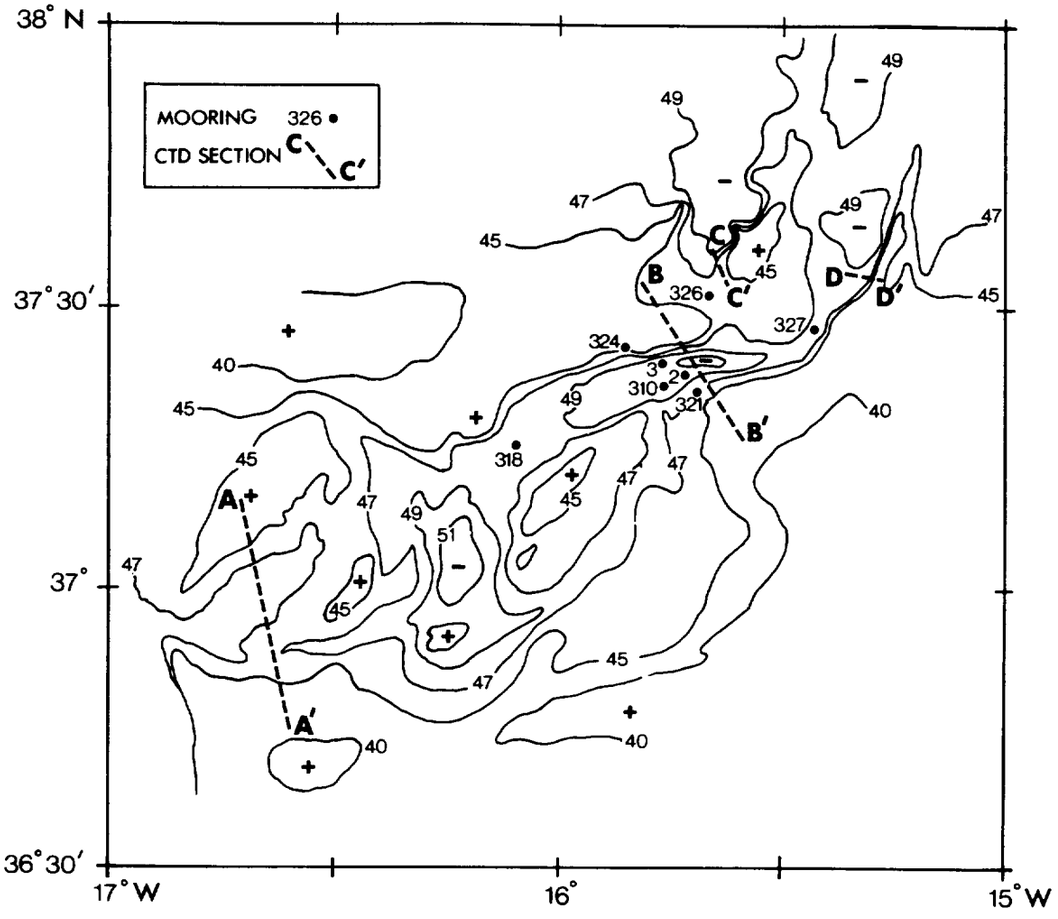

Figure 5.i.4 Bathymetric map of Discovery Gap, depths in 100m. The location of moorings and temperature sections is also shown.

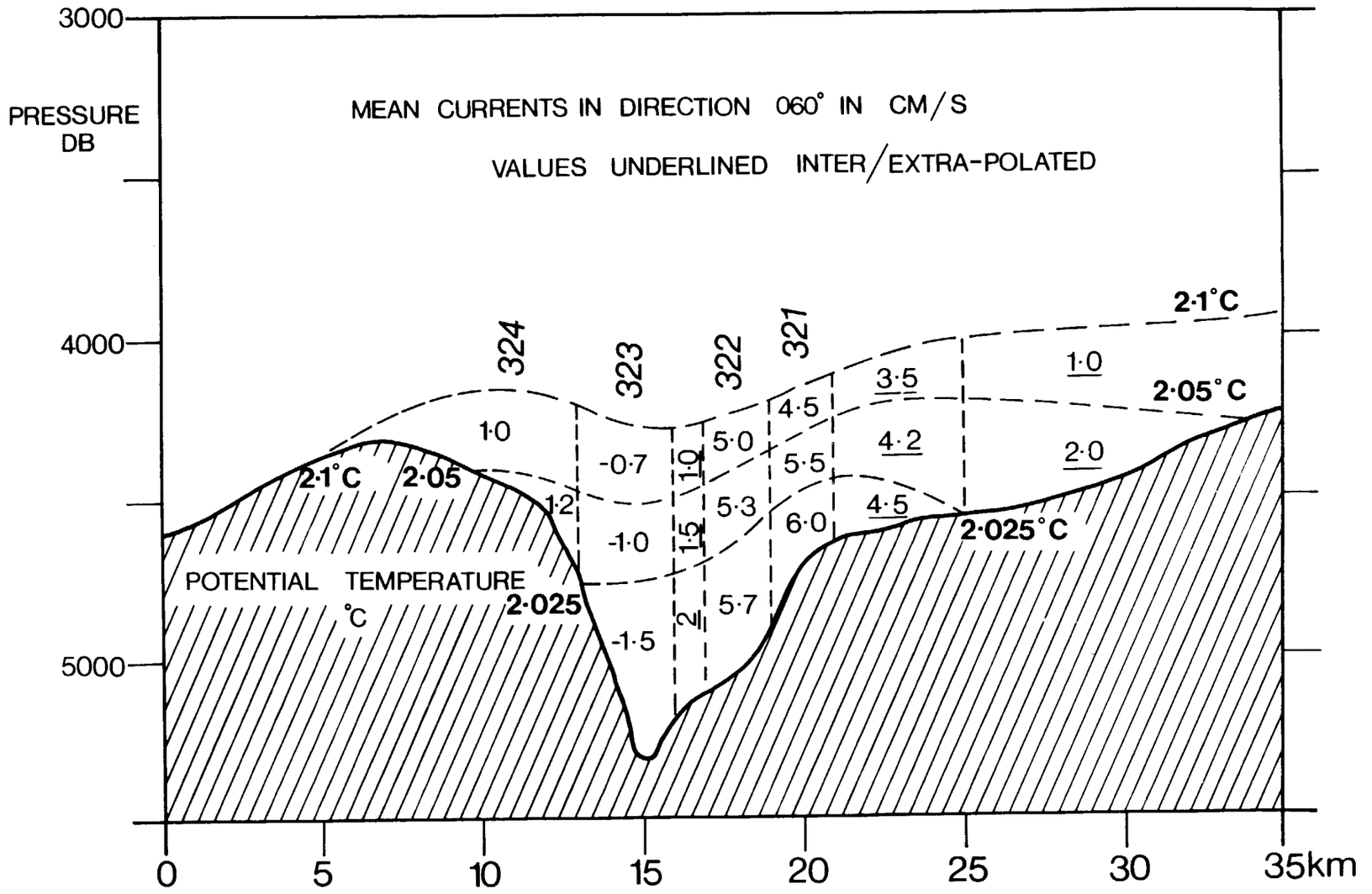

Figure 5.i.5 The computation of flux of water through Discovery Gap. Based on 1 year records.

5.ii MEASUREMENTS OF DISPERSION IN THE DEEP OCEAN

5.ii.a Contract Objectives

The contract has the ultimate aim of directly measuring the dispersion of a cluster of neutrally buoyant floats at subthermocline depths over a long (up to 2 year) period. The main components of the present contract were:

(a) Determination of acoustic propagation characteristics of the north east Atlantic ocean.

(b) Design and construction of prototype neutrally buoyant floats.

(c) Construction of autonomous listening stations.

(d) Deployment of floats and listening stations for trial period.

All of these objectives have been achieved and the study is now proceeding towards the first operational deployment of floats and listening stations.

5.ii.b Background to the Experimental Technique

Neutrally buoyant floats were developed at the IOS (then National Institute of Oceanography) in the early fifties (Swallow, 1955). These units which followed a predetermined pressure surface were tracked from an attendant ship by means of high frequency ($\sim$10kHz) sound signals and thus the float operations were restricted to relatively short duration experiments limited by the ship cruise endurance and the relatively short ($\sim$20km) acoustic propagation range. Such floats have been used in the experimental investigation of the benthic boundary layer reported in Section 5.i. The concept of a neutrally buoyant float capable of being tracked over much greater distances originated with Stommel (1955), but was not achieved until the early seventies (Rossby & Webb, 1971).

Float tracking over large (>1000km) distances is achieved by the use of low frequency sound signals and relies for its long range acoustic propagation on the "wave-guide like" nature of the sound speed profile over much of the world's ocean.

A typical vertical profile of sound speed is as shown in Figure 5.ii.1 with a near surface maximum due to the relatively high surface temperature and a deep increase in the homogenous deep water due to the effect of pressure. The minimum at depths of typically 1000m causes sound rays to be focussed and refracted about the depth of the minimum (the Sound Fixing and Ranging, SOFAR channel).

Experiments conducted in the northwest Atlantic by US scientists (Freeland, Rhines & Rossby, 1975) were confined to the tracking of floats ballasted to be near the SOFAR axis depth. Their sound signals were received by military, land based hydrophones. The development of moored internally recorded Autonomous Listening Stations (ALS) allowed experiments to be conducted in areas away from the western Atlantic hydrophone network.

The requirements of the radioactive waste disposal project were for measurements of dispersion at greater depths than were accessible to the depth-limited (2000m) US floats. Thus an investigation was embarked upon to assess the feasibility of using SOFAR float technology to make such dispersion measurements.

5.ii.c. Sound Ranging Trials

The presence of the warm, salt layer of Mediterranean water at approximately 1000m in the north east Atlantic has a marked effect on the local sound speed profile (Figure 5.ii.2). It causes an intermediate maximum which effectively provides a double SOFAR channel with the deep channel axis at levels as deep as 1900m in some instances. Sound signals will be propagated over large distances without surface or bottom reflections (and hence with low energy loss) over the range of depths where the sound speed is less than the near surface value. For a profile such as is shown in Figure 5.ii.2, this would be true for depths as great as 4000m. In the summer of 1982, trials were carried out to assess the ability of low frequency (250Hz) acoustic signals to be detected over distances of up to 1000km.

Sound sources (in effect moored neutrally buoyant floats) were constructed, and were deployed on a peak in the East Azores Fracture Zone. The sources were located at the local deep minimum in the sound speed profile. The audibility of the 80 sec-long swept-frequency pulse was measured by lowering a hydrophone at increasing ranges from the source and recording the correlation heights achieved at a series of depths throughout the water column. Simultaneous CTD stations enabled the local sound speed profile to be determined.

The results were reported by Gould, 1982 and demonstrated that under the summer stratification conditions (optimum propagation) the sources could be detected at depths of up to 3500m for ranges as great as 1000km from the source site.

5.ii.d Float Construction

As has been mentioned previously the floats used in experiments in the western N. Atlantic were limited to a maximum depth of around 2000m by the collapse depth of the large diameter aluminium tube used to provide the main instrument housing. Similar tube of greater wall thickness would have been prohibitively expensive to produce in the quantity needed for the deep SOFAR float project, therefore glass spheres were used to provide instrument housings. These, although relatively inexpensive and unlimited in their operational depth range, required four spheres to provide the necessary housing (one for electronics, two for batteries and a fourth for additional buoyancy) and hence required external electrical connections between batteries and electronics and between electronics and sound transducer. An additional problem lies in the less well defined compressibility characteristics of the glass spheres and their protective housings compared with that of a simple aluminium tube.

Four floats were constructed for the trials experiment carried out in the summer of 1983. Two were modifications of the sound sources used in the previous year and two were new floats.

5.ii.e Autonomous Listening Stations (ALS)

The autonomous listening stations used in the USA are of a relatively old design and thus a new type employing microprocessor circuitry which allowed easier modification to the recording characteristics of the listening station was chosen. The design was one originating from France (Centre Océanologique de Bretagne, COB) produced by Tillier for intermediate range (1500Hz) floats. The deployment in the summer of 1983 was the first sea trial of the 250Hz version of the Tillier listening station (TLS). Three of these units were built at IOS.

The listening stations record, every 10 minutes, the times and correlation heights of the three best correlated signals on each of two channels. (Channel 7 will be used for all experiments carried out in the Eastern Basin of the N. Atlantic, Channel 5 is used by workers west of the mid-Atlantic ridge).

5.ii.f The Summer 1983 Trials

In Summer 1983 on Discovery Cruise 138 a deployment was made of the three TLSs and four floats (two ballasted to a depth of 3500m and two incorporated in fixed moorings). The experiment was carried out in the Madeira basin approx. 200km NE of the GME site.

The uncertainties of predicting the compressibility of all the float components meant that although the floats had been ballasted at atmospheric pressure in the laboratory an in situ check on the depth of neutral buoyancy was required prior to their deployment. In order to achieve this the two free floats were initially launched with a short range (5kHz) float attached (Swallow, McCartney & Millard, 1974) so that the SOFAR float depth could be measured independently and the float pair recovered for payload adjustment prior to the final float launch of the SOFAR floats alone. (Photo, Figure 5.ii.3.)

The first float pair launch showed that neutral buoyancy was achieved at 3950m (450m deeper than intended) but an empirically derived ballasting adjustment to the second float pair enabled the correct depth to be reached at the first attempt.

The floats transmit their signals at 8 hour intervals at predetermined times by which each float is identified. The signal is an 80 sec long swept frequency pulse. The arrival time of the signal is determined in the TLS or ALS by correlating the pulse with a reference signal to a resolution of 0.1 sec (equivalent to a float range of 150m).

Additional information is transmitted from the float by a delayed pulse transmitted after the first transmission of each day. The delays on alternate days are proportional to pressure and temperature. During deployment the float runs in a fast-cycle mode and telemeters the pressure so that the level at which neutral buoyancy is reached can be determined. The floats used in the trial employed a pressure/temperature telemetry circuit which had not previously been used at these depths and low temperatures and the P/T telemetry did not work correctly. (The production series of floats will employ a French designed P/T board capable of accommodating any range of pressures and temperatures.)

The floats and listening stations were deployed at the positions shown in Figure 5.ii.4 (Gould, 1983). As stated previously the free floats were ballasted for 3500m, the moored floats were at 4000m (near the centre of the TLS array) and at 3500m (the southern float). The array was deployed in early July and recovery of the moored floats and listening stations carried out on Discovery Cruise 141 in November (McCartney, 1984).

One listening station was missing from its deployment site. Its loss is attributed to a, now recognised, failure of the acoustic release. The loss of one listening station degrades the float tracking since three stations are needed to eliminate clock drift errors and sound speed variations from the data analysis.

The two remaining TLS had functioned perfectly as had the two moored floats. Subsequent analysis of the TLS data carried out at the University of Rhode Island showed that all the floats had worked for the full experiment duration.

5.ii.g Results

Figure 5.ii.5 shows an analogue plot of the float signal arrivals at the northern-most listening station. The main signal arrivals as well as the data telemetry pulses can be seen. The free and fixed floats can be readily identified by their variable and constant arrival times. A very striking feature is the decrease in correlation height with time (dot size is proportional to correlation height). This deterioration is attributed not to float or listening station malfunction, since these were checked on recovery, but to the seasonal erosion of the near surface thermal structure which resulted in a progressive shoaling of lower limit of the sound channel.

The fixed float at the centre of the TLS array was detectable at both listening stations throughout the experiment (ranges of $\sim$300km) as was the southern fixed float at the southern TLS (450km).

Float trajectories were calculated assuming a zero clock drift on the floats and constant sound speed. The tracks are shown in Figure 5.ii.6. Clock drifts on the two moored floats were in one case zero and in the other 8 seconds, the latter equivalent to a position error of 12km.

The floats launched with an initial north-south separation of 10km moved steadily northwards at mean speeds of over 2cm/sec throughout the four month experimental trial. Towards the end of their trajectories they were turning eastwards perhaps due to blocking by the east Azores Fracture Zone.

The floats will, under prolonged exposure to the high ambient pressures, compress steadily and hence lose buoyancy and sink. In normal operation the pressure telemetry circuitry is used to detect departures from the intended operational depth and, by electrolytic erosion of a sacrificial anode, to compensate. In the two free floats the pressure telemetry did not work correctly, each in such a way that the floats would sink below their intended operational depth of 3500m. An approxiamte measure of this depth increase can be gained from one float which did telemeter pressure but with a shifted calibration. The indicated depth change was 250m over a period of 60 days. This might well account partly for the deterioration of acoustic propagation.

5.ii.h International Aspects of the Float Project

Four other laboratories are involved in SOFAR float work in the NE Atlantic. Close liaison is maintained with all of them. The objectives of the experiments differ but will all contribute to an improved knowledge of dispersion and mean circulation in the NE Atlantic. The other projects and their relation to the IOS work is summarised below and in Figure 5.ii.7.

(a) Centre Océanologique de Bretagne, France (COB)

Investigation of the cross mid Atlantic Ridge circulation south of the Azores. An array of 4 TLS is used to track a float cluster deployed at 700m depth near 35°N 40°W in July 1983. These floats will move eastward into the north Madeira basin. Piere Tillier from COB has visited IOS and there has been close cooperation at a technical and scientific level between IOS and COB.

(b) Woods Hole Oceanographic Institution, USA (WHOI)

Floats at a depth of 1100m will be launched in October 1984 to study dispersion in the Mediterranean Water core southeast of the Azores. They will be tracked by an array of 4 ALS in the Madeira-Canary basin over a 2 year period. These ALS will be used to provide tracking coverage for the IOS floats.

(c) University of Rhode Island USA (URI)

In addition to the WHOI work, small numbers of floats will be deployed into intense "blobs" of Mediterranean water in an attempt to observe their migration and dynamical characteristics (Armi & Stommel, 1983). These floats will be tracked by the WHOI ALS network. URI have also taken the lead in float data processing and their facilities were used to process data from the IOS Summer 1983 trial.

(d) MAFF Fisheries Laboratory, UK

In pursuit of studies of circulation in the Iberian basin, MAFF will launch a cluster of floats in September 1984 near 42°N 14°W. These will be tracked by IOS TLSs the southernmost of which will also supplement the WHOI ALS net. MAFF have relied entirely on IOS for technical support.

A new float data processing suite of programmes is under development at WHOI which will be implemented on the IOS GEC minicomputer to be delivered in late Summer 1984.

5.ii.i Present Status of Project and Future Plans

An initial batch of six floats for IOS plus a MAFF order have been shipped from the US manufacturer, Webb Research Corp (built to a design based on IOS experience). They will be assembled at IOS by Webb and ballasted in the IOS tank. A ballasting test, similar to that carried out in summer 1983, will be performed on a cruise of the MAFF RV Cirolana in the Summer of 1984. IOS floats and TLS moorings will be deployed on RRS Charles Darwin cruise 5/84 October 4th - November 1st with the 13 IOS floats deployed at 3000m depth at locations to the east of GME. The first IOS TLS recovery will be in April 1985 and will produce data on the MAFF float cluster dispersion. The WHOI ALS net will be recovered in October '85 and will provide the first direct results of the IOS floats. Opportunities will be taken during both IOS cruises to use shipboard lowered hydrophones to monitor float performance.

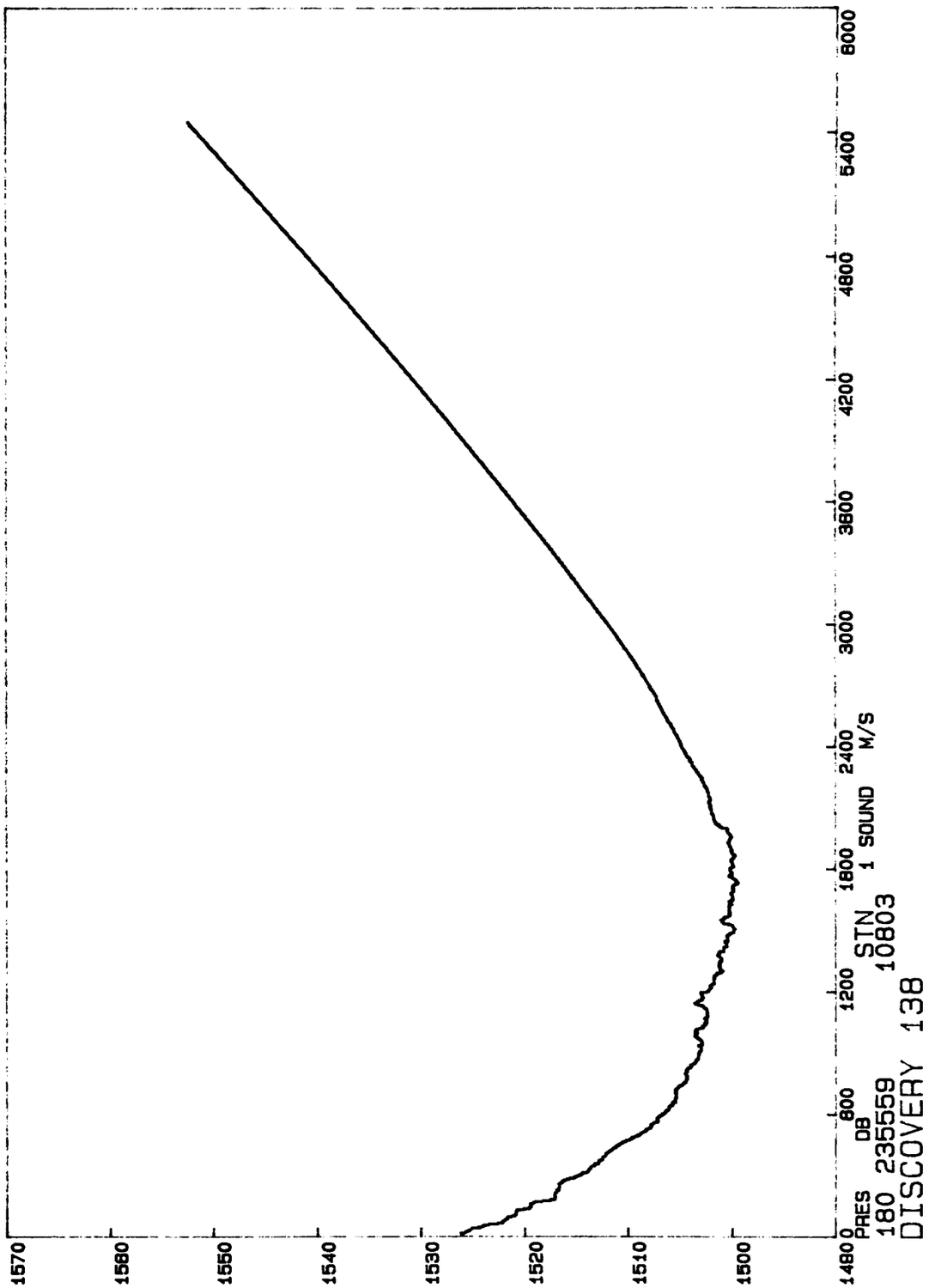

Figure 5.ii.1 Typical vertical profile of sound speed.

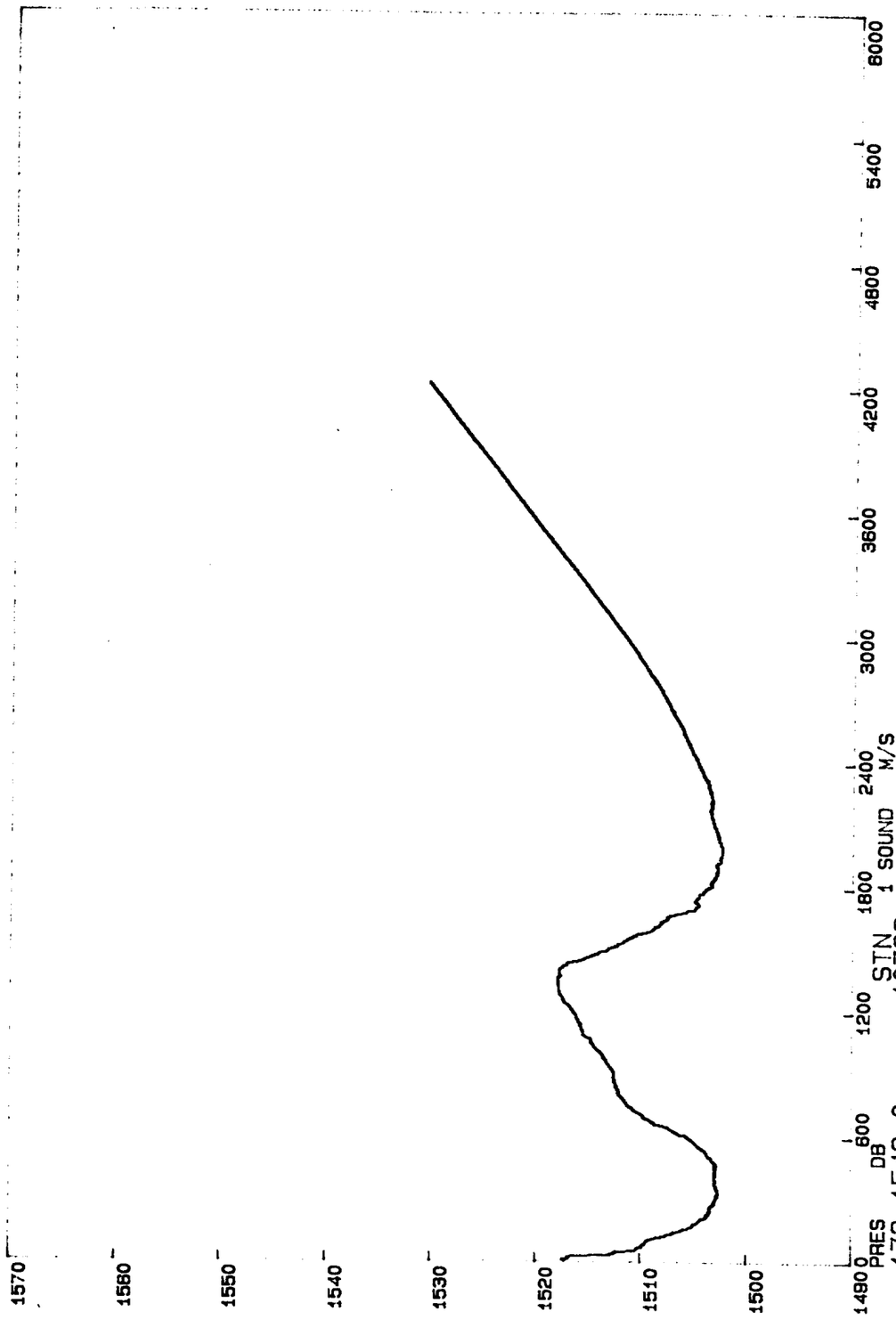

Figure 5.ii.2 Vertical profile of sound speed from NE Atlantic showing the intermediate maximum due to the Mediterranean water.

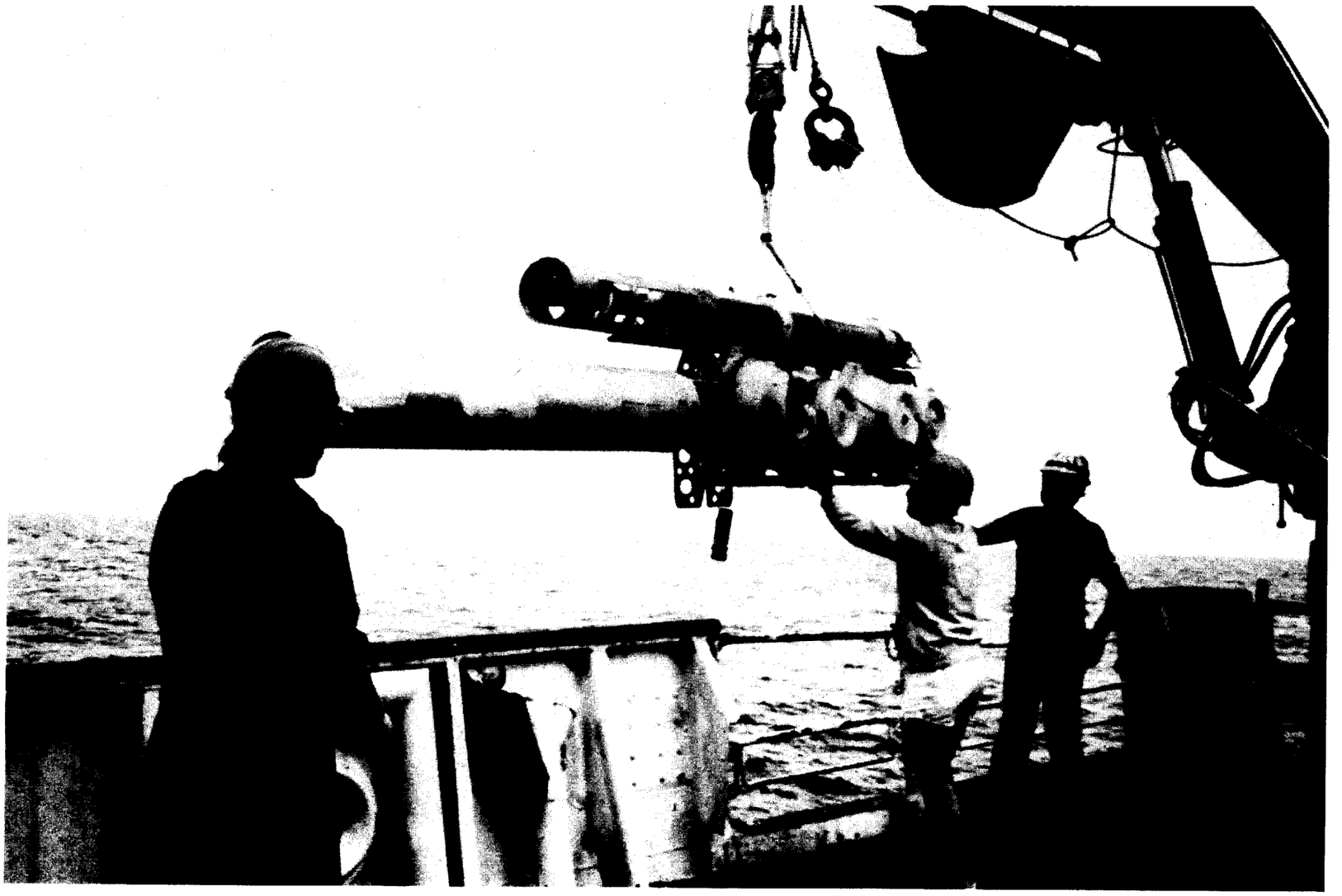

Figure 5.ii.3 SOFAR float as used in the summer 1983 trials. Small diameter cylinder is the 5kHz Minimode float used for determining the float depth.

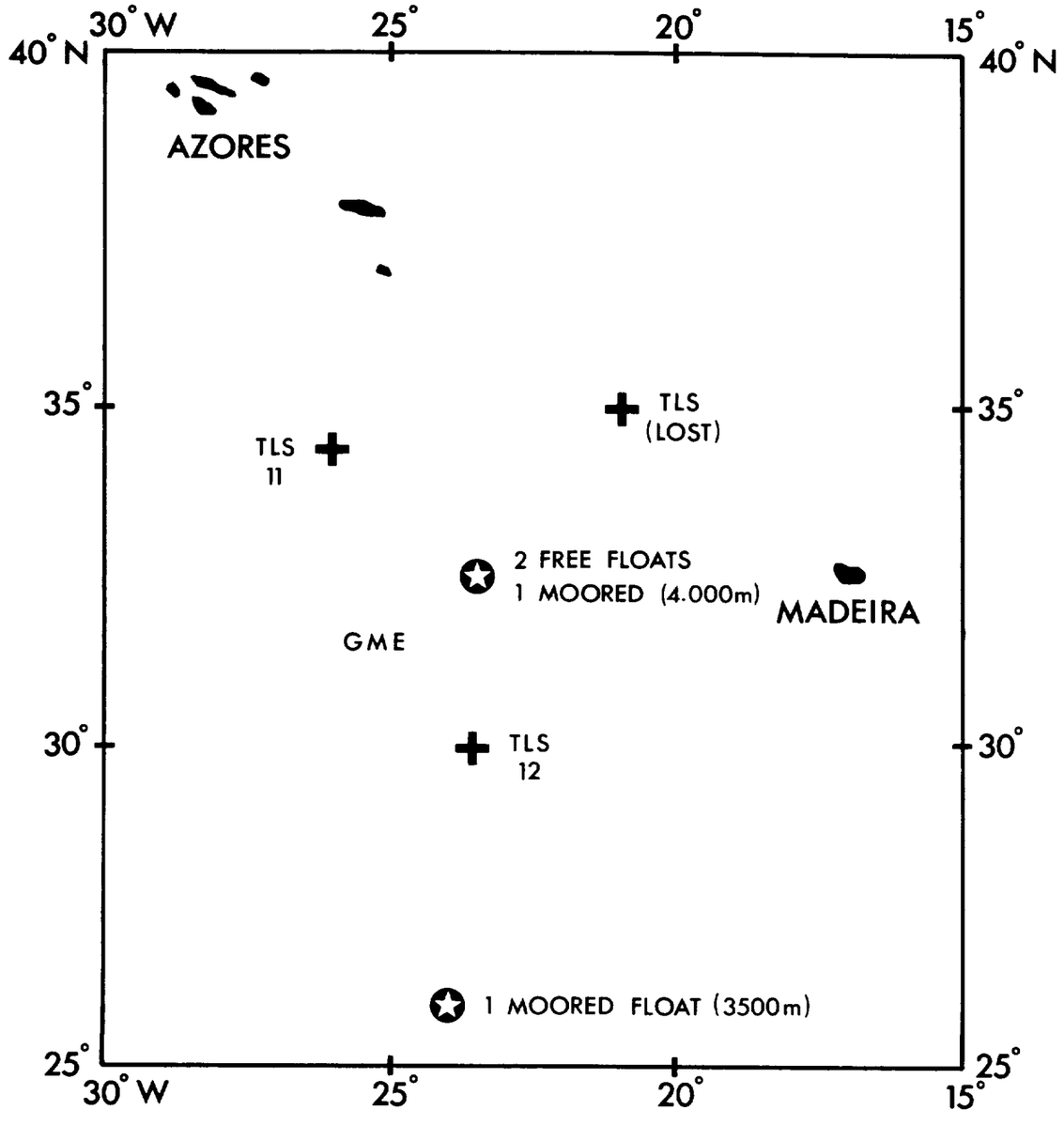

Figure 5.ii.4 Float and TLS deployment positions for the summer 1983.

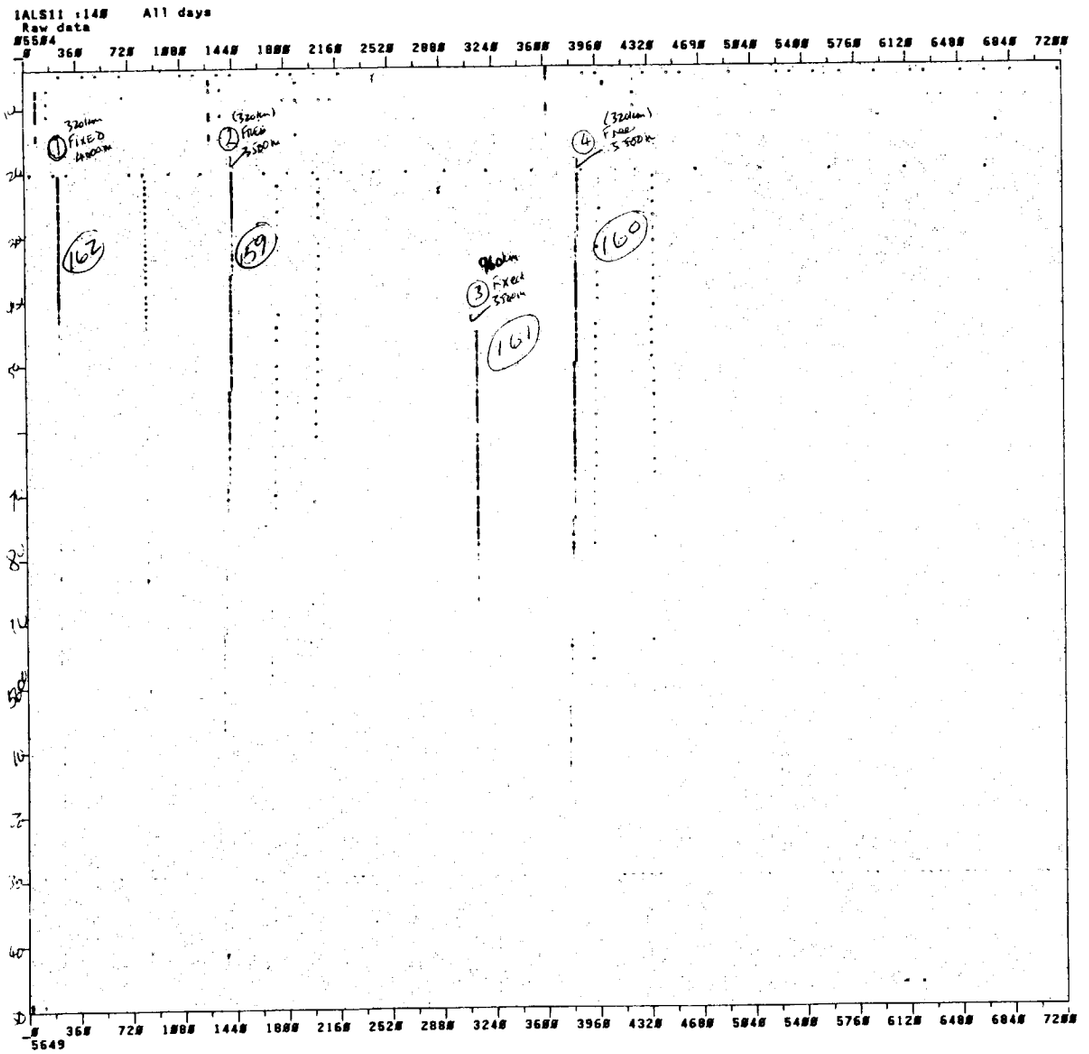

Figure 5.ii.5 Float signal arrivals at ALS 11. Arrival time is displayed horizontally on a 0 to 8 hour scale. The vertical coordinate is truncated Julian day number.

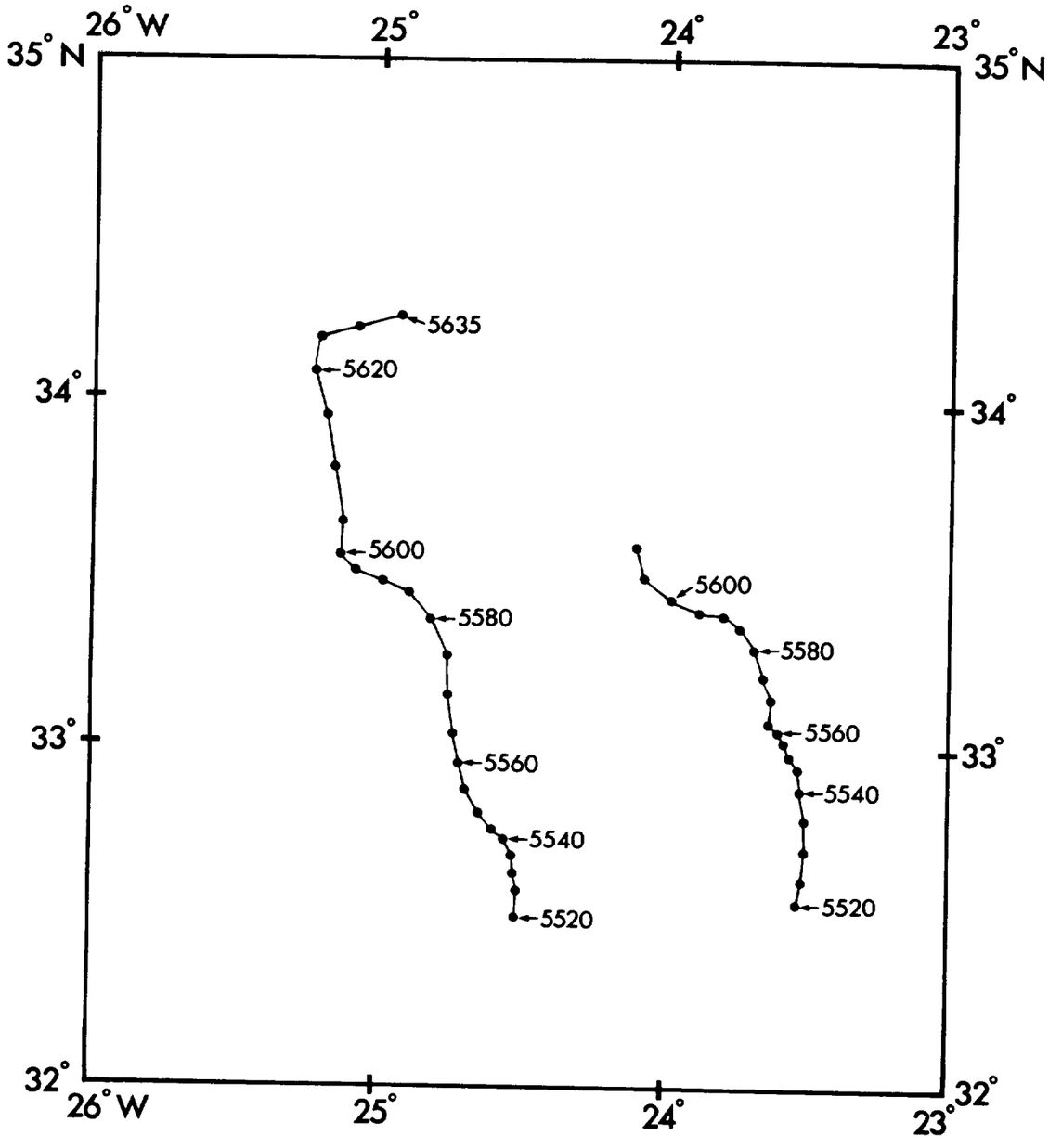

Figure 5.ii.6 Tracks of SOFAR floats. Western track is shifted west by 1° longitude for clarity. Day 5520 - 5 July 1983.

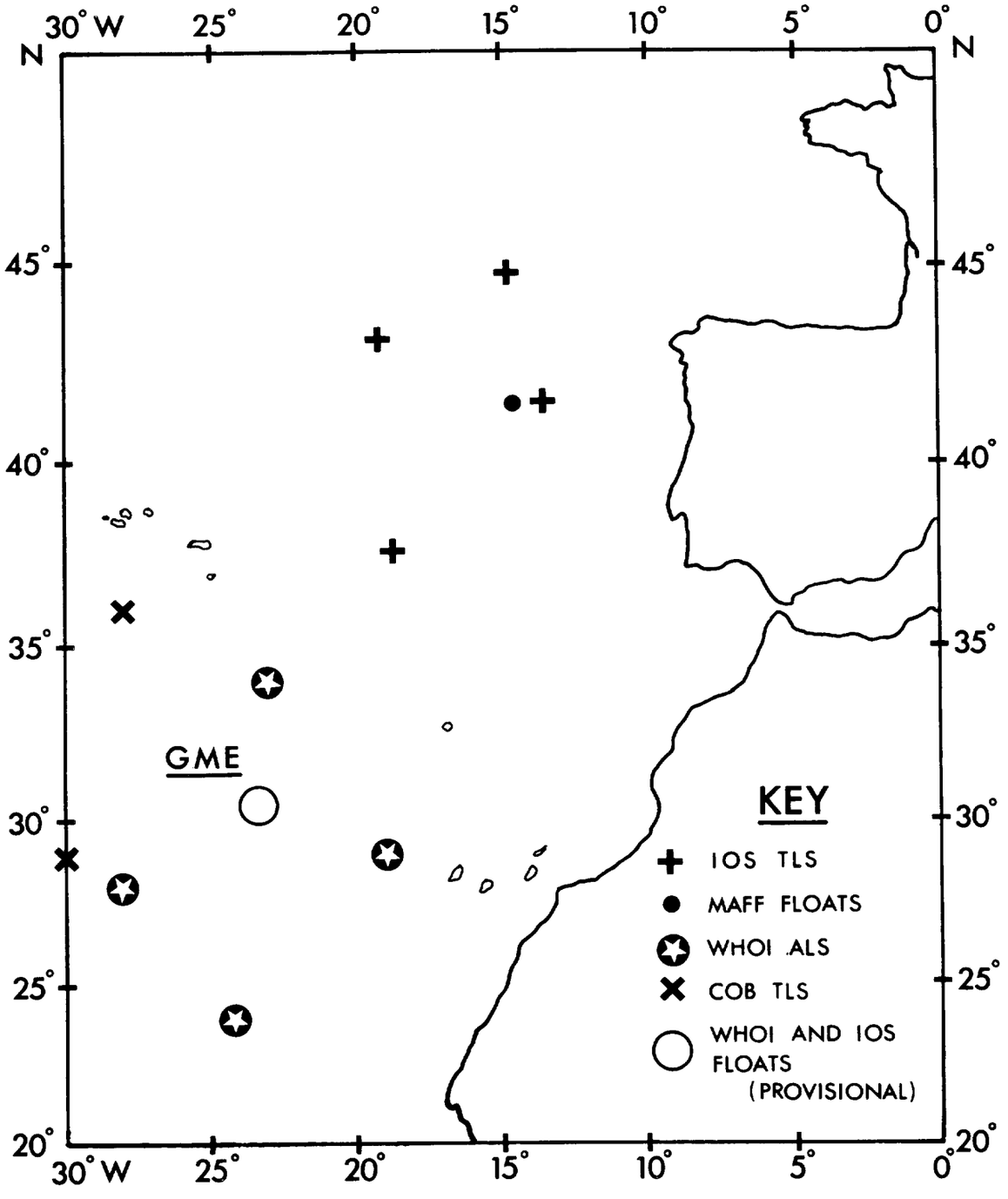

Figure 5.ii.7 Float and listening station deployments for all experiments in the NE Atlantic starting October 1984.

5.iii BIOLOGICAL PROCESSES

5.iii.a Objectives

Two major biological questions need to be answered before the risks associated with the disposal of any materials beneath the oceans can be adequately assessed. First are there any biological transport mechanisms which could return sufficient quantities of the material back up to the surface, where they could result in unacceptably high doses either reaching individuals or the total human population? Secondly would such disposal result in widespread and/or long term deleterious effects on any parts of the oceanic ecosystem. This report concentrates on the first of these questions, although much of the information provided herein is of direct relevance to the second.

In considering the possibility of biological transport from the bed of the deep ocean back to Man, two distinct scenarios must be considerd. First is the possibility that the mass transport of the contaminant material will occur in sufficient quantities to pose a threat to extensive sections of the population. The second is whether there are any critical pathways along which sufficient quantities of the contaminant material can reach and threaten specific small sections of the community, although the total amounts of contaminant involved will present no danger to the population as a whole. A hypothetical example described in GESAMP (1983) report was that of a 'bathys restaurant' specialising in deep-sea bottom-living fish which if caught close to the near-field of a disposal site, could result in the cooks receiving unacceptably high doses if they constantly tasted their dishes.

The distinction between questions of mass transport and critical path transport is important because the research requirements needed to answer them are quite distinct.

If biological processes are to result in a mass transport which is significant relative to the transport by physical processes, then large quantities of biomass containing high concentrations of contaminant material relative to the water must be involved. A critical pathway, on the other hand, will involve much smaller quantities of both biomass and contaminant, and so much more detailed information is required to identify a pathway or more importantly to demonstrate that none exists.

Following disposal into the sea bed, the first community to be subjected to disturbance or to exposure to the contaminant material will be the benthos which live within or on the sea floor. Benthic organisms may play an important role in the dispersion of contaminants via their bioturbation of the sediments, by transferring the materials to other parts of the oceanic ecosystem, or more directly by becoming a resource directly exploited by Man for food or pharmaceuticals.

Once a contaminant substance has dispersed into the water column it will be subject to physical mixing and transport, chemical modification while in solution or bound on to particulates, and possible influence by midwater biological activity. The question then arises as to whether the biological activity will have an effect which is detectable from the overwhelmingly massive physical influences. The danger of contaminants reaching the human population intensifies if and when any reach the oceanic euphotic zone, and increases still further if they are carried into upper slope and shelf waters where most of the marine fisheries are concentrated.

Biological research at IOS is concentrated in two main areas, benthic studies and pelagic research. In both areas the main thrust has been to improve the general understanding of the structure and function of oceanic ecosystems. The contract funding has been used to support an integration of the results of the main IOS biology programme to answer questions connected with disposal.

5.iii.b The Benthic Ecosystem

Benthic communities consist of organisms which live intimately associated with the sea bed, either in it (infauna), or on it (epifauna), or just above it (benthopelagic). The deep-sea benthos is usually considered under four main categories although the divisions are arbitrarily based on sampling techniques so there is considerable overlap between them:

The microflora consists of bacteria, yeasts and fungi. Little is known about the biology of these organisms in the dep-sea but, because their turnover rates are likely to be rapid compared with other elements of the benthos, it is likely they are responsible for a major portion of benthic production. It also seems likely that the microflora plays a major role in the guts of larger organisms through their conversion of non-labile organic compounds into labile forms more

readily assimilated by the host organism. Studies of hydrothermal vents have suggested that the abundant and rich fauna inhabiting the immediate surroundings of the vents are very largely supported by chemosynthetic production by bacteria. It has been suggested that certain benthic organisms such as the Pogonophora depend at least in part on chemosynthesis by bacteria beyond the environs of the vents. Otherwise most benthic organisms including the microflora ultimately depend on energy converted into organic material by the photosynthesis of autotrophs in sunlit surface layers of the ocean.

The meiobenthos is usually considered to be composed of those organisms which pass through screens of 300-500μm mesh size, but which are retained on 42μm mesh. The systematics of these communities are inadequately known. The dominant forms are nematodes, foraminiferans and copepods which live within the superficial layers of the sediments. There is a small but growing body of evidence for some of these organisms playing a significant role in metal chemistry at the sediment/water interface.

The macrobenthos consists of the animals which are retained on screens of around 500μm mesh. Beneath productive waters these animals are sufficiently abundant to be sampled reasonably effectively by large corers and grabs.

The megabenthos is rather loosely defined as those organisms which are sufficiently large to be recognised in good quality in situ photographs and are only sampled adequately, if at all, by dredges and trawls. The megabenthos therefore contains representatives of all the main animal taxa from protozoans to fish.

Within the megabenthos there are three main feeding styles which tend to be reflected in the life styles adopted. Suspension feeders capture particulates from the water which are either sedimenting down from the surface or have been resuspended from the sea bed. Because animals which rely on this feeding strategy have their food brought to them by water currents or gravity, they have little need to move and so most are sessile. Deposit feeders consume sediment either from within the substrate or from off its surface. They tend to have rather limited foraging ranges and are sluggish. Their main importance in this context is that they are responsible for much of the bioturbation that occurs. Scavenging/predatory feeders tend to be the most actively mobile component of the benthic community because their food supply is patchily distributed in both time and space.

The benthic studies at IOS have concentrated on the megafauna, but inevitably we have been led to investigate some specific aspects of other sections of the communities. The following review of benthic biology relevant to the problem of radioactive waste disposal is largely restricted to those areas in which IOS has direct involvement. More general assessments will be found in IOS (1978) and Angel, Fasham & Rice (1981), and more specifically from a modelling viewpoint GESAMP (1983).

5.iii.c Mass Transport and the Deep-Sea Benthos

Several attempts have been made to assess the possible extent of mass transport mechanisms from the deep sea to Man. Most of the early studies either ignored biological mechanisms or treated them cursorily. Two recent attempts, both of which received input from IOS biologists, considered biological mechanisms extensively (Robinson & Mullin, 1981; GESAMP, 1983). Both studies concluded that mass transport by biological processes would be insignificant compared with that resulting from physical processes.

In the two studies a 'worst case' situation was considered in which the theoretical biological transport was maximised by assuming that all the exportable benthic biomass is transferred up to the surface, but no mechanism was specified. Robinson & Mullin (1981) based their estimate of exportable biomass on the best available data on deep-sea benthic biomass and assumptions on turn-over rates. GESAMP (1983) constructed a carbon budget based on the organic input to the deep sea ecosystem estimated from sediment trap data. Rowe (1981) also provided estimates of exportable benthic biomass. Assuming the philosophy on which these models are based is correct, the conclusions of these studies will only be misleading if those estimates of exportable biomass are grossly wrong by orders of magnitude.

5.iii.d Biomass

The data for the meiofaunal and macrofaunal biomasses used in the models of Robinson & Mullin (1981) and GESAMP (1983) are based on a reasonably large number of measurements, and are unlikely to be grossly wrong. The data available for megabenthos are less reliable. They have been derived, for the most part, from catches of trawls and dredges with unknown fishing efficiencies. The best quantitative data are those of Haedrich & Rowe (1977) who estimated abundances from photographic

surveys and used trawl catches to estimate mean weights. All available megafaunal biomass estimates are based on wet weights which do not take into account the very wide differences in water and in organic contents between taxa. IOS have sought to obtain better estimates by combining photographic surveying with the sampling by the development of the IOS epibenthic sledge (Figure 5.iii.1) (Rice, Aldred, Darlington & Wild, 1976) and by measuring wet, dry and ash-free dry weights of organisms sampled.

Data from a series of 35 hauls collected from a broad range of bathymetric depths show a clear trend for biomass to decrease with increasing depth which overrides the wide range of small-scale variability seen along individual transects and between hauls from similar depths. Biomass, in terms of ash-free dry weights decline from around 0.4g m^{-2} at 500m to about 0.01g m^{-2} at 4000m (Figure 5.iii.2). The data also suggest that wet weight estimates are a better index of overall biomass than was expected considering the inter-taxa variations in chemical composition. These biomass figures do not vary substantially from those used in the models, and, since there is no reason to consider the Porcupine Abyssal Plain as being in any way atypical, they give no cause to doubt the general conclusions of the models.

However, the epibenthic sledges does not catch the mobile fish fauna effectively. The distribution of biomass of the benthic fish in the Porcupine Seabight has been studied using a relatively conventional trawl (Figure 5.iii.3). There was an increase in fish biomass down from the shelf-break at about 200m to a broad maximum extending from 600 to 1600m. Below this maximum fish biomass declines steadily to 3000m, but from 3000m down to the limit of sampling at 4500m the biomass apparently remained constant. Overall fish biomass decreased by an order of magnitude from the maximum level to the deep minimum. While it is recognised that there are quite serious problems associated with sampling inefficiencies and patchiness when studying all benthic communities, none of the IOS data provide any evidence which questions the figures used in the models of Robinson & Mullin (1981).

5.iii.e Potential Vertical Exchange based on Carbon Budgets

The input terms of the GESAMP models were based on data derived from sediment trap data. These traps have been deployed over periods ranging from days to months,

mostly at tropical or subtropical latitudes. The data have then been extrapolated to give an annual flux by assuming that there is no significant seasonal variation. Recent sediment trap studies (e.g. Deuser & Ross, 1979; Honjo, 1982) have indicated that this assumption is invalid in tropical seas, while our work in the Porcupine Seabight at a much higher latitude has revealed a substantial seasonal variation in the flux of organic material to the sea floor. Billett et al (1983) showed that large quantities of phytodetritus arrive on the sea bed at depths of at least 4000m within a few weeks of the onset of the spring bloom. This is by far the most far-reaching result of the IOS benthic programme because not only does it demonstrate that seasonal variation in sedimentary input cannot be ignored, but it also explains the seasonality in the reproduction cycles of a variety of benthic invertebrates (Tyler et al, 1982). It may also explain why there are marked seasonal variations in community respiration observed beneath oligotrophic waters in the eastern North Pacific (Smith & Baldwin, 1984). In addition the phytodetritus appears to scavenge naturally occurring radioactive isotopes out of the water column. An isotope of particular interest is ^{234}Th which has a half life of only 24 days and an atmospheric input. This isotope is detectable in the detritus on the sea bed and is incorporated into the superficial layers of the sediment possibly through biological processes. Hence this highly pulsed seasonal flux of organic detritus may not only be of considerable biological and chemical significance, but also be a major consideration in evaluating the hazards of pollutants in the ocean.

5.iii.f. Bioturbation

GESAMP (1983) concluded that bioturbation was one biological process that may have a major influence on the mass transport of contaminants. Bioturbation is the disturbance of the superficial layers of sediment by biological processes. It can affect the sediment in three ways:

The reworking of the superficial sediments by the burrowing of infaunal organisms or deposit feeding epifauna. This reworking may expose contaminants whose source is within the sediments, or bury those coming from the water column. It may also influence the porosity of the sediments. Extensive reworking is generally considered to be limited to the top 10cm of the bottom deposits, in which the chemical characteristics are usually uniform. However, a number of burrowing organisms are known to penetrate deeper and their burrows are likely to alter the chemical

environment within their immediate vicinity as well as greatly increase sediment porosity. Photographic surveys in the Porcupine Seabight have shown that the apparent degree of reworking can vary quite substantially between quite small adjacent areas (Figure 5.iii.4).

Direct resuspension can result from the effects of exhalent respiratory currents and burrowing of the infauna and the more vigorous movements of the scavenger/ carnivore community.

Roughening of the sediment water interface caused by the tracks, burrows and mounds alters the frictional drag between sediment and water. In quiet current conditions this may inhibit resuspension, but if the water movements exceed a critical limit the roughness may increase the rate of erosion.

No direct studies of bioturbation have been carried out at IOS, but photographic time sequences of small areas of sea bed resulting from the use of Bathysnap (Figure 5.iii.5) (Lampitt & Burnham, 1983) can provide data on the persistence of 'lebenspurren' (any visible feature on the sediment caused by biological activity). The abundance of the lebenspurren along photographic transects in the same vicinity can then be translated into an estimate of bioturbation activity (see Lampitt, Rice & Thurston, 1984 for an example on the persistence of faecal casts of a holothurian).

5.iii.g Conclusions on the importance of benthic biological processes to mass transport

The two modelling studies which thoroughly examined the relative importance of biological vis-a-vis physical mechanisms in the possible mass transport of contaminant substances released at the sea bed up to surface layers, both concluded that biological mechanisms would probably be less effective by several orders of magnitude. None of the IOS results have called into question either the validity of the models' underlying assumptions or the approximate correctness of the input data. Although a continuing assessment will need to be maintained, as knowledge of deep-sea ecosystems improves, the main thrust needs to be towards the investigation of critical pathways to Man.

5.iii.h Critical Pathways and Benthic Ecology

The existence of critical pathways is dependent on either the direct exploitation of contaminated organisms or direct trophic links with highly efficient transfer of contaminants between exploited populations and those which are contaminated.

The economic feasibility of direct exploitation is limited because of the decrease in biomass which occurs with depth and the rarity of large concentrations of biomass at great depths. Unless a highly valued specialised resource is discovered, the exploitation of living communities from below the present extreme limit of commercial fishing of ∿2000m seems unlikely. The prospects of any such development need to be assessed continually in the future in this context.

The main question then is centred around whether there are individual organisms that can migrate from the source of contamination and whether they can directly or indirectly contribute to an exploited resource. For benthic organisms this raises two main questions including (a) what is the maximum range over which benthic organisms move horizontally, and (b) how far up into the water column do benthic organisms migrate.

5.iii.i Maximum Ranges of Benthic Organisms

Deep-living benthic organisms tend to have very widespread geographical distributions, but tend to occur within quite limited bathymetric ranges. Data on the bathymetric ranges of benthopelagic fishes and two echinoderm groups in the Porcupine Seabight are illustrated in Figures 5.iii.6, 7 and 8. All these data show that no species inhabiting deep abyssal depths >4500m normally penetrate shallower than 2000m. The life-time ambit of an individual will be much more restricted than the total range of the species to which it belongs. This is exemplified by the morphological changes associated with depth observed in the gastropod mollusc Troschelia berniciensis. In this buccinid there is a marked decrease in the size of the shell aperture relative to the spire height, across its observed depth range in the Porcupine Seabight of 400-2100m. There were also differences in morphology between animals sampled at the same bathymetric depths on opposite flanks of the Seabight. Whether this variation is genotypic or phenotypic in origin (i.e. reflects either a difference in the genetic make-up, or is the response of a community of animals with a common genetical make-up to differences

in the environment) is unresolved, but it does indicate how much more limited is an individual's ambit compared with the total distribution range of the species.

Average speeds for the rather sluggish deposit-feeding megabenthos, estimated from Bathysnap photo-sequences, are shown in Table 5.iii.1. The maximum speeds of half a metre per hour by an unidentified worm is equivalent to 4½km per year. Such speeds make it most unlikely that the movements of deposit-feeders will be of the slightest importance as a contribution to a critical path, but the migrations of the more active benthopelagic scavengers/carnivores need to be considered. Photographic time-series are providing data about the patterns of arrival of this more mobile fauna at baits. The data from one sequence are illustrated in Figure 5.iii.9. In this sequence two fishes Coryphaenoides armatus and Echinomacrurus mollis were attracted within four hours of the bait being dropped onto the sea bed. A few amphipods also arrived soon after the drop, and continued to build up in numbers. The rate of build up appeared to be related to the tidal cycle, being faster during the periods of slow tidal current. The numbers of amphipods on the bait declined following the arrival of the fish Paraliparis bathybius, a facultative amphipod predator, which seem to coincide with the end of the periods of high tidal current. The build up in numbers of the large amphipod Eurythenes gryllus appeared to be independent of the tidal cycle. It should be possible using available technology to devise experiments which will shed some light on the daily ambit of these scavengers, and so set limits on their dispersion.

The most mobile elements in the benthic community are the fish. It is likely that at least some fish species will have life cycles which involve extensive migrations. Like its freshwater counterparts the eel, Synaphobranchus kaupi which is numerically dominant at mid-slope depth in the Porcupine Seabight is believed to undertake breeding migrations to the Sargasso Sea. Similar migrations either horizontally or up and down slope while unlikely to result in significant mass transport (e.g. GESAMP, 1983) could provide a route for critical path transport.

5.iii.j Vertical Migrations by Benthic Species up into the Water Column

The most commonly quoted example is the specimen of the amphipod Eurythenes gryllus taken at a depth of 800m over a sounding in excess of 5000m in the Pacific (McGowan 1974); this species has been taken at the surface in cold water at high latitudes. During Discovery Cruise 114 two specimens of the tripod fish, Bathypterois sp.,

were taken at 1000m depth over a sounding of 3200m to the south west of the Azores. At 42°N 17°W single specimens of juvenile Halogyreus johnsoni and Paraliparis sp., were taken at 1000m over a sounding of about 5000m (Angel et al, 1982b). There are a number of reports in the literature of benthopelagic fishes with mesopelagic prey in their stomach contents which have been interpreted as evidence for the occurrence of migrations by bottom-living fishes up into midwater to feed (see IOS 1978 for summary).

A number of reports have described holothurians in midwater well above the sea floor. However, many of the species involved are now known to be truly pelagic (e.g. Peniagone diaphana and Scotothuria spp), the only species normally considered to be benthic which have been taken with any regularity in midwater are Benthodytes typica and juveniles of Psychropotes spp.

The function of these migrations is not clear. Most of the specimens taken have been juveniles, so breeding is not the underlying reason in most cases. The deep midwater zones are more sparsely inhabited than the near-seafloor region, so feeding seems also to be an unlikely function except possibly in slope regions (e.g. Hargreaves et al, 1984a). One possibility is that the juveniles are undertaking some sort of ontogenetic migration that is related to a dispersal phase of the life-cycle. One of a number of other alternatives is that the overlying water column may be used as a refuge from the higher predation pressures on the sea floor.

Other activities may result in upward transport of material. A number of benthic species produce buoyant eggs which float up into the water column and undergo pelagic development (e.g. some macrourid fishes). Feeding by predators and scavengers which involves the breaking up of food before consumption can result in the release of buoyant substances such as lipids into the water. However, such processes involve small-sized particles and are most unlikely to provide a critical pathway.

5.iii.k The Pelagic Ecosystem

In the vast majority of oceanic areas the dominant sources of energy are the primary production in the sunlit (euphotic) zone and terrestrial material via riverine or aeolian inputs. Consequently the major inputs occur in the surface few

tens of metres of the water column, and there is an exponential decrease in standing crop of biomass with depth. The flux of energy, in the form of organic material, results from a number of processes such as the sedimentation of a vast spectrum of particulates and the migrations of organisms. Despite extensive recycling within the surface few hundred metres the net flux is downwards.

At three widely-spaced stations in the Northeast Atlantic Angel and Baker (1982a) demonstrated that the slopes of the linear regressions of log biomass against depth were surprisingly consistent for both plankton and micronekton (Figure 5.iii.10). The slopes of all the regressions implied that the standing crop decreased by around two orders of magnitude between the surface and a depth of 4000m. Then, assuming production is proportional to standing crop, production too, will decrease by two orders of magnitude over the same depth range. However, the ratio between production (or biological rates in general) and standing crop is likely to vary with depth, but by less than an order of magnitude.

5.iii.1 Vertical Structure of Midwater Communities

Five major ecological zones can be recognised in deep oceanic communities. The surface 200-250m of the water column extending through the euphotic zone to the base of the seasonal thermocline is termed the epipelagic zone. From the base of the epipelagic to around 1000m, which coincides roughly both with the greatest depth to which detectable daylight penetrates in the clearest ocean and with the base of the permanent thermocline in tropical and subtropical waters, is the mesopelagic zone. Below the mesopelagic zone extends the bathypelagic zone whose lower limit coincides with the disappearance of fishes as a major constituent of the communities at around 2500-2700m. The significant environmental factors which result in the change in community structure from bathypelagic to abyssopelagic have not yet been determined. The abyssopelagic zone extends either to the depths at which the proximity of the sea bed begins to have an influence on the community structure i.e. the top of the benthopelagic zone, or to hadal depths (>6000-6500m) over trench systems. The determination of the upper limit of the benthopelagic zone is of interest, because the standing crop increases quite sharply relative to the overlying abyssopelagic zone. The extent of this zone probably encompasses the nepheloid layer which is recognised (a) by inflections in chemical profiles produced by the resuspension of sediments, (b) by increases in the turbidity of the water close to the sea bed and (c) by the layer of water

which is homogeneous as a result of the frictional drag of the sea bed causing turbulent mixing. The sea bed acts as a sediment trap for sedimenting particulates and so it is relatively enriched with organic material. It is the vertical extent of the resuspension of superficial sediments with their organic material which determines the height to which the nepheloid layer extends above the sea bed. At abyssal depths perturbations in chemical profiles have been observed up to 1000m above the sea floor (Brewer et al, 1976), whereas increases in biomass have only been detected within 100m of the sea bed (e.g. Wishner, 1980; Hargreaves et al, 1984a).

Vertical excursions by organisms may contribute towards the upward transport of material and contaminants by biological processes. They may be undertaken in order to feed, to avoid predation, or as a life-cycle adaptation. Migrations can be of high frequency (e.g. sperm whales diving to feed, or plankton moving up and down according to the cycle of the light regime) or low frequency associated with cycles of productivity (seasonal migrations) or with life history stages (ontogenetic migrations).

5.iii.m Vertical Ranges

Perhaps the most complete data set describing the vertical structure of a midwater community available for the North Atlantic was derived from samples collected at Discovery station 9801 in April 1978 in the vicinity of 42°N 17°W. The planktonic ostracods (Angel, 1983) and the micronektonic euphausiids, mysids and decapods (Hargreaves, 1984b) have been analysed in some detail. These data can be interpreted in the context of a series of repeated tows taken at a depth of 1000m at the same station (Angel et al, 1982b) and the IOS biological data base which includes most of the information on the vertical distributions of pelagic organisms in the NE Atlantic accumulated over the last 15 years. The vertical distribution data for the ostracods, decapods, mysids and euphausiids are summarised in Figures 5.iii.11 and 5.iii.12. Hargreaves (1984b) analysed her data by factor analysis and demonstrated a clear pattern of zonation (Figure 5.iii.13). These data show that there were no direct faunistic links between the abyssopelagic community and the mesopelagic or epipelagic communities. Hence any upward biological transport will only occur through a series of trophic interactions, and if it is to provide a critical pathway not only will there need to be concentration of the contaminant as it moves along the trophic pathway, but also there must be a

mechanism that stops the dispersal of the organisms. Hargreaves (1984b) has shown that similar community changes occur in at least some taxa in the deep water column of the Porcupine Seabight and the Rockall Trough regions to the west of Britain. Trophic interactions may occur between species inhabiting different vertical zones during their vertical migrations.

5.iii.n Vertical Migrations

Many pelagic organisms are known to make vertical migrations in midwater. The function of these migrations can vary from escape from predation, finding food and life-cycle adaptations, to apparently motiveless random movements. Sampling techniques can detect migrations within populations or identifiable sections of a species' population if all the movements are synchronised. Roe (1974) and later Pearre (1979), have pointed out that at present we have no methods that will allow us to detect the occurrence or range of asynchronous movements. However, the extent of such migrations must be confined within the known total vertical range of a species, and so long as this range is small relative to the total water column depth, asynchronous migrations are unlikely to provide a faster transport mechanism than synchronised movements. These sorts of migrations could be important in slope regions where species' vertical ranges may span the total water depth.

To provide a 'measurable' transport mechanism a migration must either involve the movement of very large quantities of biomass or have a very high frequency of migration. If contaminants are absorbed out of solution at one phase of the migration, they must either be released back again very rapidly or mortality must be substantial during the other phase. Alternatively, if the contaminants are taken up in food, the fraction that is not ingested must be retained in the gut for long enough for the organism to complete its migration, and the fraction that is ingested will only be released during the alternate phase through mortality or excretion. Because the standing crop of pelagic organisms is small relative to the mass of the water, high frequency migrations are more likely to result in measurable transport of contaminants than low frequency migrations. So here the types of migration are considered in descending order of frequency.

Feeding Migrations: The vertical migrations of highest frequency are probably the feeding migrations of marine mammals; they are linked to the surface by their need to breathe air and yet they need to dive to feed. Most large and small whales

dive no deeper than a few hundred metres, but sperm whales have been recorded as diving to considerable depths. However, Lockyer (1977) found that only 5% of sperm whale dives were to as deep as 800m though there is circumstantial evidence that they may be capable of diving to as much as 3000m (e.g. Clarke in Wood, 1972). Sperm whales feed either on squid or, in a few areas, on fish, prey which tends to be predatory and have high energy demands. The general exponential decline with depth of standing crop observed both in the pelagic and benthic realms, make it unlikely that below 2000m there will be enough food for the sperm whale's prey to be sufficiently abundant for it to be metabolically worthwhile for the whale to regularly dive to such depths.

Diel Vertical Migrations (DVM): A striking phenomenon in many oceanic regions is the regular movement of midwater organisms from deep daytime depths up into the superficial layers at night. A number of theories have been put forward to explain these migrations (see Longhurst, 1976 for summary), none of which is adequate to explain them all. The theory that is held to be most acceptable at present is that the downward migration is to avoid the danger of visual predation at shallow well-lit depths by day. The movement back to shallower depths at around sunset is to return to where the food supply is more abundant. This would predict that at very high latitudes in midsummer or midwinter during conditions of constant light or dark the migrations should be suppressed, and indeed what evidence is available does support this, although this could result from the migration becoming asynchronous. At temperate latitudes where production is seasonally variable, the expression of DVM would be expected to be similarly variable, and preliminary seasonal data collected from Discovery implies this is so. The maximum range of the migration occurs in the subtropical regions but is reduced in the tropics (e.g. in planktonic ostracods, Angel & Fasham, 1975).

In Figure 5.iii.14 are plotted the day and night profiles of cumulative percentages of the total biomass in the top 1200m at five stations all within 300 nautical miles of each other to the southwest of the Azores. The stations were occupied to study the influence of a major oceanic front on the vertical distribution of plankton and micronekton in the vicinity. The profiles illustrate that there can be quite large variations in the migration patterns over quite limited distances. There was no detectable daily re-distribution of planktonic biomass below 800m, but in the micronekton there was probably some re-distribution down to at least 1200m at most stations. Deeper samples were taken at some of the stations

which suggested that 1200m was the lower limit for DVM in the majority of micronekton, but one fish Ceratoscopelus warmingi was migrating up from daytime depths of at least 1600m into the surface 100m at night. At another position further north (42°N 17°W), Angel et al (1982) showed that at a depth of 1000m only a single fish species, the myctophid Notoscopelus elongatus kroyeri, out of 192 micronektonic and planktonic species examined, showed the cyclic variability in abundance consistent with it performing DVM. Thus the lower limit for most DVM in plankton is at about 800m, and in micronekton it is at about 1000-1200m or occasionally 1600m.

The quantities of biomass moving during these migration cycles have rarely been estimated. The data from the five Discovery stations off the Azores have been analysed to provide such flux estimates (Table 5.iii.2). No attempt was made to try to estimate the errors of these estimates but, on the basis of repeat samples taken elsewhere, they are not thought to exceed 25-50%.

Data are available from four of the five stations, from which comparisons can be made between the biomass fluxes of four taxonomic groups which are major contributors to the standing crop (Table 5.iii.3). The fluxes varied substantially between the two water masses. Fish provided the largest flux up into the top 500m at all four stations and at three stations up into the top 200m. Fish also migrated over the greatest vertical distances.

The significance of these fluxes to the transportation of contaminants will depend on how the contaminants are taken up and released. There are no available estimates of daily mortality rates during these migration cycles but they are unlikely to be substantial. Transport in gut contents may prove to be the most important quantitatively, but this will be determined by feeding chronology, gut retention times and sinking rates of faeces.

Data on the feeding chronology of fish and decapods in relation to their diel vertical migrations during spring at 44°N 13°W are available from Roe (1984a), and Roe & Badcock (1984b). These data were collected in a major sampling programme which examined the variability of the majority of the planktonic and micronektonic species at four depths (100m, 250m, 450m and 600m), each of which was sampled repeatedly over a 48 hour period. The decapods fed continuously throughout the daily cycle and as far as could be judged from their stomach contents some but

not all showed selectivity in their feeding. The fish showed signs of periodicity in their feeding, and the migrants tended to feed more at night than by day. There are few data available on gut retention times.

The region studied near the Azores is a typical poorly productive mid-oceanic region. The estimates of vertical flux resulting from DVM are likely to be exceeded in more productive areas, but evidence available in the literature and collected by IOS implies the vertical range of the flux is most unlikely to be greater. If this is confirmed then fluxes resulting from DVM by plankton will be restricted to the top 800m of the water column and from DVM by nekton to the top 1000-1500m.

Ontogenetic migrations: Many midwater species undergo changes in their vertical ranges during their life cycles, and these migrations are termed ontogenetic (e.g. Miller et al, 1984). In species with annual life cycles, these ontogenetic migrations will be indistinguishable from seasonal migrations (see below). The usual pattern is for the young smaller stages to occupy shallower depths where there is greater availability of food but where the predation pressures tend to be greater. Merely the fact they are smaller in size gives young stages an element of protection against detection by visually-hunting predators. As they grow and mature, so they become more visible, so if they are still to avoid detection they must continue to descend deeper into the water column to stay below the depth to which enough daylight penetrates for them to be perceived visually. This descent may be either a slow gradual sinking of the distributional range or a quite rapid descent accompanied by a dramatic metamorphosis as is seen in a number of benthopelagic fishes such as the ceratioid anglers.

Any upward flux associated with ontogenetic migrations will probably be via reproductive products or early stage larvae. It will depend on the duration of the life cycle, the life history strategy of the organism, and the amount of metabolic investment in reproduction. The duration of life cycles tends to increase with decreasing water temperatures and increasing depths; associated with this is a low investment in reproduction until the final stage of maturation is reached. Childress & Price (1978) examined the life history characteristics of the bathypelagic mysid Gnathophausia ingens and found that it has a low rate of oxygen consumption, a long development time (7 years), a large size at maturity, and, rather unexpectedly, a single brood of 150-350 larvae, whereas many other deep-sea organisms tend to produce very small broods (1-2) iteroparously (i.e. repeated

successive broods). Most of these characteristics are energy conserving and help to optimise the efficiency with which the energy invested in reproduction is utilised. Even so, the proportion of ingested food invested in reproduction is likely to be far less than 50% of that invested in the growth and metabolism needed to maintain the standing crop of adult organisms in those species which undertake ontogenetic migrations. These ontogenetic migrations may provide quite a large upward flux at shallow depths, but from depths greater than 2000m the flux is likely to be relatively trivial because of (a) the low standing crop at such depths, (b) the relatively few species that are known to perform extensive migrations and (c) the small proportion of the population that is mature and breeding within the water column.

Seasonal Migrations: In regions in which the production cycle is markedly pulsed many organisms undertake quite extensive vertical migrations, spending the seasons of low productivity at relatively great depths, often in a state of diapause (e.g. Miller et al, 1984). Diapause is comparable to the state of hibernation or aestivation in terrestrial organisms, and is characterised by the organisms reducing their metabolic activity. It is often accompanied by the laying down of substantial quantities of lipid, both as an energy reserve and possibly as a mechanism helping the organism to maintain neutral buoyancy. The organisms cease to feed and the gut regresses. Diapause usually occurs at a specific stage in the life cycle; egg or late-stage larval stages are most common. For example, the species of copepod which dominates plankton communities in northern waters around Britain, Calanus finmarchicus, overwinters as the fifth copepodite at depths down to 2000m. The descent into deep water occurs in the autumn and the ascent occurs soon after the onset of the spring bloom. The copepodites immediately mature after the ascent and start to breed.

In the Pacific the life-history characteristics of the main grazers are much more finely tuned to the cycle of productivity. Also the Pacific species appear able to enter and break diapause with much greater facility and two or even three times during an individual's life time (Miller et al, 1984). One consequence of this finer tuning is that the grazing pressure of the herbivores prevents the spring surge of production appearing as a bloom and results in a substantial increase in phytoplankton biomass, a phenomenon which is characteristic of the spring in the temperate waters of the northeast Atlantic. Hence it is possible that the whole pelagic structure and function in the North Atlantic is quite different

from that in the North Pacific, notably in the sedimentation regime (see section on flux of organic matter, 5.iii.o).

The function of seasonal vertical migrations seems to be for the organisms to find cooler conditions, where their metabolic expenditure is less, and safer conditions, where predation pressures are not so intense. The migrations probably optimise the efficiency with which energy is used and stored in conditions of variable production.

The biomass flux associated with these seasonal migrations has rarely been estimated. Hargreaves et al (1984a) used data from Williams & Conway (1981) to estimate the total upward flux resulting from the seasonal migration of the very abundant hydromedusan Aglantha digitale as being only 40 mg m^{-2} ; the downward flux in the autumn is probably higher, possibly by a factor of 2. The total integrated community movement will be much larger, but cannot exceed the total standing crop of plankton and micronekton observed during the early spring. Angel & Baker (1982a) observed that in the Porcupine Seabight in April the total community standing crop in the whole water column (to 3500m) gave a displacement volume of 126 mℓs m^{-2} of which 75% occurred in the top 900m. Assuming all this standing crop had undergone a seasonal migration, and that dry weight is equivalent to about 5% of the displacement volume, the maximum possible total flux up through the water column will be of the order of 5g m^{-2}, but the true values will be much less than this figure. Scattered evidence in the literature suggests that all of this flux occurs within the top 2000m of the water column. Also, because a large proportion of the migrants do not feed at depth (i.e. they are in a state of diapause) much of the uptake of any contaminants at depth will not be via food, but by direct absorption from the ambient seawater.

5.iii.o Flux of Organic Material to the Sea Floor

Probably the most significant observation made by the IOS Biology Department is the rapidity with which large quantities of detrital organic material, much of it of phytoplanktonic origin, sediments out of the water column. In 1982 when the spring bloom probably occurred in early April, Bathysnap (Lampitt & Burnham, 1983) photo-sequences showed that at a depth of 2000m in the Porcupine Seabight the first signs of the detritus appeared on 30th April (Billett et al, 1983); by the end of May there were substantial quantities of the detritus lying on the

sea bed. In 1983 a cruise was planned to study the development of the spring bloom and the subsequent formation and sedimentation of the detritus. Bathysnaps were deployed at 2000m and 4000m. Unfortunately a succession of storms moved through the area keeping the surface layers well mixed and inhibiting the development of the bloom until the end of the cruise in the first week of May. In addition, the Bathysnap deployed at 2000m failed to release and so data on the arrival time of the detritus on the sea bed are available only at 4000m, where it began to appear in late June. Much of the material was arriving in the form of large aggregates up to 10mm in diameter. Tidal currents, which can reach speeds of up to 13 cm s^{-1}, resuspend some of the detrital layer but the large aggregates tend to remain in place.

Samples of the detritus have been collected using the SMBA multicorer. In May 1981, at 2000m, it consisted principally of diatoms together with amorphous organic matter in some instances bound into aggregations. In July 1982 samples from a range of soundings of 1340-4475m again showed an abundant diatomaceous content but included faecal pellets and gelatinous aggregations up to 10mm in diameter. The aggregations included coccoliths, dinoflagellates, crustacean eggs, small faecal pellets and amorphous organic material. In all these samples the specific composition of the phytoplankton reflected the seasonal composition of the phytoplankton communities present at the time in the surface layers. The chlorophyll and other chloropigments indicated that the source of the pigments was marine and there was evidence of some bacterial degradation. The C : N ratio of 24 was unexpectedly high suggesting that preferential microbial degradation of nitrogeneous material had occurred.

Sinking experiments on the aggregates gave rates mostly within the range 400-800 m d^{-1}, quite fast enough to account for the minimum rate of 100-150 m d^{-1} needed to explain the rapid arrival of the detritus on the sea bed so soon after the start of the spring bloom in April 1982. These rates are also fast enough to account for the rapid transportation of the naturally occurring isotope ^{234}Th which is derived from an atmospheric input, and has a half life of 24d. The ^{234}Th and ^{210}Pb have been used to calculate preliminary estimates of sediment-mixing coefficients in the surface few centimetres.

The intensity of the seasonal pulsing of the supply of organic material to the deep living communities in the Seabight appears to be far more extreme than has

been observed in sediment trap experiments for which results have been published to date. However, all these sediment trap observations have been conducted at subtropical and tropical latitudes where the production cycle is more uniform. It is probable that this rapid sedimentation of phytoplankton detritus will prove to be a more widespread phenomenon in temperate and sub-polar latitudes where the climatic cycle of winter cooling and summer warming results in a highly seasonal production cycle. If this can be demonstrated then it implies that annually there will be a large rapid flux of organic material sedimenting out of the water which is capable of chemically scavenging trace elements from the water column, as has been shown for the short-lived ^{234}Th isotope. This phenomenon, besides being of considerable intrinsic interest in the study of deep sea ecology, geochemistry and sedimentary geology, may prove to be extremely important in the evaluation of pollution problems in the deep ocean.

5.iii.p Continental Slope Environments

The region extending from the margin of the continental shelf at the shelf break out over the continental slope is of key interest to this problem. It forms the interface between the shelf (or neritic) ecosystem which is heavily exploited by Man, and the more remote deep water oceanic ecosystems. It is a region where future developments in the exploitation of both living and non-living resources will probably be extensive. Oceanographic processes tend to be much more dynamic over the slopes and so the potential for high fluxes is greater.

Productivity is often enhanced along the shelf break, at the shelf break front, and there is often a striking increase in the numbers of sea birds at this boundary. Although the shelf break is not a physical barrier to organisms and indeed a number of fishes perform regular on and off the shelf migrations (e.g. salmon and eels), it does act an important boundary both to the zoogeographic distributions of many species and to the way in which the ecosystems function.

On the shelf, the surface pelagic communities are intimately linked with the benthic communities and the two strongly interact, whereas in the deep ocean the shallow pelagic ecosystems are hardly influenced at all by the benthic biological processes. Over the slope this linkage between the shallow pelagic and benthic systems progressively weakens as the depth increases. So slope regions are transition zones between the shelf and the deep ocean. In some areas the slope transition

is blurred by the hydrographic processes. For example, along the northeast coast of the United States warm-core eddies which are spawned from the meandering of the Gulf Stream system, carry oceanic species in over the shelf. However, incursions of oceanic species over the shelf break off Europe seem not to be so frequent although in some years warm water oceanic species (sometimes termed the Lusitanian fauna) get advected round Scotland and enter the North Sea from the north.

Hargreaves, Ellis & Angel (1984a) carried out an assessment of the biological processes occurring close to the sea bed in the slope region of the Goban Spur which lies to the south of the entrance to the Porcupine Seabight. Their observations were supplemented by some observations made on the northern flank of the Seabight. They demonstrated a clear increase in the standing crop of biomass in the 50-100m of water immediately overlying the sea floor. They attributed this increase to the greater availability of food created by the sea floor acting as a sediment trap. However, in contrast to the great depth to which the influence of primary production in the euphotic zone extends the biological effects of the sea floor were seen only a short distance up into the water column.

Specific analysis of the catches showed that certain taxonomic groups displayed a greater response than others; polychaetes for example exhibited a very striking increase in biomass, whereas planktonic ostracods showed little. The total community increase was dominated by decapods and copepods which were the main constituents of these deep communities. Comparisons with midwater catches taken nearby in deeper water showed that two decapods, Sergestes arcticus and Gennadas elegans, not only increased substantially in abundance close to the sea bed but also extended their distributions into greater depths over the slopes (Hargreaves, 1984b). In both these species the shallower portion of the population performed diel vertical migrations, but it was not possible to establish if animals inhabiting the near sea floor undertook such migrations. Some of the data suggested that some of the bathypelagic species were being displaced by this submergence of normally mesopelagic species. However, many species appeared to be unaffected by the presence of the sea bed and their abundances and vertical ranges over the slope were similar to those observed over deep water. One bathypelagic species, the ostracod Conchoecia pusilla spread up from shallow bathypelagic depths to mesopelagic depths over the slope.

These changes in vertical distributions over slope regions offer an alternative explanation for the observations of benthopelagic fishes having midwater species in their stomachs. This had been used to argue that these fishes, which are seldom taken more than a few metres above the sea floor, were making regular, extensive migrations up into the midwater to feed, but from the observations of Hargreaves et al (1984a) the migrations may be by the pelagic species moving down. However, this does highlight the probability of much greater vertical exchange of biomass occurring via feeding migrations in slope regions.

In the Porcupine Seabight region, the sampling extended down to depths of 1650m. There was little evidence of a highly novel fauna as had been found in near sea bed samples collected at 4000m off NW Africa. Studies on benthic zonation suggest that there is a considerable change in benthic community structure at around 2000-2500m, corresponding approximately to the midwater change from bathypelagic and abyssopelagic. If there is a comparable deep-slope faunal boundary in the near bottom pelagic fauna, this could imply that biological exchange across this boundary is inhibited relative to other depths. It is important to establish whether or not there is any faunal continuity between upper and mid-slope regions and abyssal depths particularly amongst the more highly mobile pelagic forms.

Hargreaves et al (1984a) concluded that slope regions are likely to be a dynamic interface between the deep-living benthic and benthopelagic communities and the shallower-living shelf communities. If substantial quantities of contaminants do get transported up to mid-slope depths (i.e. < 2000m) then biological processes could play a significant role in moving them onto the shelf. There are some potential critical pathways (i.e. fish migrations and whale feeding) that need more careful study and evaluation.

5.iii.q Revised Research Requirements

In IOS (1978) a range of specific research requirements were drawn up and they are reassessed in the light of the advances made in the intervening six years.

Identification and Taxonomy: There is a continuing need for a thorough systematic foundation on which to base assessment studies. This need is more important to the problems of environmental impact than to the dose to Man. It will be important to demonstrate convincingly that no fragile deep sea community and no rare deep

sea organism is threatened with irreversible damage or extinction. Without a thorough knowledge of what species occur and how the community is structured and functions, it will be impossible to convince anyone that no important element in the deep sea ecosystem is threatened.

Spatial Patchiness: A thorough understanding of the patterns of heterogeneity in time and space of benthic and pelagic organisms is needed so that, (a) accurate quantititative estimates of abundances can be made; (b) the noise generated by sampling artefacts, as well as by the patchiness of organisms in time and space, can be distinguished from effects of man-made contaminants on community structure i.e. no monitoring programme will be effective without a proper baseline; (c) effective models of community interactions can be constructed. Despite the rapid advances made in the last few years, there is still uncertainty as to the relevant time/space scales at which the most meaningful data can be accrued.

Community Analysis and Zoogeography: The acquisition of such data is slow and expensive, and to be fully effective needs a major international biological data exchange. The need for such analysis is related both to questions of environment impact and to setting limits to transport mechanisms (e.g. some of the 'worst case' analyses described above).

Biomass Estimations: These data are being gradually accumulated for deep living pelagic communities, usually based on displacement volumes. Displacement volumes are only very approximate because of the extreme variations in water content and structure of various taxa, for example, salps are not only extremely watery compared to fishes but also trap more water within their bodies because of their 'bag-like' anatomy. This has partially been taken into account by efforts made to partition the biomass between taxa. However, efforts should be made to extend these estimates to the measurement of dry weight, carbon content and broad biochemical analyses (e.g. into protein, carbohydrate and fat) which would provide data on calorific value and C : N ratios. The latter data in particular are likely to prove extremely useful in providing holistic support for ecosystem models describing the flow of material through the communities. However, seasonal changes will need to be assessed at any site selected.

For benthic communities, biomass estimates for macro- and mega-fauna have been accumulated for the Porcupine Seabight region and there has been some seasonal

coverage. The problems of high spatial variability (patchiness) have been partly tackled by the use of photography in conjunction with the standard sampling (Billett & Hansen, 1982; Lampitt et al, 1984). There is a need for more quantitative estimates of the meiofaunal and microbial fractions of the benthic communities.

Direct quantification will probably continue to be a major unknown in the assessment of risk of contaminants being released in the deep sea. Biomass estimates will never provide more than a very rough estimate unless they are supplemented by some measure of 'activity'. The best measure of activity is probably total community respiration, but more extensive observations will be needed.

Feeding Strategies: Data have been painstakingly accumulated on the diets and periodicity of feeding in pelagic and benthic organisms. Quantification of feeding rates in the natural environment are available for only a few oceanic species. Some indirect methods offer hope of gaining at least some insight, for example for midwater organisms the ^{210}Po : ^{210}Pb ratios show unexpected anomalies which if investigated could well prove to be useful natural tracers for following the flow of organic carbon through midwater communities.

Reproductive Strategies: These have received more attention from the benthic biologists than those studying midwater communities. 'Worst case' models suggest that ontogenetic migrations are unlikely to provide a significant mechanism for the mass transport of contaminants, but this needs to be confirmed by estimating the fraction of available resources invested in reproduction. Perhaps the most important aspect is that reproductive processes are extremely sensitive to pollutants. If an adequate background knowledge of the reproduction of deep living organisms can be assembled, then signs of change in gametogenesis may prove to be the most sensitive indicator of chronic pollution, which can be used for monitoring.

Migrations: Diel vertical, seasonal and ontogenetic migrations appear, at present not to be significant in terms of total mass transport. They are still of considerable intrinsic interest and research will continue to address problems associated with these migrations.

Deposition: The single most important observation which has emerged out of the work of the Biology Department during the last six years, is the rapidity with which phytoplankton detritus is sedimenting out of the water column after the onset of the spring bloom. This phenomenon may be of critical importance to problems of the dispersion of chemical contaminants because of the scavenging of some trace elements and other compounds from the water column by the rapidly sinking particulates and aggregates. It is possible that this rapid sedimentation only occurs at relatively high latitudes, i.e. to the poleward side of the subtropical convergences.

Continental Slope Regions: The continental slopes have been shown to be more dynamic, both biologically and physically, than the open ocean. They are key areas of interaction between the heavily exploited shelf environments and the sparsely exploited deep ocean. Horizontal spread of contaminants into such areas could result in their rapid transportation onto the shelf. Technology is available to study many slope processes where the bottom topography is smooth, but not for where it is rough and precipitous. The problem of investigating the existence of on-off shelf migrations may remain insoluble until a methodology for mark and recapture or for in situ tracking can be developed for deep living organisms. Investigations of these areas may be hampered in future because they lie within the Exclusive Economic Zones of coastal states which could prevent adequate data being collected by withholding permission for research to be carried out.

Modelling: Modelling has two aims and objectives, to provide a predictive capability and to explore the scientific connotations of what is known. Although the final objective will be prediction, at present the main value of modelling biological oceanographic processes is to explore areas of ignorance and focus attention on key areas where more research is needed. The development of large ecosystem models has led neither to the corresponding development of our understanding nor to a reliable predictive capability. Modelling studies of limited aspects of ecosystem function have provided valuable insights which are being fed back into the design of programmes of investigation and sampling regimes. In the short term, models with limited objectives, e.g. to determine the fate of contaminants entering surface communities using more holistic approaches, are more likely to be useful than larger more complicated conceptual constructs.

Table 5.iii.1 Speeds of mobile epibenthic megafauna measured from bathysnap sequences taken in the Porcupine Seabight

	Body Length	Maximum Speed	
	cm	cm h^{-1}	Body Lengths h^{-1}
Asteroidea			
Hymenaster membranaceus	4-9	310	50
Bathybiaster vexillifer	16	100	6
Holothurioidea			
Benthogone rosea	17	89	5
Echinoidea			
Echinus affinis	4	47	12
Gastropoda			
Misc.	4	154	38
Decapoda			
Glyphocrangon sculpta	7	270	39
Vermes	3.2	525	165

Table 5.iii.2 Estimated upward flux of biomass measured in ccs displacement volume (≈ g wet weight) per square metre of sea surface occurring during a migration cycle at five ' Discovery ' stations occupied to the southwest of the Azores in summer 1981, in two water masses Western Atlantic Water (WAW) and Eastern Atlantic Water (EAW), in and close to (WAWF) the front between the two water masses, and in a cold-core eddy of EAW formed two months prior to sampling at the front, but by then surrounded by WAW.

Flux into surface 200m

	WAW	WAWF	Front	EAW	Eddy
Nekton	1.09	1.72	4.23	1.75	1.18
Plankton	1.98	3.40	6.58	8.99	5.42

Flux into surface 500m

Nekton	1.45	2.46	5.40	2.35	1.56
Plankton	0.96	4.82	7.55	8.44	3.92

Table 5.iii.3 Estimated upward fluxes occurring during each migration cycle of biomass (cc displacement volume per m^2) of the four taxonomic groups of nekton which contributed the majority of the standing crop, at four of the 'Discovery' stations occupied to the south-west of the Azores in summer 1981.

	WAW	WAWF	EAW	Eddy
Into surface 200m				
Chaetognatha	-0.023	-0.025	-0.031	-0.012
Decapoda	0.032	0.219	0.199	0.163
Euphausiaceae	0.155	0.110	0.245	0.238
Fish	0.097	0.343	0.669	0.399
Into surface 500m				
Chaetognatha	-0.084	-0.044	-0.013	-0.141
Decapoda	0.212	0.515	0.428	0.488
Euphausiaceae	0.185	0.143	0.297	0.278
Fish	0.394	0.596	0.918	1.100

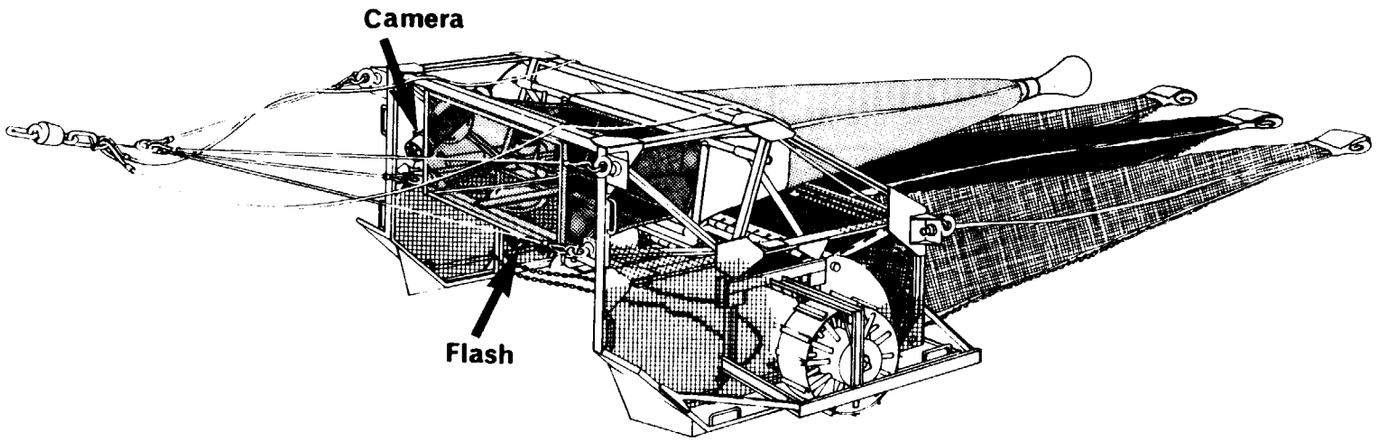

Figure 5.iii.1 Diagram of the IOS epibenthic sledge.

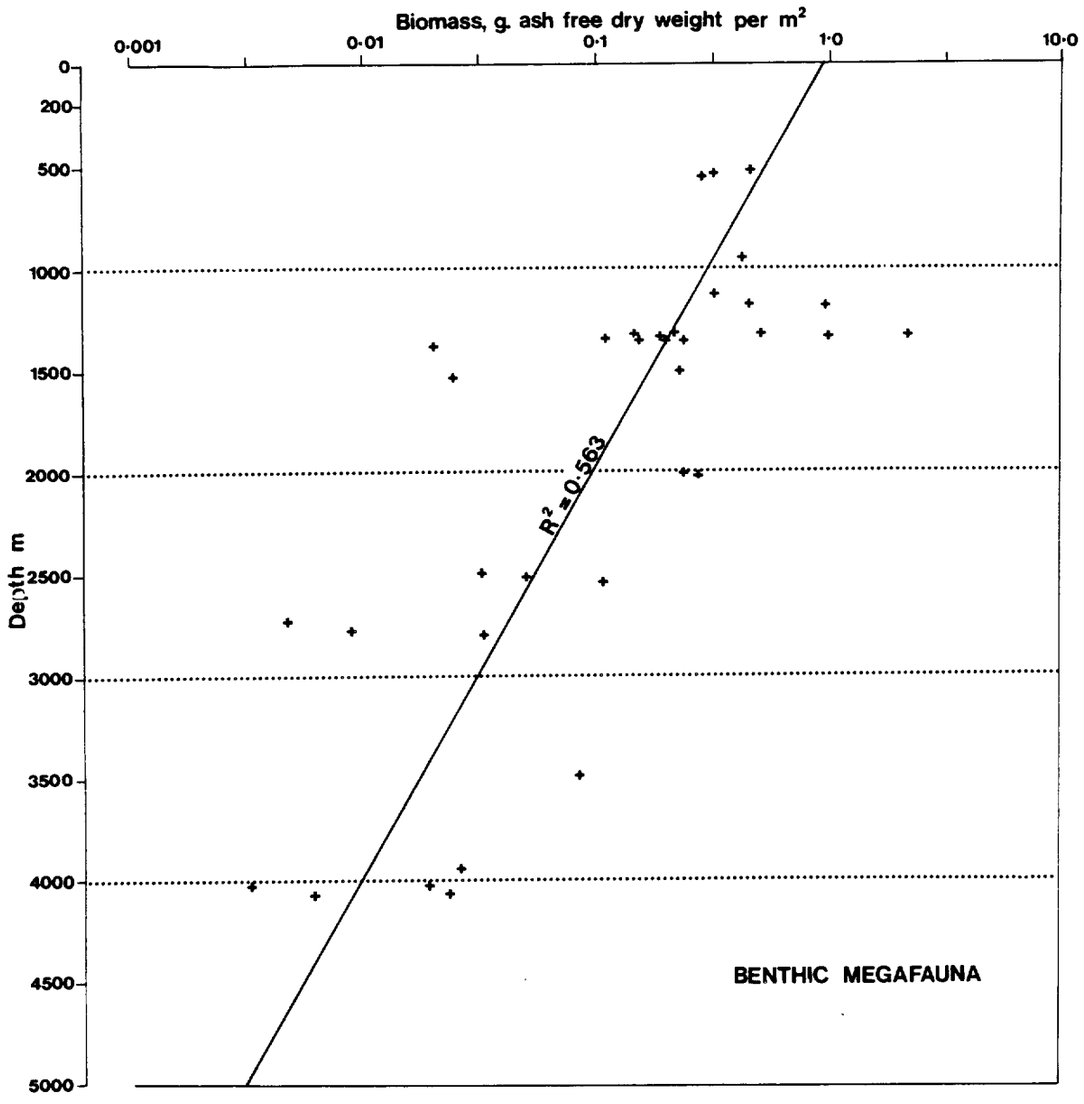

Figure 5.iii.2 Vertical profile of megabenthic biomass expressed as grammes ash-free dry weight per m^2 observed in the Porcupine Seabight region during the IOS benthic programme.

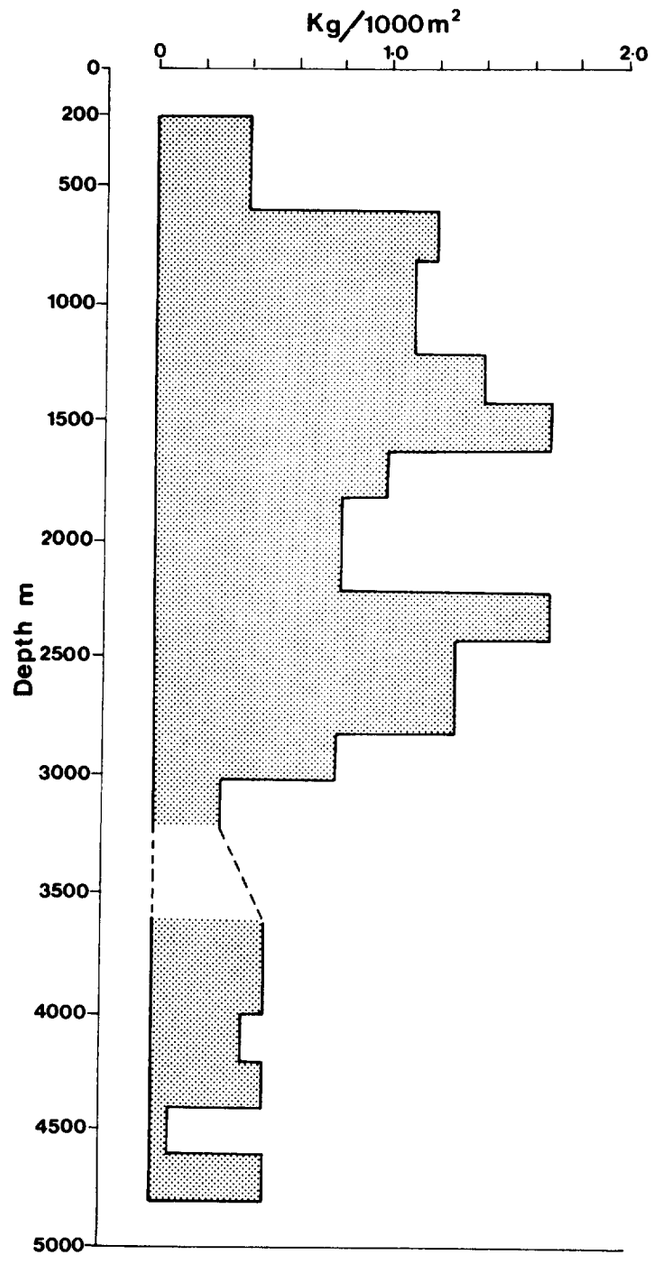

Figure 5.iii.3 Vertical distribution of benthopelagic fish biomass expressed as kilogrammes wet weight per 1000m^2 observed in the Porcupine Seabight region during the IOS deep trawling survey using a semi-balloon otter trawl.

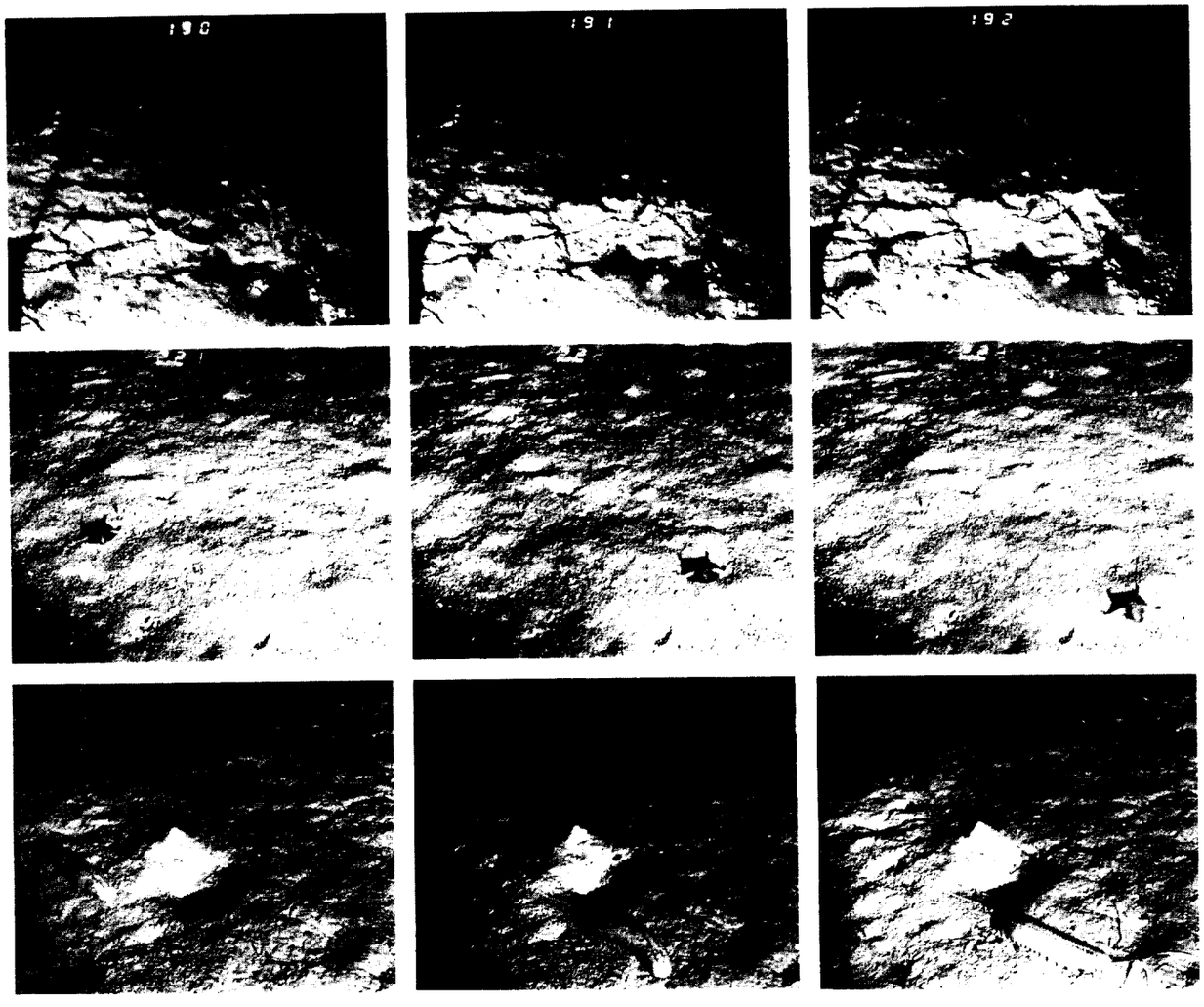

Figure 5.iii.4 Sequences of Bathysnap photographs taken in the Porcupine Seabight showing bioturbation can vary within short distances along the sea bed.

Upper sequence (frame interval 16 mins): at 2000m shows the starfish Bathybiaster vexillifer ploughing up the sediment surface covered with phytodetritus.

Middle sequence (frame interval 16 mins): at 2700m shows the starfish Hymenaster membranaceus leaving almost no visible trail over a relatively smooth, but pock-marked sediment surface.

Lower sequence (frame interval 64 mins): at 2008m with a holothurian Benthogone rosea slowly crawling over a bottom marked with starfish and brittle star (Ophiomusium lymani as in the last frame) activity.

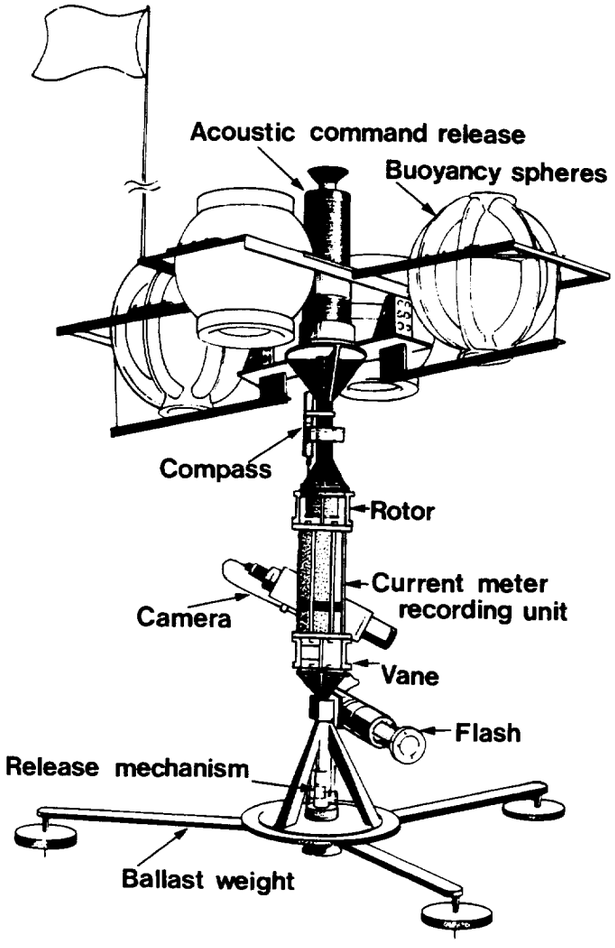

Figure 5.iii.5 Diagram of Bathysnap prior to deployment. It stands 2.4m high and weighs 2611kg. The modified Aanderaa current meter is an integral part of the single vertical central spar to which is attached the camera. A 10m polypropylene lazyline with a 25cm float which is not illustrated, is attached to the top of the device and is used to launch and retrieve it.

Figure 5.iii.6 The vertical ranges of the 95 species of benthopelagic fishes captured during the IOS deep-trawling survey of the Porcupine Seabight region.

1. Argentina sphyraena
2. Trisopterus sp.
3. Microchirus variegatus
4. Lepidorhombus whiffiagonis
5. Merluccius merluccius
6. Lepidorhombus boscii
7. Gadiculus argenteus thori
8. Micromesistius poutassou
9. Helicolenus dactylopterus
10. Malacocephalus laevis
11. Argentina silus
12. Paraliparis hystrix
13. Phycis blennoides
14. Glyptocephalus cynoglossus
15. Echiodon drummondi
16. Coelorinchus coelorinchus
17. Etmopterus spinax
18. Synaphobranchus kaupi
19. Molva dypterygia macrophthalma
20. Chimaera monstrosa
21. Notacanthus bonapartei
22. Polymetme corythaeola
23. Nezumia aequalis
24. Coelorinchus occa
25. Epigonus telescopus
26. Molva dypterygia dypterygia
27. Galeus melastomus
28. Trachyrincus trachyrincus
29. Mora moro
30. Trachyrincus murrayi
31. Lepidion eques
32. Scymnorhinus licha
33. Halargyreus johnsoni
34. Hoplostethus mediterraneus
35. Scymnodon ringens
36. Notacanthus chemnitzi
37. Alepocephalus rostratus
38. Coryphaenoides (Coryphaenoides) rupestris
39. Hydrolagus mirabilis
40. Centrolophus niger
41. Polyacanthonotus rissoanus
42. Etmopterus princeps
43. C. (Chalinura) mediterraneus
44. Scopelosaurus lepidus
45. Trachyscorpaea cristulata echinata
46. Melanostigma altanticum
47. Alepocephalus bairdii
48. Coelorinchus abditilux
49. Hoplostethus atlanticus
50. Antimora rostrata
51. Myxine ios
52. Laemonema latifrons
53. Cottunculus thompsoni
54. Bathypterois dubius
55. Raja fylae
56. Aphanopus carbo
57. Centroscymnus coelolepis
58. Cataetyx laticeps
59. Raja nidarosiensis
60. C.(Coryphaenoides) guentheri
61. Ilyophis blachei
62. Rouleina attrita
63. Rhinochimaera atlantica
64. Halosaurus johnsonianus
65. Conocara murrayi
66. Halosauropsis macrochir
67. Harriotta raleighana
68. Conocara macroptera
69. Alepocephalus productus
70. Ilyophis brunneus
71. Alepocephalus australis
72. Bathysaurus ferox
73. Hydrolagus affinis
74. Polyacanthonotus challengeri
75. Spectrunculus grandis
76. Ilyophis arx
77. Alepocephalus agassizi
78. Histiobranchus bathybius
79. Bathytroctes microlepis
80. Raja bigelowi
81. C. (Chalinura) brevibarbis
82. Narcetes stomias
83. Bathyraja richardsoni
84. C.(Lionurus) carapinus
85. C. (Chalinura) leptolepis
86. Bathyraja pallida
87. C. (Nematonurus) armatus
88. Echinomacrurus mollis
89. Sciadonus sp.
90. Batysaurus mollis
91. Bellocia koefoedi
92. Rinoctes nasutus
93. Conocara salmonea
94. C. (Chalinura) profundicola
95. Bathypterois longipes

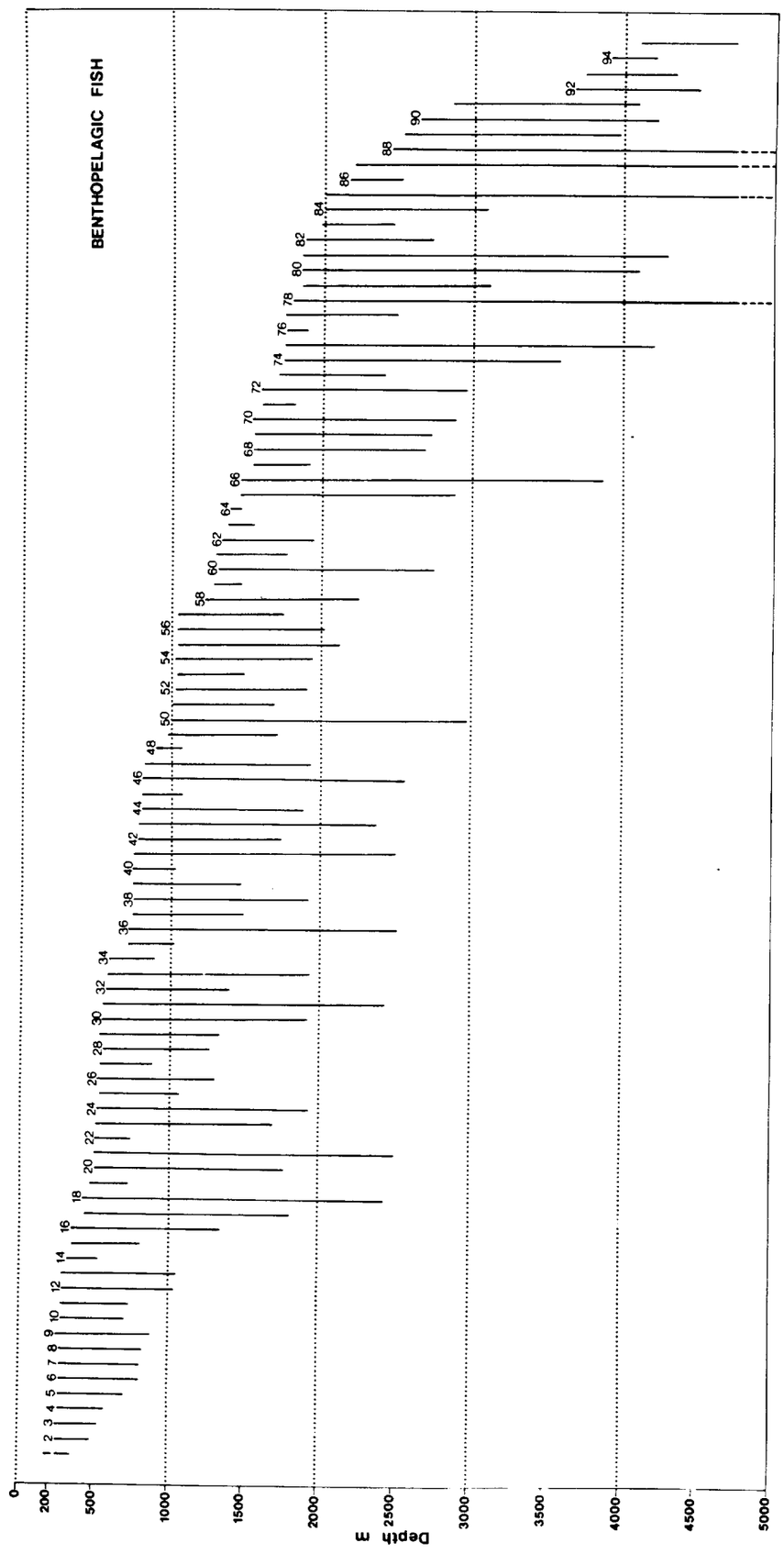

Figure 5.iii.6

Figure 5.iii.7 The vertical ranges of Asteroidea (Starfish) taken during the IOS benthic programme in the Porcupine Seabight.

1. Asterias rubens
2. Luidia sarsi
3. Stichastrella rosea
4. Astropecten irregularis
5. Psilaster spp
6. Nymphaster arenatus
7. Pontaster tenuispinus
8. Pseudarchaster spp
9. Henricia sp.
10. Brisingella coronata
11. Poraniomorpha borealis
12. Stichastrella ambigua
13. Odontaster mediterraneus
14. Plinthaster dentatus
15. Poranicmorpha hispida
16. Zoroaster fulgens
17. Plutonaster bifrons
18. Ceramaster grenadensis
19. Hymenaster giganteus
20. Radiaster tizardi
21. Pteraster personatus
22. Chondraster grandis
23. Hymenaster sp.
24. Brisinga endecacnemos
25. Solaster sp.
26. Pectinaster filholi
27. Benthopecten simplex
28. Bathybiaster vexillifer
29. Diplopteraster multipes
30. Hymenaster membranaceus
31. Hoplaster spinosus
32. Poraniomorpha hispida rosea
33. Paragonaster subtilis
34. Dytaster grandis
35. Zoroaster longicauda
36. Hyphalaster inermis
37. Porcellanaster ceruleus
38. Freyella spinosa
39. Styracaster chuni
40. Styracaster armatus
41. Thoracaster cylindratus
42. Freyella sexradiata
43. Pteraster alveolatus

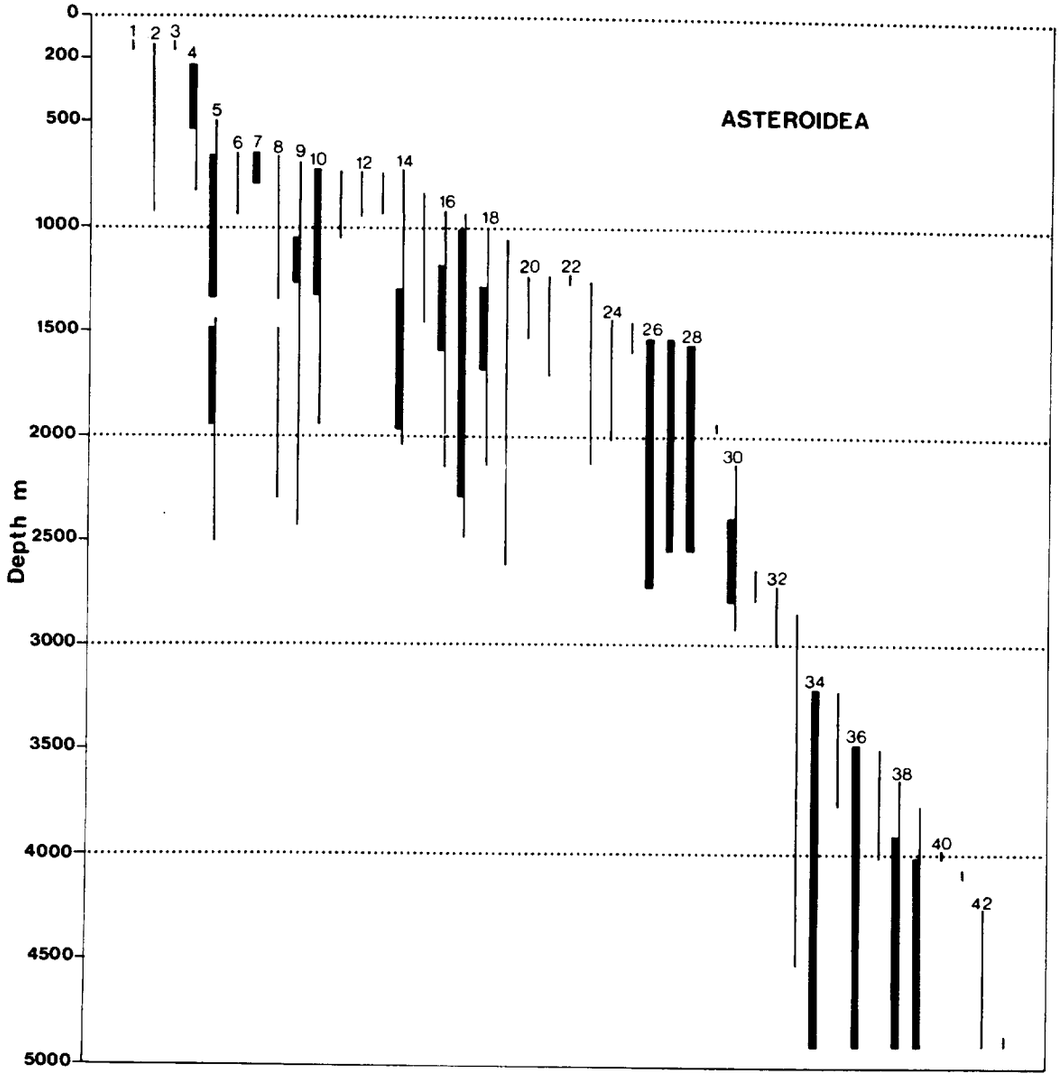

Figure 5.iii.7

Figure 5.iii.8 The vertical ranges of Holothurioidea (sea cucumbers) taken during the IOS benthic programme in the Porcupine Seabight.

1. Stichopus tremulus
2. Thyone fusus
3. Laetmogone violacea
4. Bathyplotes natans
5. Echinocucumis hispida
6. Psolus squamatus
7. Mesothuria intestinalis
8. Ypsilothuria talismani talismani
9. Mesothuria verrilli
10. Benthogone rosea
11. Mesothuria lactea
12. Mesothuria macroccana
13. Paroriza pallens
14. Elpidia echinata
15. Kolga hyalina
16. Mesothuria cathedralis
17. Paelopatides grisea
18. Mesothuria bifurcata
19. Mesothuria nov. sp. 1
20. Peniagone diaphana
21. Peniagone azorica
22. Psychropotes depressa
23. Benthothuria funebris
24. Labidoplax sp.
25. Nov. gen. Apoda
26. Myriotrochus sp.
27. Molpadia blakei
28. Oneirophanta mutabilis mutabilis
29. Cherbonniera utriculus
30. Benthodytes sordida
31. Deima validum validum
32. Siniotrochus nov.sp.
33. Protankyra brychia
34. Myriotrochus bathybius
35. Mesothuria nov. sp. 2
36. Psychropotes longicauda
37. Pseudostichopus villosus
38. Mesothuria candelabri
39. Amperima rosea
40. Pseudostichopus atlanticus
41. Paroriza prouhoi
42. Pseudostichopus marenzelleri
43. Pseudostichopus nov. sp
44. Psychropotes semperiana

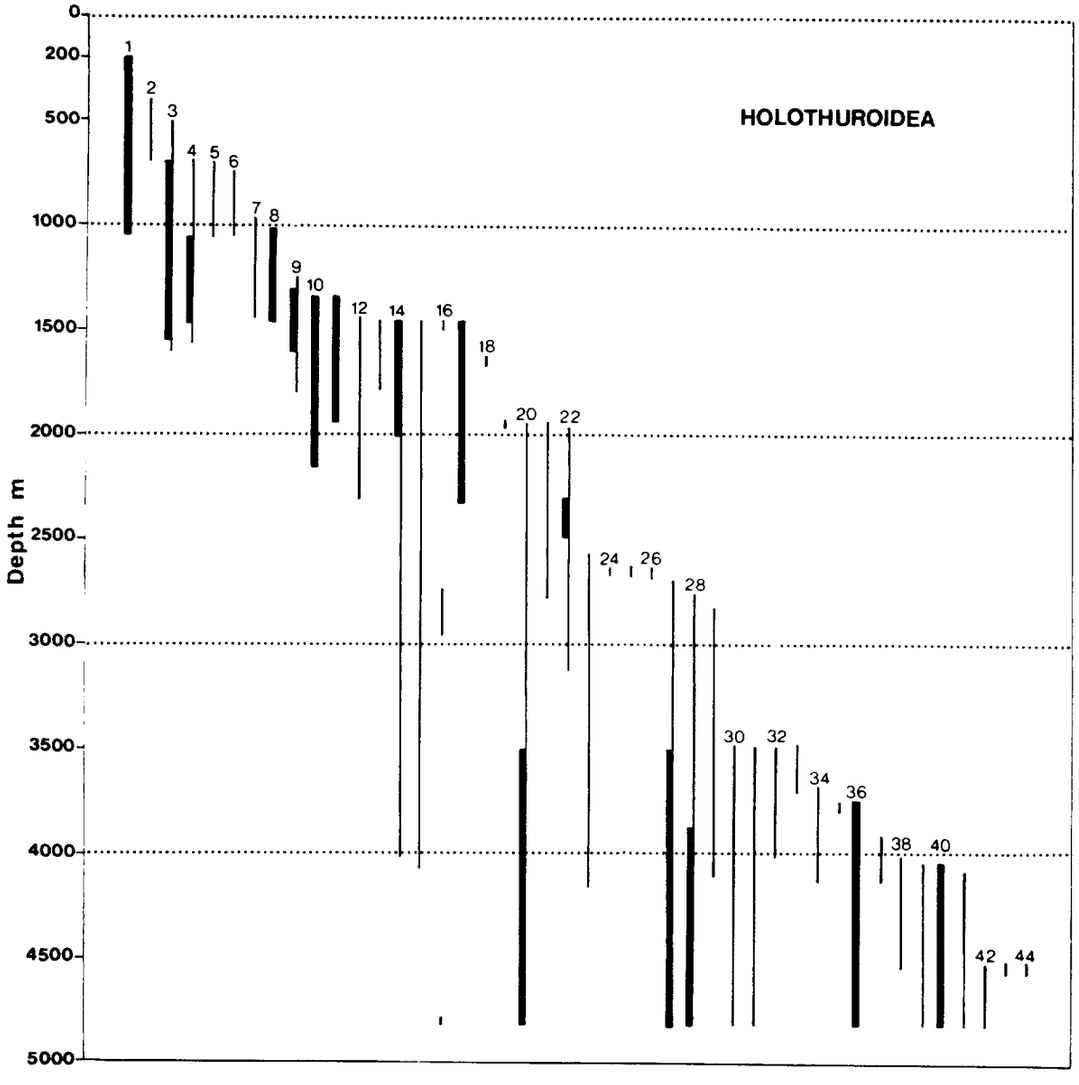

Figure 5.iii.8

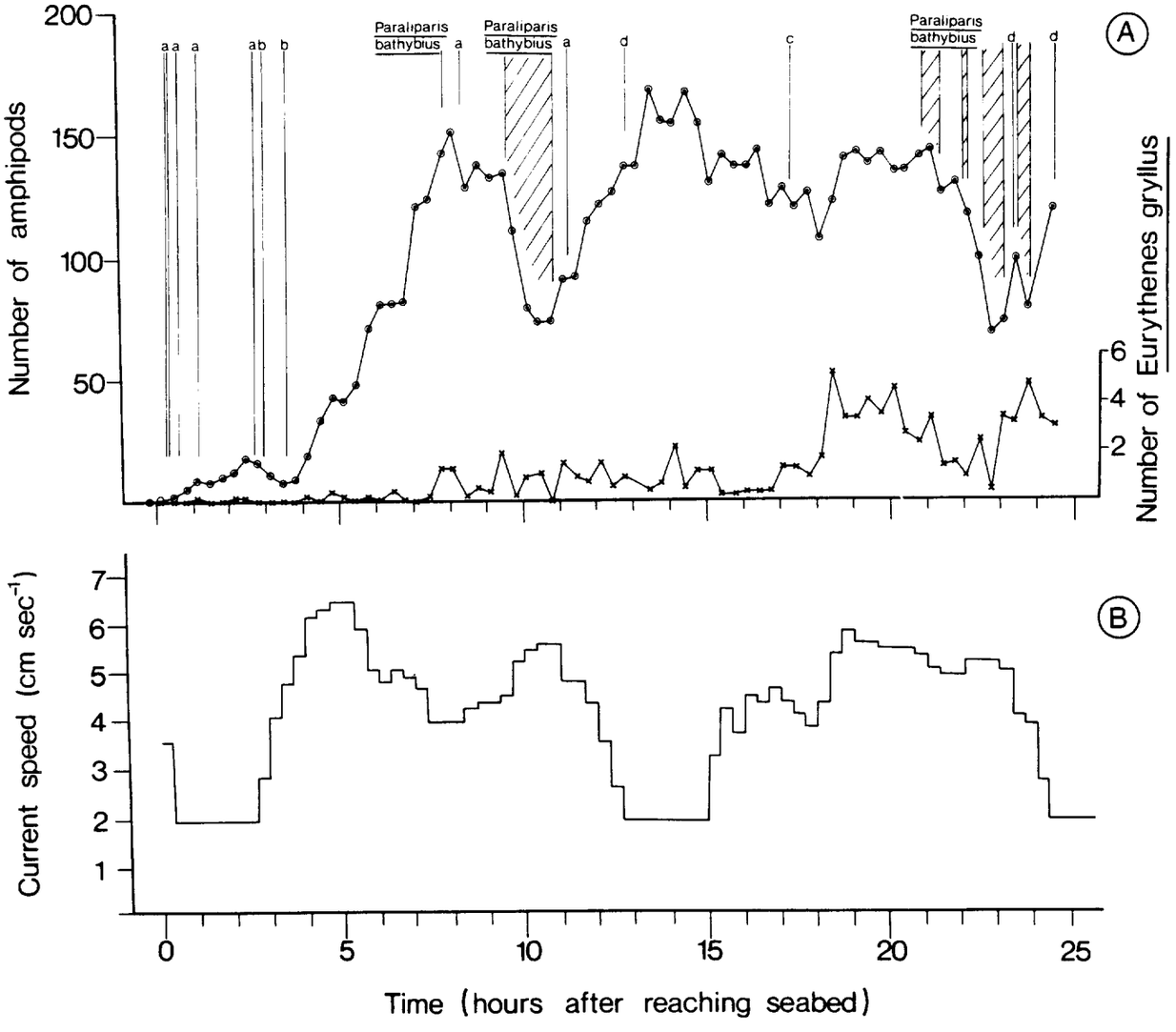

Figure 5.iii.9 Results of a bait experiment conducted at a depth of 4009m in the Porcupine Seabight using Bathysnap showing:

A. The total numbers of amphipods visible on the bait throughout the photographic sequence, together with the numbers of a single amphipod species Eurythenes gryllus, and the occurrences of the fish predator of amphipods Paraliparis bathybius. The letters indicate the occurrences of other fish species:-

a) Coryphaenoides armatus,
b) Echinomacrurus mollis,
c) unidentified fish,
d) Pleisiopenaeus armatus.

B. Current velocities (note the periods of constant velocity of 1.8 cm s^{-1} are artefacts of current meter sensitivity).

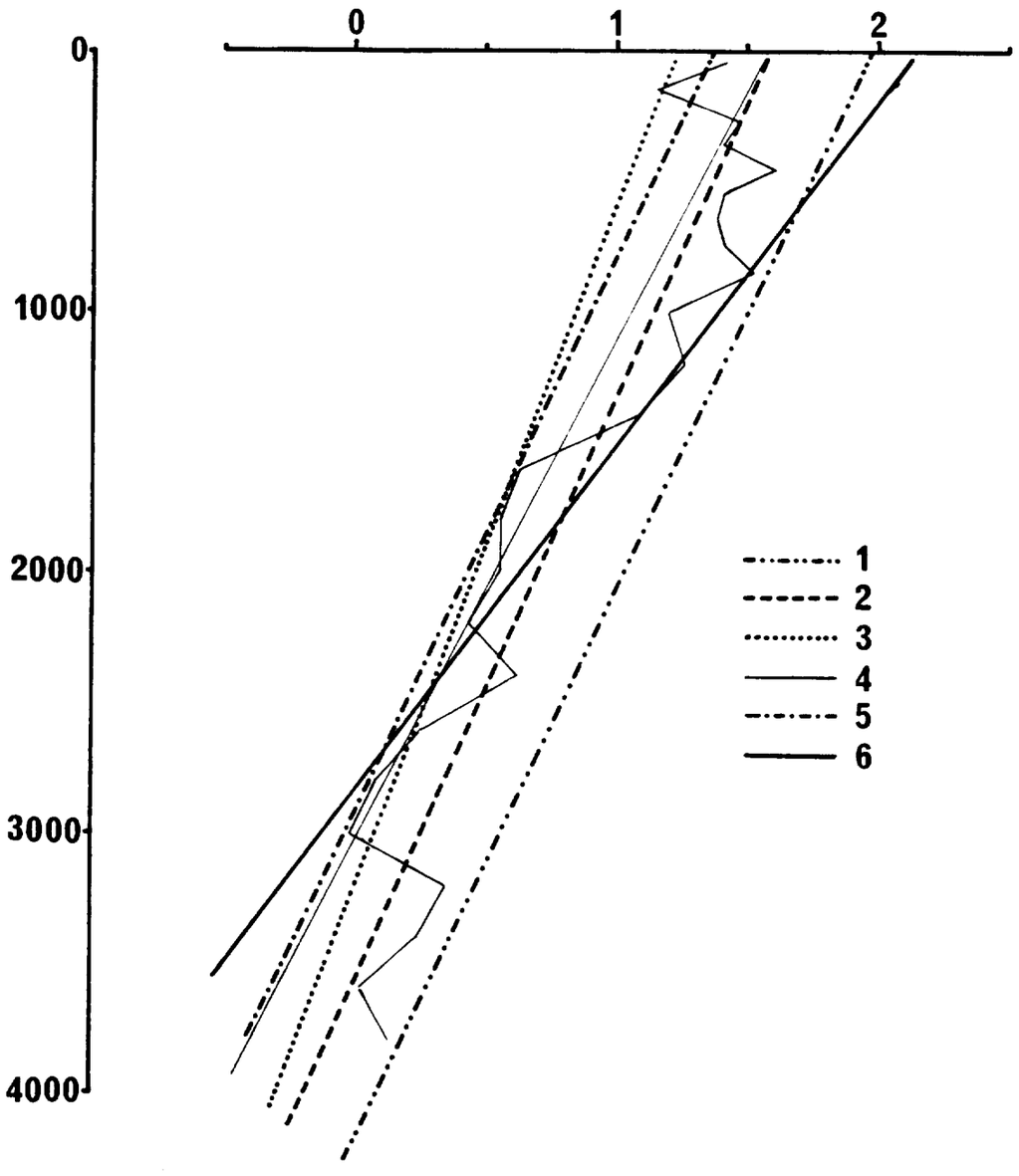

Figure 5.iii.10 Regression lines of the vertical profiles of log (biomass) against log (depth in metres) for plankton and micronekton at three stations in the Northeast Atlantic:

1) For micronekton at 20°N 21°W;
2) For plankton at 42°N 17°W;
3) For micronekton at 42°N 17°W;
4) For plankton at 49°40'N 17°W;
5) For micronekton at 49°40'N 17°W;
6) For plankton in the Northeast Atlantic according to Wishner (1980).

Superimposed is the raw data profile for micronekton at 42°N 17°W with the day and night values <900m averaged.

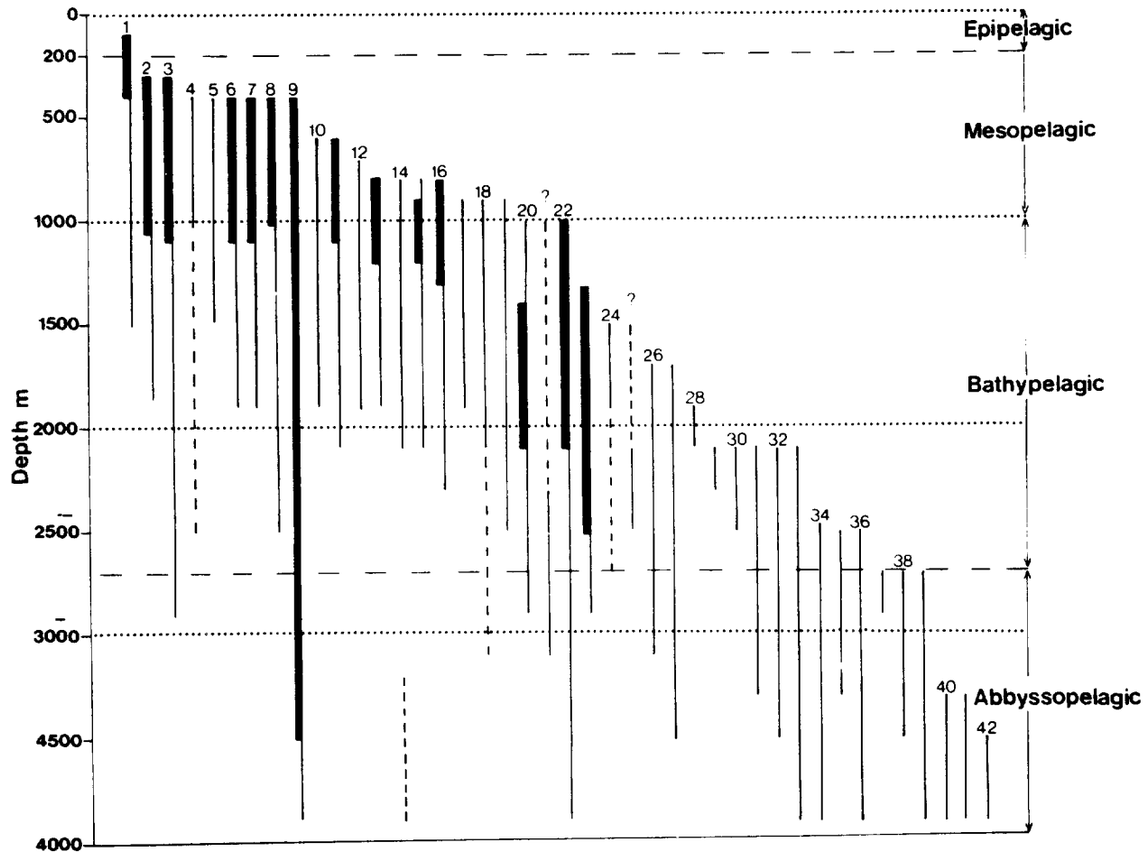

Figure 5.iii.11 Vertical ranges of the planktonic ostracods caught at depths of 1000m and from 1500-3900m at 42°N 17°W, the ranges of species only found shallower than 1000m are not shown:-

1. Conchoecia curta
2. C. elegans
3. C. hyalophyllum
4. C. ctenophora
5. C. acuticosta
6. C. loricata
7. C. rhynchena
8. C. haddoni
9. C. stigmatica
10. C. magna
11. C. lophura
12. C. nanomamillata
13. C. discoveryi
14. Halocypria globosa
15. C. kampta
16. C. ametra
17. C. dorsotuberculata
18. C. gaussi
19. C. brachyaskos
20. C. dichotoma
21. C. acutimarginata
22. A. cucullata
23. C. arcuata
24. Archiconchoecia gastrodes
25. C. borealis
26. C. tyloda
27. C. dasyophthalma
28. Archiconchoecia n. sp. 1
29. Archiconchoecia n. sp. 2
30. Gigantocypris dracontovalis
31. C. glandulosa
32. C. plinthina
33. C. mamillata
34. C. eltaninae
35. A. longiseta
36. C. vitjazi
37. C. n. sp. 1
38. C. n. sp. 2
39. C. lunata
40. A. versicula
41. C. brachyaskos (large)
42. A. n. sp. 3

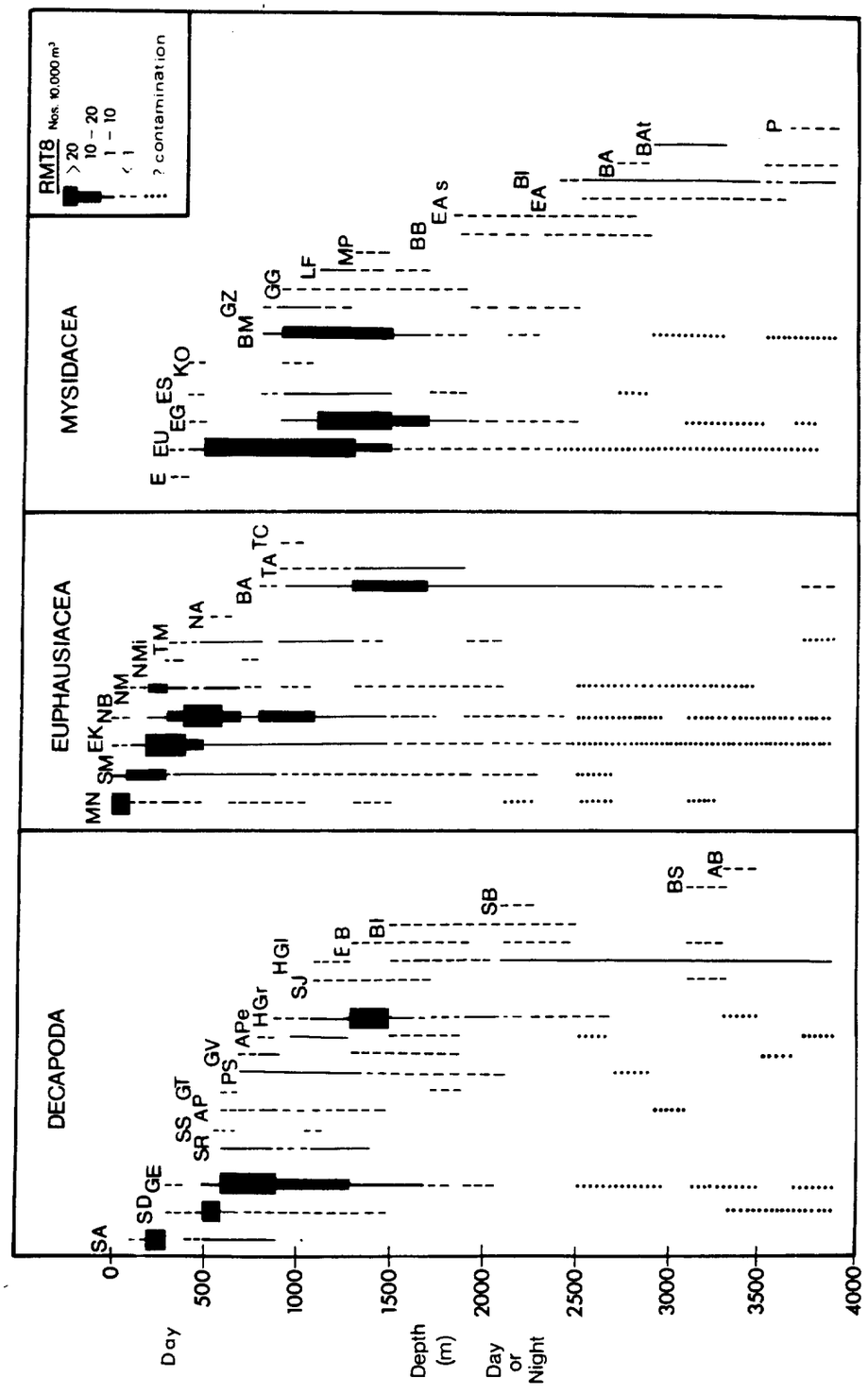

Figure 5.iii.12 Vertical ranges of three groups of micronektonic crustaceans at 42°N 17°W; Decapoda (18 species), Euphausiacea (11 species), and Mysidacea (17 species) from the surface to 3900m.

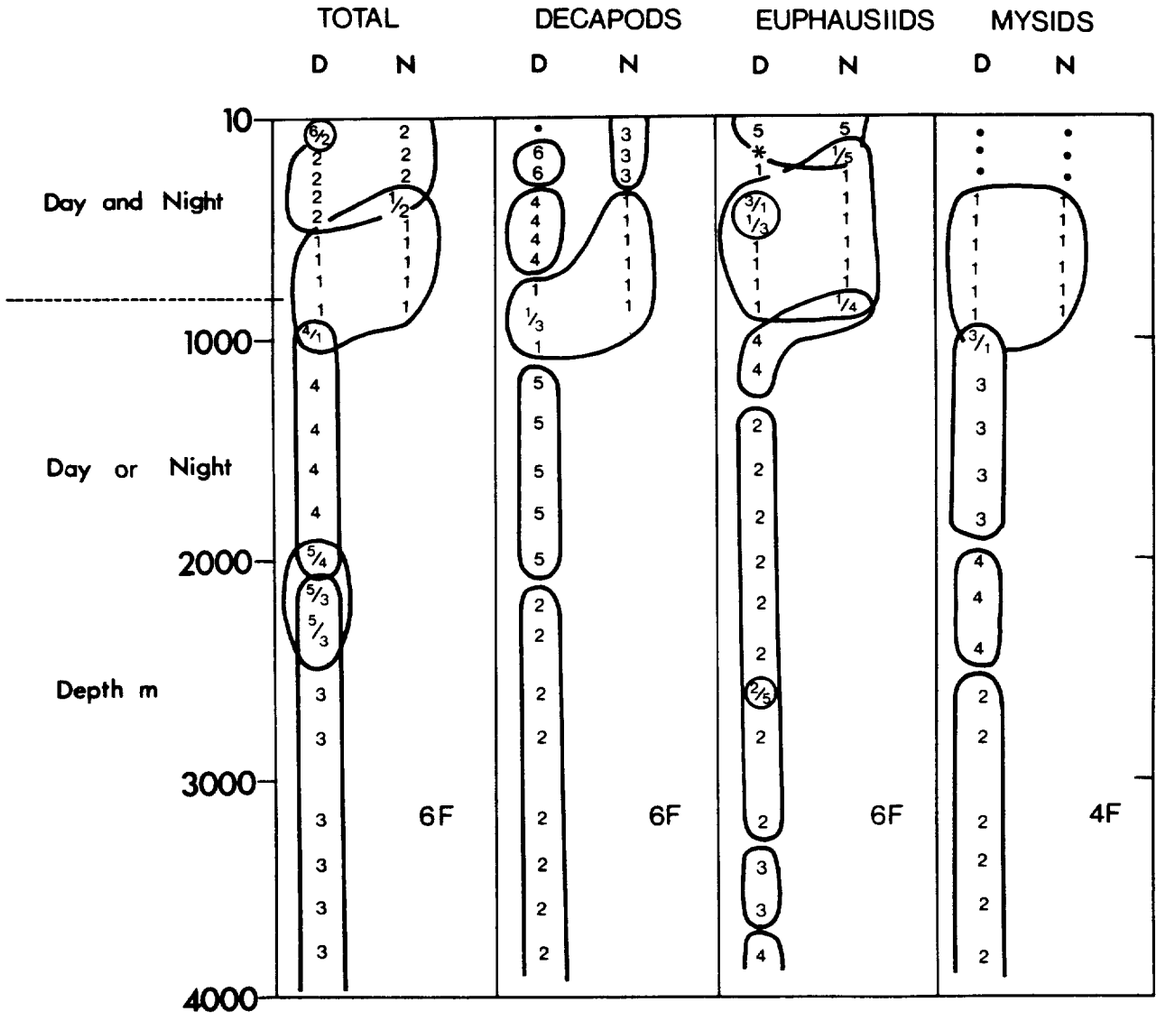

Figure 5.iii.13 Results of factor analyses of the data for the micronektonic crustaceans from 42°N 17°W. Data from depths <900m include both day and night samples; data collected from depths >900m have been assumed not to show any significant day/night variation. (Note that the deep zonation of euphausiids is seriously affected by contamination).

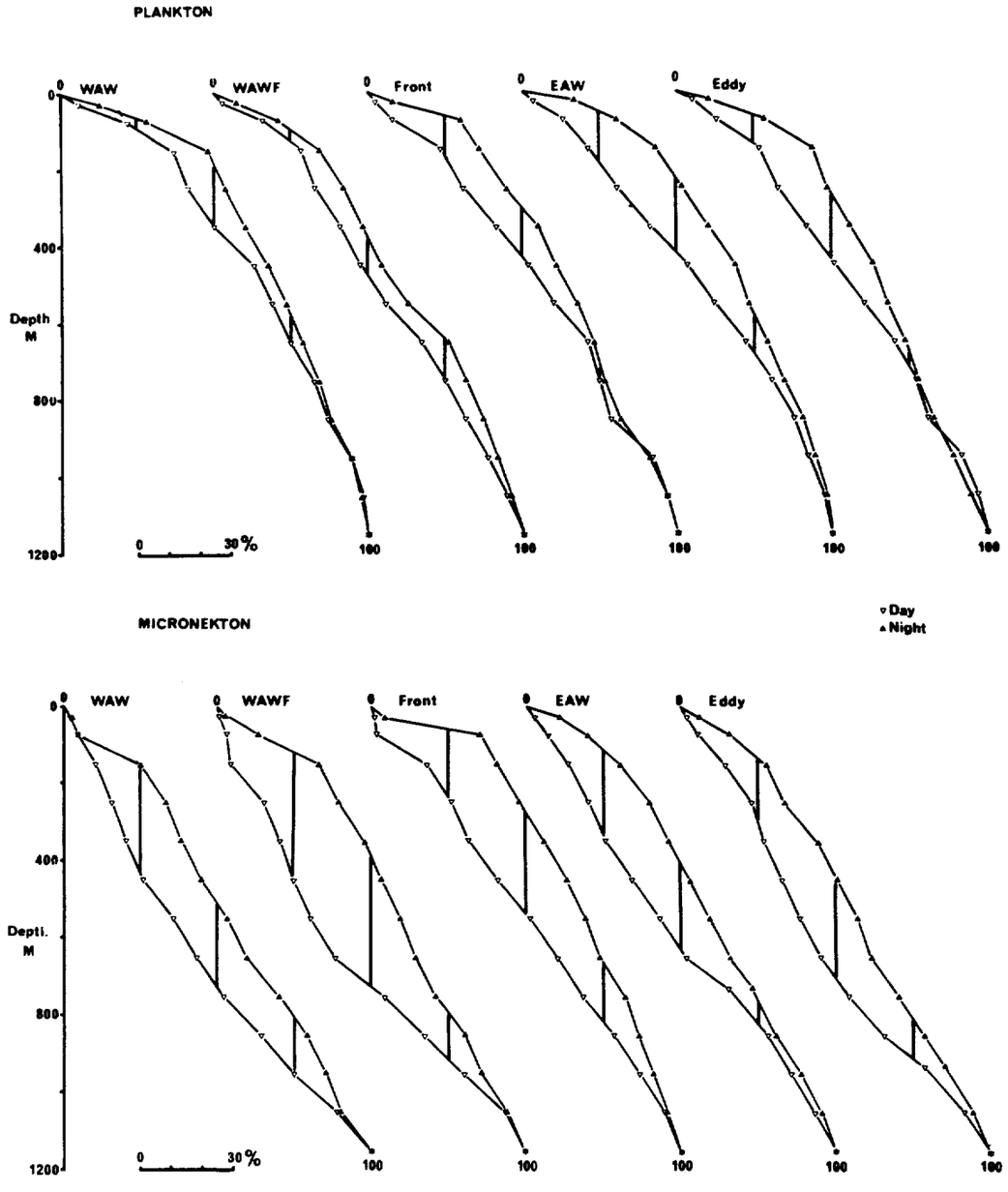

Figure 5.iii.14 Biomass profiles for plankton and micronekton at five stations in the North Atlantic to the southwest of the Azores. Each profile is expressed as the accumulative percentage of displacement volume to a depth of 1200m. The vertical lines show the vertical shift in the quartiles (25%, 50% and 75%) between day and night. Note that in most of the day profiles day and night values were very similar at depths >800m, whereas the limit of 1200m does not encompass the total range over which diel vertical migration causes a shift in the distribution of micronektonic biomass.

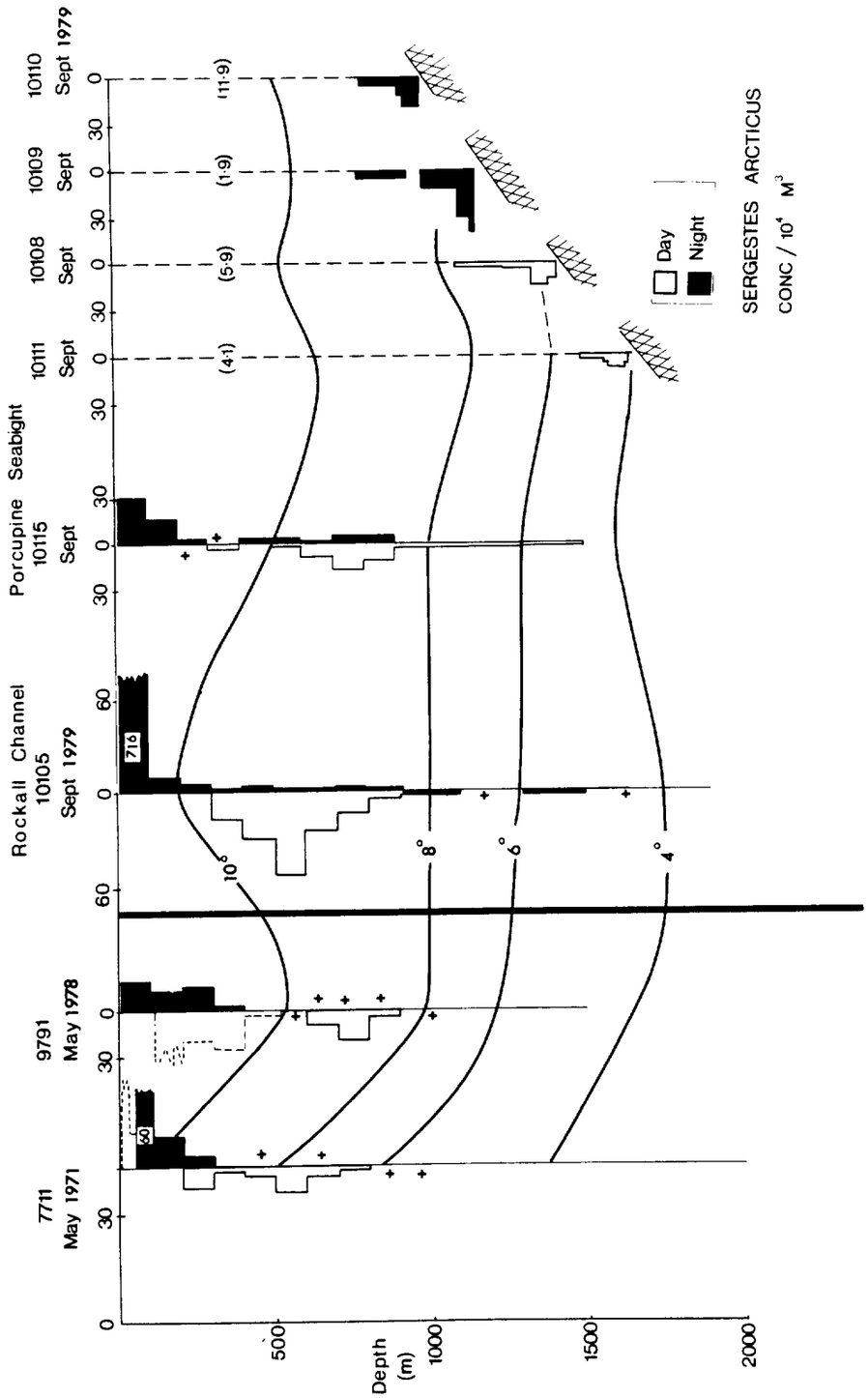

Figure 5.iii.15 Vertical profile of abundance of the decapod Sergestes arcticus (numbers per 10^4 m^3) near-bottom over the slope on the Goban Spur (Stations 10108-10111), at two deep water stations sampled at the same time nearby in the Porcupine Seabight and also in the Rockall Channel, and at 42°N 17°W (station 9791) and at 53°N 20°W (station 7711). The profiles illustrate the considerable extent to which this species extends its vertical range in the benthopelagic zone over the slope.

5.iv CHEMICAL PROCESSES

Process-related Studies

A detailed study of post-depositional migration of several redox-sensitive elements has been carried out on two cores collected in an area of brown clay sedimentation situated to the west of the Cape Verde Abyssal Plain. A report of this work has been published (Colley et al, 1984).

While many examples of post-depositional mobility of redox-sensitive elements (particularly Mn, but also Co, Ni, Cu and U) within the sediment column, as a result of changing Eh conditions with depth, are steady state (Lynn & Bonatti, 1965; Li et al, 1969; Bonatti et al, 1971; Hartmann et al, 1976), this study was concerned with cores from an area dominated by pelagic sedimentation, but also subject to occasional turbidite incursions. Organic carbon concentrations are low in the pelagic brown clay sediment (<0.2%) but the interposition of turbidite units has introduced relatively organic-rich material. Subsequent organic carbon oxidation has affected the local redox conditions in the previously oxic pelagic sediment column. This is a similar but much simpler situation than at GME, where organic-rich turbidites are more frequent within the succession. An investigation of the metal distributions within the sediment from this brown clay area was undertaken prior to a more detailed appraisal of the GME sediment column when porewater data were also available.

Core Locations, Descriptions, Sampling and Analysis

One of the few brown clay areas of the North East Atlantic is situated to the west of the Cape Verde Abyssal Plain. The area has a rugged relief with basins below 6000m and hills rising to 5000m water depth. It is bounded in the east by the abyssal plain, to the south by an extension of the Cape Verde plateau and to the north by the Great Meteor Seamount. To the west the rugged terrain extends, rising steadily, to the Mid-Atlantic Ridge.

Two gravity cores from the deep basin, taken on RRS Discovery cruises, are investigated here. Core 10311 was collected using a stainless steel gravity corer with a 10cm diameter, 2m long barrel at 25°39.2'N, 30°57.6'W in a water depth of 6129m. This core consists of an upper 60cm layer of brown clay (Munsell Code

5YR 4/4), underlain by 157cm of sediment with a grey hue. There is a sharp colour change within this unit from yellow-grey (5Y7/2) to olive-grey (5Y5/2) material at 127cm.

Core 10400 was collected using a Kastenlot gravity corer with a 2m x 15cm square barrel at 25°42.4'N, 30°57.7'W in a water depth of 6044m. This core consists of brown clay (2.5YR 4/4) interrupted by a green (10Y 5/4) layer at 47-55cm and an underlying red band (5YR 5/4) from 55-71cm.

Shipboard sampling of the cores was carried out on retrieval and the subsamples were returned to the laboratory where they were dried at 110°C and ground in agate. When larger samples from 10311 were required for XRF analysis the core was re-sampled at the laboratory, where it had been stored at 4°C. No porewater analyses were made on either of these cores.
XRF, carbonate and organic carbon, ferrous iron, and U and Th -emitting isotopic analyses were carried out using standard IOS methods. The data are tabulated as Tables 5.iv.1 to 5.iv.5.

Accumulation Rates and Timing of Turbidite Emplacement

Figure 5.iv.1 shows the $^{230}Th_{excess}$ data plotted versus depth for the two cores. The mean accumulation rates shown are estimated by the conventional method (Ku, 1976) from the decay of $^{230}Th_{excess}$ with increasing depth in the sediment column.

The $^{230}Th_{excess}$ profile for core 10400 demonstrates that the pelagic sedimentation of brown clay is interrupted only in the green band (47-55cm). The lower contact of this band is sharp, showing little disturbance by bioturbation. Disturbance by organisms is evident at the upper contact, however, and brown mottling, due to this process, is seen throughout the band. The green band is believed to be a turbidite. From the $^{230}Th_{excess}$ profile in the brown sediment, the date of emplacement is estimated at 170,000 years before present. An important feature of the interpretation is that the red band below the turbidite, at 55-71cm, is shown to be part of the brown clay section. The consistent $^{230}Th_{excess}$ data in the red band contrast with the low off-trend $^{230}Th_{excess}$ values found in the turbidite itself.

Table 5.iv.2 Major and trace element data for core 10400

Depth Interval cm	Major element data, % wt (dry basis)															Trace element data, ppm										
	SiO_2	Al_2O_3	Fe_2O_{3T}	MnO	MgO	CaO	K_2O	Na_2O	TiO_2	P_2O_5	LOI	Total	NaCl*	$CaCO_3$	C_{org}	Rb	Sr	Y	Zr	Nb	Ni	Co	V	Cr	Cu	Zn
10-12	53.09	17.18	7.54	0.41	2.94	2.39	2.86	1.29	0.96	0.20	9.84	98.70	1.96	3.42	0.01	114	193	39	227	27	117	60	169	89	146	116
16-18	51.13	16.46	7.41	0.39	2.87	0.88	2.89	2.02	0.95	0.17	12.37	97.54	2.55	ND	ND	112	141	37	215	27	123	54	160	86	141	116
24-26	53.77	17.73	7.92	0.39	2.93	0.74	2.97	1.88	0.96	0.16	8.97	97.42	2.34	0.83	0.11	120	143	34	214	28	121	48	167	90	155	116
44-46	54.93	16.97	7.28	0.28	3.10	1.07	2.83	1.33	0.94	0.19	9.23	98.15	2.85	1.75	0.03	116	145	40	229	27	121	45	155	99	120	113
47-49	58.88	13.23	5.17	0.19	2.73	1.96	2.29	2.05	0.89	0.22	7.18	94.79	2.38	3.50	0.09	92	151	36	324	24	77	28	115	79	77	82
49-51	63.63	12.61	4.90	0.18	2.83	2.31	2.51	2.43	0.97	0.20	7.48	100.05	2.36	4.25	0.10	95	171	41	378	25	74	28	109	78	74	83
51-53	61.84	13.52	5.23	0.12	2.95	2.10	2.55	2.30	0.95	0.19	7.68	99.43	2.19	4.92	0.05	90	165	41	393	26	68	23	106	76	72	79
53-55	63.35	12.05	4.75	0.17	2.85	2.32	2.46	2.05	0.97	0.19	8.30	99.46	2.53	ND	ND	96	154	38	324	24	64	24	114	85	85	84
61-63	53.59	17.58	8.75	0.05	2.93	0.58	2.93	1.49	0.97	0.17	8.94	97.98	2.16	0.50	0.15	120	129	38	211	26	74	20	161	91	105	116
69-71	53.67	18.01	8.74	0.06	2.86	0.55	2.91	1.35	0.98	0.17	8.84	98.14	2.05	ND	ND	120	133	41	216	29	70	21	167	91	130	116
71-73	52.03	17.88	7.91	0.28	2.74	0.58	2.70	1.34	0.95	0.23	8.05	94.69	2.13	0.33	0.12	116	134	39	215	29	105	106	165	89	138	112
73-75	54.02	13.22	8.17	0.37	2.88	0.55	2.88	1.53	1.01	0.17	8.56	98.36	1.96	0.42	0.10	119	138	38	223	32	115	89	168	92	147	116
83-85	53.70	17.90	8.11	0.47	2.86	0.58	2.93	1.49	0.99	0.18	8.72	97.93	2.36	ND	ND	123	148	40	226	31	120	62	169	91	137	120
113-115	53.83	17.79	8.03	0.47	2.76	0.56	2.96	1.41	0.99	0.17	8.72	97.69	2.02	ND	ND	125	148	40	224	28	115	64	170	89	123	117
133-135	53.75	18.21	8.14	0.49	2.91	0.64	2.96	1.48	1.01	0.21	8.59	98.39	2.13	1.25	ND	120	141	47	223	30	117	66	174	90	131	119
163-165	53.54	18.49	8.20	0.46	2.84	0.65	3.01	1.31	1.01	0.19	8.33	98.03	2.16	ND	ND	125	146	44	217	28	120	60	172	90	142	117
173-175	54.21	18.21	8.17	0.50	2.86	0.82	3.06	1.47	1.02	0.19	8.33	98.44	1.96	ND	ND	123	148	46	224	30	123	61	171	89	145	120
183-185	53.76	18.19	8.11	0.48	2.73	0.64	2.99	1.51	1.00	0.17	8.23	97.45	2.22	0.50	0.08	123	144	39	213	26	136	57	165	83	183	148

* Cl + equivalent Na, assuming (wt % Na)/(wt % Cl) = 0.555

We believe that the organic material originally present in the upper part of the turbidite has been destroyed by oxidation by a similar process to that acting on the green turbidites at GME. The rate of this process would be controlled by the rate of diffusion of oxygen downward from the sea bed, and thus would become slower as the oxidation front became more deeply buried. Such oxidation of organic matter is believed to be bacterially-mediated and results from reduction of the available oxidant producing the greatest free energy change (Froelich et al, 1979; Emerson et al, 1980). After oxygen itself has been consumed, the predicted sequence for reduction is NO_3 and MnO_2, Fe_2O_3 and then SO_4. Since no porewater data for core 10311 are available, the point reached in this sequence is unknown, but MnO_2 does appear to have been utilised. Subsequently the overall process is referred to simply as oxidation, although an Eh gradient must exist in the column.

A semi-quantitative numerical treatment using the assumed linear slope of the oxygen diffusion profile has been used to calculate the flux of oxygen, and hence the carbon oxidised, during each timestep for 10311. (This treatment has since been developed to model the situation at GME where the processes acting are thought to be similar, and where direct dissolved O_2 and other porewater data are available.) The new, deeper position of the organic-rich surface is calculated from this information. This in turn determines the new slope of the oxygen profile for the succeeding timestep. The accumulation of new sediment is also included. Table 5.iv.7 summarises the input data appropriate to station 10311. Curves of the depth of the organic-rich layer against time are shown in Figure 5.iv.3 for various values of surficial sediment oxygen consumption.

The stoichiometry of the reaction assumed is:

$$138\ O_2 + C_{106}H_{263}O_{110}N_{16}P + 18HCO_3^- \rightarrow 124CO_2 + 16NO_3^- + HPO_4^{2-} + 140H_2O$$

This composition of the organic material corresponds to the Redfield ratios normally assumed for deep-ocean organic material (Jahnke et al, 1982).

It is assumed that consumption of oxygen occurs only at the sediment-water interface and at the upper surface of the organic-rich layer (the 'oxidation front'), a similar situation to that prevailing at GME. Hence, the oxygen diffusion profile between these sites is linear. The respiration at the sediment-water interface causes an offset to the diffusion profile, so that the latter, when extrapolated

upward, intersects the sediment-water interface at an oxygen value less than the bottom-water value. At the depth of the oxidation front, oxygen is assumed to fall to zero concentration. Hence, the linear oxygen gradient is defined by the known bottom water value for dissolved oxygen, the instantaneous depth of the oxidation front, and the assumed offset.

The magnitude of this oxygen profile offset has been estimated by inspection of oxygen profile data from oxic sediments in the literature (Wilson, 1978; Murray & Grundmanis, 1980; Grundmanis & Murray, 1982): the effect of various estimates is shown in Figure 5.iv.3. Lack of such data at site 10311 constitutes a major uncertainty in the application of this model. Further development of the model has been possible at GME, where an oxygen profile is available. A further uncertainty at site 10311 is the possible upward diffusion of reduced chemical species from deeper within the sediment.

The rather crude model developed at site 10311 serves to illustrate the important point that the downward diffusive flux of oxygen to the buried reaction front is adequate to oxidise the organic carbon of the turbidite layer to the 65cm depths observed at station 10311. It is, in fact, likely to underestimate this oxidation depth, since diagenesis attributable to electron-acceptors other than oxygen is not included. The most significant such acceptor is nitrate. Simple assumptions suggest a maximum nitrate flux to the front equivalent to about 30% of the oxidative diagenesis. It is thus possible that anaerobic diagenesis makes a significant contribution to the total diagenetic process.

A notable feature of Figure 5.iv.2 is the peak in U concentration just beneath the colour change boundary at 127cm. This is interpreted as a progressive post-depositional relocation of U in the turbidite as a result of the downward advance of the oxidation front. The initial U content of the turbidite is high, 3.3ppm in the linear unaffected section at 175-200cm. Assuming an initial [U] of 3.3ppm, around 65% (68 $\mu g/cm^2$) of the U deficit (106 $\mu g/cm^2$) of the upper oxidised section of the turbidite is now present in the peak. The U mobilised from the oxidised section appears to have been originally associated with the organic matter of the turbidite, since the U levels now present in the oxidised section are 2.7ppm on a carbonate-free basis, similar to the values in pelagic clay (Tables 5.iv.3 and 5.iv.4). An association of authigenic U with C_{org} in marine sediments is well-known (Mangini & Dominik, 1979).

The greater part of the uranium mobilised during oxidation has moved progressively downwards. Bonatti et al (1971) similarly found that uranium was enriched at depth in an organic-rich, hemipelagic environment in the Eastern Pacific. It is probable that the remaining 35% of U lost from the upper section of the turbidite has diffused upwards, and possibly has even been lost from the sediment to seawater.

To a first approximation the radioactive decay sequence nuclides ^{238}U, ^{234}U and ^{230}Th have similar activity profiles (Figure 5.iv.4 for ^{234}U and ^{230}Th). The ^{230}Th maximum, however, occurs at a slightly shallower depth than those for the U isotopes, as would be expected if the U isotope peaks are still moving downwards slowly and increasing in size. There is also clear evidence of ^{234}U movement relative to ^{238}U, as some of the highest $^{234}U/^{238}$ activity ratios yet reported in marine sediments occur on the upper side of the U concentration peak (Figure 5.iv.5). This isotope differentiation is well documented, and is believed to be due to a preferential migration of ^{234}U in the (VI) oxidation state following in situ production from ^{238}U in the (IV) oxidation state. Only 30% of the ^{234}U so produced is susceptible to this effect (Ku, 1965; Kolodny & Kaplan, 1970; Mangini & Dominik, 1979). Upward migration of ^{234}U has been dominant in this core as the high $^{234}U/^{238}U$ ratios are in the oxidised section immediately above the U peak (Figure 5.iv.5).

The mechanism invoked above to explain the uranium peak has similarities to that suggested for the formation of the roll-front uranium deposits found at the interface between oxidised and unoxidised sandstone (Maynard, 1983), although the level of concentration reached here is much less and diffusive rather than advective transport is involved. Of the elements measured in this core only V and Cu show signs of similar behaviour (Figure 5.iv.6). These two metals are also found in association with U in the Colorado Plateau deposits which may be genetically similar to roll-front deposits (see Maynard (1983), p.171). Bonatti et al, (1971) similarly found enrichments of U, V and Cr at depth in Pacific hemipelagic sediments. No evidence for such behaviour by Cr is found in this core, and we conclude that it was not present in association with the original turbidite organic matter, unlike U, V and Cu.

Other trace metals appear to have been mobilised, but in these cases movement has been predominantly upwards so that the progressive intensification seen on

the downward migration of U is absent. Manganese has been concentrated in a peak immediately above the turbidite/clay boundary at 57cm (Figure 5.iv.6). In terms of the model, this would have occurred on resumption of pelagic sedimentation after deposition of the turbidite. At that time the depth of the pelagic clay cap would be at a minimum and diffusion of oxygenated seawater into the turbidite less hindered, with the result that the rate of downwards oxidation would be at a maximum. On utilisation of MnO_2 as an oxidant, Mn(II) would diffuse in solution and be oxidised to the solid phase again at higher levels in the sediment column (Froelich et al, 1979; Burdige & Gieskes, 1983). The Mn peak so produced would then remain unaffected by subsequent oxidation as it would always be located in a zone of oxidised porewater, although the locus of manganese immobilisation would move downwards in time as oxidation proceeded. It can be seen from Figure 5.iv.6 that the oxidised turbidite section does indeed have higher Mn levels than the lower section. A similar behaviour is observed for Ni (Figure 5.iv.6). Bonatti et al,(1971) also found a predominant upward movement of Mn, Ni and Co in a hemipelagic environment, where precipitation occurred in an upper oxidised zone.

Diagenetic Processes in Core 10400

The major compositional contrasts between the short green section (47-55cm) and the over- and underlying pelagic clay in this core are its higher contents of SiO_2, CaO, and Zr, and lower contents of Rb, Al_2O_3, V, Cr and Th (Table 5.iv.6). This is interpreted as being due to higher heavy mineral (SiO_2 and Zr) and calcium carbonate (Ca and Sr) contents in the green section, with the remaining elements lower because of dilution. These differences reinforce the $^{230}Th_{excess}$ interpretation that this unit is a turbidite with a different genesis from the remainder of the pelagic clay section. In contrast, Table 5.iv.6 shows that the longer red section (55-71cm) in the core is similar in composition to the pelagic clay in terms of SiO_2, Al_2O_3, CaO, Zr, Cr, Rb, TiO_2, V and Th contents, and confirms the $^{230}Th_{excess}$ interpretation that this section is modified pelagic clay. The only compositional differences observed between the red band and the underlying brown clay are its higher Fe content (increased by 0.65% with all Fe expressed at Fe_2O_3) and its lower contents of Mn, Co, Ni and possibly Cu (Figure 5.iv.7 and Table 5.iv.6). The red band is therefore interpreted as a diagenetic 'halo' caused by the overlying turbidite.

The compositional distinction of the red band indicates that the alteration involved ion transport of iron into the halo and removal from it of redox-sensitive Mn and its congeners. A redox replacement reaction of the type:

$$Mn_s^{4+} + 2Fe_{aq}^{2+} \rightarrow Mn_{aq}^{2+} + 2Fe_s^{3+}$$

was therefore considered. Inventory calculations for the red band show that there is an excess of 54 mg/cm^2 Fe whereas 46 mg/cm^2 Mn has been removed. There is therefore a shortfall of Fe for a reaction such as (1), but more importantly oxidation state analyses (Table 5.iv.5) demonstrate that an amount of Fe(II) is present in the red band sufficient to account for all the iron excess. Iron therefore appears to have been concentrated as an Fe(II) mineral (such as siderite). The action of another unidentified reductant must therefore be invoked to explain the observed manganese mobilisation.

Because high C_{org} values are not observed anywhere in this core, organic oxidation is probably now inactive or proceeding at a slow rate on the refractory organic fraction (Muller & Suess, 1979; Muller & Mangini, 1980). The most reducing site in this sediment column would have been in the turbidite, because it initially contained the C_{org} to fuel the diagenetic process. No sulphide was detected in the solid phase of either the green or red bands by the methylene blue method following acidification by 5MHCL (Gustafsson, 1960). We conclude that reduction in this thin turbidite was sufficient to utilise iron oxides, but insufficient to utilise SO_4^{2-}, and that this was the source for the Fe(II) enrichment now observed in the red band.

Of Mn and the trace elements associated with manganese oxides (Ni and Co) only Co gives any indication of subsequent immobilisation. Refixation of Co appears in a peak immediately below the lower boundary of the red band (Figure 5.iv.7), which contains excess Co amounting to 40% of that removed. No corresponding Mn and Ni relocalisations are observed, suggesting that these elements have been lost by upward diffusion. This would require an anoxic overlying column. The most likely period for such a condition would have been shortly after emplacement of the turbidite before further pelagic sediment accumulated.

Despite the indications that oxidation of the turbidite organic matter was achieved quickly (loss of Mn and Ni) and is complete (low C_{org}), there is another indication

which suggests that fully oxic conditions have not yet been established. The evidence for this is the existence of traces of Fe(II) at all depths to 75cm. While the Fe(II) contents of the green and red bands are highest and similar, the Fe(II)/Fe (total) values in the green band are higher (Figure 5.iv.7). As discussed previously, Lyle (1983) interprets such green colours as indicative of reducing conditions. The red band sediment can be turned green experimentally by treatment with sodium dithionite as described by Lyle, so its natural Fe(II) content is evidently insufficient to develop green colouration. The red colour of this halo must be a reflection of its decreased Mn content rather than its additional Fe(II).

It is noteworthy on this interpretation that only the authigenic component of Mn, Co and Ni in the red band appears to have been remobilised, presumably by reduction of grain coatings. The residual levels of these elements now observed (Figure 5.iv.7 and Table 5.iv.6) are similar to those of shale, suggesting that the sediment matrix remains unaffected. For these elements, the diagenetic alteration causing the halo has therefore been analogous to the operation desired of a good selective leaching agent.

In summary, the discovery of two turbidites of different character within pelagic clay sections sampled from the Cape Verde Abyssal Plain, has allowed investigation of metal mobility in response to organic diagenesis. These interpretations have been based on the generalised scheme which has emerged for deep-sea organic oxidation, and must be seen as conditional because no porewater information is available. Nevertheless, a simple model can be constructed for 10311 involving the destruction of organic matter within the turbidite as a result of the downward diffusion of oxygen from the seabed. This appears to be an important process in some areas of the North East Atlantic, and the model, together with observations of metal mobility and relocation has been further expanded with a more quantitative approach in the GME area, where porewater data have also been included.

Table 5.iv.1 Major and trace element data for core 10311

Depth Interval cm	Major element data, % wt (dry basis)												Trace element data, ppm									
	SiO_2	Al_2O_3	Fe_2O_{3T}	MnO	MgO	CaO	K_2O	Na_2O	TiO_2	P_2O_5	LOI	Total	NaCl*	Rb	Sr	Y	Zr	Nb	Ni	Co	V	Cr	Cu	Zn
10-13	54.33	17.73	7.93	0.44	2.95	1.26	2.77	1.31	0.95	0.29	8.13	98.09	2.29	120	155	41	218	34	121	57	166	92	148	118
20-23	55.07	17.71	7.76	0.40	3.11	0.93	2.60	1.37	0.92	0.29	7.99	98.15	2.39	121	144	38	210	29	118	55	166	91	142	117
31-33.5	54.06	17.99	8.01	0.44	2.98	0.80	2.76	1.33	0.94	0.29	8.61	98.21	2.39	120	148	38	227	30	123	53	163	91	114	118
52-55	54.57	17.46	7.43	0.48	3.16	1.03	2.84	1.30	0.92	0.17	8.79	98.05	2.35	120	147	33	210	26	132	67	154	96	126	120
57	53.32	17.03	7.08	0.71	3.27	1.17	2.87	ND	0.90	0.18	9.30	95.83	3.17											
80	30.32	9.82	4.17	0.14	2.18	23.97	0.52	ND	0.39	0.13	26.15	97.79	2.21											
77-80														66	821	20	106	10	42	14	85	69	44	69
90	30.19	9.59	4.38	0.05	2.16	24.09	0.40	ND	0.37	0.13	26.70	98.06	1.94											
99	30.05	9.79	4.06	0.12	2.21	24.30	0.46	ND	0.39	0.13	26.44	97.95	2.05											
97-99.5														65	832	22	109	11	39	14	92	69	42	66
109	29.75	9.58	4.03	0.12	2.15	24.36	0.48	ND	0.37	0.13	27.18	98.15	1.85											
107-110														65	822	19	104	8	50	13	89	70	43	66
125	27.95	9.10	3.51	0.03	2.00	25.39	0.30	ND	0.35	0.13	29,49	98.25	1.75											
125-127														64	852	19	100	10	36	11	101	61	66	70
127.5	27.72	9.07	3.49	0.03	2.15	25.74	0.27	ND	0.35	0.14	29.28	98.24	1.76											
130	26.43	9.01	3.19	0.04	2.01	26.54	0.33	ND	0.34	0.14	30.02	98.05	1.95											
136	26.37	8.88	3.19	0.03	1.99	26.87	0.32	ND	0.34	0.15	30.15	98.29	1.71											
140-144														61	877	17	96	10	37	13	79	63	46	62
148	26.30	8.91	3.22	0.03	1.88	27.02	0.31	ND	0.33	0.15	30.50	98.65	1.35											
156	26.40	8.84	3.24	0.04	1.94	26.97	0.29	ND	0.33	0.15	30.37	98.57	1.43											
155-159														63	893	18	104	3	38	13	77	64	47	62
188	26.97	8.79	3.33	0.04	1.96	27.11	0.35	ND	0.34	0.14	29.08	98.11	1.89											
188.5-191														64	901	18	105	8	42	12	78	64	48	60

* Cl + equivalent Na, assuming (wt % Na)/(wt % Cl) = 0.555

ND = Not determined

Table 5.iv.2 Major and trace element data for core 10400

Depth Interval cm	Major element data, % wt (dry basis)															Trace element data, ppm										
	SiO_2	Al_2O_3	Fe_2O_{3T}	MnO	MgO	CaO	K_2O	Na_2O	TiO_2	P_2O_5	LOI	Total	NaCl*	$CaCO_3$	C_{org}	Rb	Sr	Y	Zr	Nb	Ni	Co	V	Cr	Cu	Zn
10-12	53.09	17.18	7.54	0.41	2.94	2.39	2.86	1.29	0.96	0.20	9.84	98.70	1.96	3.42	0.01	114	193	39	227	27	117	60	169	89	146	116
16-18	51.13	16.46	7.41	0.39	2.87	0.88	2.89	2.02	0.95	0.17	12.37	97.54	2.55	ND	ND	112	141	37	215	27	123	54	160	86	141	116
24-26	53.77	17.73	7.92	0.39	2.93	0.74	2.97	1.88	0.96	0.16	8.97	97.42	2.34	0.83	0.11	120	143	34	214	28	121	48	167	90	155	116
44-46	54.93	16.97	7.28	0.28	3.10	1.07	2.83	1.33	0.94	0.19	9.23	98.15	2.85	1.75	0.03	116	145	40	229	27	121	45	155	99	120	113
47-49	58.88	13.23	5.17	0.19	2.73	1.96	2.29	2.05	0.89	0.22	7.18	94.79	2.38	3.50	0.09	92	151	36	324	24	77	28	115	79	77	82
49-51	63.63	12.61	4.90	0.18	2.83	2.31	2.51	2.43	0.97	0.20	7.48	100.05	2.36	4.25	0.10	95	171	41	378	25	74	28	109	78	74	83
51-53	61.84	13.52	5.23	0.12	2.95	2.10	2.55	2.30	0.95	0.19	7.68	99.43	2.19	4.92	0.05	90	165	41	393	26	68	23	106	76	72	79
53-55	63.35	12.05	4.75	0.17	2.85	2.32	2.46	2.05	0.97	0.19	8.30	99.46	2.53	ND	ND	96	154	38	324	24	64	24	114	85	85	84
61-63	53.59	17.58	8.75	0.05	2.93	0.58	2.93	1.49	0.97	0.17	8.94	97.98	2.16	0.50	0.15	120	129	38	211	26	74	20	161	91	105	116
69-71	53.67	18.01	8.74	0.06	2.86	0.55	2.91	1.35	0.98	0.17	8.84	98.14	2.05	ND	ND	120	133	41	216	29	70	21	167	91	130	116
71-73	52.03	17.88	7.91	0.28	2.74	0.58	2.70	1.34	0.95	0.23	8.05	94.69	2.13	0.33	0.12	116	134	39	215	29	105	106	165	89	138	112
73-75	54.02	13.22	8.17	0.37	2.88	0.55	2.88	1.53	1.01	0.17	8.56	98.36	1.96	0.42	0.10	119	138	38	223	32	115	89	168	92	147	116
83-85	53.70	17.90	8.11	0.47	2.86	0.58	2.93	1.49	0.99	0.18	8.72	97.93	2.36	ND	ND	123	148	40	226	31	120	62	169	91	137	120
113-115	53.83	17.79	8.03	0.47	2.76	0.56	2.96	1.41	0.99	0.17	8.72	97.69	2.02	ND	ND	125	148	40	224	28	115	64	170	89	123	117
133-135	53.75	18.21	8.14	0.49	2.91	0.64	2.96	1.48	1.01	0.21	8.59	98.39	2.13	1.25	ND	120	141	47	223	30	117	66	174	90	131	119
163-165	53.54	18.49	8.20	0.46	2.84	0.65	3.01	1.31	1.01	0.19	8.33	98.03	2.16	ND	ND	125	146	44	217	28	120	60	172	90	142	117
173-175	54.21	18.21	8.17	0.50	2.86	0.82	3.06	1.47	1.02	0.19	8.33	98.44	1.96	ND	ND	123	148	46	224	30	123	61	171	89	145	120
183-185	53.76	18.19	8.11	0.48	2.73	0.64	2.99	1.51	1.00	0.17	8.23	97.45	2.22	0.50	0.08	123	144	39	213	26	136	57	165	83	183	148

* Cl + equivalent Na, assuming (wt % Na)/(wt % Cl) = 0.555

Table 5.iv.3 Uranium and thorium isotopic data for core 10311 together with $CaCO_3$ and C_{org} analyses

Depth cm	U ppm	Th ppm	Th/U	$\frac{^{234}U}{^{238}U}$ Activity Ratio	$\frac{^{230}Th}{^{232}Th}$ Activity Ratio	^{234}U dpm/g	^{230}Th dpm/g	$^{230}Th_{excess}$ dpm/g	C_{org} %	$CaCO_3$ %
0	2.66±0.12	17.0 ± 0.5	6.4 ±0.3	1.00±0.05	12.7 ±0.2	1.99±0.09	52.4 ±1.3	50.4 ±1.3	ND	ND
10	2.52±0.08	12.9 ± 0.1	5.1 ±0.4	0.95±0.04	7.9 ±0.3	1.80±0.06	24.7 ±1.3	22.9 ±1.3	0.30	1.08
20	2.74±0.10	16.8 ± 0.9	6.1 ±0.4	0.98±0.04	9.7 ±0.2	2.00±0.07	39.6 ±2.0	37.6 ±2.0	0.24	0.67
30	2.45±0.09	14.5 ± 0.1	5.9 ±0.3	0.92±0.04	6.3 ±0.1	1.68±0.06	22.3 ±0.6	20.6 ±0.6	ND	ND
44	2.54±0.09	12.9 ± 0.1	5.1 ±0.3	0.95±0.04	2.59±0.06	1.80±0.07	8.1 ±0.3	6.30 ± 0.30	0.13	2.92
49	2.56±0.07	13.1 ± 0.4	5.1 ±0.2	0.91±0.03	3.43±0.07	1.73±0.05	10.9 ±0.3	9.20 ± 0.30	ND	ND
57	2.36±0.07	12.4 ± 0.5	5.3 ±0.3	0.88±0.03	2.41±0.07	1.56±0.05	7.2 ±0.2	5.60 ± 0.20	0.28	2.17
62	2.10±0.07	11.5 ± 0.4	5.5 ±0.3	0.83±0.03	1.69±0.04	1.30±0.05	4.7 ±0.1	3.40 ± 0.10	0.14	15.7
80	1.47±0.05	6.2 ± 0.2	4.2 ±0.2	0.99±0.04	1.39±0.05	1.09±0.04	2.09±0.07	1.00 ± 0.08	0.16	41.4
90	1.57±0.05	8.2 ± 0.4	5.2 ±0.3	0.94±0.03	1.39±0.06	1.11±0.03	2.77±0.37	1.66 ± 0.37	0.11	43.3
99	1.46±0.05	7.8 ± 0.3	5.3 ±0.3	1.10±0.04	1.60±0.06	1.20±0.04	3.03±0.12	1.83 ± 0.13	0.06	44.2
109	1.58±0.05	6.3 ± 0.3	4.0 ±0.2	1.10±0.04	2.01±0.08	1.30±0.04	3.09±0.11	1.79 ± 0.12	0.07	47.3
116	1.50±0.05	6.2 ± 0.4	4.1 ±0.3	1.27±0.06	2.44±0.14	1.42±0.05	3.70±0.17	2.28 ± 0.18	ND	ND
120	2.00±0.09	6.8 ± 0.2	3.4 ±0.2	1.32±0.07	3.70±0.13	1.97±0.08	6.10±0.10	4.10 ± 0.10	ND	ND
125	1.86±0.06	6.6 ± 0.2	3.5 ±0.2	1.50±0.05	3.99±0.11	2.08±0.06	6.40±0.20	4.30 ± 0.20	0.54	45.5
127.5	7.40±0.20	7.3 ± 0.2	0.99±0.04	1.11±0.02	4.10±0.10	6.10±0.10	7.30±0.20	1.20 ± 0.20	0.51	46.5
130	12.2 ±0.3	6.2 ± 0.2	0.51±0.02	1.11±0.03	3.98±0.13	10.1 ±0.3	6.00±0.10	-	0.69	48.3
132	12.6 ±0.3	6.9 ± 0.2	0.54±0.02	1.05±0.02	3.76±0.11	9.9 ±0.3	6.30±0.20	-	ND	ND
134	11.2 ±0.4	7.2 ± 0.3	0.65±0.03	1.03±0.03	3.43±0.12	8.7 ±0.3	6.00±0.20	-	ND	ND
136	8.1 ±0.4	6.4 ± 0.2	0.79±0.04	1.01±0.04	2.87±0.07	6.1 ±0.3	4.50±0.10	-	0.41	47.5
148	4.5 ±0.2	6.1 ± 0.3	1.35±0.08	1.06±0.04	2.32±0.09	3.5 ±0.1	3.41±0.13	-	0.79	48.3
156	5.1 ±0.2	6.4 ± 0.3	1.27±0.07	1.06±0.03	2.39±0.09	4.0 ±0.1	3.74±0.14	-	0.67	47.4
164-165	3.7 ±0.2	6.8 ± 0.2	1.84±0.07	1.03±0.05	2.13±0.05	2.83±0.13	3.51±0.09	0.68 ± 0.15	0.79	47.9
176	3.28±0.01	6.3 ± 0.3	1.92±0.10	1.02±0.03	2.12±0.08	2.49±0.08	3.25±0.12	0.76 ± 0.14	0.49	47.5
188	3.35±0.06	6.6 ± 0.2	1.96±0.06	1.06±0.02	2.09±0.05	2.66±0.05	3.34±0.07	0.68 ± 0.09	1.03	47.5
200	3.21±0.11	6.5 ± 0.3	2.03±0.11	1.05±0.04	2.23±0.08	2.53±0.08	3.53±0.12	1.00 ± 0.14	0.55	47.7

ND = Not determined

Table 5.iv.4 Uranium and thorium isotopic data for core 10400

Depth cm	U ppm	Th ppm	$^{Th}/_{U}$	$\frac{^{234}U}{^{238}U}$ Activity Ratio	$\frac{^{230}Th}{^{232}Th}$ Activity Ratio	^{234}U dpm/g	^{230}Th dpm/g	$^{230}Th_{excess}$ dpm/g
10	2.72±0.10	17.6±0.9	6.5±0.4	1.18±0.05	12.7 ±0.4	2.39±0.08	54.5 ±2.4	52.1 ±2.4
25	2.75±0.06	16.9±0.8	6.1±0.3	1.01±0.03	7.5 ±0.2	2.07±0.05	30.9 ±1.2	28.8 ±1.2
45	2.75±0.10	15.2±0.7	5.5±0.3	0.91±0.04	3.29±0.10	1.88±0.07	12.1 ±0.5	10.3 ±0.5
50	2.77±0.10	10.7±0.3	3.9±0.2	0.93±0.04	2.11±0.05	1.92±0.07	5.5 ±0.1	3.58±0.17
54	3.13±0.10	10.6±0.5	3.4±0.2	0.88±0.03	1.74±0.06	2.06±0.07	4.5 ±0.2	2.42±0.19
60	2.62±0.07	17.9±0.6	6.8±0.3	0.92±0.03	3.02±0.06	1.80±0.05	13.1 ±0.4	11.3 ±0.4
68	2.59±0.07	17.1±0.9	6.6±0.4	0.97±0.03	2.52±0.08	1.87±0.05	10.5 ±0.5	8.6 ±0.5
71-73	2.68±0.09	13.3±0.5	5.0±0.3	0.92±0.03	2.46±0.06	1.84±0.06	7.9 ±0.3	6.1 ±0.3
85	2.71±0.09	16.6±0.5	6.1±0.2	0.92±0.04	1.58±0 04	1.87±0.06	6.4 ±0.2	4.5 ±0.2
110	2.79±0.07	19.4±1.0	6.9±0.4	0.86±0.03	0.90±0.03	1.81±0.05	4.2 ±0.2	2.39±0.20
135	2.85±0.08	18.3±0.7	6.4±0.3	0.85±0.03	0.66±0.02	1.80±0.05	2.95±0.12	1.15±0.13
160	2.74±0.10	17.3±0.5	6.3±0.3	0.89±0.04	0.51±0.01	1.82±0.07	2.16±0.08	0.34±0.11
181	2.87±0.09	18.2±0.7	6.3±0.3	0.83±0.03	0.47±0.02	1.78±0.06	2.06±0.10	0.28±0.12

Table 5.iv.5 Values of Fe_T, Fe(II) and $\frac{Fe(II)}{Fe_T}$ for core 10400. Fe_T is calculated from XRF results and Fe(II) from a wet chemical analysis for FeO.

Depth Interval cm	Fe_T %	Fe(II) %	$\frac{Fe(II)}{Fe_T} \times 100$ %
10-12	5.27	0.15	2.85
16-18	5.18	0.20	3.86
24-26	5.54	0.16	2.89
44-46	5.09	0.20	3.93
47-49	3.62	0.37	10.22
49-51	3.43	0.44	12.83
51-53	3.66	0.54	14.75
53-55	3.32	0.43	12.95
61-63	6.12	0.53	8.66
69-71	6.11	0.44	7.20
71-73	5.53	0.24	4.34
73-75	5.71	0.14	2.45
83-85	5.67	0	0
113-115	5.62	0.05	0.90
133-135	5.69	0	0
163-165	5.74	0	0
173-175	5.71	0	0
183-185	5.67	0	0

Table 5.iv.6 Average major and trace element compositions for the different sediment types present in cores 10311 and 10400 compared with average shale (Wedepohl, 1971) and average Pacific pelagic clay (Turekian and Wedepohl, 1961; Bischoff, et al., 1979).

	10311 Pelagic clay a: 0-60 cm b,c: 5,4	10400 Pelagic clay 0-47 cm 4,4	10400 Pelagic clay 71-185 cm	Average Shale[d]	Average Pacific Pelagic clay[e]	10400 Red clay 55-71 cm 2,2	10400 Green Clay 47-55 cm 4,4	10311 Carbonate[f] 60-127 cm 5,4	10311 Carbonate[f] 127-212 cm 6,6
SiO_2	54.30	53.20	53.60	58.90	54.90	53.60	61.90	52.60	51.10
Al_2O_3	17.60	17.10	18.10	16.70	16.60	17.80	12.90	17.00	17.10
Fe_2O_3	7.64	7.54	8.10	6.91	7.70	8.75	5.00	7.14	6.26
MnO	0.49	0.37	0.40	0.09	0.56	0.06	0.17	0.16	0.07
MgO	3.09	2.96	2.82	2.60	3.40	2.90	2.84	3.79	3.80
CaO	1.04	1.27	0.62	2.20	0.70	0.57	2.17	-	-
K_2O	2.77	2.89	2.94	3.60	2.70	2.92	2.45	0.76	0.60
TiO	0.93	0.95	1.00	0.78	0.78	0.98	0.95	0.66	0.65
P_2O_5	0.24	0.18	0.19	0.16	0.25	0.17	0.20	0.23	0.28
Rb	120	116	122	140	110	120	93	116	122
Sr	149	156	143	300	710	131	160	-	-
Y	38	38	42	41	150	40	39	36	34
Zr	216	221	221	160	150	214	355	186	197
Nb	30	28	29	18	14	28	25	17	14
Ni	123	121	119	68	210	72	71	74	75
Co	58	52	71	19	113	21	26	23	24
V	162	163	169	130	117	164	111	164	151
Cr	93	91	90	90	64	91	80	120	123
Cu	133	141	143	45	230	118	77	87	91
Zn	118	115	121	95	165	116	82	121	119

a Interval studied

b Number of samples averaged for major elements

c Number of samples averaged for trace elements

d From Wedepohl (1971)

e From Bischoff et al.,(1979). Rb, Zr and Nb from Turekian and Wedepohl (1961)

f Expressed on a carbonate-free basis

Table 5.iv.7 A summary of the input data used to construct a numerical model appropriate to station 10311

Parameters used in model (station 10311)

Pelagic accumulation rate	=	0.18 cm/10^3yr
Organic carbon originally in turbidite	=	0.8% dry wt
Bottom sea-water oxygen content	=	0.22 m moles
Free solution diffusion coefficient (D)	=	0.85 x 10^{-5} cm^2 sec^{-1}
Porosity of sediment (assumed uniform) (Ø)	=	0.70
Depth of uniform surficial reaction layer assumed	=	2 cm

Equations:

Tortuosity $\theta = \sqrt{\emptyset F}$ where F is formation factor

$F = \emptyset^{-3}$ Ullman and Aller (1982)

Effective diffusion coefficient (D_s) = $D\theta^{-2}$ = $D\emptyset^2$

Oxygen flux in forewater = $\emptyset D_s \frac{\partial [O_2]}{\partial z}$

Results:

Penetration of the oxidation front into the turbidite (d) for various assumed values of activity at the sediment-water interface and times since emplacement

activity (moles cm^{-2} sec^{-1})	d(cm)		
	$2x10^4$ yr	10^5 yr	$2x10^5$ yr
2.70×10^{-13}	15.3	33.5	43.2
2.55×10^{-13}	17.6	39.4	50.8
2.44×10^{-13}	19.4	45.0	58.0
2.26×10^{-13}	21.1	50.2	64.4

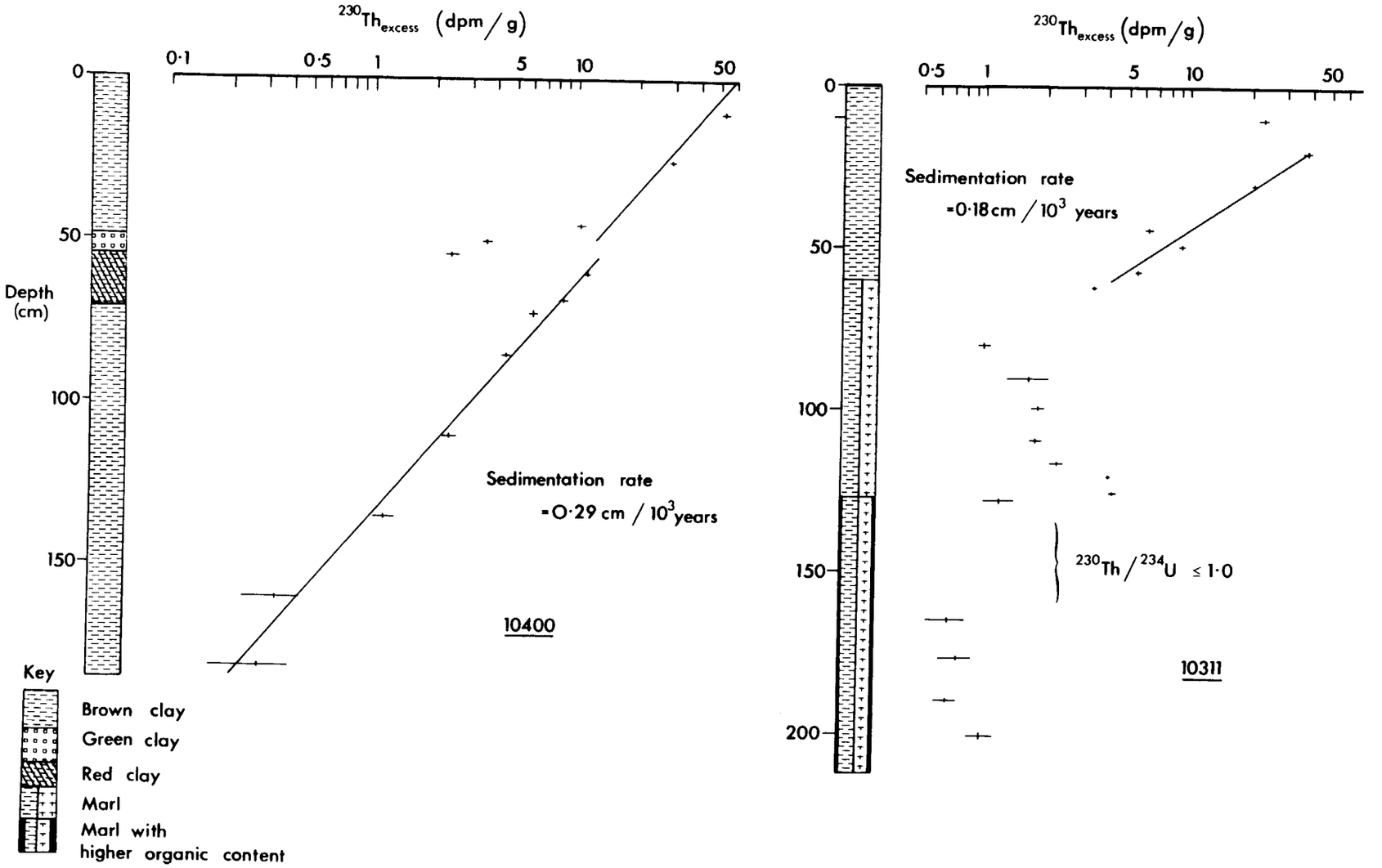

Figure 5.iv.1 Core descriptions and $^{230}Th_{excess}$ data-versus-depth for the two cores studied. Sediment accumulation rates are also shown.

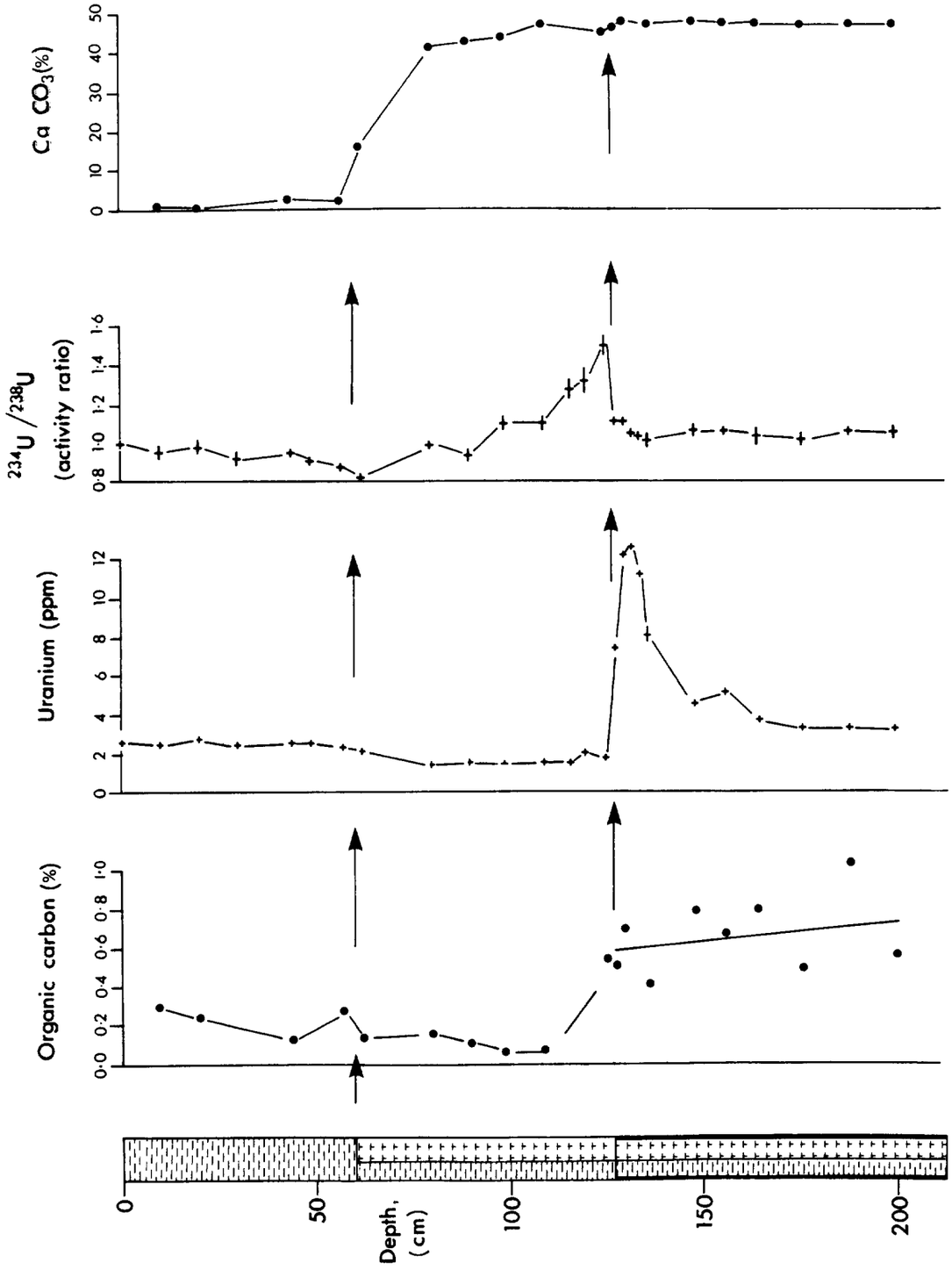

Figure 5.iv.2 Descriptive core log and profiles for C org, uranium, the $^{234}U/^{238}U$ activity ratio and $CaCO_3$-versus-depth for core 10311.

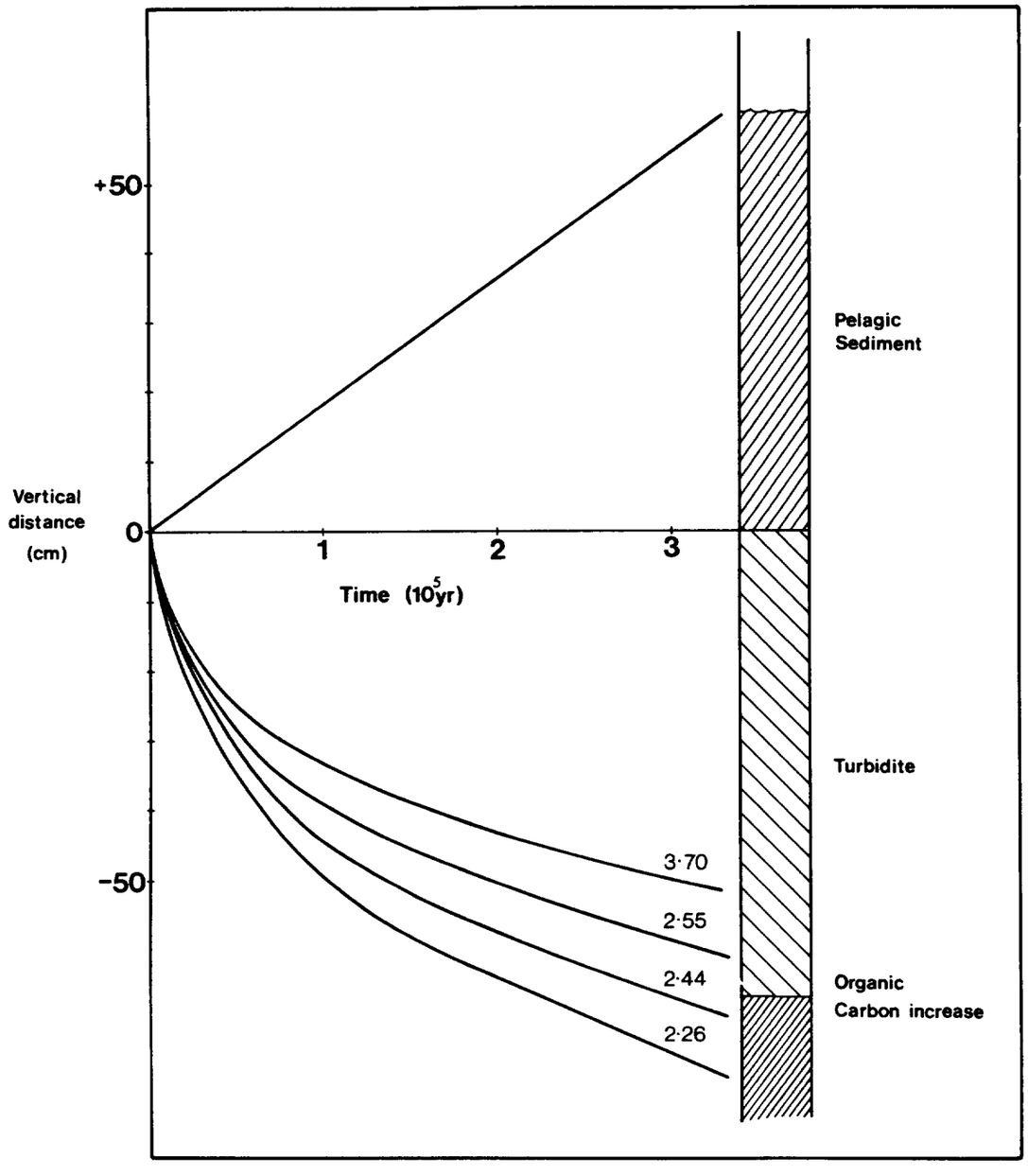

Figure 5.iv.3 The thickness of the oxidised layer plotted against time elapsed since the turbidite event at station 10311 (calculated using the model parameters given in Table 7). The upper diagonal line represents the increasing thickness of pelagic sedimentation. The lower (diagenetic) curves are drawn for various values of surficial oxygen demand in units of 10^{-13} moles cm^{-2} sec^{-1}(assumed constant over the upper 2 cm). As surficial demand rises, less oxygen is available for reaction at the surface of the deep organic-rich layer (close hatching) so that the oxidised layer deepens less rapidly.

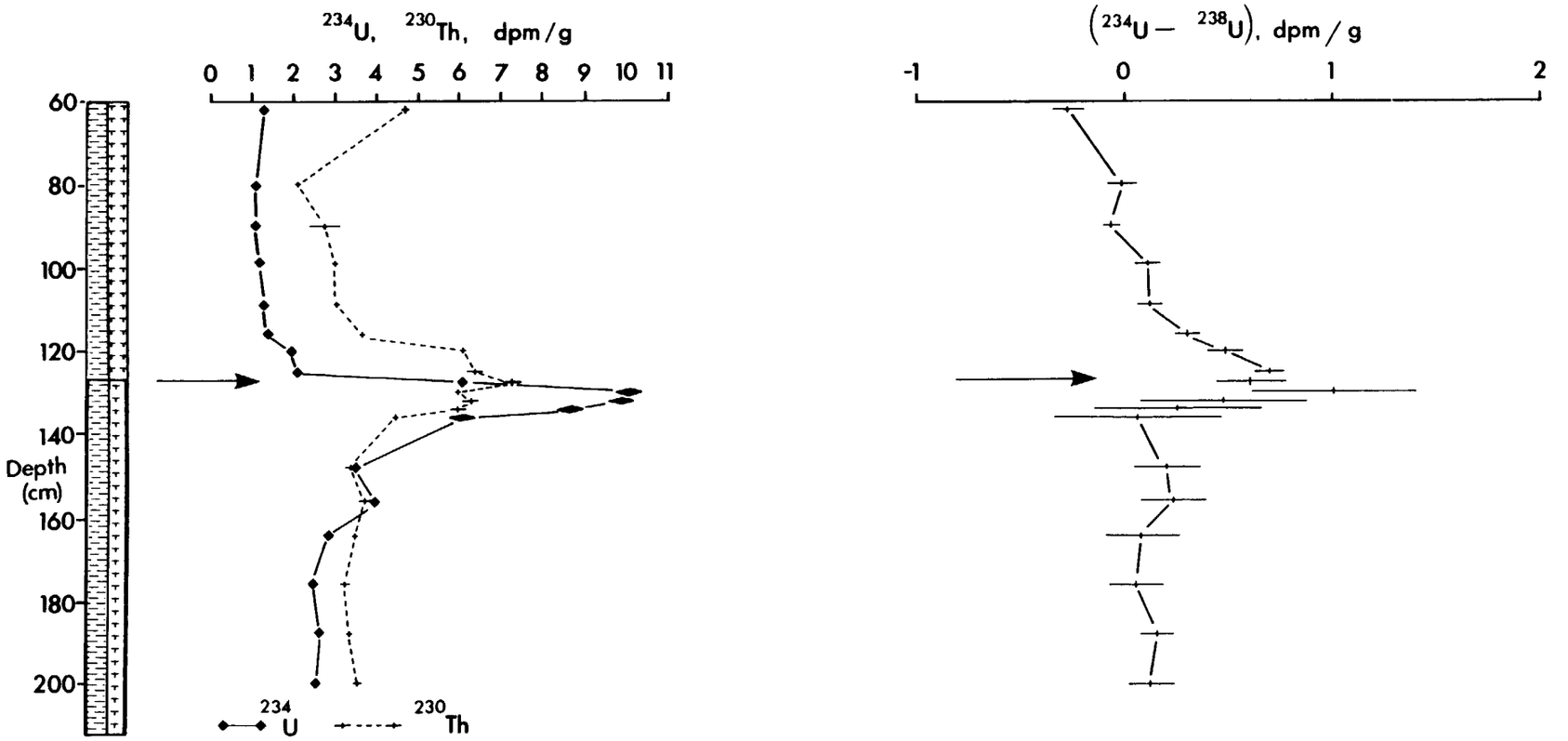

Figure 5.iv.4 Profiles of ^{234}U and ^{230}Th within the calcareous turbidite at station 10311.

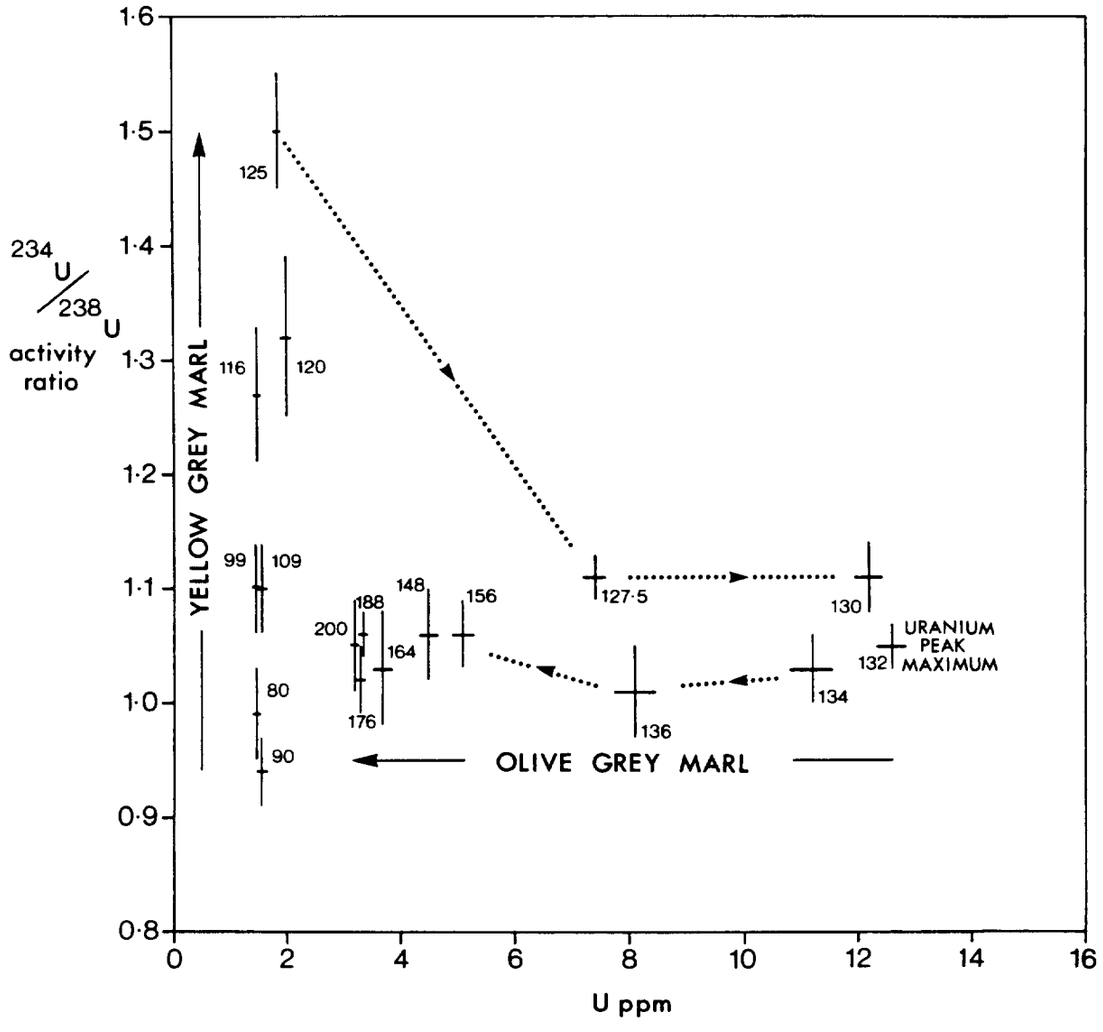

Figure 5.iv.5 Plot of the $^{234}U/^{238}U$ activity ratio-versus-U content for the turbidite section in core 10311. The numbers by the points represent sample depths (cm). High values of the activity ratio are seen in samples above the uranium peak maximum (yellow-grey marl) indicating upward migration of ^{234}U.

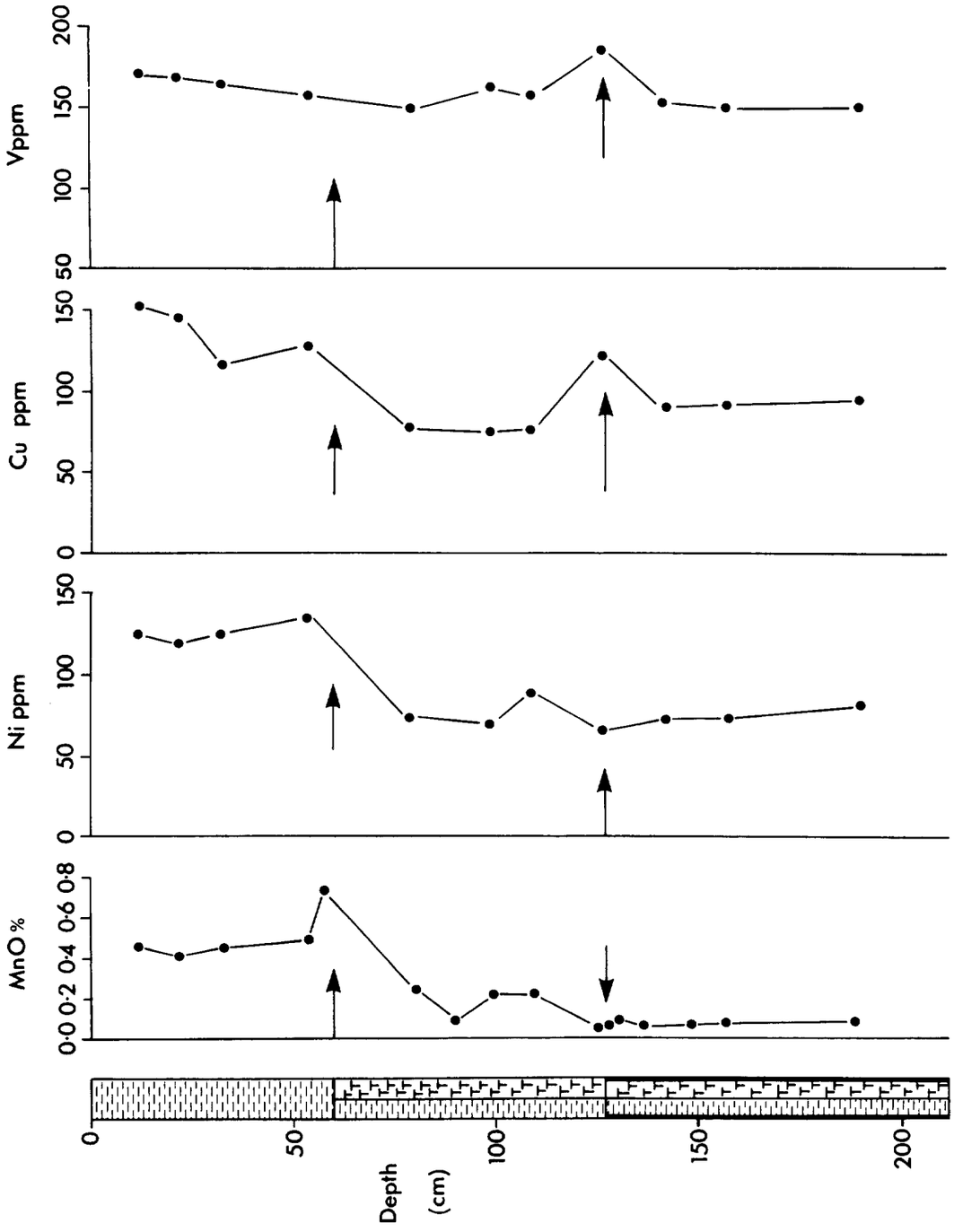

Figure 5.iv.6 Solid phase concentration-versus-depth profiles for MnO, Ni, Cu and V (expressed on a carbonate-free basis) in core 10311.

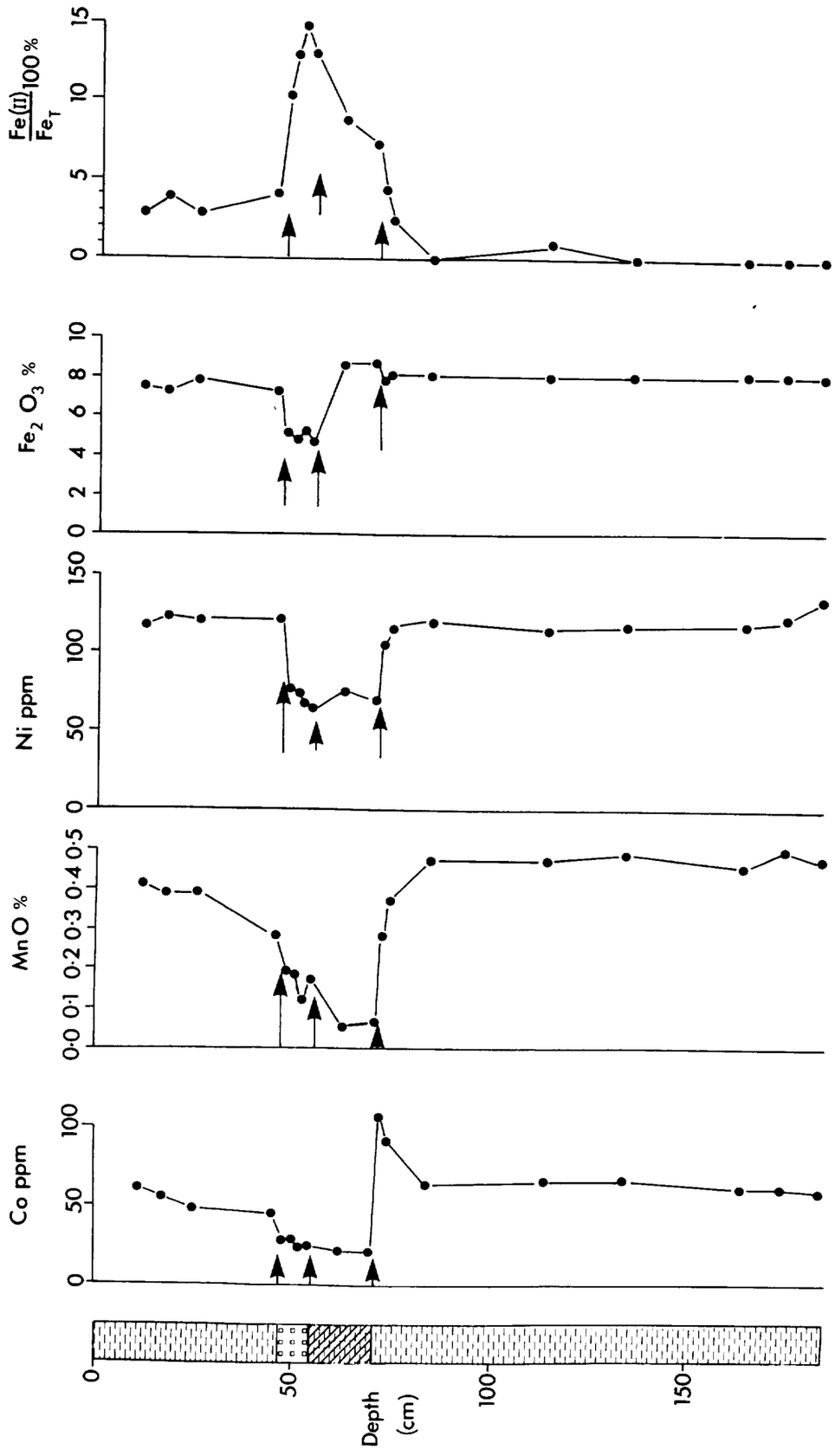

Figure 5.iv.7 Solid phase concentration-versus-depth profiles for Co, MnO, Ni and $(Fe(II)/Fe_T)$ x 100% for core 10400.

5.v TEMPERATURE, CONDUCTIVITY AND HEAT FLOW 1979-1984

In the period 1979-1984, a total of fourteen heat flow stations were occupied during five cruises in the northeast Atlantic area (Figure 5.v.1). These have yielded data from 76 individual sediment penetrations. The heat flow results have been compared to theoretical values predicted by crustal cooling models but the main interest has centred on examining sediment temperature profiles for evidence of vertical porewater movement in the KTF and GME areas selected for assessment for radioactive waste disposal.

The majority of the measurements have been made using a new model of heat flow probe specifically designed for deep ocean operation. This instrument is of the 'bowstring' type with a 4m probe and now incorporating a solid state data logger for direct, post-station, transfer of data to the ship's computer for processing. The probe is handled and deployed using a special trolley system.

Two stations were occupied in the Kings Trough Flank area, viz. 10335 and 10662 (Figure 5.v.1). The first station gave three full penetrations, one of which disclosed a marked non-linearity in the sediment temperature profile (Figure 5.v.2) which could imply upward porewater movement. When the data are modelled using conduction-convection theory the suggested velocity is 52 cm/y. The ten measurements at station 10662 also showed consistent evidence for non linear sediment temperature profiles along a $\sim$5nm transect. However, in this case the implied upward advection velocity was only $\sim$10 cm/y. Both stations may have recorded water movements which form part of a more regional scale porewater convection pattern.

Three heat flow stations were occupied in the Great Meteor East study area (Figure 5.v.1). Station 10318 was on the west extremity of the Madeira Abyssal Plain while stations S126.3 and S126.5 were in the central Madeira Abyssal Plain. These three stations recorded remarkably linear temperature profiles at a total of 10 penetrations. This may be evidence for a low rate of porewater movement. It is interesting to note that, on younger crust to the northwest, at station 10674 (Figure 5.v.1), the results suggested porewater velocities of up to 112 cm/y. These data and the results from the remaining stations are discussed at length in an IOS report (Noel, 1984b).

During cruise 144 attention focussed on an area within GME where a network of 3.5 KHz surveys have revealed 'fault-like' structures in the sediments. Using acoustic navigation, two heat flow surveys were run across a selected fault resulting in a total of 23 dips, one of which was within a few hundred metres of the fault plane. It is hoped, from an analysis of the sediment temperature data, to determine whether the fault structures are preferred paths of porewater migration through the sediment. This work is being carried out at Sheffield University under contract to the DoE.

A comprehensive study was completed of mechanisms, other than porewater migration, which can give rise to non-linear sediment temperature profiles. These include changes in bottom water temperature, the effects of rapid deposition or removal of sediment and the release or adsorption of heat by mechanical and chemical changes within the sediment column. The study suggests that caution must be applied when interpreting the sediment temperature structure (Noel, 1984a).

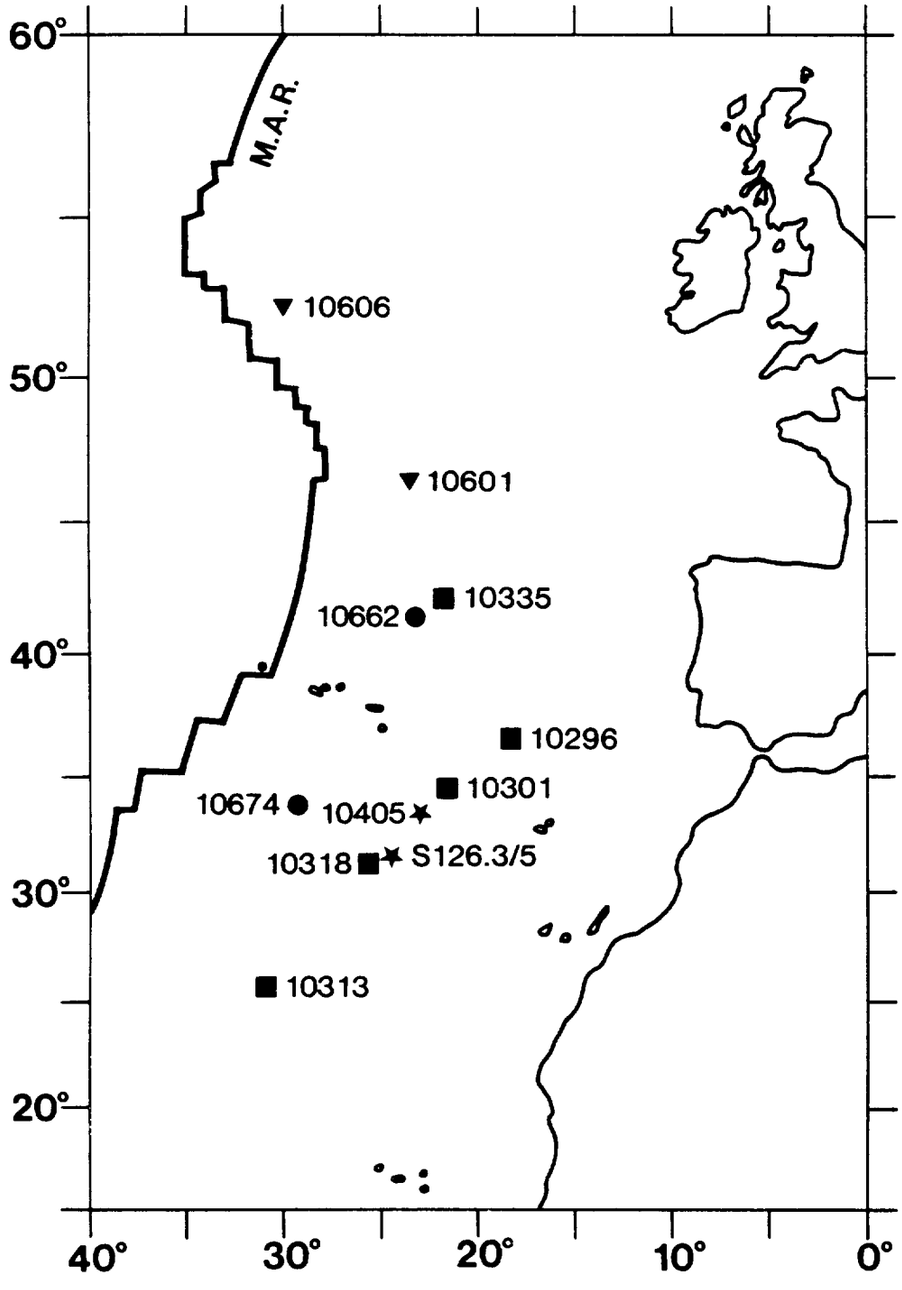

Figure 5.v.1 Location of Heat Flow Stations on Cruises:

CR 118 ■ CR 126 ★ CR 131 ▼ CR 134 ●

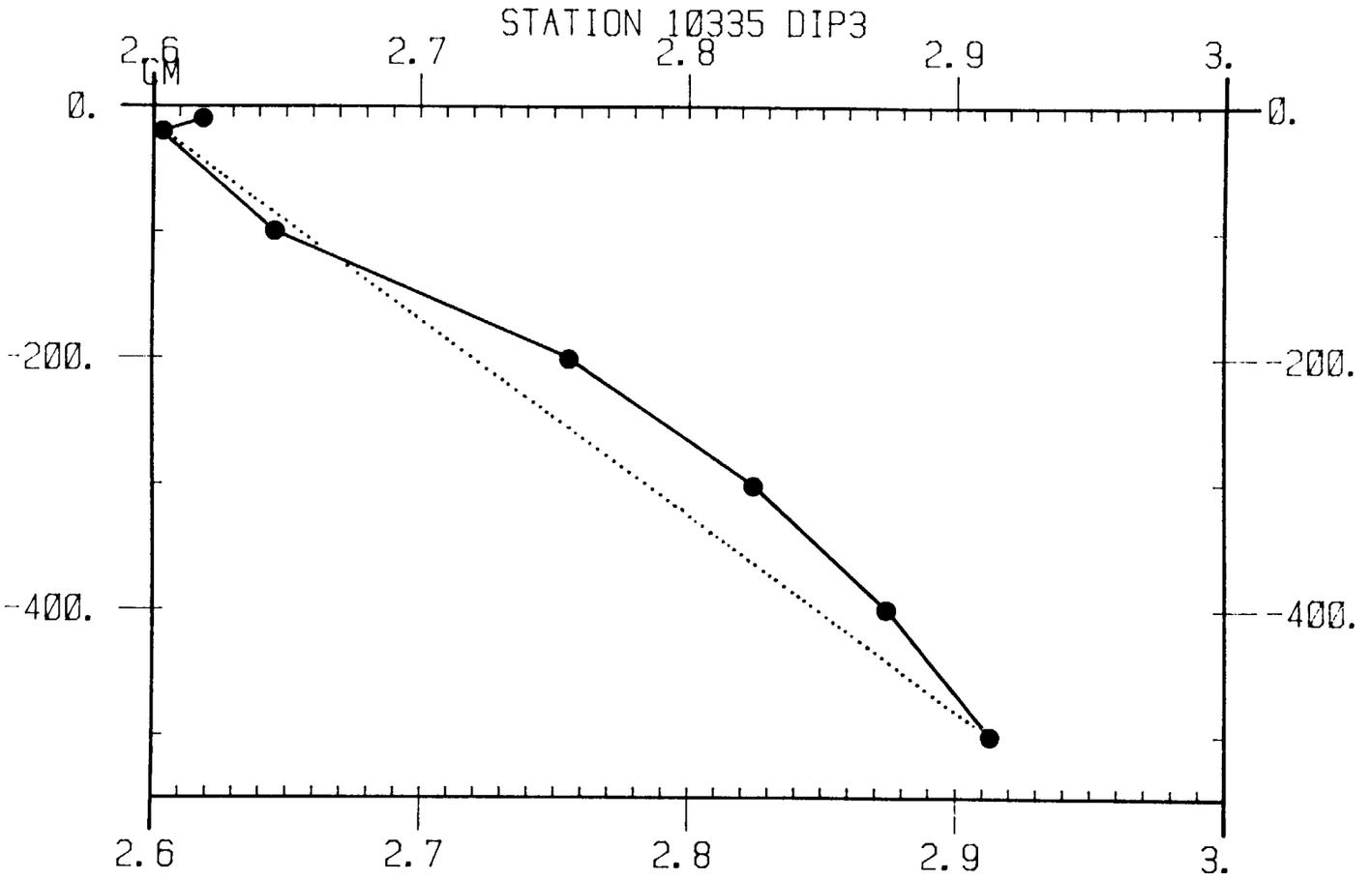

Figure 5.v.2 Sediment temperature profile at station 10335. Dip 3 in the KTF area, which might indicate upward advection of porewater of 52cm/yr.

5.vi PARTICULATE MATTER IN THE OCEANS

5.vi.a Introduction

The aim of this aspect of the radioactive waste disposal research programme was to identify the processes, especially sediment resuspension, which control the containment or dispersal of radionuclides should release occur at the sea-floor.

At the outset it was obvious that new instrumentation was required in order to collect and quantify in situ suspended particulate material to depths of 6000m and that new analytical methods needed to be developed and applied to the samples.

The design of both the instrument and the whole experiment was based on the measurement of variables commonly used in geochemical models as discussed in a report to DoE on this topic (Simpson, 1984). That discussion will not be repeated here but we shall concentrate on the data collected at the Great Meteor East study site and what has been learned from them. The trials cruise (Discovery Cruise 125) was made in January 1982 from which qualitative information was obtained on the particle morphology, especially for large particles, and was followed by Discovery Cruise 129 on which good profile data were obtained and samples analysed for elemental composition. In 1983 unsuccessful alterations were made to the instrument (Discovery Cruise 135) followed by the successful participation in Phycemed 83 Cruise in the Mediterranean.

5.vi.b Methods

Only a brief outline of the methods and instrumentation will be given since these are covered in detail in separate reports.

The Deep Water Particle Sampler (DWPS)

The instrument was designed to fulfil the following functions:

i) Filter 1000 l hr^{-1} through suitable filters.
ii) Collect water samples at the depths of filtration.
iii) Carry in-line scavengers for some dissolved radionuclides.
iv) Take four discrete samples on one cast.

v) Operate to depths of 6000m.

vi) Be controlled and monitored from the ship.

vii) Be self-contained for power.

An essential specification was to monitor the physical structure of the water column and particle distributions in real-time using sensors to measure:

viii) Particle size distribution.

ix) Particle concentration.

x) Depth.

xi) Pressure.

As a consequence of the above a suitable data transmission system was designed along with shipboard signal demodulation and display units and full computing facilities. The advantages of such a system are informed sampling and flexibility.

Details of the instrument are given in Table 5.vi.1 and Figure 5.vi.1 shows the sampler as rigged for Discovery Cruise 129. A full description is given in Simpson Gwilliam, Lawford & Lewis (1984). The main points in the development are:

i) After several trials of various combinations of filters, both in series and parallel, a 1 μm Nuclepore membrane (293mm) following a 30 μm polyester mesh prefilter (142mm) was thought to give the best compromise of large volume flow, in situ size fractionation and ease of sample handling.

ii) Mechanical flow meters give a high precision (1%) of volume filtered compared to the electronic sensors (±5%).

iii) For future cruises, the particle counter will have an upper size limit of 240 μm instead of 450 μm. (see Particle data below). The software is continually updated to optimise the real-time information on which sampling is based.

iv) The comparator settings for the particle counter as used on Discovery Cruise 129 are given in Table 5.vi.2. The diameters quoted in column 4 refer to the cumulative number distributions; the geometric means

(column 5) are applied to difference distribution data. The densities quoted are used as constants in the estimation of the mass concentration in mass difference distributions whereas the estimates of density contrast are used in mass flux calculations.

In real-time, from temperature and pressure is calculated potential temperature, depth and viscosity (without salinity correction).

From light transmission and temperature is calculated the attenuation coefficient (equivalent to particle concentration). The flow measurement from the particle counter is used to scale the raw particle counts to give the cumulative number distribution in counts per litre. The gradient and intercepts of the log $N_{>d}$ v log d are given by regression of each data cycle of 12 channels. The difference, mass and flux distributions are also estimated from the calibrated particle data.

Trials of a conductivity sensor will be made if finances allow; for the cruises under discussion, salinity, in situ water density and viscosity (salinity corrected) were taken on separate CTD casts.

Sampling

A continuous profile of the physical data is collected on the outward cast. On the basis of the information so obtained, the four filtration depths are selected. Data summaries (averages) for the hour of filtration at each depth are automatically produced at the end of the cast. On recovery, the filters are rinsed under suction with doubly distilled water and, after a period of drying in a clean hood, the filters are subsampled for the various analytical procedures. Samples are stored cold or frozen depending on the requirements of the method.

Instrumental neutron activation analysis (INAA)

INAA allows for the simultaneous measurement of many elements. The activation of the samples was carried out at the Laboratoire "Pierre Süe", CNRS-CEA, Saclay, France and the counting of the samples at CFR, Guf-sur-Yvette by C.E. Lambert and N. Rissler. As no wet chemistry is required, a very small quantity (>100µg) of material is needed to determine 25 elements of interest (Buat-Menard et al, 1980). A quarter of the filter is pelletised and irradiated in a reactor at $10^{12} - 10^{13}$ n/cm^2/s

for periods varying from 2 min (to determine Al, Cu, V, Mn, Mg, Cu) to 2 hrs (to determine Fe, Sc, REE, Ba, Cr, Zn, Sb, Th, La, Hg, etc.). The sample activity is counted on Ge-Li or Ge(HP) detectors. The activity of the sample for each element is corrected for the time elapsed since the irradiation and the detector efficiency. The concentration of the element in the sample is determined by comparing its activity to the activity of an international standard of known weight and composition. The blanks obtained on the Nuclepore membranes are given in Table 5.vi.3 and comparisons are made with those found previously by Buat-Menard (1979). Also indicated in Table 5.vi.3 are typical whole sample values for some elements to illustrate sample to blank ratios.

Scanning electron microscopy (SEM)

The SEM experiments were designed to provide information on four areas:

i) The general particle size-composition relationships (in combination with energy dispersive X-ray analysis; EDX-R).

ii) The microbial composition of the sample in terms of species distribution.

iii) The clay-type and non-biogenic mineral composition of the sample.

iv) To check the efficiency of the filtration system and compare SEM size distributions with the particle counter distributions.

The methods are discussed fully in Simpson & Gibbs (in prep.), and only i) and iv) will be discussed in the results section. Briefly, sub-samples of the filters (8mm x 8mm) were analysed for particle dimensions, description and composition. Several general categories are used: biogenic calcium carbonate (e.g. coccoliths, forams), biogenic silica (e.g. diatoms, radiolarians, silicoflagellates), organic matter (no EDX-R spectra), aggregates (e.g. faecal matter), minerals (e.g. iron oxyhydroxides, authigenic inorganic minerals), clays (e.g. chlorite, vermiculite, illite) and inorganic silica (e.g. glass shards and sand grains). Particles from 0.4μm to mm. sizes can be counted.

Originally, 100 counts were thought sufficient to give representative distributions although a minimum count of 400 is now used. For detailed biological species

analysis, e.g. coccoliths, three counts of 300 are necessary, the first establishes the percentage composition of the dominant species, and the latter two subsamples give the relative compositions of the minor species.

Particle micro-electrophoresis (PME)

Analysis of particles from subsamples (2 x 2cm) of the 1μm filters from Discovery Cruise 125 were carried out by Loder & Liss (in press). The description of the method is given in that paper. Samples were stored in filtered deep-sea water at 4°C until required in the laboratory, at which time they were sonicated prior to the electrophoretic mobility determinations (30 to 50 particles per sample). The effect on surface charge of adsorbed organics was investigated by oxidation with hydrogen peroxide before analysis on separated subsamples.

Inductively-coupled plasma emission spectroscopy (ICP)

Experiments are in progress to examine the feasibility of measuring major element particulate concentration by ICP. The methods involved are new and show promise for the determination of Al, Si, Ca and Ba.

5.vi.c Results and Discussion

CTD Data

The CTD profile for GME is shown in Figure 5.vi.2. The in situ density (σ_{tsp}) and viscosity of the water is used in the estimation of settling velocity in the Stokes' equation for particle settling.

The core and mixing of the Mediterranean water can clearly be seen at around and below 1200m. The origin of the salinity and temperature inversions at 150-200m is unknown; the salinity maxima is further north than that usually associated with the warm water sphere. The water masses show up clearly on the theta-salinity plot (Figure 5.vi.3). The complex surface structure is followed by the core of the Mediterranean water (M), Intermediate Atlantic water (I) and Deep Atlantic water (D) indicated by the steepening of the gradient.

Particle Data (Preliminary Observations)

The basic profile as obtained by the DWPS is shown in Figure 5.vi.4. Immediately apparent is the sharp increase in the transmissometer output and a decrease in total particle count to give a minima at the temperature inversion. There is a logarithmic decrease in particle concentration with depth, with evidence of slight resuspension in the bottom 1000m. The spikes in the particle counts are due to fragmentation of large particles in the cell, confirmed by examination of the 1 sec record of the channel 1 count (not shown). In Figure 5.vi.5, the attenuation coefficient, calculated from the percent transmission figures, and water viscosity, based on pressure and temperature alone, are plotted. The salinity corrected viscosity (Figure 5.vi.2) shows only a small variation from the Figure 5.vi.5 curves, the most obvious difference being in the Mediterranean water.

The ship's records and plots were primarily used to choose sampling depths for the filtration system. Also they aided the more detailed analysis in the laboratory, particularly in choosing depth intervals for averaging data. For estimating the particle mass concentration and particle mass flux the following two algorithms were used:

$$[m] = \pi . \rho . \bar{d}^3 . n/6 \qquad (\text{mg m}^{-3})$$

$$F = [m] \cdot U_s = [m] . g . \Delta \rho . \bar{d}^2 / 18\eta \qquad (\text{mg m}^{-2}\ \text{day}^{-1})$$

for η particles of given geometric mean diameter $\bar{d}$, density, ρ and density contrast with respect to water $\Delta\rho$ where η is the water viscosity and g gravity.

Thus F is ultimately dependent on a $\bar{d}^5$ term and the bias to the rare large particles is self-evident. The total water volume passing through the counter from 1000m to the bottom was 30 l and only 10 cycles produced counts of particles (15 in all) > 245 μ m mean diameter. By taking only particles up to 200 μ m and averaging over 60, 120 or 300m depth intervals the data was sufficiently smoothed to show the main trends (Table 5.vi.4). There appeared to be four distinct regions of activity:

1. The estimated mass concentration decreased rapidly from $\sim$100 μg l^{-1} in near surface waters to 17.5 μg l^{-1} at 667m. The estimated fluxes

decreased from 2229 to 38 mg m^{-2} d^{-1} over the same depth range, bounded by both the greatest values and variability in BV stability frequency.

2. The next region, 780-1736m, included the Mediterranean water in which the estimated mass concentration and flux showed greatest fluctuation. The BV stability frequency decreased linearly from 2.00 to 0.56 cycles per hour.

3. In the mid-water region, 1949-3713m, the estimated flux decreased from 162 to 77.7 mg $m^{-2}d^{-1}$ with mid-water concentrations of particulate matter of about 10 μg l^{-1}.

4. The viscosity maximum was at 4000m and, from 4000m to the bottom, as the BV stability frequency tended to zero the particle mass concentration increased, i.e. the eddy diffusion increased resulting in resuspension.

These data are still in the initial stages of interpretation. Work is yet to be done on internal variation in size spectra and the individual channel variation with depth. The loss of mass rate terms are to be evaluated, and the diffusion-advection-reaction models completed. The main consideration for the moment is, do these indirect measurements of masses and fluxes compare favourably with previous estimates? The mass estimates agree with those for the Atlantic determined during the GEOSECS experiment (Brewer et al, 1976), whereas the flux estimates are within the range quoted for the Sargasso Sea (Deuser, Ross & Anderson, 1981) and northwest Atlantic Ocean (Rowe & Gardner, 1979). There are few measurements on particle size spectra in the deep sea; the data of McCave (1975) suggested that above 20 μm the gradients tended to be between -3 and -4 for the cumulative number distributions. The analyses reported in McCave (1975) were carried out on a Coulter counter using small volumes hence problems were evident similar to those above described for 200 μm particles,i.e. the probability of detecting relatively large particles in relatively small volumes was low. The gradients (m) determined at GME for the intermediate size range particles (10-200 μm) range between -2 and -2.8 which demonstrate the importance of larger particles in mass and mass flux calculations.

Particle Morphology

The particle samples obtained from NE Atlantic stations (shown in Figure 5.vi.6 and described in Table 5.vi.5) were examined by SEM - EDX-R. The combinations of data to give descriptions for four depth intervals are also listed.

a) Size Distribution - Composition Relationships. Figure 5.vi.7 shows the percentage composition of the 1 to 10 μm size fractions. Two immediately obvious features are (a) calcium carbonate in the form of calcite (coccolithophorids) dominates all the samples, and (b) the clay material (aluminosilicates) contribution increases with depth and accounts for 25% of the small size fraction in bottom waters. The biogenic opal only appears to have any great significance in the surface water for this region during the summer cruise. The higher concentration of 'minerals' found on Discovery Cruise 125 is an artefact; these samples have higher concentrations of iron, titanium and chromium which suggests contamination from the ship. The organic material, like the calcite and opal, shows a relative decrease with depth in the northern stations. The dissolution/degradation of this material throughout the water column is the probable cause, but the effect is accentuated by resuspension of clay material in bottom water.

The distribution of the larger particles (10 to 100 μm) is shown in Figure 5.vi.8. There are fewer discrete $CaCO_3$ particles. Those between 10 and 20 μm are generally coccospheres and the larger particles are forams. The aggregates, mostly faecal material containing coccoliths, come into prominence at 25 μm as does the biogenic silica (opal) - mostly diatoms and radiolaria. Organic matter is most prevalent in the surface water and shows a gradual decrease in concentration with size whereas the clay- and mineral-dominated aggregates show a rapid tail-off to 35 μm. Thus, for the large particles, the population is again dominated by $CaCO_3$ either as discrete coccospheres or coccoliths in faecal aggregates. The organic matter is the next most common component with the silicon-containing material (biogenic and non-biogenic) forming the third group.

Since coccoliths made the main 'hard-part' contribution to the particulate matter, detailed species studies were instigated. One species, Emiliana huxleyi, dominated the species assemblage, but the holococcolith species, those made up of rhombohedric crystal units, displayed poor preservation in deep water. The reports on coccolithophorid species and distributions are in preparation (Jordan, Simpson & Chamberlain).

b) Microscope - Counter Relationships. The summed difference distributions of data in Figure 5.vi.8 are shown in Figure 5.vi.9. The curves became asymptotic at about 50 μm. When plotted as cumulative number distributions, the gradients are approximately -2 compared to the counter gradients of -2 to -2.8; the agreement is good for what is basically a subjective semiquantitative technique. However, the translation from number counts to concentration per litre was found to be unreliable as the distribution of samples on the filters was too variable.

Surface Charge

The results of Loder & Liss (1982) show that the particulate matter surface charge was remarkably constant from surface to the bottom with an electrophoretic mobility of between -0.9 and -1.1 x 10^{-8} $m^2 s^{-1} V^{-1}$. The charge was slightly more negative in near-surface samples than deep samples. After oxidation the change in charge showed that the particles were organic-coated with the indication of a greater effect in the surface (organic rich) samples.

Elemental composition of the particulate matter

Buat-Menard & Chesselet (1979) classified the elements into three main groups based upon the enrichment of elements in particulate samples with respect to crustal abundance. These groups may be summarised as (a) those directly related to crustal weathering with enrichment factors (EF) close to unity (Sc, Th, Al), (b) those closely related to the first group but with a secondary phase not associated directly with aluminosilicates; their EFs generally lay between 2 and 4 (V, Fe, Mn), and (c) those elements which were greatly enriched relative to crustal abundance (Co, Ba, Sb, Au, Ag, Hg, Se).

In the absence of data for Al, the element generally taken as the terrigenic marker for enrichment factor calculations, the enrichments were calculated taking Sc as unity. The particulate concentrations for GME in the 1 to 60 μm size range are given in Table 5.vi.6 and the crustal enrichment factors in Table 5.vi.7 with crustal concentrations from Buat-Menard (1979). The EF crust values for surface mid- and deep-waters were close to those reported by Buat-Menard (1979) and Buat-Menard & Chesselet (1979).

The same authors showed that the flux of Se, Sb, Au, Hg and Ag was biologically driven, probably in 'soft' (organic) components of the biological material. The suggested cycle for these elements was a large atmospheric input, with subsequent incorporation of the elements into organisms, and faecal material, in surface water, followed by release back into solution at depth. Cobalt, enriched to a much lesser extent, was implicated in 'soft part' biochemistry, e.g. in methylcobalamine. Barium on the other hand, was found as discrete barite crystals, possibly biogenically produced (Dehairs, Chesselet & Jedwab, 1980). Further information on barium will be useful, first because the Ba-Ra cycles are closely linked, and second because Ba SO_4 has been used as a scavenger in the laboratory for radionuclide analysis and therefore may act as an in situ scavenger for some elements. Similarly, iron also has been used in the laboratory as a scavenger to remove trace elements by coprecipitation. Iron has often been discussed as an important carrier in the removal of trace elements from solution in the oceans (e.g. Balistrieri & Murray, 1983) but the success in relating iron concentrations in particles with other element removal has been limited (Balistrieri, Brewer & Murray, 1981). The thorium crustal enrichment factors were greater than those determined using shale concentrations in the calculations. The latter gave values <2. A group of elements, hitherto not reported in any detail in particulate material, also had low enrichments. They are the most relevant group to RWD - the rare earth elements (REE) La, Ce, Eu and Yb (Table 5.vi.8).

Little is known of the rare earth element (REE) biochemical and geochemical behaviour in the oceans. Solution data for one station in the NE Atlantic, with hypotheses for the ocean cycling, were given by Elderfield and Greaves (1982) as were some theoretical considerations on the controls on REE distributions in seawater by Turner & Whitfield (1979). More recently, sediment flux estimates were made using box core samples (Thomson et al, 1984), yet no measurements were available on suspended particulate material in the ocean interior from which to derive reliable flux and residence time (τ) estimates. The variation in τ calculated from river input, aeolian and river input and sediment output was illustrative of this gap in information (Elderfield & Greaves, 1982).

Solution data from a station close to GME (Elderfield & Greaves, 1982) and the particle data were combined and from the data residence times, fluxes, apparent distribution coefficients (A_D) and enrichment factors against shale values were calculated. These results are discussed below in comparison to both the theory and previous work.

The concentrations of Sc and the REE La, Ce, Eu and Yb are listed in Table 5.vi.8. Also in Table 5.vi.8 are given the dissolved data for depth ranges comparable to the particulate sampling depths.

To reiterate the statement made by Elderfield and Greaves (1982):

a) The REE are a coherent group which possess an ordered variation in stability constants, thus fractionation between light and heavy elements may be expected.

b) Two of the elements show variation from the III oxidation state, CeIV and EuII, thus further fractionation may be expected from these two elements.

The evidence to support this statement is best appreciated by comparing the enrichment of the elements in particulate material against shale values; again, in the absence of Al data, Sc was used as the terrigenous marker. The estimates of REE concentrations in shales vary markedly, classically the Wedepohl (1971) values are used, but also included are the latest determinations for Cody Shale (Jarvis & Hockings, in press), and thus two EF_{shale} values are presented in Table 5.vi.8.

The relatively greater enrichment of Ce is indicative of the lower solubility of the 4+ oxidation state and low enrichment of Eu is due to the existence of the 2+ oxidation state. These effects, and the fractionation between the lightest, more reactive (La) and heaviest (Yb) elements is shown in the deep water residence time calculations (Table 5.vi.9) based on the model of Bacon and Anderson (1982). The order of Ce<La<Eu<Yb was consistent with the groups observed and predicted behaviour with τ in the ranges quoted previously in Elderfield & Greaves (1982).

It was suggested that the high bottom water dissolved concentrations were indicative of diffusion from sediments and that sediments were an important source of the elements to the ocean interior (Elderfield & Greaves, 1982). Evidence for extensive remobilisation (dissolution-desorption) and also resuspension of detrital material is provided by the low EF shale and the high Sc and REE particulate concentrations respectively. The primary (midwater) flux of the elements was estimated using particle data obtained from the particle counter on the DWPS

at the time of sampling. From 1200m to 4000m the mean particle concentration for <60 μm particles was calculated to be 5 μg l^{-1} and the mass flux of particles 50 mg m^{-2} day^{-1}. The resulting total primary fluxes (F_T) are in good agreement with those derived from the sediment record for clay sediments in the Nares Abyssal Plain (Thomson et al, 1984). Some geographical variability is to be expected in comparing these sites (W to E Atlantic). Furthermore seasonal variability is an important factor in water column work; these samples were collected shortly after the spring bloom as indicated by the low concentration of Sc (clay material) in the surface water.

Since remobilisation appeared to be important (Elderfield & Greaves, 1982) much of the authigenically complexed material must be recycled from the suspended particles. The bottom sample was assumed to be typical of the surface sediment, a valid assumption since there was evidence for resuspension from the DWPS sensors, microscopy and chemical data. Subtracting the detrital component from the bottom sample, the authigenic components are 6.7%, 51%, 8.9%, 7.9% for La, Ce, Eu and Yb respectively. Scaling up the detrital primary flux accordingly, total fluxes of 77-89, 194-320, 2.82-3.25 and 3.98-6.01 nmol cm^{-2} kyr^{-1} for La, Ce, Eu and Yb respectively are obtained (Table 5.vi.9, bracketed values in column 5 + column 4). Again the comparisons with the sediment flux estimates are good. The inference is that 95%, 63%, 70% and 85% of La, Ce, Eu and Yb respectively in the authigenic component are returned to solution in transit from 1000m to the sediment and at the sediment-seawater interface.

To find a plausible explanation we must return to the theory. The enrichment of the lanthanides was suggested to be by ion capture, i.e. where an ion of higher coordination and/or greater polarising power replaces the major ion within a mineral, rather than through solution chemistry (Turner & Whitfield, 1979). The replacement of calcium in calcite or aragonite, barium in barite, and strontium in celestine by REE fulfils these conditions; all these minerals have biogenic origins, e.g. coccolithophorids, foraminifera, benthic protozoa and acantharia. From 1000m to 5470m the Ca and Ba enrichments decreased greatly with depth. It is possible that the REE also have some organic association, e.g. in membranes (Williams, 1982).

Lastly, there are similarities in behaviour of the REEIII with AmIII and CeIV with PuIV. For example, compared to the data of Fowler et al (1983, points a and b)

and Livingstone & Anderson (1983 , points c to f):

a) $^{239,240}Pu$ was enriched relative to ^{241}Am in biological material during a spring bloom of dinoflagellates, c.f. Ce v La.

b) The A_D values (Table 5.vi.8) agree well with the surface sample A_D values of Pu and Am of 1.4×10^5 and 0.8×10^5 respectively.

c) The Am/Pu ratios in particles were uniform with depth in deep (> 750m) samples, c.f. 1320 and 1806m EF shale and particle concentrations.

d) with the exception of two samples Pu was enriched relative to Am, c.f. Ce v other REE.

e) Most of the Pu flux to sediments was shown to dissolve.

f) The estimated residence time of Pu was similar to that of REE.

The term A_D is the apparent distribution coefficient in that mineral and biological components contribute to the overall concentration, probably the distributions are kinetically controlled by biological uptake followed by dissolution, rather than by solution equilibria. Although this data set is limited, the indications are that the REE cycles are of importance as markers for authigenic (biological)-detrital removal processes, coupled to extensive remobilisation in deep water as a result of the recycling of biological components.

The implication is that their ultimate removal is probably at the continental boundary similar, perhaps, to that observed for naturally occurring radioisotopes like Th, Pa and Pb (Kadko, 1983; Spencer, Bacon & Brewer, 1981). Perhaps the radionuclides, Am and Pu, are also extensively remobilised at the sediment-seawater interface and scavenged at the continental margins.

5.vi.d Summary

The particle sampler operated to its specification in that it provided real-time information on which to carry out informed sampling and sufficient sample for full chemical and morphological analysis. Most of the laboratory data handling

procedures and analytical methods have been worked up. The analytical results obtained and estimates of particle mass concentration and fluxes were in good agreement to those determined by other workers. Also new and more detailed information is becoming available on particle composition and distribution.

In general, the particulate material was dominated by $CaCO_3$, in the form of coccoliths, and unidentified organic matter. The particles themselves were coated with organics and were negatively charged. There was evidence of strong recycling (and grazing?) in the top 700m. There was a loss of particle mass and decrease in flux to 4000m in the size range measured, and the chemical data suggested this primarily to be due to dissolution of calcite and possibly loss of organic material.

Below 4000m the instrumentation and analysis were sensitive to low resuspension phenomena. Early results on REE, a group that may prove to be analogous in behaviour to the heavy radionuclides, suggested an indirect method of predicting the behaviour of Am and Pu. Of particular importance is the possibility of boundary scavenging of these elements at the continental margins by incorporation in organisms.

The experiments have reached a stage where the lines of approach require drawing together for more extensive interpretation through modelling, along with more detailed sampling at the site.

5.vi.e Acknowledgements

This work is the result of the joint efforts of many people. T.J.P. Gwilliam and V.A. Lawford (IOS) designed and constructed the deep water particle sampler, Christine Lunn (IOS) and A.R. Lewis (RVS) wrote the ship's software, M.J.R. Fasham set up the laboratory data processing and advised on interpretation of data, Gill Gibbs (University of Surrey) carried out the SEM analysis and Claude Lambert and N. Risler (CFR-CNRS) ran the INAA analyses. Thanks are due to T.C. Loder, P.S. Liss and I.N. McCave for permission to utilise material prior to publication and also to the officers and crew of the RRS Discovery.

Table 5.vi.1 Summary of the deep water particle sampler

a)	MECHANICS	-	Max. flow available 2480 1 hr^{-1} with filters 1000 1 hr^{-1} in situ		
	Pumps	-	Austin centrifugal - polypropylene		
	Motors	-	Printed motors G9M4 (26V) - pressure balanced housing		
	Power	-	Chloride Cyclon lead-acid paste (5 Ah) 48 per pack in four units of 12 ≡ 24V (15 Ah). Pressure balanced		
	Filters	-	Nuclepore polycarbonate (1 μm), Estal Polyester (30 μm)		
	Volume meters	-	Kent mechanical positive displacement (1 part in 1000)		
	Selector valve	-	Rotary (cone-shaped) built in-house		
	Water samplers	-	General Oceanics Go-Flo bottles (2.5 1)		
b)	SENSORS			RANGE	ACCURACY	RESOLUTION
	Temperature	-	Pt resistance thermometer	0-20°C	± 0.005°C	0.002°C
	Pressure	-	Strain gauge	6000 m	± 4m	0.05 m
	Transmissometer	-	Seatech 1 m folded	0-100%	± 0.5%	0.02%
	Particle counter	-	Light blockage principle	10-450 μm in 16 channels		
	Flow meters	-	Appleby-Ireland pressure transducer			
			a) Venturi	300-3000 1 hr^{-1}	±5%	20 1 hr^{-1}
			b) particle cell	300-3000 ml min^{-1}	±5%	20 ml min^{-1}
	Height off bottom	-	35 kHz Acoustic sensor	9-256 m off	-	1 m
c)	DATA PROCESSING					
	From sensors	-	voltage or frequency to b.c.d. 8-bit words			
	Transmission	-	FSK line signal $3\frac{1}{3}/6\frac{1}{3}$ kHz (≡ "0" and "1")			
	Demodulator	-	IOS FSK or Neil Brown CTD deck unit			
	Displays (raw data)	-	CTD unit, purpose built unit and BBC microcomputer			
	Computer	-	PDP 11/34 run under RSX 11M with sampling software in RTL/2, processing software in C and FORTRAN IV			
	Display	-	Tektronix, H.P. graphics terminals + printers and plotters			

Table 5.vi.2 Summary of comparator settings (mV), equivalent diameters (μm) and density estimates (g cm^{-3}) by channel number

Channel (number)	Comparator (mVx10)	log d (log μm)	diam (μm)	Geometric mean (d)	Density[1] (g cm^{-3})	Density[2] Contrast
CHAN 1	96	1.0000	10.0			
				11.4	1.386	0.366
CHAN 2	102	1.1111	12.9			
				14.7	1.352	0.332
CHAN 3	148	1.2222	16.7			
				19.0	1.327	0.307
CHAN 4	223	1.3333	21.6			
				24.5	1.307	0.287
CHAN 5	338	1.4444	27.9			
				31.6	1.281	0.261
CHAN 6	512	1.5556	36.0			
				40.9	1.252	0.232
CHAN 7	775	1.6667	46.4			
				52.8	1.236	0.216
CHAN 8	1173	1.7778	59.9			
				68.2	1.214	0.194
CHAN 9	1776	1.8889	77.4			
				88.0	1.144	0.124
CHAN 10	2689	2.0000	100.0			
				114	1.110	0.090
CHAN 11	4000	2.1111	129.2			
				147	1.083	0.063
CHAN 12	6163	2.2222	166.9			
				190	1.062	0.042
CHAN 13	9328	2.3333	215.9			
				245	1.048	0.028
CHAN 14	14125	2.4444	278.5			
				316	1.039	0.019
CHAN 15	21380	2.5556	359.5			
				409	1.033	0.013
CHAN 16	32367	2.6667	464.5			

1. Based on the density contrast - diameter relationship postulated by McCave (1984).

2. Assumes a seawater density of 1.02 g cm^{-3}

Table 5.vi.3 a) Blank values for 293 mm diameter Nuclepore polycarbonate membranes (1.0 μm) and comparison with 47mm (0.4 μm) NPM - Unwashed filters.

	Blank 1 Mass(ng)	2σ(%)	Blank 2 Mass(ng)	2σ(%)	Mean (ng)		This work (ng cm^{-2})	47mm+ (ng cm^{-2})
Ce	6.56	51.2	8.64	51.8	7.60	≡	1×10^{-2}	0.16
Se	16.97	23.1	18.62	22.4	17.8	≡	3×10^{-2}	$<2 \times 10^{-2}$
Hg	30.65	10.8	36.13	9.03	33.39	≡	5×10^{-2}	-
Cr	9263	0.21	8366	0.24	8814	≡	13.1	1.6
Sc	0.1072	10.8	0.0358	23.2	0.0715	≡	1×10^{-4}	1×10^{-3}
Fe	1303.7	8.2	1265	8.48	1284	≡	1.9	26
Co	2.942	7.2	3.085	6.5	3.013	≡	4×10^{-3}	7×10^{-2}
Zn	273.1	3.4	190.7	4.1	231.9	≡	0.34	1.4
Sb	8.301	9.9	6.34	11.6	7.320	≡	1×10^{-2}	2×10^{-2}
Ba			378	35.0	378	≡	0.56	<0.4
Ag			1.396	36.0	1.396	≡	2×10^{-3}	0.1
							La	2×10^{-2}
							Sm	1×10^{-3}
							Au	1×10^{-3}
							Th	2×10^{-3}
							Ca	22
							Mn	0.2
							As	2×10^{-2}
							Al	8
							(+ Buat - Menard, 1979)	

B) Mean values of all samples (sample + filter) for some elements. Units of:- Σ ng of element per filter ± 1 s.d.

Sc	12.7	±	3.7
Fe	48,900	±	7
Zn	2440	±	9
Sb	58	±	17
Mg	108	±	47
La	89	±	21
Ba	11,620	±	20

Table 5.vi.4 Data Summary for G.M.E. 10 - 200 μm Particles

Correlations for the cumulative number distributions were >0.99 with the exception of 960-1080m and 3900-4200m(*). 1560-1680m the averaging was biased by one sample.

Key: Z = depth range of sample averaging; $\bar{Z}$ = mean depth of averaging (m)
TEMP = in situ temperature (°C), ATCO = $_{1}^{-1}$ attenuation coefficient
BVSF = Brunt-Vaisala stability frequency (cycles hr^{-1})
VISC = Water viscosity ($g\ cm^{-1}s^{-1} \times 10^{2}$)
MASS = Particle mass concentration ($\mu g\ l^{-1}$)
FLUX = Particle mass flux ($mg\ m^{-2}\ d^{-1}$)
INT = 10 μm intercept of the cumulative number distribution (log counts l^{-1})
GRAD = Gradient of cumulative number distributions, log N = a - m log d.

	Z	$\bar{Z}$	TEMP	ATCO	BVSF	VISC	MASS	FLUX	INT(a)	GRAD(m)
	0-60	40	20.96	0.452	5.04	1.08	81.3	1597	4.134	-2.62
	60-120	85	19.09	0.445	3.94	1.12	97.2	2229	3.996	-2.29
	120-240	168	18.47	0.413	1.80	1.18	67.4	1450	3.898	-2.41
	240-360	305	15.77	0.400	2.38	1.22	39.8	772	3.645	-2.25
	360-480	405	13.92	0.395	2.07	1.27	27.1	483	3.523	-2.33
	480-600	546	12.25	0.390	1.65	1.32	20.1	323	3.592	-2.84
	600-720	667	11.46	0.387	1.74	1.35	17.5	318	3.265	-2.26
	720-840	780	10.68	0.386	2.00	1.38	15.3	217	3.404	-2.60
	840-960	895	9.68	0.385	1.88	1.41	13.9	183	3.410	-2.70
*	960-1080	1024	8.81	0.384	1.71	1.43	16.7	286	3.083	-1.68
	1080-1200	1136	8.25	0.382	1.58	1.45	12.9	172	3.183	-2.09
	1200-1320	1263	7.88	0.383	1.35	1.47	16.5	297	3.208	-2.29
	1320-1440	1379	7.26	0.382	1.22	1.50	13.8	225	3.062	-1.98
	1440-1560	1505	6.43	0.382	0.94	1.53	12.0	148	3.212	-2.26
*	1560-1680	1620	5.77	0.382	0.77	1.56	29.0	621	3.063	-1.85
	1680-1800	1736	5.29	0.381	0.56	1.57	15.8	269	3.13	-2.16
	1800-2100	1949	4.56	0.381	0.65	1.61	11.5	162	3.13	-2.31
	2100-2400	2245	3.80	0.380	0.60	1.64	9.1	126	3.02	-2.34
	2400-2700	2531	3.31	0.380	0.47	1.66	10.4	153	3.10	-2.50
	2700-3000	2829	2.98	0.380	0.52	1.67	8.4	111	3.15	-2.71
	3000-3300	3143	2.75	0.380	0.42	1.675	9.6	132	3.057	-2.41
	3300-360	3447	2.62	0.381	0.36	1.688	7.6	98.3	3.025	-2.31
	3600-3900	3713	2.55	0.381	0.24	1.690	7.0	77.7	3.081	-2.56
*	3900-4200	4086	2.49	0.381	0.28	1.690	18.5	374	2.826	-1.62
	4200-4500	4344	2.46	0.381	0.23	1.689	9.7	152	3.007	-2.41
	4500-4800	4658	2.44	0.381	0.14	1.687	12.3	194	2.952	-2.07
	4800-5100	4944	2.45	0.382	0.10	1.685	12.7	204	3.020	-2.20
	5100-5220	5156	2.47	0.383	0.05	1.683	19.1	381	2.964	-2.01
	5220-5340	5280	2.48	0.384	0.00	1.681	11.2	142	3.154	-2.37
	5340-5460	5415	2.50	0.384	0.03	1.680	14.6	237	3.122	-2.11

Table 5.vi.5 Station numbers, positions and depths of sampling on cruises 125 and 129. Combinations of samples for Figures 5.vi.7 to 9 are also given.

Cruise	Station	Location	Depth	Combinations
125 (Jan '82)	10399	N25°12' W25°25'	133m, 500m, 1000m	0-200m:- 15m + 20m + 75m + 133m
	10400	N25°40' W30°59'	20m, 250m	200-1000m:- 250m + 500M + 550m +860m
	10402	N31°27' W24°34'	75m, 550m, 860, 2000m, 5370m	1000-4000m:- 1000m + 2000m + 2500m
	10404	N34°23' W12°27'	15m, 1500m, 2500m, 4400m	4000m-bottom:- 440m + 5370m
129 (June'82)	10548	N00°03' W13°15'	(25m), 80m, 300m, 850m	0-200m:- 25m + 80m + 60m
	10550	N10°00' W26°00'	60m, (500m, 1500m)	200-1000m:- 250m + 300m + 850m
	10552	N19°21' W29°51'	25m, 250m, 4705m	4000m-bottom:- 4705m
	10554	N31°26' W24°26'	28m, 134m, 1320m, 1806m, (3009m, 5152m, 5434m) and 5470m	Grouped accordingly

( ) indicate sampling failures

Table 5.vi.6 The variation of particulate elemental concentrations (ng l^{-1}) with depth at G.M.E.

	28m	134m	1320m	1806m	5470m
Sc	0.0038	0.0034	0.0105	0.0105	0.0295
Fe	50.85	13.45	36.38	54.22	87.3
Th	0.0029	0.0038	0.0116	0.0118	0.028
Co	0.1030	0.0307	0.0505	0.0799	0.0759
Zn	15.51 (?)	3.921	2.289	3.121	5.269
Hg	0.2749	0.1040	0.0513	0.1307	0.0721
Se	0.0860	0.0711	0.0516	0.0507	0.0279
Sb	0.0713	0.0279	0.0528	0.0834	0.0245
Ba	1.818	11.39	10.73	10.36	4.865
Ca	nd (?)	1242	812	503	475
La	nd (?)	0.0128	0.0788	0.0708	0.0849
Ce	0.0719	0.0606	0.2175	0.2248	0.3262
Eu	0.0012	0.0011	0.0016	0.0015	0.0034
Yb	0.0045	0.0028	0.0032	0.0033	0.0055
Hf	nd	nd	0.0044	0.0044	0.0099
Ag	0.0295	0.0103	0.2537 (?)	0.0350	0.0134
Au	0.0070	0.0042	0.0425 (?)	0.0060	0.0032
Rb	0.0534	0.0190	nd (?)	nd (?)	0.0794
Cs	nd	nd	0.0040	0.0034	0.0104
$CaCO_3$ [a]	-	3105	2030	1256	1188
AlSi [b]	30	27	84	84	126

a) from Ca and b) from Sc values

Table 5.vi.7 Crustal enrichment factors against Sc, using crustal values given in Buat-Menard (1979), for particle samples from G.M.E.

Depth	28m	134m	1320m	1860m	5470m
Cs	-	-	2.8	2.4	2.6
Th	1.8	2.6	2.5	2.7	2.2
Fe	5.2	1.5	1.4	2.0	1.2
Co	24	7.9	4.2	6.7	2.3
Ba	25	174	53	51	8.5
Ca	-	221	50	29	9.8
Sb	2064	903	553	873	91
Ag	2440	953		1048	143
Au	10100	6790	-	3140	59.6
Hg	19900	8400	1342	3419	671
Se	9970	9212	216)	2130	417

Where $E.F._{CRUST}$ =([Element] / [Sc])$_{PART}$/ ([Element] / [Sc[ )$_{CRUST}$

Table 5.vi.8 Rare Earth Element Concentrations (mol kg $x12^{12}$), Distribution Coefficients (A_D) and Shale Enrichment Factors (vs. Sc)

θ -S Region		:	Surface	Near Surface	"Mediterranean"	Deep Water	Bottom Water		
Sample Depths (m)	Water	:	0	100 & 200	1000 & 1500	2500 & 3000	4500	Shale Concentration (nmol. g^{-1}) a)	b)
	Particles	:	28	134	1320	1806	5470		
La -	dissolved+	:	36.7	15.0	22.8	31.0	54.4		
	particulate	:	n.d.	0.0897	0.0549	0.492	0.581		
	A_D	:	-	1.8×10^5	5.0×10^6	3.3×10^6	1.1×10^6		
	E.F. Shale a)	:	-	1.4	2.8	2.5	1.1	213	
	b)	:	-	1.2	2.4	2.1	0.91		295
Ce -	dissolved+	:	66.3	19.6	15.3	22.7	55.1		
	particulate	:	0.500	0.421	1.501	1.549	2.213		
	A_D	:	8.8×10^4	6.3×10^5	2.0×10^7	1.2×10^7	4.2×10^6		
	E.F. Shale a)	:	3.5	3.3	3.8	3.9	2.0	428	
	b)	:	3.0	2.6	3.2	3.4	1.7		592
Eu -	dissolved+	:	0.615	0.747	0.982	0.941	1.22		
	particulate	:	0.0077	0.0071	0.0102	0.0095	0.0213		
	A_D	:	9.1×10^4	2.8×10^5	2.2×10^6	2.0×10^6	1.8×10^6		
	E.F. Shale a)	:	3.0	3.1	1.5	1.4	1.1	7.63	
	b)	:	2.6	2.6	1.2	1.2	0.94		10.5
Yb -	dissolved+	:	3.15	3.81	4.99	5.00	5.16		
	particulate	:	0.0253	0.0158	0.0179	0.0184	0.0302		
	A_D	:	1.4×10^5	1.2×10^5	7.4×10^5	7.6×10^5	6.2×10^5		
	E.F. Shale a)	:	6.9	4.8	1.8	1.8	1.1	10.9	
	b)	:	4.4	3.1	1.1	1.2	0.7		20
Sc -	particulate	:	0.0824	0.0736	0.226	0.225	0.624	235	289

+Elderfield and Greaves (1982). In the equation described square brackets denote concentrations: $A_D = \rho . f/(1-f)[m]$ where $f = [REE]_{particles}/[REE]_{total}$ and [m] = particle mass concentration; $E.F._{shale} = ([REE]/[Sc])_{particles}/([REE]/[Sc])_{shale}$

a) Jarvis and Hockings (in press) b) Wedepohl (1971)

Table 5.vi.9 Rare Earth Element Deep Ocean Residence Times (yr) and Flux Estimates ($nmol/cm^2\ 10^3\ yr$)

1 Element	2 Residence Time (τ_E) †	3 Total Primary Flux (F_T) ≠	4 Detrital Primary Flux (F_D) #	5 Authigenic Primary Flux (F_A) §	6 Total Sediment Flux (F_S) ∞	7 Authigenic Sediment Flux (F_{SA}) ∞
La	255-510	190	72 - 84	106-118 (5.2)	110-204	8-11
Ce	65-130	560	144 - 170	390-416 (150)	272-468	34-106
Eu	505-1010	3.6	2.57 - 3.0	0.6-1.03 (0.25)	3.5-6.7	0.59
Yb	1395-2770	6.6	3.67 - 5.7	0.9-2.97 (0.31)	5.3-10	0.65

Calculations are based on 1320 m and 1806 m averages in Table 5.vi.8

† Using $\tau_E = \tau p/f$ where τp = the deep water particle residence time = 5to 10 yr (f from Table 5.vi.8)

≠ $F_T = F_p.[REE]_{part.}/[m]$ where the mass flux of material (F_p) and mass concentraiton of material, m, are 50 mg $m^{-2}\ d^{-1}$ and 5 $\mu g\ l^{-1}$ respectively for 1 to 60 μm particles.

Shale values, a and b, from Table 5.vi.8

where $[REE]_{detrital} = [Sc]_{particles} \times [REE/Sc]_{shale}$ and $F_D = F_p[REE]_{detrital}/[m]$

§ $F_A = F_T - F_D$. The numbers in brackets are based on the % authigenic component in the Bottom Water Sample using Jarvis and Hockings shale data and scaling the l.h.c. of F_D accordingly.

∞ Thomson et al (in press)

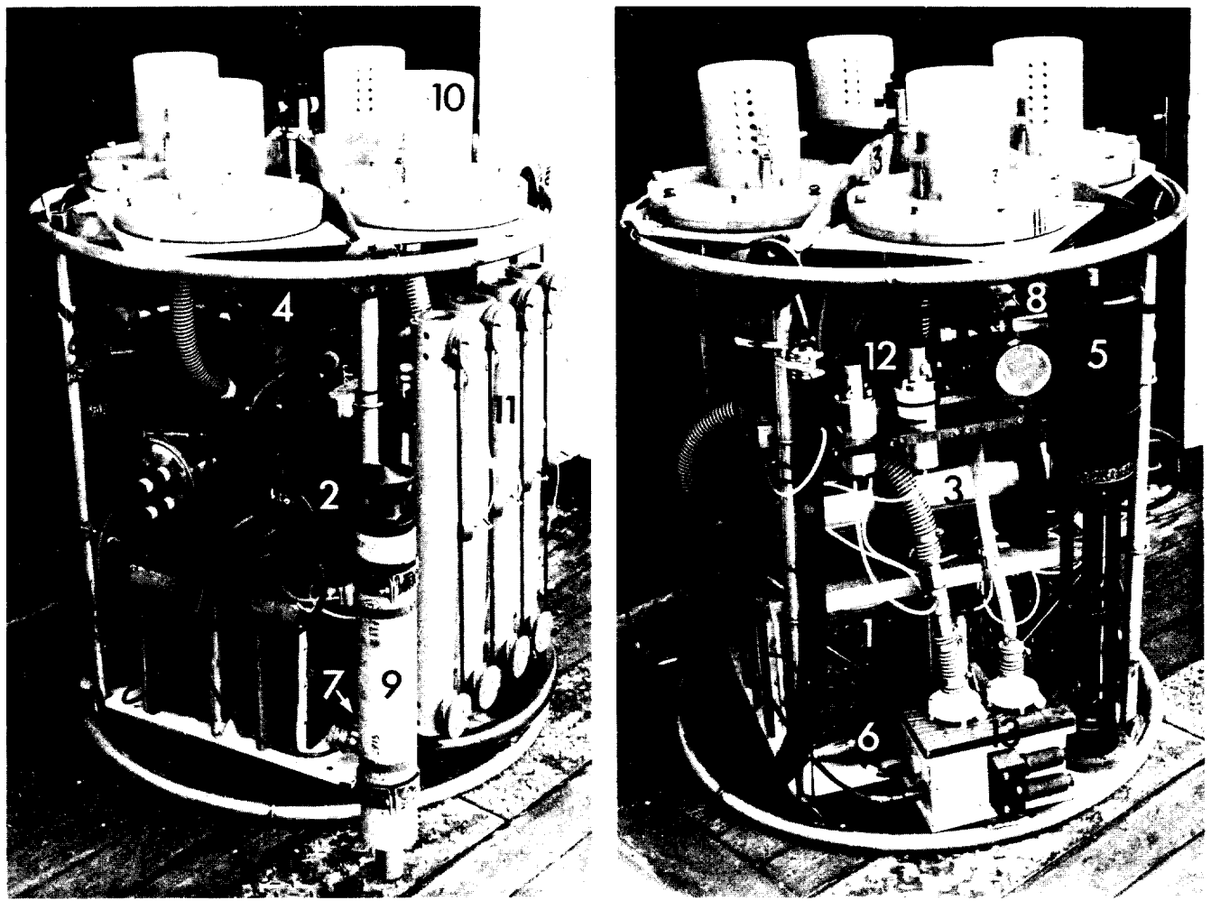

Figure 5.vi.1 The deep water particle sampler as rigged for Cruise 129:

1. Battery packs
2. Remote-control electronics tube
3. Data transmission tube
4. Filter selector valve
5. Transmissometer
6. Pressure sensor
7. Temperature sensor
8. Particle counter
9. Acoustic near-bottom echo sounder
10. Filter stacks
11. 2.5 l Go-Flo water samplers
12. Pressure transducers
13. Pumps and motor housing

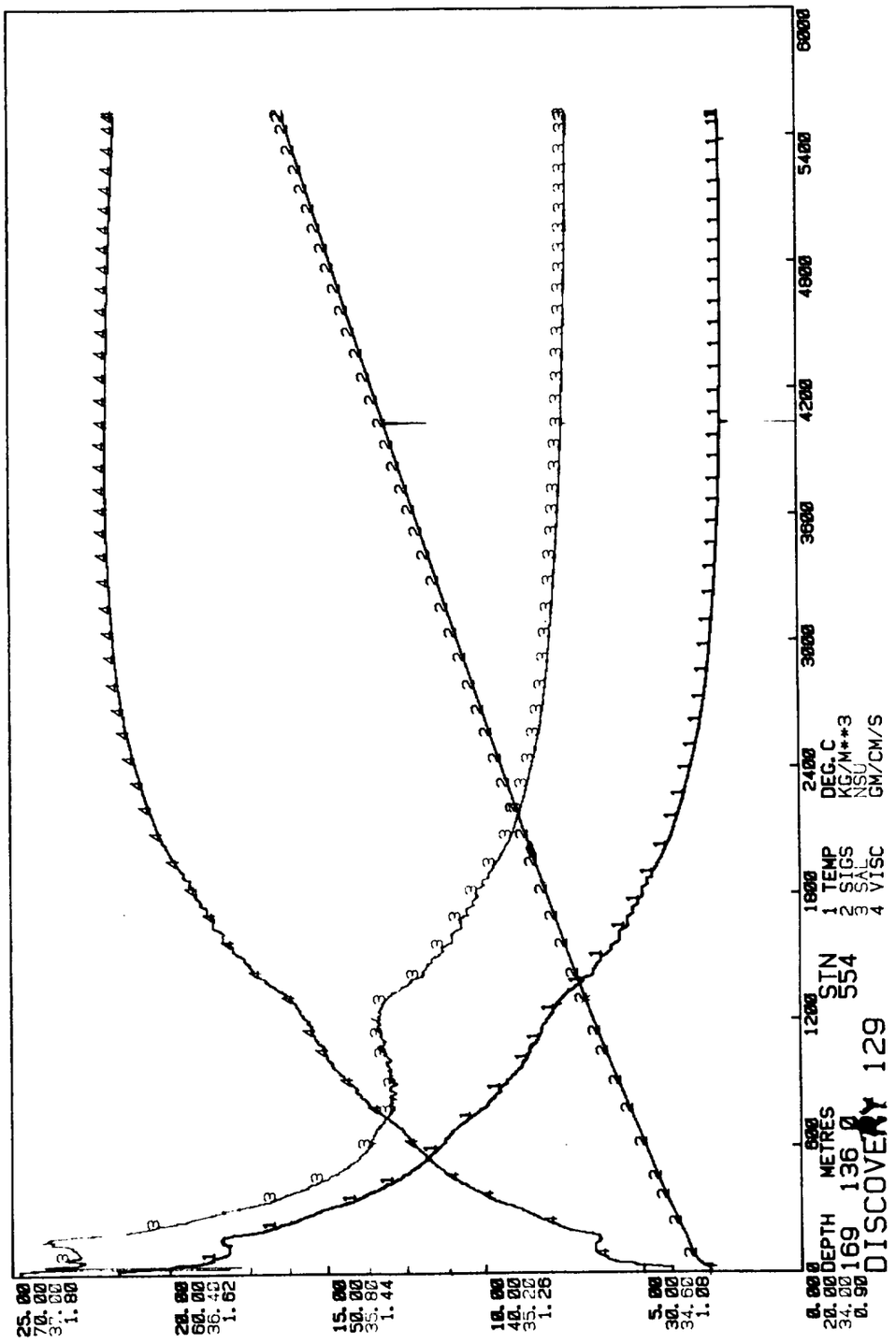

Figure 5.vi.2 Plot of CTD-derived data at G.M.E.

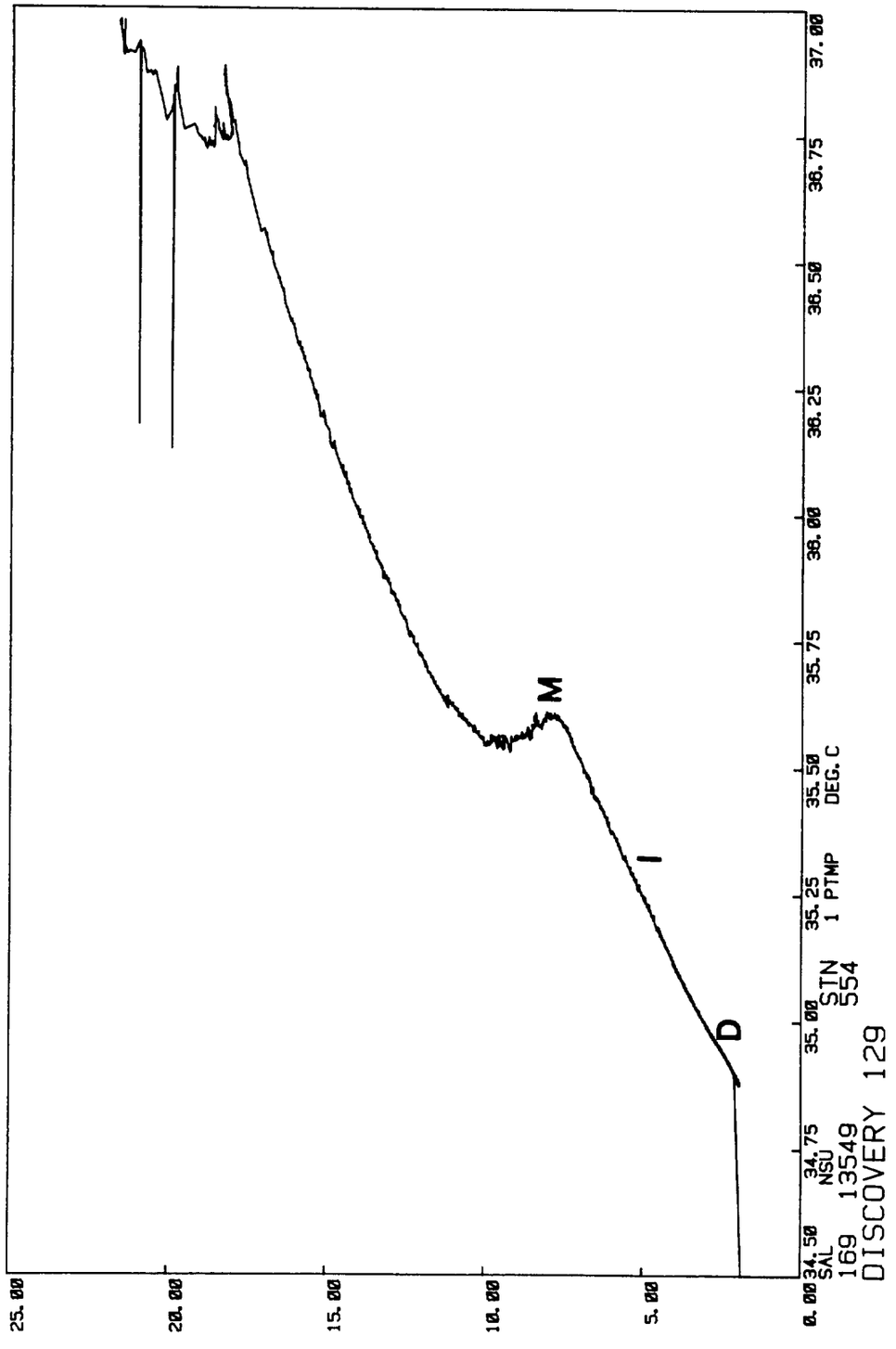

Figure 5.vi.3 Potential temperature - salinity plot showing water strucutre at G.M.E.

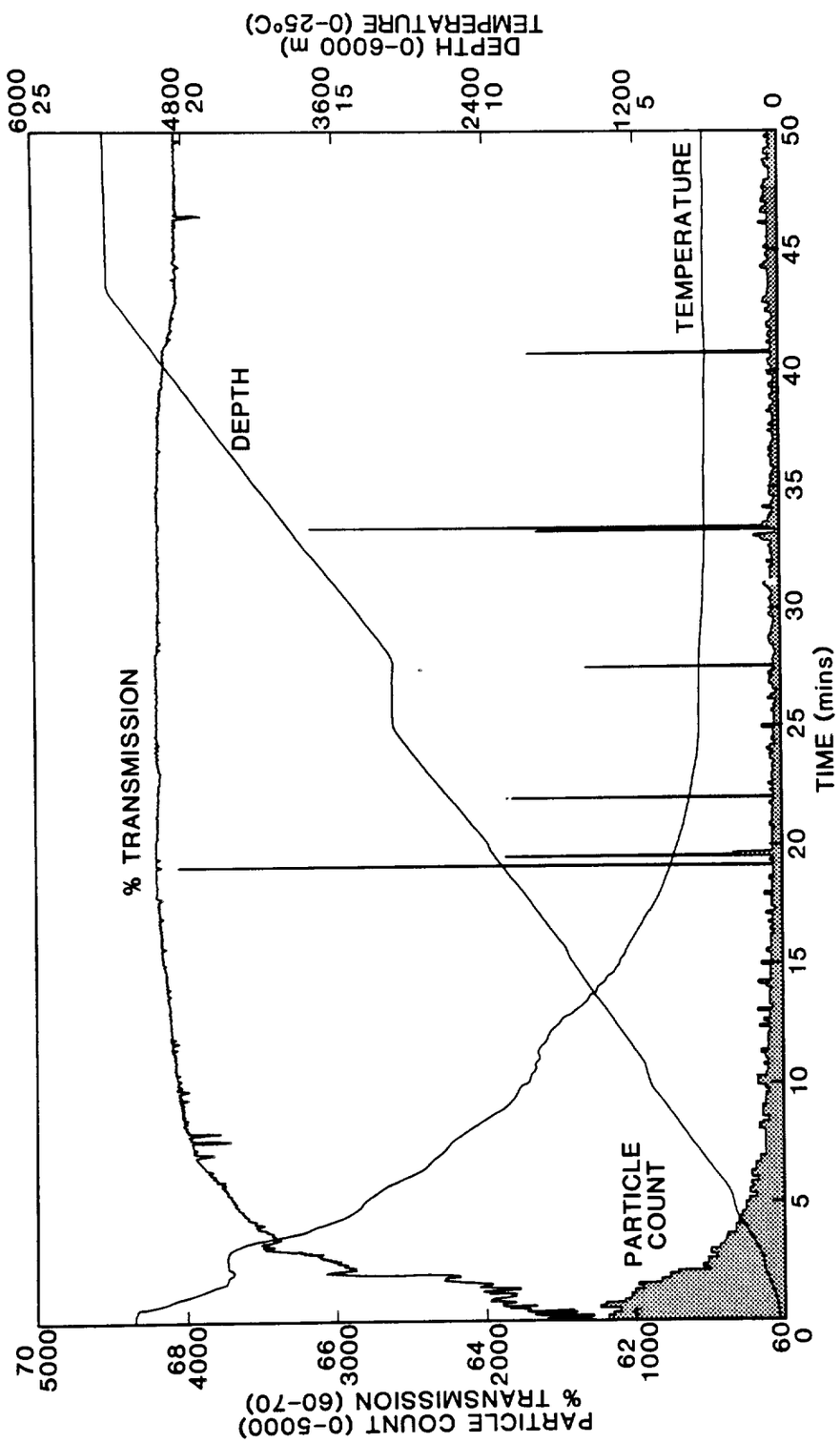

Figure 5.vi.4 Representation of real-time D.W.P.S. profile at G.M.E.

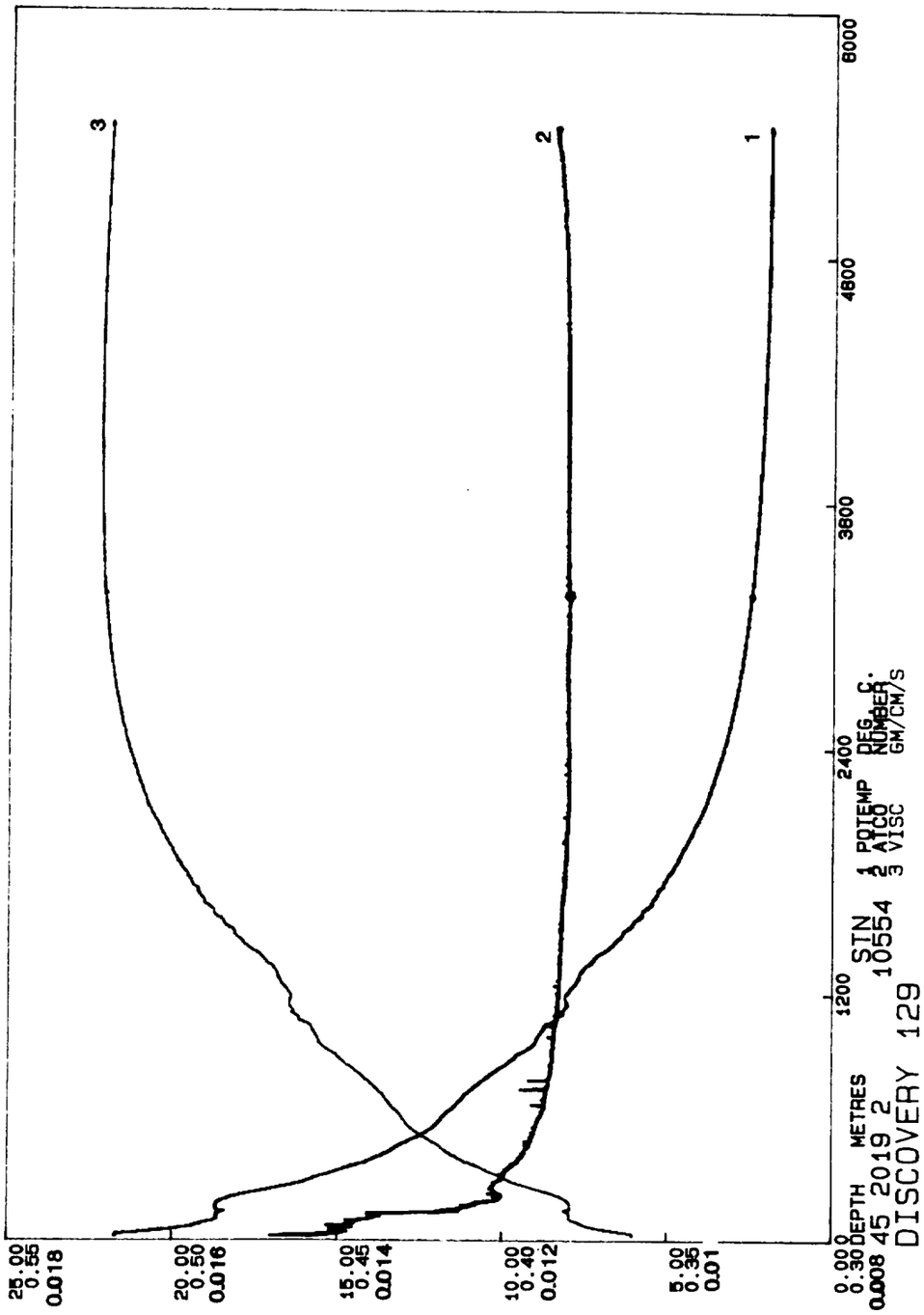

Figure 5.vi.5 Profiles of D.W.P.S. - derived data at G.M.E.

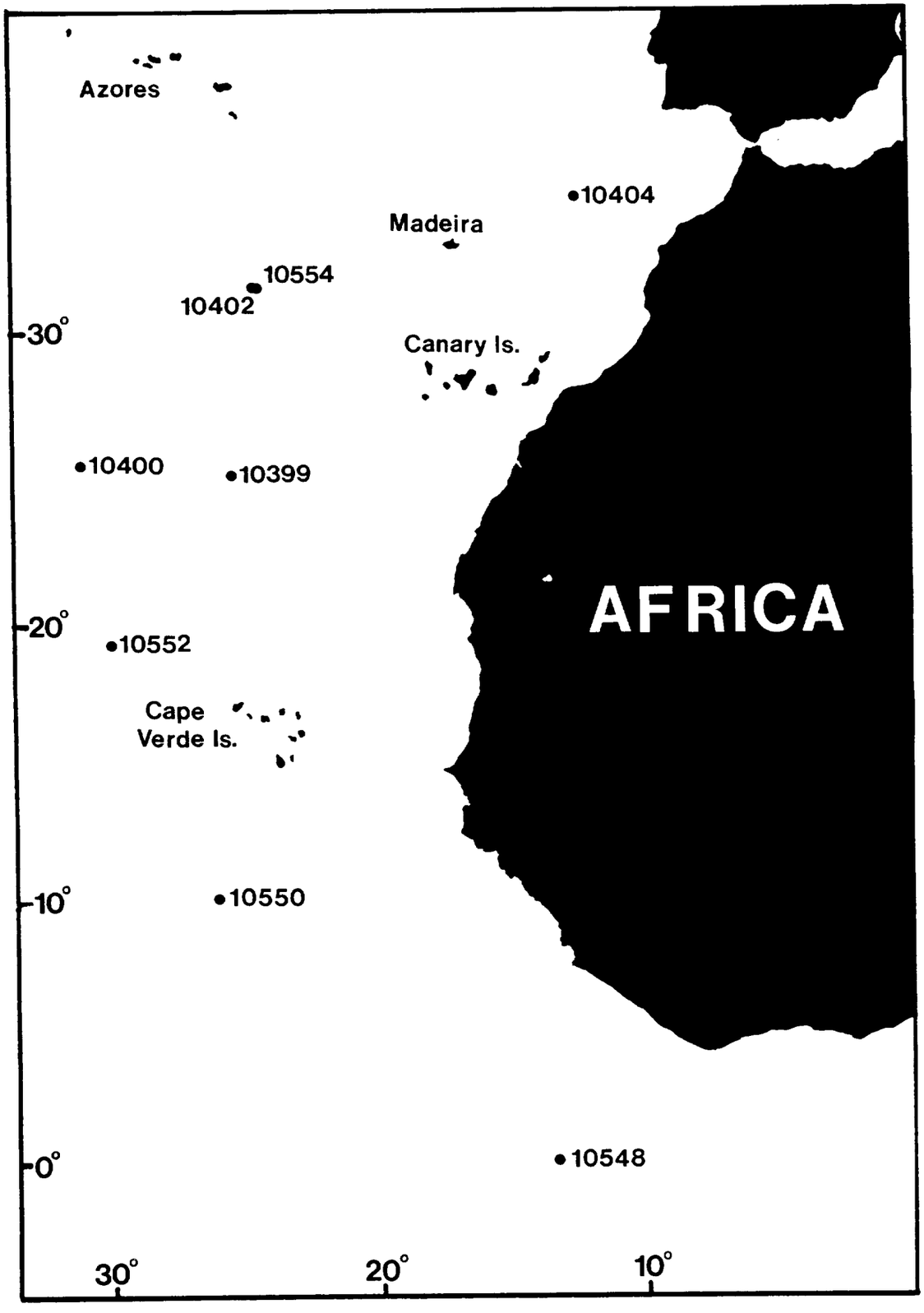

Figure 5.vi.6 Station positions works on Discovery Cruises 125 and 129. (G.M.E. at 10402 and 10554).

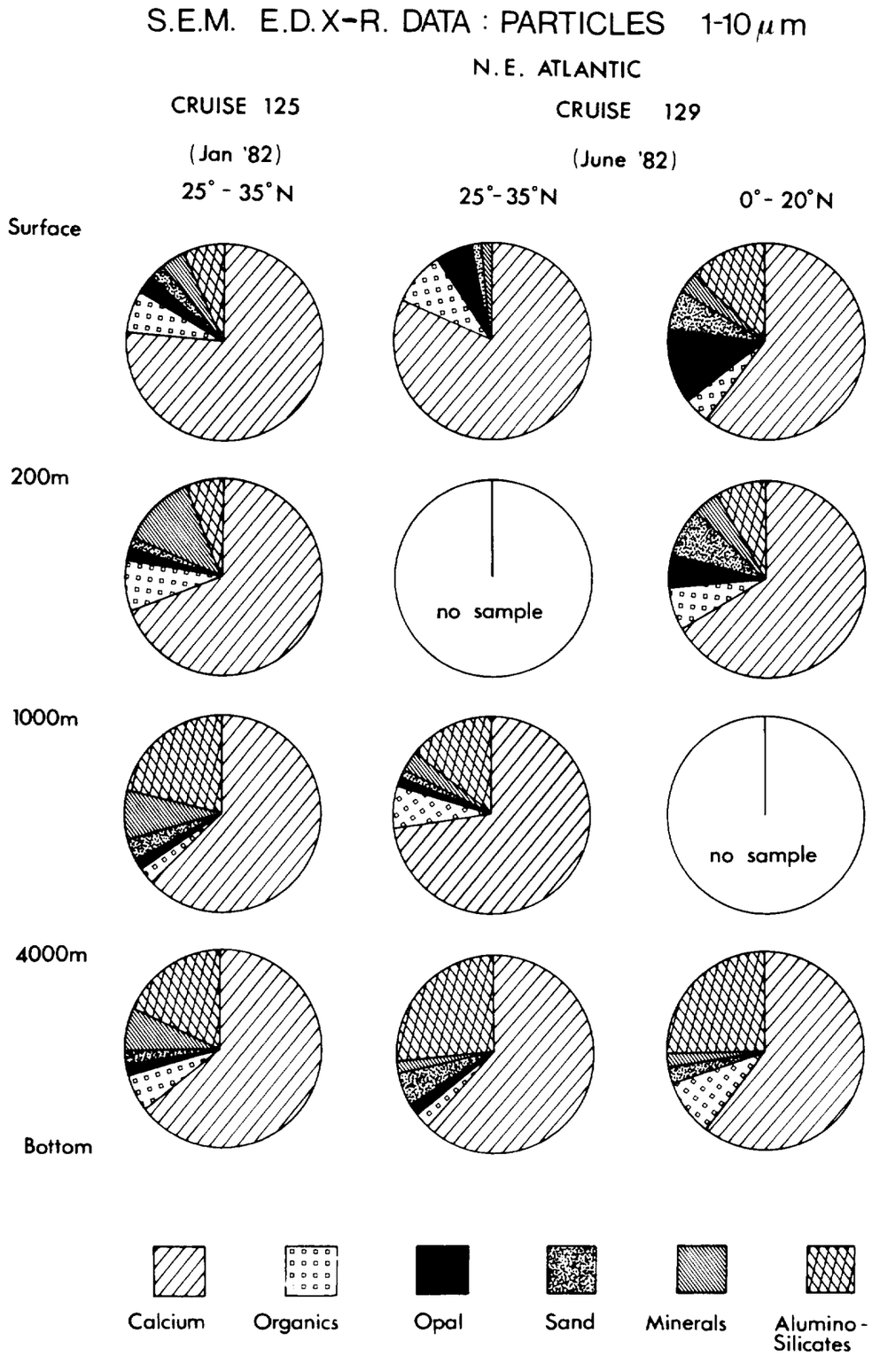

Figure 5.vi.7 Small particle S.E.M. analysis

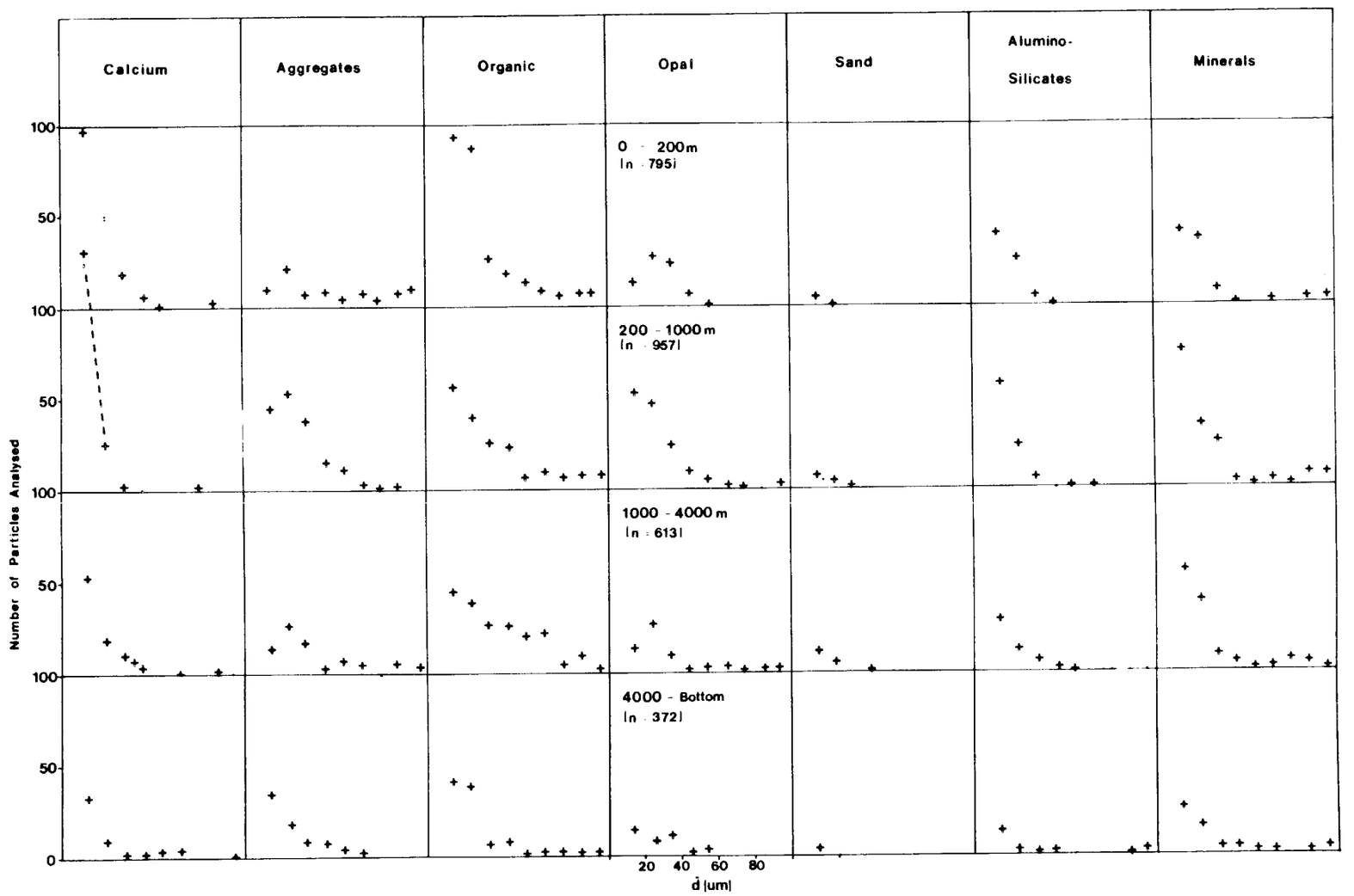

Figure 5.vi.8 Large particle S.E.M. analysis for Cruise 125.

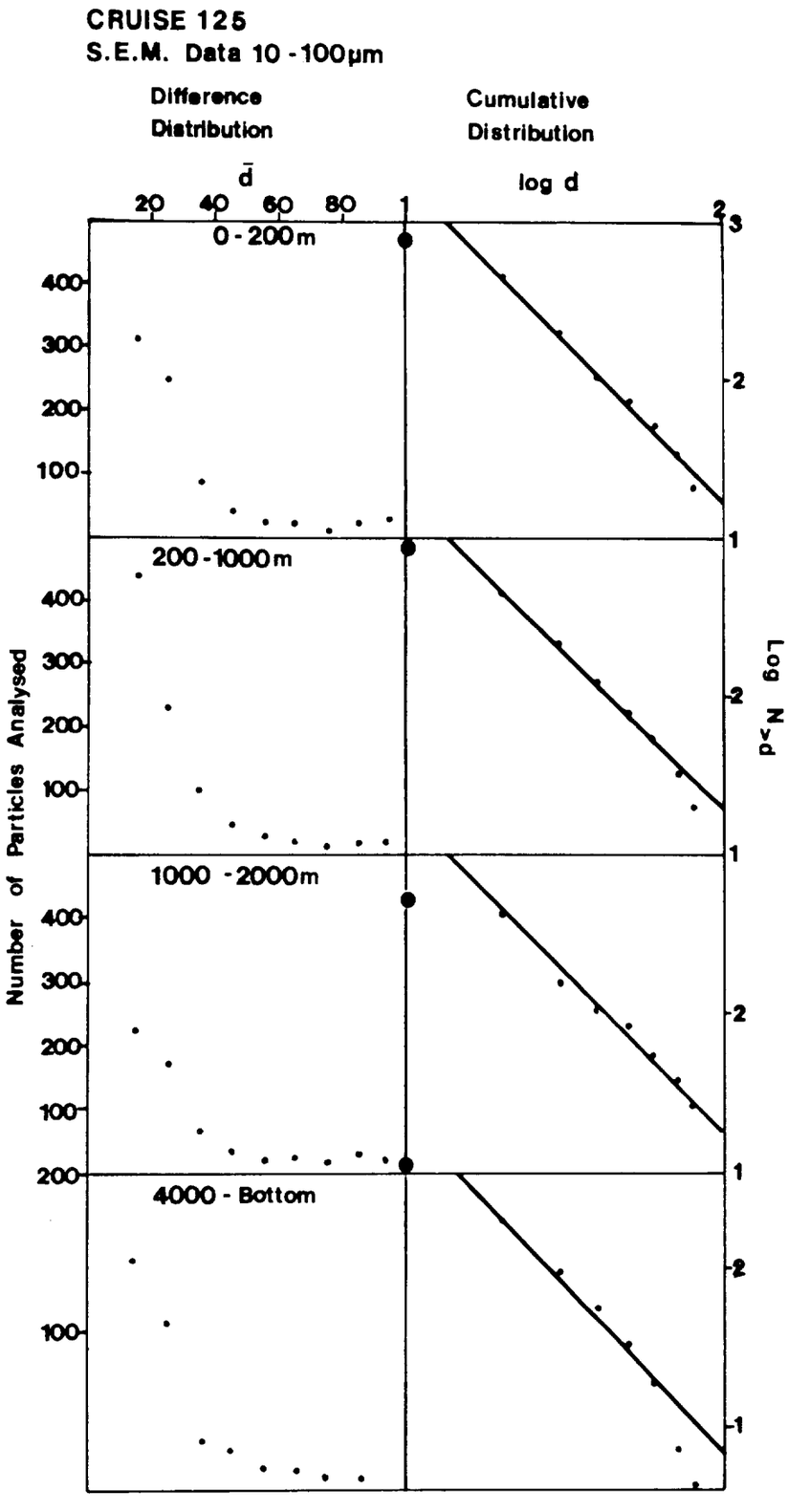

Figure 5.vi.9 Difference and cumulative number distributions derived from the large particle analysis.

CHAPTER 6

REFERENCES

ABBOT, D.H., MENKE, W. & MORIN, R. 1983
Constraints upon water advection in sediments of the Mariana Trough.
Journal of Geophysical Research, 88, 1075-1093.

ABDEL-MONEM, A., FERNANDEZ, L.A. & BOONE, G.A. 1968
Pliocene-Pleistocene minimum K-Ar ages of the older eruptive centers, eastern Azores.
Transactions of the American Geophysical Union, 49, p. 363. (Abstract).

ABDEL-MONEM, A.A., FERNANDEZ, L.A. & BOONE, G.A. 1975
K.Ar ages from the eastern Azores group (Santa Maria, Sao Miguel and the Formigas Islands).
Lithos, No. 4, 247-254.

ADDY, S.K. 1978
Distribution of Fe, Mn, Cu, Ni and Co in co-existing manganese nodules.
Marine Geology, 28, M9-M17.

ANDERSON, D.R. (Ed.) 1980
Proceedings of the Fifth Annual NEA-Seabed Working Group Meeting, Bristol, England, March 3-5, 1980.
Sandia National Laboratories, Albuquerque, NM, Report SAND-80-0754, 252pp.

ANDERSON, D.R. (Ed.) 1981
Proceedings of the Sixth Annual NEA Seabed Working Group Meeting, Paris, France, February 2-5, 1981.
Sandia National Laboratories, Albuquerque, NM, Report SAND-81-0427, 222pp.

ANDERSON, D.R. (Ed.) 1982
Seventh International NEA Seabed Working Group Meeting, La Jolla, California, 15-19 March, 1982.
Sandia National Laboratories, Albuquerque, NM, Report SAND-82-0460, 221pp.

ANDERSON, D.R. (Ed.) 1984
Eighth International NEA Seabed Working Group Meeting, Varese, Italy, 30 May - 3 June 1983.
Sandia National Laboratories, Albuquerque, NM, Report SAND-83-2122, 414pp.

ANDERSON, R.N., LANGSETH, M.G. & SCLATER, J.G. 1977
The mechanisms of heat transfer through the floor of the Indian Ocean.
Journal of Geophysical Research, 82, 3391-3409.

ANDERSON, R.N., HOBART, M.A. & LANGSETH, M.G. 1979
Geothermal convection through oceanic crust and sediments in the Indian Ocean.
Science, 204, 828-832.

ANGEL, M.V. & FASHAM, M.J.R. 1975
Analysis of the vertical and geographical distribution of the abundant species of planktonic ostracods in the north-east Atlantic.
Journal of the Marine Biological Association of the U.K., 55, 709-737.

ANGEL, M.V., FASHAM, M.J.R. & RICE, A.L. 1981
Marine biology needed to assess the safety of a program of disposal of high-level radioactive waste in the ocean.
pp. 297-312 in, Marine environmental pollution, Vol.2, Dumping and mining, (ed. R.A. Geyer).
Amsterdam: Elsevier, 574pp. (Elsevier Oceanography Series, 27B).

ANGEL, M.V. & BAKER. A. de C. 1982a
Vertical distribution of the standing crop of plankton and micronekton at three stations in the north-east Atlantic.
Biological Oceanography, 2, 1-30.

ANGEL, M.V., HARGREAVES, P.M., KIRKPATRICK, P. & DOMANSKI, P. 1982b
Low variability in planktonic and micronektonic populations at 1000m depth in the vicinity of 42N, 17W; evidence against diel migratory behaviour in the majority of species.
Biological Oceanography, 1, 287-319.

ANGEL, M.V. 1983
A vertical profile of planktonic ostracods from depths of 1500-3900m at a north-east Atlantic station.
pp. 549-559 in, Applications of Ostracoda, (ed. R.F. Maddocks).
Texas: University of Houston.

ARMI, L. & STOMMEL, H. 1983
Four views of a portion of the North Atlantic subtropical gyre.
Journal of Physical Oceanography, 13, 828-837.

AUFFRET, G., BUCKLEY, D., LAINE, E., SCHUTTENHELM, R., SEARLE, R.C. & SHEPHARD, L. 1984a
NEA Seabed Working Group status on site qualification for nuclear waste disposal within deep-sea sediment.
Sandia National Laboratories, Albuquerque, NM, Report SAND-83-2037, 64pp.

AUFFRET, G.A., LE SUAVE, R., KERBRAT, R., SICHLER, B., ROY, S., LAJ, C. & MULLER, C 1984b
Sedimentation in the southern Cape Verde Basin: seismic and sediment facies.
In, Fine-grained sediments, (ed. D.A.V. Stow & D.J.W. Piper).
Oxford: Blackwell Scientific Publications. (Geological Society Special Publication. No.15.)

BACKMAN, J. & SHACKLETON, N.J. 1983
Quantitative biochronology of Pliocene and early Pleistocene calcareous nannofossils from the Atlantic, Indian and Pacific Oceans.
Marine Micropaleontology, 8, 141-170.

BACON, M.P. & ANDERSON, R.F. 1982a
Distribution of thorium isotopes between dissolved and particulate forms in the deep sea.
Journal of Geophysical Research, 87, 2045-2056.

BACON, M.P. & ROSHOLT, J.N. 1982b
Accumulation rates of Th-230, Pa-231 and some transition metals on the Bermuda Rise.
Geochimica et Cosmochimica Acta, 46, 651-666.

BALISTRIERI, L.S., BREWER, P.G. & MURRAY, J.W. 1981
Scavenging residence times of trace metals and surface chemistry of sinking particles in the deep ocean.
Deep-Sea Research, 28A, 101-121.

BALISTRIERI, L.S. & MURRAY, J.W. 1983
Metal solid interactions in the marine environment: estimating apparent equilibrium binding constants.
Geochimica et Cosmochimica Acta, 47, 1091-1098.

BANDA, E., DANOBEITIA, J.J., SURINACH, E. & ANSORGE, J. 1981
Features of crustal structure under Canary Islands.
Earth and Planetary Science Letters, 55, 11-24.

BARRON, E.J. & WHITMAN, J.M. 1981
Oceanic sediments in space and time.
pp. 687-731 in The Sea, Vol.7: Oceanic lithosphere, (ed. C. Emiliani).
New York: John Wiley.

BATES, R.L. & JACKSON, J.A. (Eds) 1980
Glossary of geology (2nd edition).
Falls Church, Virginia: American Geological Institute, 749pp.

BECKER, K., VON HERZEN, R.P., FRANCIS, T.J.G., ANDERSON, R.N., HONNOREZ, J., ADAMSON, A.C., ALT, J.C., EMMERMANN, R., KEMPTON, P.D., Kinoshita, H., LAVERNE, C., MOTTL, M.J. & NEWMARK, R.L. 1982
In-situ electrical resistivity and bulk porosity of the oceanic crust Costa Rica Rift.
Nature, 300, 594-598.

BECKER, K. & VON HERZEN, R.P. 1983
Heat flow on the western flank of the East Pacific Rise at 21N.
Journal of Geophysical Research, 88, 1057-1066.

BELDERSON, R.H., KENYON, N.H. & WILSON, J.B. 1973
Iceberg plough marks in the north-east Atlantic.
Palaeogeography, Palaeoclimatology, Palaeoecology, 13, 215-224.

BENDER, M.L. 1971
Does upward diffusion supply the excess manganese in pelagic sediments?
Journal of Geophysical Research, 76, 4212-4215.

BERGER, W.H. & VON RAD, U. 1972
Cretaceous and Cenozoic sediments from the Atlantic Ocean.
Initial Reports of Deep Sea Drilling Project, 14, 787-954.

BERNER, R.A. 1980
Early diagenesis: a theoretical approach.
Princeton NJ: Princeton University Press. 241pp.

BILLETT, D.S.M. & HANSEN, B. 1982
Abyssal aggregations of Kolga hyalina Danielssen and Koren (Echinodermata: Holothurioidea) in the north-east Atlantic Ocean: a preliminary report.
Deep Sea Research, 29A, 799-818.

BILLETT, D.S.M., LAMPITT, R.S., RICE, A.L. & MANTOURA, R.F.C. 1983
Seasonal sedimentation of phytoplankton to the deep-sea benthos.
Nature, 302, 520-522.

BISCHOFF, J.L., GREER, R.E. & LUISTRO, A.O. 1970
Composition of interstitial waters of marine sediments: temperature of squeezing effect.
Science, 167, 1245-1246.

BISCHOFF, J.L., HEATH, G.R. & LEINEN, M. 1979
Geochemistry of deep-sea sediments from the Pacific Manganese Nodule Province: DOMES sites A, B and C.
pp. 397-436 in, Marine geology and oceanography of the Pacific Manganese Nodule Province (ed. J.L. Bischoff & D.Z. Piper).
New York: Plenum Press.

BONATTI, E., FISHER, D.F., JOENSUU, O. & RYDELL, H.S. 1971
Post-depositional mobility of some transition elements, phosphorus uranium and thorium in deep-sea sediments.
Geochimica et Cosmochimica Acta, 35, 189-201.

BOSSHARD, E. & MACFARLANE, D.J. 1970
Crustal structure of the western Canary Islands from seismic refraction and gravity data.
Journal of Geophysical Research, 75, 4901-4918.

BOUMA, A.H. 1962
Sedimentology of some flysch deposits.
Amsterdam: Elsevier. 168pp.

BOUMA, A.H. 1964
Notes on the X-ray interpretation of marine sediments.
Marine Geology, 2, 278-309.

BOUMA, A.H. 1969
Methods for the study of sedimentary structures.
New York: Wiley-Interscience. 458pp.

BOUMA, A.H. & HOLLISTER, C.D. 1973
Deep ocean basin sedimentation.
pp. 79-118 in, Turbidites and deep-water sedimentation. (Lecture notes for short course 12 May 1983.)
Los Angeles: Society of Economic Paleontologists and Mineralogists (Pacific Section). 158pp.

BOYCE, R.E. & BODE, G.W. 1972
Carbon and carbonate analyses, Leg 9.
Initial Reports of the Deep Sea Drilling Project, 9, 797-816.

BOYLE, E.A., SCLATER, F.R. & EDMOND, J.M. 1977
The distribution of dissolved copper in the Pacific.
Earth and Planetary Science Letters, 37, 38-54.

BOYLE, E.A., HUESTED, S.S. & JONES, S.P. 1981
On the distribution of copper, nickel and cadmium in the surface waters of the North Atlantic and North Pacific Oceans.
Journal of Geophysical Research, 86, 8048-8066.

BREDEHOEFT, J.D. & PAPADOPULOS, I.S. 1965
Rates of vertical groundwater movement estimated from the Earth's thermal profile.
Water Resources Research, 1, 325-328.

BREWER, P., SPENCER, D.W., BISCAYE, P.G., HANLEY, A., SACHS, P.L., SMITH, C.L., KADAR, S. & FREDERICKS, J. 1976
The distribution of particulate matter in the Atlantic Ocean.
Earth and Planetary Science Letters, 32, 393-402.

BRULAND, K.W. 1980
Oceanographic distributions of cadmium, zinc, nickel and copper in the North Pacific.
Earth and Planetary Science Letters, 47, 176-198.

BRYANT, W.R., DEFLACHE, A.P. & TRABANT, P.K. 1974
Consolidation of marine clays and carbonates.
pp. 209-244 in, Deep sea sediments: physical and mechanical properties, (ed. A.L. Inderbitzen).
New York: Plenum.

BUAT-MENARD, P. 1979a
Influence de la retombee atmospherique sur la chimie des metaux en trace dans la matiere en suspension de l'Atlantique nord.
Universite de Paris VII, Docteur es Science These. 434pp.

BUAT-MENARD, P. & CHESSELET, R. 1979b
Variable influence at the atmospheric flux on the trace metal chemistry of oceanic suspended matter.
Earth and Planetary Science Letters, 42, 399-411.

BUAT-MENARD, P., ARNOLD, M., BARON, D., BERNARD, H. & CHESSELET, R. 1980
Particulate trace metal chemistry in the open ocean and western Mediterranean: a comparative study.
pp. 1005-1010 in, Ves Journees d'Etudes sur les pollutions marines en Mediterranee, Cagliari 1980.
Monaco: Commission International pour l'Exploration Scientifique de la Mer Mediterranee.

BUCHAN, S., DEWES, F.C.D., JONES, A.S.G., MCCANN, D.M. & SMITH, D.T. 1971
The acoustic and geotechnical properties of North Atlantic cores. Vols 1 & 2
University College of North Wales, Marine Science Laboratories, Geological Report No. 71-1. (200pp. in 2 volumes).

BULLARD, E.C. 1954
The flow of heat through the floor of the Atlantic Ocean.
Proceedings of the Royal Society of London, A, 222, 408-429.

BURDIGE, D.J. & GIESKES, J.M. 1983
A pore water/solid phase diagenetic model for manganese in marine sediments.
American Journal of Science, 283, 29-47.

BURGESS, M. & JUDGE, A. 1981
Heat-flow studies in the Sohm Abyssal Plain and their relevance to nuclear waste disposal investigations.
Canada, Energy Mines & Resources, Earth Physics Branch, Open File No. 81-15, 21pp. & figs.

BURNS, R.E. 1963
A note on some possible misinformation from cores obtained by piston-type coring devices.
Journal of Sedimentary Petrology, 33, 950-952.

CANN, J.R. & FUNNELL, B.M. 1967
Palmer Ridge: a section through the upper part of the ocean crust?
Nature, 213, 661-664.

CARPENTER, M.S.N., COLLEY, S., ELDERFIELD, H., KENNEDY, H.A., THOMSON, J. & WILSON, T.R.S. 1983
Geochemistry of the near surface sediments of the Nares Abyssal Plain.
Institute of Oceanographic Sciences, Report No. 174, 66pp.

CASAGRANDE, A. 1936
The determination of the preconsolidation load and its practical significance.
p.60 in, Proceedings 1st International Conference of Soil Mechanics and Foundation Engineers, Cambridge, Massachusetts, 1936.

CHAPMAN, E., HYDES, D.J. & COX, A. 1983
A method for determining Cd, Cu, and Ni in marine sediment pore water samples.
Institute of Oceanographic Sciences, Internal Document No. 194, 21pp. (Unpublished manuscript.)

CHESTER, R. & MESSIHA-HANNA, R.G. 1970
Trace element partition patterns in North Atlantic deep-sea sediments.
Geochimica et Cosmochimica Acta, 34, 1121-1128.

CHESTER, R. & JOHNSON, L.R. 1971
Trace element geochemistry of North Atlantic aeolian dusts.
Nature, 231, 176-178.

CHESTER, R., JOHNSON, L.R., MESSIHA-HANNA, R.G. & PADGHAM, R.C. 1973
Similarities between Mn, Ni and Co contents of deep-sea clays and manganese nodules from the south-west region of the North Atlantic.
Marine Geology, 14, M15-M20.

CHESTER, R. & ASTON, S.R. 1976
The geochemistry of deep-sea sediments.
pp. 281-390 in, Chemical oceanography (2nd ed.) vol.6 (ed. J.P. Riley and R. Chester).
London: Academic Press.

CHILDRESS, J.J. & PRICE, M.H. 1978
Growth rate of the bathypelagic crustacean Gnathophausia ingens (Mysidacea: Lophogastridae). I. Dimensional growth rate and population structure.
Marine Biology, 50, 47-62.

CLINE, J.D. & RICHARDS, F.A. 1972
Oxygen deficient conditions and nitrate reduction in the eastern tropical North Pacific Ocean.
Limnology & Oceanography, 17, 885-900.

COCHRAN, K.J. & KRISHNASWAMI, S. 1980
Radium, thorium, uranium and 210Pb in deep-sea sediments and sediment pore waters from the north equatorial Pacific.
American Journal of Science, 280, 849-889.

COHEN, Y. 1978
Consumption of dissolved nitrous oxide in an anoxic basin, Saanich Inlet, British Columbia.
Nature, 272, 235-237.

COLLETTE, B.J., SLOOTWEG, A.P. VERHOEF, J. & ROEST, W.R. 1984
Geophysical investigations of the floor of the Atlantic Ocean between 10 and 38N (Kroonflag-Project).
Proceedings, K. Nederlandse akademie van wetenschappen, B. 87(1).

COLLEY, S., THOMSON, J., WILSON, T.R.S. & HIGGS, N.C. 1984
Post-depositional migration of elements during diagenesis in brown clay and turbidite sequences in the north-east Atlantic.
Geochimica et Cosmochimica Acta, 48, 1223-1235.

CRANK, J. 1956
The mathematics of diffusion.
Oxford: Clarendon Press. 347pp.

CREAGER, J.S. & STERNBERG, R.W. 1963
Comparative evaluation of three techniques of pipette analysis.
Journal of Sedimentary Petrology, 33, 462-466.

CRONIN, T.M. 1983
Rapid sea level and climate change: evidence from continental and island margins.
Quaternary Science Reviews, 1, 177-214.

CROWE, J. & MCDUFF, R.E. 1979
Temperature and pore water chemistry profiles of sediments in the equatorial Pacific: incompatible results?
EOS, Transactions of the American Geophysical Union, 60, p.863. (Abstract.)

CROWLEY, T.J. 1981
Temperature and circulation changes in the eastern North Atlantic during the last 150,000 years: evidence from the planktonic foraminiferal record. Marine Micropaleontology, 6, 97-129.

CROWLEY, T.J. 1983
Calcium carbonate preservation patterns in the central North Atlantic during the last 150,000 years.
Marine Geology, 51, 1-14.

CULKIN, F. et al 1980
RRS 'Discovery' Cruise 108, 18 February - 3 March 1980.
Geochemical sampling on the Nares Abyssal Plain.
Institute of Oceanographic Sciences, Cruise Report No.99, 7pp. & figs.

DAMUTH, J.E. 1980
Use of high-frequency (3.5-12 KHz) echograms in the study of near-bottom sedimentation processes in the deep-sea: a review.
Marine Geology, 38, 51-75.

DEHAIRS, F., CHESSELET, R. & JEDWAB, J. 1980
Discrete suspended particles of barite and the barium cycle in the open ocean.
Earth and Planetary Science Letters, 49, 528-550.

DELANY, A.C., DELANY, A.C. PARKIN, D.W., GRIFFIN, J.J., GOLDBERG, E.D. & REIMANN, B.E.F. 1967.
Airborne dust collected at Barbados.
Geochimica et Cosmochimica Acta, 31, 885-909.

DEMASTER, D.J. & COCHRAN, K.J. 1982
Particle mixing rates in deep-sea sediments determined from excess 210Pb and 32Si profiles.
Earth and Planetary Science Letters, 61, 257-271.

DEUSER, W.G. & ROSS, E.H. 1979
Seasonal change in the flux of organic carbon to the deep Sargasso Sea.
Nature, 283, 364-365.

DEUSER, W.G., ROSS, E.H. & ANDERSON, R.F. 1981
Seasonality in the supply of sediment to the deep Sargasso Sea and implications for the rapid transfer of matter to the deep ocean.
Deep-Sea Research, 28A, 495-505.

DE VRIES, D.A. 1958
Simultaneous transfer of heat and moisture in porous media.
EOS, Transactions of the American Geophysical Union, 39, 909-916.

DUIN, E.J.T. & KUIJPERS, A. 1983
Contribution to the Seabed Working Group Programmes. Progress report 1982.
Geological studies on abyssal plains in the North Atlantic.
Haarlem: Rijks Geologische Dienst. 107pp. & 7 charts. (Unpublished manuscript)

DUIN, E.J.T., MESDAG, C.S. & KOK, P.T.J. 1984
Faulting in Madeira Abyssal Plain sediments.
Marine Geology, 56, 299-308.

DUNN, D.A. 1980
Revised techniques for quantitative calcium carbonate analysis using the 'Karbonat-bombe' and comparisons to other quantitative carbonate analysis methods.
Journal of Sedimentary Petrology, 50, 631-636.

ELDERFIELD, H. & GREAVES, M.J. 1982
The rare earth elements in seawater.
Nature, 296, 214-219.

ELLIOT, A.J. & THORPE, S.A. 1983
Benthic observations on the Madeira Abyssal Plain.
Oceanologica Acta, 6, 463-466.

EMBLEY, R.W. 1975
Studies of deep-sea sedimentation processes using high frequency seismic data.
Columbia University, PhD. thesis, 332pp.

EMBLEY, R.W. 1976
New evidence for occurrence of debris flow deposits in the deep sea.
Geology, 4, 371-374.

EMBLEY, R.W. & JACOBI, R.D. 1977
Exotic middle Miocene sediment from Cape Verde Rise and its relation to Piercement structures.
American Association of Petroleum Geologists Bulletin, 61, 2004-2009.

EMBLEY, R.W. 1980
The role of mass transport in the distribution and character of deep-ocean sediments with special reference to the North Atlantic.
Marine Geology, 38, 23-50.

EMBLEY, R.W. 1982
Anatomy of some Atlantic Margin sediment slides and some comments on ages and mechanisms.
pp. 189-213 in, Marine slides and other mass movements, (ed. S. Saxov & J.K. Nieuwenhuis).
New York: Plenum. 353pp.

EMBLEY, R.W., HOBART, M.A., ANDERSON, R.N. & ABBOTT, D. 1983
Anomalous heat flow in the north-west Atlantic: a case for continued hydrothermal circulation in 80-M.Y. crust.
Journal of Geophysical Research, 88, 1067-1074.

EMERSON, S., JAHNKE, R., BENDER, M.L., FROELICH, P.N., KLINKHAMMER, G.P., BOWSER, C & SETLOCK, G. 1980
Early diagenesis in sediments from the eastern equatorial Pacific. 1. Pore water nutrient and carbonate results.
Earth and Planetary Science Letters, 49, 57-80.

EMILIANI, C. 1955
Pleistocene temperatures.
Journal of Geology, 63, 538-578.

EWING, J. & EWING, M. 1959
Seismic-refraction measurements in the Atlantic Ocean basins, in the Mediterranean Sea, on the Mid-Atlantic Ridge, and in the Norwegian Sea.
Bulletin of the Geological Society of America, 70, 291-318.

FANNING, K.A. & PILSON, M.E.Q. 1974
The diffusion of dissolved silica out of deep-sea sediments.
Journal of Geophysical Research, 79, 1293-1297.

FLOOD, R.D. 1978
Studies of deep-sea sedimentary microtopography in the North Atlantic Ocean.
Woods Hole Oceanographic Institution/Massachusetts Institute of Technology, Doctoral Dissertation WHOI-78-64, 394pp. (Unpublished manuscript).

FLOOD, R.D. 1980
Deep-sea sedimentary morphology: modelling and interpretation of echo-sounding profiles.
Marine Geology, 38, 77-92.

FOWLER, S.W., BALLESTRA, S. LA ROSA, J. & FUKAI, R. 1983
Vertical transport of particulate-associated plutonium and americium in the upper water column of the north-east Pacific.
Deep-Sea Research, 30A, 1221-1233.

FRANCIS, T.J.G. et al 1981a
RRS 'Shackleton' Cruise 8/79, 31 August - 30 September 1979. Geology and geophysics in the north-east Atlantic and on the Mid-Atlantic Ridge.
Institute of Oceanographic Sciences, Cruise Report No. 110, 9pp.

FRANCIS, T.J.G. et al 1981b
RRS 'Discovery' Cruise 118, 11 February - 30 March 1981. Geophysics and sediment sampling in the north-east Atlantic.
Institute of Oceanographic Sciences, Cruise Report No.117, 33pp.

FRANCIS, T.J.G. et al 1983
RRS 'Discovery' Cruise 126, 4 March - 3 April 1982. Geological and geophysical studies between the Azores and the Canaries.
Institute of Oceanographic Sciences, Cruise Report No.141, 21pp. & figs.

FRANCIS, T.J.G. et al 1984
RRS 'Discovery' Cruise 134, 1-26 March, 1983.
Institute of Oceanographic Sciences, Cruise Report. (In preparation.)

FREELAND, H.J., RHINES, P.B. & ROSSBY, H.T. 1975
Statistical observations of the trajectories of neutrally buoyant floats in the North Atlantic.
Journal of Marine Research, 33, 383-404.

FREEMAN, T.J., CARLYLE, S.G., FRANCIS, T.J.G. & MURRAY, C.N. 1984
The use of large-scale penetrators for the measurement of deep-ocean sediment properties.
pp. 0I.1.8/1 - 1.8/8 in, Oceanology International exhibition and conference, 1984, Brighton.
Kingston-upon-Thames: Spearhead Publications Ltd.

FROELICH, P.N., KLINKHAMMER, G.P., BENDER, M.L., LUEDTKE, N.A., HEATH, G.R., CULLEN D., DAUPHIN, P., HAMMOND, D., HARTMAN, B. & MAYNARD, V. 1979
Early oxidation of organic matter in pelagic sediments of the eastern equatorial Atlantic: suboxic diagenesis.
Geochimica et Cosmochimica Acta, 43, 1075-1090.

GARDNER, J.V. 1975
Late Pleistocene carbonate dissolution cycles in the eastern equatorial Atlantic.
pp. 129-141 in, Dissolution of deep-sea carbonates, (ed. W.V. Sliter, A.W.H.Be & W.H. Berger).
Cushman Foundation for Foraminiferal Research, Special Publication, 13, 129-141.

GARTNER, S. & EMILIANI, C. 1976
Nannofossil biostratigraphy and climate stages of Pleistocene Brunhes Epoch.
American Association of Petroleum Geologists Bulletin, 60, 1562-1564.

GESAMP. 1983
An oceanographic model for the dispersion of wastes disposed of in the deep-sea.
GESAMP Reports and Studies, No.19, 182pp.

GLACCUM, R.A. 1978
The mineralogical and elemental composition of marine aerosols over the North Atlantic: the influence of Saharan dust.
University of Miami, Ph.D. Thesis. 160pp.

GOERING, J.J. 1968
Denitrification in the oxygen minimum layer of the eastern tropical Pacific Ocean.
Deep-Sea Research, 15, 157-164.

GOLDBERG, E.D. & BRULAND, K.W. 1974
Radioactive geochronologies.
pp. 451-489 in, The Sea. Vol.5: Marine chemistry, (ed. E.D. Goldberg).
New York: John Wiley & Sons.

GOLOWAY, F. & BENDER, M. 1982
Diagenetic models of interstitial nitrate profiles in deep sea suboxic sediments.
Limnology & Oceanography, 27, 624-638.

GOULD, W.J., HENDRY, R.M. & HUPPERT, H.E. 1981
An abyssal topographic experiment.
Deep-Sea Research, 28A, 409-440.

GOULD, W.J. 1982
Long range acoustic propagation trials June-July 1982, RRS 'Discovery' Cruise 130.
Institute of Oceanographic Sciences, Internal Document No. 167, 5pp & figs. (Unpublished manuscript.)

GOULD, W.J. et al 1983
RRS 'Discovery' Cruise 138, 17 June - 9 July 1983. Current studies and CTD stations in the Discovery Gap and in the Madeira Basin.
Institute of Oceanographic Sciences, Cruise Report No. 152, 25pp.

GRIFFIN, J.J., WINDOM, H.L. & GOLDBERG, E.D. 1968
The distribution of clay minerals in the world ocean.
Deep-Sea Research, 15, 433-459.

GRIMAUD, S., BOILLOT, G., COLLETTE, B.J., MAUFFRET, A., MILES, P.R. & ROBERTS, D.G. 1982
Western extension of the Iberian-European plate-boundary during the early Cenozoic (Pyrenean) convergence: a new model.
Marine Geology, 45, 63-77.

GRUNDMANIS, V. & MURRAY, J.W. 1982
Aerobic respiration in pelagic marine sediments.
Geochimica et Cosmochimica Acta, 46, 1101-1120.

GUSTAFSSON, L. 1960
Determination of ultramicro amounts of sulphate as methylene blue: 1. The colour reaction.
Talanta, 4, 227-235.

HAEDRICH, R.L. & ROWE, G.T. 1977
Megafaunal biomass in the deep sea.
Nature, 269, 141-142.

HAMBLIN, W.K. 1965
Origin of 'reverse drag' on the downthrown side of normal faults.
Geological Society of America Bulletin, 76, 1145-1164.

HAMILTON, E.L. 1979
Sound velocity gradients in marine sediments.
Journal of the Acoustical Society of America, 65, 909-922.

HAMILTON, E.L. 1980
Geoacoustic modeling of the sea floor.
Journal of the Acoustical Society of America, 68, 1313-1340.

HARGREAVES, P.M., ELLIS, C.J. & ANGEL, M.V. 1983
An assessment of biological processes close to the sea-bed in a slope region and its significance to the assessment of sea-bed disposal of radioactive waste.
Institute of Oceanographic Sciences, Report No. 185, 114pp.

HARGREAVES, P.M. 1984
The distribution of Decapoda (Crustacea) in the open ocean and near-bottom over an adjacent slope in the northern north-east Atlantic Ocean during Autumn 1979.
Journal of the Marine Biological Association of the UK, 64, 829-857.

HARLAND, W.B., COX, A.V., LLEWELLYN, P.G., PICKTON, C.A.G, SMITH, A.G. & WALTERS,R. 1982
A geologic time-scale.
Cambridge: Cambridge University Press. 131pp.

HARTMANN, M., MULLER, P.J., SUESS, E. & VAN DER WEIJDEN, C.H. 1976
Chemistry of Late Quaternary sediments and their interstitial waters from the NW African continental margin.
'Meteor' Forschungsergebnisse, C. No. 24, 1-67.

HASKIN, M.A. & HASKIN, L.A. 1966
Rare earths in European shales: a redetermination.
Science, 154, 507-509.

HAYES, D.E., PIMM, A.C. et al. 1972
Initial Reports of Deep Sea Drilling Project, Vol.14.
Washington: U.S. Government Printing Office, 975pp.

HEEZEN, B.C. & HOLLISTER, C.H. 1971
The face of the deep.
New York: Oxford University Press. 659pp.

HEM, J.D. 1978
Redox processes at surfaces of manganese oxide and their effects on aqueous metal ions.
Chemical Geology, 21, 199-218.

HOFFMAN, J. 1957
Hyperbolic curves applied to echo-sounding.
International Hydrographic Review, 34(2), 45-55.

HOGG, N., BISCAYE, P., GARDNER, W. & SCHMITZ, W.J. 1982
On the transport and modification of Antarctic Bottom Water in the Vema Channel.
Journal of Marine Research, 40, Supplement, 231-263.

HOLLISTER, C.D., ANDERSON, D.R. & TALBERT, D.M. 1976
The first international workshop on seabed disposal of high-level wastes. pp.639-657 in, Proceedings of the International Symposium on the Management of Wastes from the LWR Fuel Cycle, Denver, Co., 11-16 July 1976.
Washington, D.C.: Energy Research & Development Administration. 759pp.

HOLLISTER, C.D., FLOOD, R. & MCCAVE, I.N. 1978
Plastering and decorating in the North Atlantic.
Oceanus, 21(1), 5-13.

HONEA, J.W. 1956
Sam Fordyce - Vanderbilt fault system of southwest Texas.
Transactions of the Gulf-Coast Association of Geological Societies, 6, p.51.

HONJO, S. 1982
Seasonality and interaction of biogenic and lithogenic particulate flux at the Panama Basin.
Science, 218, 883-884.

HOUTZ, R.E. & EWING, J.T. 1963
Detailed sedimentary velocities from seismic refraction profiles in the western North Atlantic.
Journal of Geophysical Research, 68, 5233-5258.

HSU, K.J. et al 1978
Initial reports of the Deep Sea Drilling Project, Vol.42, Part 1.
Washington: U.S. Government Printing Office. 1249pp.

HUGGETT, Q.J. & KIDD, R.B. 1984
The distribution of ice-rafted and other exotic material in deep-sea dredge hauls.
Geo-Marine Letters, 3, 23-29.

HYDES, D.J. 1984
A manual of methods for continuous flow analysis.
Institute of Oceanographic Sciences, Report No. 177. (In press).

IAGA Division I, Working Group 1. 1981
International Geomagnetic Reference Fields: DGRF 1965, DGRF 1970, DGRF 1975 and IGRF 1980.
EOS, Transactions of the American Geophysical Union, 62, p.1169.

INMAN, D.L. 1952
Measures for describing the size distribution of sediments.
Journal of Sedimentary Petrology, 22, 125-145.

I.O.S. 1978
Oceanography related to deep-sea waste disposal.
Institute of Oceanographic Sciences, Report No.77, 261pp.

JACOBI, R.D. 1976
Sediment slides on the north-western continental margin of Africa.
Marine Geology, 22, 157-173.

JACOBI, R.D. & HAYES, D.E. 1982
Bathymetry, microphysiography and reflectivity characteristics of the West African Margin between Sierra Leone and Mauritania.
pp. 182-212 in, Geology of the northwest African continental margin, (ed. U. Von Rad, K. Hinz, M. Sarnthein & E. Seibold).
Berlin: Springer-Verlag. 703pp.

JAHNKE, R.A., EMERSON, S.R. & MURRAY, J.W. 1982a
A model of oxygen reduction, denitrification, and organic matter mineralisation in marine sediments.
Limnology & Oceanography, 27, 610-623.

JAHNKE, R.A., HEGGIE, D., EMERSON, S. & GRUNDMANIS, V. 1982b
Pore waters of the central Pacific Ocean: nutrient results.
Earth and Planetary Science Letters, 61, 233-256.

JARVIS, I. & HOCKINGS, K.E. 1984
Rare earth element geochemistry of standard sediments: a study using inductively coupled plasma spectrometry.
Chemical Geology. (In press.)

JESSOP, A.M., HOBART, M.A. & SCLATER, J.G. 1976
The world heat flow data collection, 1975.
Canada, Energy Mines & Resources, Earth Physics Branch, Geothermal Series No.5, 125pp.

KADKO, D. 1980
230Th, 226Ra and 222Rn in abyssal sediments.
Earth and Planetary Science Letters, 49, 360-380.

KADKO, D. 1983
A multitracer approach to the study of erosion in the north-east Equatorial Pacific.
Earth and Planetary Science Letters, 63, 13-33.

KASTENS, K.A. 1984
Earthquakes as a triggering mechanism for debris flows and turbidites on the Calabrian Ridge.
Marine Geology, 55, 13-33.

KELLER, G.H. & LAMBERT, D.N. 1979
Variation of sediment geotechnical properties between the Greater Antilles Outer Ridge and the Nares Abyssal Plain.
Marine Geotechnology, 4, 125-143.

KENNEDY, W.J. & ODIN, G.S. 1982
The Jurassic and Cretaceous timescale in 1981.
pp. 557-592 in, Numerical dating in stratigraphy, Part 1. (ed G.S. Odin).
Chichester: John Wiley. 630pp.

KIDD, R.B. & DAVIES, T.A. 1978
Indian Ocean sediment distribution since the Late Jurassic.
Marine Geology, 26, 49-70.

KIDD, R.B. et al 1980
RRS 'Discovery' Cruise 106, 5 December - 22 December, 1979. Trans-Atlantic passage with equipment trials and high-resolution seismic profiling.
Institute of Oceanographic Sciences, Cruise Report No.90, 16pp. & figs.

KIDD, R.B. 1982a
Long-range sidescan sonar studies of sediment slides and the effects of slope mass-sediment movements on abyssal plain sedimentation.
pp. 289-303 in, Marine slides and other mass movements, (ed. S. Saxov & J.K. Nieuwenhuis).
New York: Plenum. 353pp.

KIDD, R.B. & ROBERTS, D.G. 1982b
Long-range sidescan sonar studies of large-scale sedimentary features in the North Atlantic.
Bulletin de l'Institut de Geologie du Bassin d'Aquitaine, No.31-32, 11-29.

KIDD, R.B., SEARLE, R.C., RAMSAY, A.T.S., PRICHARD, H. & MITCHELL, J. 1982c
The geology and formation of King's Trough, north-east Atlantic Ocean.
Marine Geology, 48, 1-30.

KIDD, R.B., SEARLE, R.C., WEAVER, P.P.E., JACOBS, C.L., HUGGETT, Q.J., NOEL, M.J. & SCHULTHEISS, P.J. 1983a
King's Trough Flank: geological and geophysical investigations of its suitability for high-level radioactive waste disposal.
Institute of Oceanographic Sciences, Report No. 166, 103pp.

KIDD, R.B. et al 1983b
Sediment drifts and intraplate tectonics in the North Atlantic. (Paper prepared by DSDP Leg 94 staff).
Nature, 306, 532-533.

KIDD, R.B., SIMM, R.W. & SEARLE, R.C. 1984a
Acoustic and sediment facies on the Saharan Continental Rise - a calibration of long-range sidescan sonar data. (In preparation.)

KIDD, R.B. & SEARLE, R.C. 1984b
Sedimentation in the southern Cape Verde Basin: regional observations by long range sidescan sonar.
pp. 145-151 in, Fine-grained sediments, (ed. D.A.V. Stow & D.J.W. Piper). Oxford: Blackwell Scientific Publications. (Geological Society Special Publication. No.15.)

KIDD, R.B. 1984c
Preliminary results of Deep Sea Drilling Project Leg 94, North Atlantic Ocean. Institute of Oceanographic Sciences, Internal Document No. 200, 26pp & appendices. (Unpublished manuscript.)

KIPP, N.G. 1976
New transfer function for estimating past sea-surface conditions from sea-bed distribution of planktonic foraminiferal assemblages in the North Atlantic pp. 3-41 in, Investigation of Late Quaternary paleoceanography and paleoclimatology, (ed. R.M.Cline & J.D. Hays).
Boulder, Co.: Geological Society of America, 464pp. (Geological Society of America, Memoir No. 145.)

KLINKHAMMER, G.P. & BENDER, M.L. 1980
The distribution of manganese in the Pacific Ocean.
Earth and Planetary Science Letters, 46, 361-384.

KLINKHAMMER, G.P. HEGGIE, D.T. & GRAHAM, D.W. 1982
Metal diagenesis in oxic marine sediments.
Earth and Planetary Science Letters, 61, 211-219.

KNAUER, G.A., MARTIN, J.H. & GORDON, R.M. 1982
Cobalt in north-east Pacific waters.
Nature, 297, 49-51.

KOLODNY, Y. & KAPLAN, I.R. 1970
Uranium isotopes in sea-floor phosphorites.
Geochimica et Cosmochimica Acta, 34, 3-24.

KOMINZ, M.A., HEATH, G.R., KU, T.L. & PISIAS, N.G. 1979
Brunhes time scales and the interpretation of climate change.
Earth and Planetary Science Letters, 45, 394-410.

KRAUSE, D.C. 1962
Interpretation of echo sounding profiles.
International Hydrographic Review, 39(1), 65-123.

KRAUSE, D.C. & WATKINS, N.D. 1970
North Atlantic crustal genesis in the vicinity of the Azores.
Geophysical Journal of the Royal Astronomical Society, 19, 261-283.

KRISHNASWAMI, S., LAL, D., MARTIN, J.M. & MAYBECK, M. 1971
Geochronology of lake sediments.
Earth and Planetary Science Letters, 11, 407-414.

KRISHNASWAMI, S. 1976
Authigenic transition elements in Pacific pelagic clays.
Geochimica et Cosmochimica Acta 40, 425-434.

KRUMBEIN, W.C. 1936
Application of logarithmic moments to size frequency distribution of sediments
Journal of Sedimentary Petrology, 6, 64-72.

KUIJPERS, A. 1982
Contribution to the Seabed Working Group Programme. Progress report 1981. The sedimentology of two north-east Atlantic study areas: the western Madeira Abyssal Plain and the area west of Great Meteor Seamount.
Haarlem: Rijks Geologische Dienst. 61pp. (Unpublished manuscript.)

KU, T.L. 1965
An evaluation of the U234/U238 method as a tool for dating pelagic sediments.
Journal of Geophysical Research, 70, 3457-3474.

KU, T.L. 1976
The uranium-series methods of age determination.
Annual Review of Earth and Planetary Science, 4, 347-379.

KU, T.L., KNAUSS, K.G. & MATHIEU, G.G. 1977
Uranium in open ocean: concentration and isotopic composition.
Deep-Sea Research, 24, 1005-1017.

LACHENBRUCH, A.M. 1968
Rapid estimation of the topographic disturbance to superficial thermal gradients.
Reviews of Geophysics, 6, 365-400.

LAMBE, T.W. & WHITMAN, R.V. 1979
Soil mechanics.
New York: John Wiley, 553pp.

LAMPITT, R.S. & BURNHAM, M.P. 1983
A free-fall time lapse camera and current meter system ('Bathysnap') with notes on the foraging behaviour of a bathyal decapod shrimp.
Deep-Sea Research, 30A, 1009-1017

LAMPITT, R.S., RICE, A.L. & THURSTON, M.H. 1984
The use of in situ photography in studies of the deep-sea benthos at IOS.
Institute of Oceanographic Sciences, Internal Document No. 198, 33pp. (Unpublished manuscript.)

LANDING, W.M. & BRULAND, K.W. 1980
Manganese in the North Pacific.
Earth and Planetary Science Letters, 49, 45-56.

LANGSETH, M.G. & HERMAN, B.M. 1981
Heat transfer in the oceanic crust of the Brazil Basin.
Journal of Geophysical Research, 86, 10805-10819.

LANGSETH, M.G., CANN, J.R., NATLAND, J.H. & HOBART, M. 1983
Geothermal phenomena at the Costa Rica Rift: background and objectives for drilling sites 501, 504 and 505.
Initial Reports of Deep Sea Drilling Project, 69, 5-29.

LAUGHTON, A.S. & WHITMARSH, R.B. 1974
The Azores - Gibraltar plate boundary.
pp. 63-81 in, Geodynamics of Iceland and the North Atlantic area, (ed. L. Kristjansson).
Dordrecht, Holland: Reidel.

LAUGHTON, A.S., ROBERTS, D.G. & GRAVES, R. 1975
Bathymetry of the north-east Atlantic: Mid-Atlantic Ridge to southwest Europe.
Deep-Sea Research, 22, 791-810 & Admiralty Chart C6568.

LAUGHTON, A.S. & SEARLE, R.C. 1979
Tectonic processes on slow spreading ridges.
pp. 15-32 in, Deep drilling results in the Atlantic Ocean: ocean crust, (ed. M. Talwani, C.G. Harrison & D.E. Hayes).
Washington, DC: American Geophysical Union, 431pp. (Maurice Ewing Series, 2.)

LAUGHTON, A.S. 1981
The first decade of GLORIA
Journal of Geophysical Research, 86, 11511-11534.

LE PICHON, X., HOUTZ, R.E., DRAKE, C.L. & NAFE, J. 1965
Crustal structure of the mid-ocean ridges. 1. Seismic reflection measurements.
Journal of Geophysical Research, 70, 319-339.

LE PICHON, X., FRANCHETEAU, J. & BONNIN, J. 1973
Plate tectonics.
Amsterdam: Elsevier. 300pp.

LILWALL, R.C. 1982
Intraplate seismicity and seismic risk in the Atlantic Ocean based on teleseismically observed earthquakes.
Institute of Oceanographic Sciences, Report No. 136, 40pp.

LISITZIN, A.P. 1982
Sedimentation in the World Ocean.
Tulsa: Society of Economic Paleontologists & Mineralogists. 218pp. (SEPM Special Publication No. 17.)

LISTER, C.R.B. 1979
The pulse-probe method of conductivity measurement.
Geophysical Journal of the Royal Astronomical Society, 57, 451-461.

LIVINGSTONE, H.D. & ANDERSON, R.F. 1983
Large particle transport of plutonium and other fallout radionuclides to the deep ocean.
Nature, 303, 228-231.

LI, Y.H., BISCHOFF, J. & MATTHIEU, G. 1969
The migration of manganese in the Arctic basin sediments.
Earth and Planetary Science Letters, 7, 265-270.

LI, Y.H. & GREGORY, S. 1974
Diffusion of ions in sea water and in deep-sea sediments.
Geochimica et Cosmochimica Acta, 38, 703-714.

LOCKYER, C. 1977
Observations on diving behaviour of the sperm whale Physeter catodon.
pp. 591-609 in, A Voyage of Discovery, (ed. M.V. Angel).
Oxford: Pergamon, 696pp.

LODER, T.C. & LISS, P.S. 1984
The role of organic matter in determining the surface charge of suspended particles in estuarine and oceanic waters.
Thalassia Jugoslavica. (In press.)

LONGHURST, A.R. 1976
Vertical migration.
pp. 116-140 in, The Ecology of the Seas, (ed. D.H. Cushing & J.J. Walsh).
Oxford: Blackwell Scientific Publications.

LOWRIE, W. & ALVAREZ, W. 1981
One hundred million years of geomagnetic polarity history.
Geology, 9, 392-397.

LYLE, M. 1983
The brown-green color transition in marine sediments: a marker for the Fe(III)-Fe(II) redox boundary.
Limnology & Oceanography, 28, 1026-1033.

LYNN, D.C. & BONATTI, E. 1965
Mobility of manganese in diagenesis of deep sediments.
Marine Geology, 3, 457-474.

MANGINI, A. & DOMINIK, J. 1969
Late Quaternary sapropel on the Mediterranean Ridge: U-budget and evidence for low sedimentation rates.
Sedimentary Geology, 23, 113-125.

MANSURE, A.J. & REITER, M. 1979
A vertical groundwater movement correction for heat flow.
Journal of Geophysical Research, 84, 3490-3496.

MATTHEWS, D.H., LAUGHTON, A.S., PUGH, D.T., JONES, E.J.W., SUNDERLAND, J., TAKIN, M. & BACON, M. 1969
Crustal structure and origin of Peake & Freen Deeps, north-east Atlantic.
Geophysical Journal of the Royal Astronomical Society, 18, 517-542.

MAUVIEL, A., NGUYEN, M.V., CHESSELET, R., SIBUET, M., YOKOYAMA, Y. & AUFFRET, G. 1982
Etude des variations des taux de bioturbations par la spectrometrie gamma non destructive (GeHP), dans trois zones sedimentaires de l'Atlantique nord, a 2000m et a plus de 4000m de profondeur.
Bulletin de l'Institut de Geologie du Bassin d'Aquitaine, No. 31-32, 257-274.

MAYNARD, J.B. 1983
Geochemistry of sedimentary ore deposits.
New York: Springer-Verlag. 305pp.

MCCARTNEY, B.S. et al 1984
RRS 'Discovery' Cruise 141, 26 October - 17 November 1983.
Mooring recoveries, instrumentation trials and engineering tests.
Institute of Oceanographic Sciences, Cruise Report No. 156, 27pp.

MCCAVE, I.N. 1975
Vertical flux of particles in the ocean.
Deep-Sea Research, 22, 491-502.

MCCAVE, I.N. 1984
Size spectra and aggregation of suspended particles in the deep ocean.
Deep-Sea Research, 31A, 329-352.

MCGIVERON, S. 1980
A compilation of seismic reflection profile and core data for the north-east Atlantic, 30-45N, 6-35W.
Institute of Oceanographic Sciences, Internal Document No. 108, 9pp. & figs. (Unpublished manuscript.)

MCGIVERON, S. 1981
Distal abyssal plain limit, Madeira Abyssal Plain, 24-26N, 27-31W.
Institute of Oceanographic Sciences, Internal Document No. 133, 9pp. & figs. (Unpublished manuscript.)

MCGOWAN, J.A. 1974
The nature of oceanic ecosystems.
pp. 9-28 in, The biology of the oceanic Pacific, (ed. C.B. Miller).
Corvallis: Oregon State University Press. 157pp.

MCINTYRE, A., RUDDIMAN, W.F. & JANTZEN, R. 1972
Southward penetrations of the North Atlantic Polar Front: faunal and floral evidence of large-scale surface water mass movements over the last 225,000 years.
Deep-Sea Research, 19, 61-77.

MCINTYRE, A., KIPP, N.G., BE, A.W.H., CROWLEY, T., KELLOG, T., GARDNER, J.V., PRELL, W. & RUDDIMAN, W.F. 1976
Glacial North Atlantic 18,000 years ago: a CLIMAP reconstruction.
pp. 43-76 in, Investigation of Late Quaternary paleoceanography and paleo-climatology, (ed. R.M. Cline & J.D. Hays).
Boulder, Co.: Geological Society of America. 464pp. (Geological Society of America, Memoir No. 145.)

MCKENZIE, D.P. 1972
Active tectonics of the Mediterranean region.
Geophysical Journal of the Royal Astronomical Society, 30, 109-185.

MILLER, C.B., FROST, B.W., BATCHELDER, H.P., CLEMONS, M.J. & CONWAY, R.E. 1984
Life histories of large, grazing copepods in a subarctic ocean gyre: Neocalanus plumchrus, Neocalanus cristatus and Eucalanus bungii in the northeast Pacific.
Progress in Oceanography, 13, 201-243.

MILLER, D.G. & RICHARDS, A.F. 1969
Consolidation and sedimentation-compression studies of a calcareous core, Exuma Sound, Bahamas.
Sedimentology, 12, 301-316.

MILNE-EDWARDS, A. 1883
L'expedition du Talisman faite dans l'Ocean Atlantique.
Bulletin de l'Association Scientifique francais, Ser.2, 7, 138-139.

MOORE, W.S., KU, T.L., MCDOUGALL, J.D., BURNS, V.M., BURNS, R., DYMOND, J., LYLE, M.W. & PIPER, D.Z. 1981
Fluxes of metals to a manganese nodule: radiochemical, chemical, structural and mineralogical studies.
Earth and Planetary Science Letters, 52, 151-171.

MORRIS, R.J., MCCARTNEY, M.J., GROGAN, W.C. & SMITH, D.J. 1984
Post-depositional changes in the geochemistry of an organic-rich turbidite from sediments on the Madeira Abyssal Plain. (In preparation.)

MULLER, G. 1961
Die Rezenten Sedimente im Golf von Neapel 2: Mineral-neeund-umbildungen in den rezenten sedimenten des Golfes Pozzuoli. Ein Beitreig zur Unwandlung vulcanischer Glaser durch Hamyrolyse.
Beitrage zur Mineralogie und Petrographie, 8, 1-20.

MULLER, G. & GASTNER, M. 1971
The Karbonat-bombe: a simple device for the determination of the carbonate content in sediment soils and other materials.
Neues Jahrbuch fur Mineralogie. Monatshefte, 10, 466-469.

MULLER, P.J. & SEUSS, E. 1979
Productivity, sedimentation rate and sedimentary organic matter in the ocean - 1. Organic carbon preservation.
Deep-Sea Research, 26A, 1347-1362.

MULLER, P.J. & MANGINI, A. 1980
Organic carbon decomposition rates in sediments of the Pacific manganese nodule belt dated by 230Th and 231Pa.
Earth and Planetary Science Letters, 51, 94-114.

MULLER, T.J. 1981
Current and temperature measurements in the north-east Atlantic during NEADS.
Berichte aus dem Institut fur Meereskunde, Christian-Albrechts-Universitat, Kiel, No.90. 98pp.

MURRAY, J.W. & BREWER, P.G. 1977
Mechanisms of removal of manganese, iron and other trace metals from sea water.
pp. 291-325 in, Marine manganese deposits, (ed. G.P. Glasby).
Amsterdam: Elsevier.

MURRAY, J.W. & GRUNDMANIS, V. 1980
Oxygen consumption in pelagic marine sediments.
Science, 209, 1527-1530.

NELSON, D.M., CAREY, A.E. & BOWEN, V.T. 1984
Plutonium oxidation state distributions in the Pacific Ocean during 1980-1981.
Earth and Planetary Science Letters, 68, 422-430.

NOEL, M. 1984a
Origins and significance of non-linear temperature profiles in deep-sea sediments.
Geophysical Journal of the Royal Astronomical Society, 76, 673-690.

NOEL, M. 1984b
Measurements of sediment temperatures, conductivity and heat flow in the North Atlantic and their relevance to radioactive waste disposal.
Institute of Oceanographic Sciences, Report No. 172, 27pp & figs.

NUCLEAR ENERGY AGENCY. 1984
Seabed disposal of high-level radioactive waste. A status report on the NEA coordinated research programme.
Paris: Organisation for Economic Cooperation and Development. 245pp.

OFFICER, C.B. & LYNCH, D.R. 1983
Determination of mixing parameters from tracer distributions in deep-sea sediment cores.
Marine Geology, 52, 59-74.

OLAUSSON, E. 1960
Description of sediment cores from the North Atlantic.
Reports of the Swedish Deep Sea Expedition, 1947-1948, 7(5), 229-286.

OVE ARUP & PARTNERS 1982
Ocean disposal of radioactive waste, an initial study into penetrator shape and size for emplacement in deep ocean sediments.
Department of the Environment, Report No. DOE/RW/82-102.

OVENSHINE, A.T. 1970
Observations of iceberg rafting in Glacier Bay, Alaska, and the identification of ancient ice-rafted deposits.
Geological Society of America Bulletin, 81, 891-894.

PEARRE, S. 1979
Problems of detection and interpretration of vertical migration.
Journal of Plankton Research, 1, 29-44.

PEDDIE, N.W. 1982
International geomagnetic reference field 1980: a report by IAGA Division I, Working Group 1.
Geophysical Journal of the Royal Astronomical Society, 68, 265-268.

PERRY, R.K., FLEMMING, H.S. VOGT, P.R., CHERKIS, N.Z., FEDEN, R.H., THIEDE, J., STRAND, J.E. & COLLETTE, B.J. 1981
North Atlantic Ocean: bathymetry and plate tectonic evolution. 1:8,753,909 at Equator.
Geological Society of America, Map and Chart Series, MC-35.

PIPER, D.J.W. 1978
Turbidite muds and silts on deepsea fans and abyssal plains.
pp. 163-176 in, Sedimentation in submarine canyons, fans and trenches, (ed. D.J. Stanley & G. Kelling).
Stroudsberg, Pa.: Hutchinson & Ross.

PIPER, D.Z. 1974
Rare earth elements in the sedimentary cycle: a summary.
Chemical Geology, 14, 285-304.

PISIAS, N.G. & MOORE, T.C. 1981
The evolution of Pleistocene climate: a time series approach.
Earth and Planetary Science Letters, 52, 450-458.

PRATT, R.M. 1963
Great Meteor Seamount
Deep-Sea Research, 10, 17-25

PRELL, W.L., GARDNER, J.V. et al 1982
Initial Reports of Deep Sea Drilling Project, Vol.68.
Washington: U.S. Government Printing Office. 495pp.

PUJOL, C. 1980
Les foraminiferes planctoniques de l'Antique nord au Quaternaire: ecologie - stratigraphie - environnement.
Memoires de l'Institut de Geologie du Bassin d'Aquitaine, No.10, 1-254.

RAMPINO, M.R. 1981
Revised age estimates of Brunhes palaeomagnetic events: support for a link between geomagnetism and eccentricity.
Geophysical Research Letters, 8, 1047-1050.

RAMSAY, A.T.S. 1970
The pre-Pleistocene stratigraphy and palaeontology of the Palmer Ridge area, north-east Atlantic.
Marine Geology, 9, 261-285.

RATCLIFFE, E.H. 1960
The thermal conductivities of ocean sediments.
Journal of Geophysical Research, 65, 1535-1541.

REEBURGH, W.S. 1983
Rates of biogeochemical processes in anoxic sediments.
Annual Review of Earth and Planetary Sciences, 11, 269-298.

REES, A.I. 1965
The use of anisotropy of magnetic susceptibility in the estimation of sedimentary fabric.
Sedimentology, 4, 257-271.

REIMERS, C.E., KALHORN, S., EMERSON, S.R. & NEALSON, K.H. 1984
Oxygen consumption rates in pelagic sediments from the central Pacific: first estimates from microelectrode profiles.
Geochimica et Cosmochimica Acta, 48, 903-910.

REVIE, J.A. et al 1983
MV 'Farnella' Cruises 8, 9/82, 26 February - 26 March, 1982. Geophysical studies in the Nares Abyssal Plain and King's Trough Flank. Recovery of tide gauges deployed in December 1981.
Institute of Oceanographic Sciences, Cruise Report No. 145, 17pp.

RICE, A.L., ALDRED, R.G., DARLINGTON, E. & WILD, R.A. 1982
The quantitative estimation of the deep-sea megabenthos: a new approach to an old problem.
Oceanologica Acta, 5, 63-72.

RICHARDS, A.F. 1961
Investigations of deep-sea sediment cores. I: Shear strength, bearing capacity and consolidation.
U.S. Navy Hydrographic Office, Technical Report No.63, 70pp.

RICHARDS, K.J. 1982
Modeling the benthic boundary layer.
Journal of Physical Oceanography, 12, 428-439.

RICHARDS, K.J. 1984a
The interaction between the bottom mixed layer and mesoscale motions of the ocean: a numerical study.
Journal of Physical Oceanography, 14, 754-768.

RICHARDS, K.J. 1984b
Benthic boundary layer modelling studies.
Institute of Oceanographic Sciences, Report No.181, 29pp.

RIDLEY, W.I., WATKINS, N.D. & MACFARLANE, D.J. 1974
The oceanic islands: Azores.
pp. 445-483 in, Ocean basins and margins, Vol.2. The North Atlantic, (ed. A.E.M. Nairn & F.G. Stehli).
New York: Plenum.

ROBERTS, D.G. & JONES, M.T. 1979a
Magnetic anomalies in the north-east Atlantic. North sheet: Reykjanes Ridge to the British Isles.
Wormley: Institute of Oceanographic Sciences. 1:2,400,000 at 41N.

ROBERTS, D.G. & KIDD, R.B. 1979b
Abyssal sediment wave fields on Feni Ridge, Rockall Trough: long-range sonar studies.
Marine Geology, 33, 175-191.

ROBERTS, D.G. & JONES, M.T. 1984
Magnetic anomalies in the north-east Atlantic. South sheet: Mid-Atlantic Ridge to southeast Europe.
Wormley: Institute of Oceanographic Sciences. 1:2,400,000 at 41N.

ROBINSON, A.R. & MULLIN, M.M. 1981
A model for physical-biological transfer.
Sandia National Laboratories, Albuquerque, NM, Report No. SAND-81-0012, 29-31.

ROE, H.S.J. 1974
Observations on the diurnal vertical migrations of an oceanic animal community
Marine Biology, 28, 99-113.

ROE, H.S.J. 1984a
The diel migrations and distributions within a mesopelagic community in the north-east Atlantic. 2. Vertical migrations and feeding of mysids and decapod Crustacea.
Progress in Oceanography, 13, 269-318.

ROE, H.S.J. & BADCOCK, J. 1984b
The diel migrations and distributions within a mesopelagic community in the north-east Atlantic. 5. Vertical migrations and feeding of fish.
Progress in Oceanography, 13, 389-424.

ROSSBY, H.T. & WEBB, D.C. 1971
The four month drift of a Swallow float.
Deep-Sea Research, 18, 1035-1039.

ROWE, G.T. & GARDNER, W.D. 1979
Sedimentation rates in the slope water of the north-west Atlantic Ocean measured directly with sediment traps.
Journal of Marine Research, 37, 581-600.

ROWE, G.T. 1981
The deep-sea ecosystem.
pp. 235-267 in, Analysis of Marine Ecosystems, (ed. A.R. Longhurst).
London: Academic. 741pp.

RUDDIMAN, W.F. & GLOVER, L.K. 1972
Vertical mixing of ice-rafted volcanic ash in North Atlantic sediments.
Geological Society of America Bulletin, 83, 2817-2836.

RUDDIMAN, W.F. & MCINTYRE, A. 1976
North-east Atlantic paleoclimatic changes over the past 600,000 years.
pp. 111-146 in, Investigation of Late Quaternary paleoceanography and paleoclimatology, (ed. R.M. Cline & J.D. Hays).
Boulder, Col: Geological Society of America. 464pp. (Geological Society of America, Memoir No. 145.)

RUDDIMAN, W.F. 1977
Late Quaternary deposition of ice-rafted sand in the sub-polar North Atlantic (Lat.40 to 65N).
Geological Society of America Bulletin, 88, 1813-1827.

RUDDIMAN, W.F. & MCINTYRE, A. 1981
The North Atlantic Ocean during the last deglaciation.
Palaeogeography, Palaeoclimatology, Palaeoecology, 35, 145-214.

SARNTHEIN, M. 1978
Neogene sand layers off N.W. Africa: composition and source environment.
Initial Reports of Deep Sea Drilling Project, 41, Supplementary Volume, 939-959.

SAUNDERS, P.M. 1982
Circulation in the eastern North Atlantic.
Journal of Marine Research, 40, Supplement, 641-657.

SAUNDERS, P.M. 1983a
Benthic boundary layer, IOS Observational Programme. Interim report January 1983.
Institute of Oceanographic Sciences, Report No.163, 33pp.

SAUNDERS, P.M. 1983b
Benthic observations on the Madeira Abyssal Plain: currents and dispersion.
Journal of Physical Oceanography, 13, 1416-1429.

SAUNDERS, P.M. 1984
Benthic boundary layer - IOS Observational Programme. Technical report, Discovery Gap measurements, March 1984.
Institute of Oceanographic Sciences, Report No.180, 44pp.

SAWLAN, J.J. & MURRAY, J.W. 1983
Trace metal remobilisation in the interstitial waters of red clay and hemipelagic marine sediments.
Earth and Planetary Science Letters, 64, 213-230.

SAYLES, F.L. 1979
The composition and diagenesis of interstitial solutions. 1. Fluxes across the seawater sediment interface in the Atlantic Ocean.
Geochimica et Cosmochimica Acta, 43, 527-545.

SCHINK, D.R., GUINASSO, N.L. & FANNING, K.A. 1975
Processes affecting the concentration of silica at the sediment-water interface of the Atlantic Ocean.
Journal of Geophysical Research, 80, 3013-3031.

SCHMINCKE, H.U. 1979
Age and crustal structure of the Canary Islands.
Journal of Geophysics, 46, 217-224.

SCHMINCKE, H.U. 1982
Volcanic and chemical evolution of the Canary Islands.
pp.273-306 in, Geology of the northwest African continental margin, (ed. U. Von Rad, K. Hinz, M. Sarnthein & E. Seibold.)
Berlin: Springer-Verlag. 703pp.

SCHREIBER, E. & FOX, P.J. 1973
Compressional wave velocities of oceanic rocks and the geology of the oceanic crust: a brief summary.
EOS, Transactions of the American Geophysical Union, 54, 1033-1035.

SCHULTHEISS, P.J. 1984a
Consolidation and permeability of North Atlantic sediments.
Institute of Oceanographic Sciences, Report (in preparation).

SCHULTHEISS, P.J., MCPHAIL, S.D., PACKWOOD, A.R. & HART, B. 1984b
An instrument to measure differential pore pressures in deep-ocean sediments: Pop-Up-Pore-Pressure-Instrument (PUPPI). (In preparation.)

SCHULTHEISS, P.J. et al 1984c
RRS 'Discovery' Cruise 144, 22 January - 20 February 1984.
Geology and geophysics of an area east of the Great Meteor Seamount.
Institute of Oceanographic Sciences, Cruise Report No.161, 37pp.

SCHULTHEISS, P.J., WEAVER, P.P.E. & PRICE, M.C. 1984d
Electro-osmotic core cutting. (In preparation.)

SCLATER, J.G. & FRANCHETEAU, J. 1970
The implications of terrestrial heat-flow observations on current tectonic and geochemical models of the crust and upper mantle of the Earth.
Geophysical Journal of the Royal Astronomicasl Society, 20, 509-542.

SCLATER, J.G., LAWYER, L.A. & PARSONS, B. 1975
Comparison of long-wavelength residual elevation free air gravity anomalies in the North Atlantic and possible implications for the thickness of the lithospheric plate.
Journal of Geophysical Research, 80, 1031-1052.

SCOTT, M.R. 1968
Thorium and uranium concentrations and isotope ratios in river sediments.
Earth and Planetary Science Letters, 4, 245-252.

SEARLE, R.C. 1976
Lithospheric structure of the Azores Plateau from Rayleigh wave dispersion.
Geophysical Journal of the Royal Astronomical Society, 44, 537-546.

SEARLE, R.C. 1977
Geophysical studies of the Atlantic seafloor near 40N, 24W and its relation to King's Trough and the Azores.
Marine Geology, 25, 299-320.

SEARLE, R.C. & WHITMARSH, R.B. 1978
The structure of King's Trough, north-east Atlantic, from bathymetric, seismic and gravity studies.
Geophysical Journal of the Royal Astronomical Society, 53, 259-287.

SEARLE, R.C. 1979
Guidelines for the selection of sites for disposal of radioactive waste on or beneath the ocean floor.
Institute of Oceanographic Sciences, Report No.91, 44pp.

SEARLE, R.C. 1980
Tectonic pattern of the Azores spreading centre and triple junction.
Earth and Planetary Science Letters, 51, 415-434.

SEARLE, R.C., MONAHAN, D. & JOHNSON, G.L. 1982a
General Bathymetric Chart of the Oceans, 5th ed., Sheet 5.08.
Ottawa: Canadian Hydrographic Service. (Scale 1:10,000,000 at the Equator.)

SEARLE, R.C. et al 1982b
MV 'Farnella' Cruise 3/81, 7 November - 26 November, 1981. GLORIA studies of lower continental rise and abyssal plain sedimentation in the Canary Basin.
Institute of Oceanographic Sciences, Cruise Report No.122, 14pp. & figs.

SEARLE, R.C. 1984a
Guidelines for the selection of sites that might prove suitable for radioactive waste disposal on or beneath the ocean floor.
Nuclear Technology, 64, 166-174.

SEARLE, R.C. et al 1984b
Great Meteor East (distal Madeira Abyssal Plain): geological studies of its suitability for disposal of heat-emitting radioactive wastes.
Institute of Oceanographic Sciences, Report. (In preparation.)

SEED, H.B. & IDRISS, I.M. 1971
A simplified procedure for evaluating soil liquefaction potential.
Journal of the Soil Mechanics and Foundations Division, American Society of Civil Engineers, 97, 1249-1273.

SHACKLETON, N.J. 1969
The last interglacial in the marine and terrestrial records.
Proceedings of the Royal Society of London, B. 174, 135-154.

SHACKLETON, N.J. & OPDYKE, N.D. 1973
Oxygen isotope and palaeomagnetic stratigraphy of equatorial Pacific core V28-238: oxygen isotope temperatures and ice volume on a 10^5 and 10^6 year scale.
Quaternary Research, 3, 39-55.

SHAW, A.B. 1964
Time in stratigraphy.
New York: McGraw-Hill. 365pp.

SHIPLEY, T.H. 1978
Sedimentation and echo characteristics in the abyssal hills of the west-central North Atlantic.
Geological Society of America Bulletin, 89, 397-408.

SIBUET, J.C. & LE PICHON, X. 1971
Structure gravimetrique du Golfe de Gascogne et le fosse marginal nord-espagnol.
pp.VI.9.1 - VI.9.17 in, Histoire structural du Golfe de Gascogne. Tom.2.
Paris : Editions Technip.

SIGURDSSON, H. & CAREY, S.N. 1981
Marine tephrochronology and Quaternary explosive volcanism in the Lesser Antilles Arc.
pp.255-280 in, Tephra studies. (Proceedings of the NATO Advanced Study Institute 'Tephra studies as a tool in Quaternary research', Laugarvatn and Reykjavik, Iceland, 18-29 June 1980).
Dordrecht, Holland: D. Reidel.

SIMM, R.W. & KIDD, R.B. 1984
Submarine debris flow deposits detected by long-range sidescan sonar 1000km from source.
Geo-Marine Letters, 3, 13-16.

SIMPSON, W.R. 1982
Particulate matter in the oceans - sampling methods, concentration, size distribution and particle dynamics.
pp.119-172 in, Oceanography and marine biology: an annual review, vol.20, (ed. M. Barnes).
Aberdeen: Aberdeen University Press.

SIMPSON, W.R. 1984a
Particulate matter in the oceans - I. Aims models and experimental design.
Department of the Environment, Report No. DOE/RW/84.014, 31pp.

SIMPSON, W.R., GWILLIAM, T.J.P., LAWFORD, V.A. & LEWIS, A.R. 1984b
Particulate matter in the oceans - II. A deep water particle sampler.
Department of the Environment, Report No. DOE/RW/84, 30pp.

SMITH, K.L. & BALDWIN, R.J. 1984
Seasonal fluctuations in deep-sea sediment community oxygen consumption: central and eastern North Pacific.
Nature, 307, 624-626.

SMITH, S.G. 1977
A reflection profile modelling system.
Geophysical Journal of the Royal Astronomical Society, 49, 723-737.

SOMERS, M.L., CARSON, R.M., REVIE, J.A., EDGE, R.H., BARROW, B.J. & ANDREWS, A.G. 1978
'GLORIA II' - an improved long range sidescan sonar.
pp.16-24 in, Oceanology International '78, Technical Session J.
London: BPS Exhibitions Ltd. 610pp.

SORENSEN, J. 1982
Reduction of ferric iron in anaerobic marine sediment and interaction with reduction of nitrate and sulphate.
Applied and Environmental Microbiology, 43, 319-324.

SOUTHARD, J.B., YOUNG, R.A. & HOLLISTER, C.D. 1971
Experimental erosion of calcareous ooze.
Journal of Geophysical Research, 76, 5903-5909.

SPENCER, D.W., BACON, M.P. & BREWER, P.G. 1981
Models of the distribution of 210Pb in a section across the north equatorial Atlantic Ocean.
Journal of Marine Research, 39, 119-138.

STALIMAN, R.W. 1963
Computation of groundwater velocity from temperature data.
U.S. Geological Survey, Water Supply Paper, 1544-H, 36-46.

STEBBINS, J. & THOMPSON, G. 1978
The nature and petrogenesis of intra-oceanic plate alkaline eruptive and plutonic rocks: King's Trough, north-east Atlantic.
Journal of Volcanology and Geothermal Research, 4, 333-361.

STOMMEL, H. 1955
Discussions on the relationships between meteorology and oceanography.
Journal of Marine Research, 14, 504-510.

SVERDRUP, H.U., JOHNSON, M.V. & FLEMMING, R.H. 1942
The oceans, their physics, chemistry and general biology.
Englewood Cliffs, N.J.: Prentice-Hall, 1987pp.

SWALLOW, J.C. 1955
A neutral-buoyancy float for measuring deep currents.
Deep-Sea Research, 3, 74-81.

SWALLOW, J.C., MCCARTNEY, B.S. & MILLARD, N.W. 1974
The Minimode float tracking system.
Deep-Sea Research, 21, 573-595.

TENDAL, O.S. & HESSLER, R.R. 1977
An introduction to the biology and systematics of Komokiacea (Textulariina, Foraminiferida).
Galathea Report, 14, 165-194. & pls.

THIERSTEIN, H.R., GEITZENAUER, K.R. MOLFINO, B. & SHACKLETON, N.J. 1977
Global synchroneity of late Quaternary coccolith datum levels: validation by oxygen isotopes.
Geology, 5, 400-404.

THOMSON, J. et al 1982
RRS 'Discovery' Cruise 125, 30 January - 25 February 1982. Geochemical sampling over the Madeira/Cape Verde Abyssal Plains.
Institute of Oceanographic Sciences, Cruise Report No.125, 14pp. & figs.

THOMSON, J., CARPENTER, M.S.N., COLLEY, S., WILSON, T.R.S., ELDERFIELD, H. & KENNEDY, H. 1984
Metal accumulation rates in north-west Atlantic pelagic sediments.
Geochimica et Cosmochimica Acta. 48, 1935-1948.

THORPE, S.A. 1983
Benthic observations on the Madeira Abyssal Plain: fronts.
Journal of Physical Oceanography, 13, 1430-1440.

THUNNELL, R.C. 1982
Carbonate dissolution and abyssal hydrography in the Atlantic Ocean.
Marine Geol.ogy, 47, 165-180.

TOOLE, J., THOMSON, J., WILSON, T.R.S. & BAXTER, M.S. 1984
A sampling artefact affecting the uranium content of deep-sea pore waters obtained from cores.
Nature, 308, 263-266.

TRASK, P.D. 1932
Origin and environment of source sediments of petroleum.
Houston, Texas: American Petroleum Institute/Gulf Publishing Co. 323pp.

TUCHOLKE, B.E. & VOGT, P.R. 1979
Western North Atlantic: sedimentary evolution and aspects of tectonic history.
Initial Reports of Deep Sea Drilling Project, 43, 791-825.

TUCHOLKE, B.E. 1980
Acoustic environment of the Hatteras and Nares Abyssal Plains, western North Atlantic Ocean, determined from velocities and physical properties of sediment cores.
Journal of the Acoustical Society of America, 68, 1376-1390.

TUCHOLKE, B.E. & LUDWIG, W.J. 1982
Structure and origin of the J Anomaly Ridge, western North Atlantic.
Journal of Geophysical Research, 87, 9389-9407.

TUCHOLKE, B.E., FRY, VA. & SHEPARD, L.E. 1983
Interim report on Nares Abyssal Plain studies for sub-seabed disposal of high-level nuclear waste. (Unpublished manuscript).

TUREKIAN, K.K. & WEDEPOHL, K.H. 1961
Distribution of the elements in some major units of the Earth's crust.
Geological Society of America Bulletin, 72, 175-192.

TUREKIAN, K.K. 1965
Some aspects of the geochemistry of marine sediments.
pp.81-126 in, Chemical oceanography, vol.2. (ed. J.P. Riley & G. Skirrow).
London: Academic Press.

TUREKIAN, K.K. 1967
Estimates of the average Pacific deep-sea clay accumulation rate from material balance considerations.
pp.227-244 in, Progress in oceanography, vol.4.
Oxford: Pergamon.

TUREKIAN, K.K., COCHRAN, J.K. & DEMASTER, D.J. 1978
Bioturbation in deep-sea deposits: rates and consequences.
Oceanus, 21(1), 34-41.

TURNER, D.R. & WHITFIELD, M. 1979
Control of seawater composition.
Nature, 281, 468-469.

TYLER, P.A., GRANT, A., PAIN, S.L. & GAGE, J.D. 1982
Is annual reproduction in deep-sea echinoderms a response to variability in their environment?
Nature, 300, 747-750.

TYLER, P.A. & MUIRHEAD, A. 1984
Studies of the reproductive biology of deep-sea megabenthos. 1. The echinoderm species Laetmogone violacea and Benthogone rosea (Elasipoda, Holothuroidea).
(Unpublished manuscript.)

UDINTSEV, G.B., YEL'NIKOV, I.N. LUNARSKIY, G.N., KRASIL'SHCHIKOVA, G.N., GRIN'KO, B.N., PEREVOZCHIKOV, A.V. & BEREZYUK, V.M. 1976
Results of deep seismic soundings southwest of the Azores.
Oceanology, 16, 360-362.

UDINTSEV, G.B., YEL'NIKOV, I.N. & LUNARSKIY, G.N. 1977
New data on the deep structure of the Earth's crust to the northwest of the Cape Verde Islands.
Oceanology, 17, 163-166.

ULLMAN, W.J. & ALLER, R.C. 1980
Dissolved iodine flux from estuarine sediments and implications for the enrichment of iodine at the sediment-water interface.
Geochimica et Cosmochimica Acta, 44, 1177-1184.

ULRICH, J. 1969
Topographie und Morphologie.
pp.21-23 in, Atlantische Kuppenfahrten 1967 mit dem Forschungschiff 'Meteor' - Reisebericht.
'Meteor' Forschungsergebnisse, A. No.5, 1-71

U.S. NAVY OCEANOGRAPHIC OFFICE 1968
Oceanographic atlas of the North Atlantic Ocean. III. Ice.
U.S. Navy Oceanographic Office Publication 700(III), 157pp.

VAN ANDEL, T.H. 1975
Mesozoic/Cenozoic calcite compensation depth and the global distribution of calcareous sediments.
Earth and Planetary Science Letters, 26, 187-194.

VERHOEF, J. 1983a
The sedimentation pattern around the Atlantis-Meteor Seamount complex: a model study. 26pp. & figs. (Unpublished manuscript.)

VERHOEF, J. & COLLETTE, B.J. 1983b
A tear fault system beneath the Atlantic - Meteor Seamount Group.
Annales Geophysicae, 1, 199-206.

VERHOEF, J. 1984
Geophysical study of the Atlantis - Meteor Seamount Complex.
University of Utrecht, Ph.D. Thesis. 153pp.
(Geologica Ultraiectina No.38)

VON RAD, U. 1974
Great Meteor and Josephine Seamounts (eastern North Atlantic): composition and origin of bioclastic sands, carbonate and pyroclastic rocks.
'Meteor' Foreschungsergebnisse, C. No.19, 1-62.

VON RAD, U. & WISSMANN, G. 1982
Cretaceous - Cenozoic history of the west Saharan continental margin (NW Africa): development, destruction and gravitational sedimentation.
pp.106-131 in, Geology of the northwest African continental margin, (ed. U. Von Rad, K. Hinz, M. Sarnthein & E. Seibold).
Berlin: Springer-Verlag. 703pp.

WATKINS, N.D. 1973
Palaeomagnetism of the Canary Islands and Madeira.
Geophysical Journal of the Royal Astronomical Society, 32, 249-267.

WATTS, A.B., COCHRAN, J.R. & SELZER, G. 1975
Gravity anomalies and flexure of the lithosphere: a three-dimensional study of the Great Meteor Seamount, north-east Atlantic.
Journal of Geophysical Research, 80, 1391-1398.

WEAVER, C.E. & POLLARD, L.D. 1973
The chemistry of clay minerals.
Amsterdam: Elsevier. (Developments in Sedimentology, 15)

WEAVER, P.P.E. 1983a
An integrated stratigraphy of the upper Quaternary of the King's Trough Flank area, NE Atlantic.
Oceanologica Acta, 6, 451-456.

WEAVER, P.P.E. & KUIJPERS, A. 1983b
Climatic control of turbidite deposition on the Madeira Abyssal Plain.
Nature, 306, 360-363.

WEAVER, P.P.E. & SCHULTHEISS, P.J. 1983c
Vertical open burrows in deep-sea sediments 2m in length.
Nature, 301, 329-331.

WEAVER, P.P.E. & SCHULTHEISS, P.J. 1983d
Detection of repenetration and sediment disturbance in open-barrel gravity cores.
Journal of Sedimentary Petrology, 53, 649-654.

WEDEPOHL, K.H. 1960
Spurenanalytische Untersuchungen an Tiefseetonen aus dem Atlantik.
Geochimica et Cosmochimica Acta, 18, 200-231.

WEDEPOHL, K.H. 1968
Chemical fractionation in the sedimentary environment.
pp.999-1016 in, Origin and distribution of the elements, (ed. L.H. Ahrens).
Oxford: Pergamon Press.

WEDEPOHL, K.H. 1971
Environmental influences on the chemical composition of shales and clays.
pp.305-333 in, Physics and chemistry of the Earth, vol.8, (ed. L.H. Ahrens, F. Press, S.K. Runcorn and H.C. Urey).
Oxford: Pergamon Press.

WENDT, I., KREUZER, H., MULLER, P., VON RAD, U. & RASCHKA, H. 1976
K-Ar age of basalts from Great Meteor and Josephine seamounts (eastern North Atlantic).
Deep-Sea Research, 23, 849-862.

WHITEHEAD, J.A. & WORTHINGTON, L.V. 1982
The flux and mixing rates of Antarctic bottom water within the North Atlantic.
Journal of Geophysical Research, 87, 7903-7924.

WHITMARSH, R.B. & LILWALL, R.C. 1982a
A new method for the determination of in-situ shear-wave velocity in deep-sea sediments.
Paper No.4.2 in, Oceanology International exhibition and conference, 2-5 March, 1982, Brighton.
Kingston-upon-Thames: Spearhead Exhibition Ltd. 21pp.

WHITMARSH, R.B. GINZBURG, A. & SEARLE, R.C. 1982b
The structure and origin of the Azores-Biscay Rise, north-east Atlantic Ocean.
Geophysical Journal of the Royal Astronomical Society, 70, 79-107.

WILLIAMS, D.L., VON HERZEN, R.P., SCLATER, J.G. & ANDERSON, R.N. 1974
The Galapagos spreading centre: lithospheric cooling and hydrothermal circulation.
Geophysical Journal of the Royal Astronomical Society, 38, 587-608.

WILLIAMS, D.L., GREEN, K., VAN ANDEL, T.H., VON HERZEN, R.P., DYMOND, J.R. & CRANE, K. 1979
The hydrothermal mounds of the Galapagos Rift: observations with DSRV Alvin and edetailed heat flow studies.
Journal of Geophysical Research, 84, 7467-7484.

WILLIAMS, R. & CONWAY, D.V.P. 1981
Vertical distribution and seasonal abundance of Aglantha digitale (O.F.Muller) (Coelenterata: Trachymedusae) and other planktonic coelenterates in the north-east Atlantic Ocean.
Journal of Plankton Research, 3, 633-643.

WILLIAMS, R.J.P. 1982
The chemistry of Lanthanide ions in solutions and biological systems.
Structure and Bonding, 50, 79-119.

WILSON, T.R.S 1978
Evidence for denitrification in aerobic pelagic sediments.
Nature, 274, 354-356.

WILSON, T.R.S. et al 1982
RRS 'Discovery' Cruise 129, 22 May - 22 June 1982. Geochemical sampling in the tropical and subtropical eastern Atlantic.
Institute of Oceanographic Sciences, Cruise Report No.138, 18pp.

WILSON, T.R.S., THOMSON, J., HYDES, D.J. & COLLEY, S. 1983
Status report on geochemical field results from Atlantic study sites.
Institute of Oceanographic Sciences, Report No.175, 57pp.

WILSON, T.R.S., THOMSON, J., COLLEY, S., HYDES, D.J. HIGGS, N.C. & SORENSEN, J. 1984a
Early organic diagenesis; the significance of progressive subsurface oxidation fronts in pelagic sediments.
Geochimica et Cosmochimica Acta. (In press.)

WILSON, T.R.S. et al 1984b
RRS 'Discovery' Cruise 135, 30 March - 24 April 1983.
Geochemical sampling in the north-east Atlantic and the Mediterranean.
Institute of Oceanographic Sciences, Cruise Report No.160, 18pp.

WINDOM, H.L. 1976
Lithogenous material in marine sediments.
pp.103-135 in, Chemical oceanography, (2nd edition), vol.5, (ed. J.P. Riley & R. Chester).
London: Academic Press.

WISHNER, K.F. 1980
The biomass of the deep-sea benthopelagic plankton.
Deep-Sea Research, 27A, 203-216.

WONG, G.T.F. & BREWER, P.G. 1977
The marine chemistry of iodine in anoxic basins.
Geochimica et Cosmochimica Acta, 41, 151-159.

WOOD, G.L. 1972
The Guinness Book of animal facts and feats.
Enfield, Middlesex: Guinness Superlatives Ltd., 384pp.

ZIMMERMAN, H.B. 1982
Fine-grained sediment distribution in the Late Pleistocene/Holocene North Atlantic.
Bulletin de l'Institut de Geologie du Bassin d'Aquitaine, No.31-32, 337-357.

CHAPTER 7

FURTHER WORK

Assessment of Possible Disposal Areas

IOS work on the first contracts (up to the end of 1983-84) has concentrated on a general assessment of disposal options in the North Atlantic and on developing the field and analytical techniques needed for assessing the potential of particular sites (IOS Report No. 153).

A number of areas have been identified as showing promise and the next stage will be to study sites within one or two of these in more detail to try to establish whether they contain sites that would, in principle, be suitable for one or other of the disposal options.

A number of factors must be investigated before the feasibility of any option can be fully evaluated. Details will differ depending on the emplacement method but the options fall into two main groups.

Seabed Burial Options

In these options the sediment acts as a barrier to, or an adequate delay in the migration of, material released from primary containment. For detailed site assessment the principal questions to be answered may be summarised as follows:

1. What total area is needed for disposal, how much of this area would form an economic disposal site and what form would a repository take?

2. Can a suitable site or sites be found in the study area?

Both require information to be obtained from an oceanographic research programme though the answer to the first primarily requires assessments of the amount of material to be disposed of and of the economics of transport and emplacement. The second requires information about geological, chemical, physical and biological regimes to permit realistic safety assessments of the types of site available.

On the Seabed Options

The questions to be answered are formally the same as for the in the seabed options but the emphasis is different. Instead of acting as a barrier the sediments act as a substrate or foundation on which the disposed material is to be placed and may, if released, be reabsorbed. Their potential stability remains important because of the possibility of erosion or burial but their chemical or physical properties become less so since all they have to do is bear what is placed on them. Because there is no sediment barrier the performance of the repository itself is relatively more important as are the physical, chemical and biological processes in the water column.

A Site Assessment Research Strategy for Seabed Options

The research requirements for the two types of option have much in common and work relevant to one will contribute to the other. The difference between the two concepts lies in the additional sediment barrier if waste is buried. For the purposes of research, therefore, it is convenient to consider one option as forming part of the other and to assess both programmes in terms of multi-barrier seabed disposal. A suitable strategy is outlined here.

Work will aim at assessing the potential of a site within the GME study area in the Northeast Atlantic to provide a full geological appraisal of the site and to provide raw material for laboratory studies the results of which will be combined at the end of the research to give a comprehensive description of the site. This combined with engineering data will help provide a basis for radiological and environmental safety assessments.

The greatest emphasis will be on the study of the seabed itself, the initial stages of which will be devoted to the selection of a study site of approximately 10-20km on a side. Work will include photographic and geophysical surveys, with surface and deep towed equipment, the systematic acquisition of high grade sediment samples from the top 20m and in situ measurements of geotechnical properties, heat flow and sampling for porewater chemistry. Long term seismic monitoring of the areas with ocean bottom seismographs will commence at an early date.

By the end of 1985 it will be possible to decide to concentrate work on one study site. The remainder of the period will be directed to complete detailed geophysical mapping and to the application of advanced in situ techniques for studying sediment properties. Long term seismic monitoring will continue and further high quality samples of superficial sediments will be required for laboratory study.

Work on processes in the water column and on possible biological effects will need to continue during this period. The work will be specific to the chosen study site in the sense that it will be directly applicable to it though because it deals with possible transport of material to distant locations some observations will be widely distributed. The work will include long term local observations of oceanic variables in order to establish a base for statistical prediction of extreme events.